Energy conversion from electroactive materials and Modeling of behaviour on these materials

Chatchai Putson

N° d'ordre 2010-ISAL-0097 Année 2010

Energy conversion from electroactive materials and Modeling of behaviour on these materials

By

Chatchai Putson

**A thesis submitted in fulfilment
of the requirements for the degree of**

Doctor of Philosophy

School of doctorate: Electronic, Electrotechnic and Automatic (EEA)

INSA-Lyon

Lyon, France

18 November 2010

Advisory Committee:

Prof. Daniel GUYOMAR (Advisor)	LGEF, INSA-Lyon
Prof. Laurent LEBRUN (Co-Advisor)	LGEF, INSA-Lyon
Prof. Amen AGBOSSOU (Reviewer)	Université de Savoie
Prof. Jean François ROUCHON (Reviewer)	LAPLACE, GREM3, INPT
Dr. Eric DUHAYON (Committee Member)	LAPLACE, GREM3, INPT
Dr. Olivier GIRAUDO (Committee Member)	ONERA

LGEF Laboratory, Department of Electrical Engineering, INSA-Lyon

SIGLE	ECOLE DOCTORALE	NOM ET COORDONNEES DU RESPONSABLE
CHIMIE	**CHIMIE DE LYON** **http://sakura.cpe.fr/ED206** M. Jean Marc LANCELIN Insa : R. GOURDON	M. Jean Marc LANCELIN Université Claude Bernard Lyon 1 Bât CPE 43 bd du 11 novembre 1918 69622 VILLEURBANNE Cedex Tél : 04.72.43 13 95 Fax : lancelin@hikari.cpe.fr
E.E.A.	**ELECTRONIQUE, ELECTROTECHNIQUE, AUTOMATIQUE** **http://www.insa-lyon.fr/eea** M. Alain NICOLAS Insa : C. PLOSSU ede2a@insa-lyon.fr Secrétariat : M. LABOUNE AM. 64.43 – Fax : 64.54	M. Alain NICOLAS Ecole Centrale de Lyon Bâtiment H9 36 avenue Guy de Collongue 69134 ECULLY Tél : 04.72.18 60 97 Fax : 04 78 43 37 17 eea@ec-lyon.fr Secrétariat : M.C. HAVGOUDOUKIAN
E2M2	**EVOLUTION, ECOSYSTEME, MICROBIOLOGIE, MODELISATION** **http://biomserv.univ-lyon1.fr/E2M2** M. Jean-Pierre FLANDROIS Insa : H. CHARLES	M. Jean-Pierre FLANDROIS CNRS UMR 5558 Université Claude Bernard Lyon 1 Bât G. Mendel 43 bd du 11 novembre 1918 69622 VILLEURBANNE Cédex Tél : 04.26 23 59 50 Fax 04 26 23 59 49 06 07 53 89 13 E2m2@biomserv.univ-lyon1.fr
EDISS	**INTERDISCIPLINAIRE SCIENCES-SANTE** Sec : Safia Boudjema M. Didier REVEL Insa : M. LAGARDE	M. Didier REVEL Hôpital Cardiologique de Lyon Bâtiment Central 28 Avenue Doyen Lépine 69500 BRON Tél : 04.72.68 49 09 Fax :04 72 35 49 16 Didier.revel@creatis.uni-lyon1.fr
INFOMATHS	**INFORMATIQUE ET MATHEMATIQUES** http://infomaths.univ-lyon1.fr M. Alain MILLE	M. Alain MILLE Université Claude Bernard Lyon 1 LIRIS - INFOMATHS Bâtiment Nautibus 43 bd du 11 novembre 1918 69622 VILLEURBANNE Cedex Tél : 04.72. 44 82 94 Fax 04 72 43 13 10 infomaths@bat710.univ-lyon1.fr - alain.mille@liris.cnrs.fr
Matériaux	**MATERIAUX DE LYON** M. Jean Marc PELLETIER Secrétariat : C. BERNAVON 83.85	M. Jean Marc PELLETIER INSA de Lyon MATEIS Bâtiment Blaise Pascal 7 avenue Jean Capelle 69621 VILLEURBANNE Cédex Tél : 04.72.43 83 18 Fax 04 72 43 85 28 Jean-marc.Pelletier@insa-lyon.fr
MEGA	**MECANIQUE, ENERGETIQUE, GENIE CIVIL, ACOUSTIQUE** M. Jean Louis GUYADER Secrétariat : M. LABOUNE PM : 71.70 –Fax : 87.12	M. Jean Louis GUYADER INSA de Lyon Laboratoire de Vibrations et Acoustique Bâtiment Antoine de Saint Exupéry 25 bis avenue Jean Capelle 69621 VILLEURBANNE Cedex Tél :04.72.18.71.70 Fax : 04 72 43 72 37 mega@lva.insa-lyon.fr
ScSo	**ScSo*** M. OBADIA Lionel Insa : J.Y. TOUSSAINT	M. OBADIA Lionel Université Lyon 2 86 rue Pasteur 69365 LYON Cedex 07 Tél : 04.78.77.23.88 Fax : 04.37.28.04.48 Lionel.Obadia@univ-lyon2.fr

*ScSo : Histoire, Geographie, Aménagement, Urbanisme, Archéologie, Science politique, Sociologie, Anthropologie

RESUME

Le besoin de systèmes auto-alimentés et sans fils est à l'origine d'une activité intense de recherches sur la récupération d'énergie électrique à partir de sources ambiantes d'origine thermique ou mécanique. Cette récupération ne peut se faire que si l'on dispose de matériaux de conversion adaptés, objet de cette thèse et de méthodes efficaces d'extraction d'énergie. Parmi les différents types de matériaux, les polymères électro-actifs occupent une place de choix car ils sont faciles de mise en œuvre et peuvent être déposés sur de très grandes surfaces quelles soient planes ou non.

Dans un premier temps, un modèle analytique a été réalisé pour obtenir l'expression du courant électrique et de la puissance disponible lorsqu'on récupère l'énergie électrique avec un film polymère collé sur une poutre métallique excitée mécaniquement sur son premier mode de flexion. Ce modèle a par exemple montré que la permittivité du film polymère est un des paramètres clefs pour augmenter la conversion. Ce modèle a été validé expérimentalement en utilisant des polymères du commerce et a permis aussi d'évaluer l'effet de l'épaisseur du film et de la fréquence de travail.

Dans un deuxième temps, des composites utilisant des charges conductrices de taille nanométriques ou micrométriques dispersées en volume dans le polymère ont été synthétisés. Il a été montré que l'emploi de charges conductrices permet d'augmenter la permittivité grâce à un mécanisme de polarisation interfaciale et, conformément à ce que le modèle prédit, d'accroitre les performances en récupération d'énergie.

ABSTRACT

The need of self-powered and wireless systems is at the origin of intense research activity on the electrical energy harvesting from surrounding sources of thermal or mechanical origin. This energy harvesting can be made only if adapted materials of conversion, object of this thesis and efficient methods of extraction of energy are available. Among different types of materials, electro-active polymers occupy a place of choice because they are easy of implementation and can be deposited on of very large surfaces.

Firstly, an analytical model was proposed to model the expression of electric current and available power that can be harvested by using a polymeric film glued together on a metallic beam mechanically excited on its first flexural mode. This model showed for instance that the permittivity of the polymeric film is one of the key parameters to improve the conversion. This model was experimentally validated by using polymers of trade and also allowed to assess the effect of the thickness of the film and working frequency.

Secondly, polymers filled in volume by nanometric or micrometric conductive powders have been synthesized. It was shown that the use of such fillers allows increasing the permittivity thanks to a mechanism of interfacial polarization and, in accordance with the results predicted by the model, also allows enhancing the performances of energy harvesting.

To my son NaPat

To my wife and my parents

Acknowledgments

I would like to thank my advisor, Professor Daniel Guyomar, for his advices, encouragement and supervision throughout my graduate studies. His warm guidance and complete support made my working and learning experience. Also, I would like to express my sincere gratitude and appreciation to my co-advisor, Professor Laurent Lebrun, for his help, enlightening guidance and enthusiastic encouragement throughout the work. Especially, his knowledge, interest and commitment to excellence impress me greatly.

I also would like to express my gratitude to the committee members:
Pr. Amen Agbossou, Pr. Jean François Rouchon, Dr. Eric Duhayon and Dr. Olivier Giraudo for their invaluable, insightful comments and suggestions that improved the quality of this work.

I wish to thank Dr.Nantakan Muensit from material physics laboratory, Prince of Songkhla University for her help, advices and encouragement throughout research work.

I would like to thank Dr. Bernoit Guiffard, Dr. Laurence Seveyrat for providing help and advices in completing this research. I also would like to specially thank Pierre-Jean Cottinet and Komkrid Wongtimnoi for their kindness help and support. Thanks also go to Mr. Frederic Defromerie and Verinique Perin for machining the art-like device for my design and experiment.

I also would like to thank Evelyne Dorieux, secretary of Laboratory for her supporting.

In addition, I would like to thank my colleagues in the Génie Electrique and Ferroélectricité laboratory (Dr.Rabah, Dr.Akram, Dr.Xingjun, Jiawei, Kaixiang, Hongying, Masae, Dan, Qin…).

I will not be able to list the names of all whom I feel grateful to, but I would like to express my gratitude to all of the members of LGEF, scientific and administrative for their help and support during my work.

I would like to acknowledge LGEF, INSA-Lyon and the support of the Prince of Songkhla University Ph.D. Scholarship.

Finally, I want to thank my father, mother and sisters for enormous support. I also would like to thank my wife Suteeraporn for her considerable understanding and strong support. This thesis is dedicated to her and my son Napat.

Table of Contents

continuous

continuous

Nomenclature

A	area of sputtered electrode on the polymer
A_c	cross-sectional area of the beam
C_p	capacitance of the composite
c_{ijkl}^{E}	stiffness
c	specific heat capacity
D	Electric flux density
d_{ijm}	piezoelectric constants
E	electric field
F	electromagnetic force
f	frequency
G	Gibbs function
I	harvested current
k	coupling factor
L	beam length
M_{ijkl}	electric-field-related electrostriction coefficient
M_M	contribution of the Maxwell effect
M_T	contribution of the thermal effect
P	polarization
$P_{harvesting}$	harvested power
Q_{ijmn}	polarization related electrostriction coefficient
R	the sample resistance
R_c	matched load
S	Strain
S^M	Maxwell stress
s_{ijkl}^{E}	elastic compliance
T	stress
T_T	temperature
T_g	glass temperature
T_m	melting temperature
T_c	recrystallization temperature
t	thickness of the sample
t_b	thickness of the beam

u	displacement of the beam
V	voltage
w	width of rectangular cross-section
Y	Young modulus of the sample
Y_B	Young modulus of the beam
e_{mn}	linear dielectric permittivity
$e¢$	real part of the dielectric constant
$e¢¢$	imaginary part of the dielectric constant
e_r	dielectric constant
e_o	vacuum permittivity, $8.854´ 10^{-12}$ F/m
c_{mn}	dielectric susceptibility
b_{nm}	dielectric stiffness
s	conductivity
r	density of the beam
w_n	natural frequency
b_i	mode shape constants
f_c	percolation threshold volume fraction of loading
f_i	volume fraction of loading in the composite
$\tan d$	loss tangent

Introduction

The process of extracting energy from the environment or from a surrounding system and converting it to useable electrical energy is known as *energy harvesting or energy scavenging*. A variety of different methods exist for harvesting energy, such as solar power, ocean tides, piezoelectricity, thermodielectricity, magnetoelectricity and physical motion. Scavenging energy from ambient vibrations, heat or light could enable smart sensors to be functional indefinitely. Over the past decade, the amount of literature published on the topic of energy harvesting has increased drastically due to renewed interest in alternative energy sources. Recently, there has been a surge of research in the area of energy harvesting. This increase in research has been brought on by modern advances in wireless technology and low-power electronics such as MEMS devices.

Energy conversion in coupled materials and energy harvesting on ambient sources have become a crucial issue since they directly impact the self-powered devices performances. The past few years have witnessed an increasing focus in the research and development of wireless sensor networks and/or self power generating devices. Wireless sensors with ability for self power generation can potentially be employed in devices for wireless data transmitting and receiving as well as in structural health monitoring equipment. Given the wireless nature of some emerging sensors, it becomes necessary that they contain their own power supply, which is, in most cases, conventional batteries. If ambient energy in the surrounding medium can be obtained and utilized, this captured energy can then be used to prolong the life of the power supply or, ideally, provide unlimited energy for the lifespan of the electronic device. Therefore, the amount of research devoted to energy harvesting has been rapidly increased, and the energy harvesters have been investigated as an alternative power source for the next generation of embedded sensing systems.

The vibration energy harvesting is one such attractive technique for the potential powering of wireless sensors and low-power devices. A significant amount of papers have been published on energy harvesting on vibration with piezoelectric materials. Piezoelectric materials exhibit high electromechanical coupling but are heavy, brittle and have to be accurately located in the high-stress zones. Electrostrictive polymers

present a lower coupling but can be easily spread over large surfaces and are conformable to any regular surface.

Electrostrictive polymers exhibit very attractive characteristics, and as a result, they have been widely studied either for the purpose of understanding the electrostriction phenomenom**[YIM 1999][GUI 2003][SU 1998]** or in view of practical applications **[HER 1982][COH 2001]**. Numerous reports are devoted to the characterization of the electrostrictive behavior versus applied electric fields **[SU 1999][GUI 2006][PET 2008]**. Under moderate electric fields, electrostrictive polymers have been found to produce large strains of >10%, and for this reason they are considered as good candidates for actuation **[BHA 1999]**. As an example, polyurethane (PU) elastomers are of great interest for a wide range of transducer and actuator applications when considering their significant electrical-field-induced strains, high specific energy, and small response. Furthermore, these materials are lightweight, very flexible, presenting low manufacturing costs, and can be readily molded into any desirable shape **[PET 2008]**. In addition, it has recently been shown that the incorporation of nanofillers such as carbon nanotubes into a polymer matrix can greatly enhance the expected strain versus electric field **[PAR 2008]**.

In recent years, EAPs have been proposed for harvesting energy, or mechanical to electrical energy conversion. These polymers show their potential such as a large strain, elastic energy density, and high energy conversion efficiency. The total weight of systems based on EAPs is proposed to be significantly lower than those based on piezoelectric materials.

Several papers have published modeling studies to explain the generation of strain and the dynamic characteristics of materials. As an example, Lam *et al.* generated modeling to describe the deformation or small strain and the effect of accumulated charges at the inclusion matrix **[LAM 2005]**. A majority of modeling is based on the electrical equivalent circuit to describe the electromechanical behavior. Liu Y *at el.* discussed the mechanical and electrical boundary conditions based on elelctroactive polymer to predict the energy harvesting density. The energy harvesting density and coupling factor, or the ratio of electrical energy output-to-mechanical energy input, related to boundary conditions which passive diode circuit provided low energy harvesting density, while an open circuit obtained the maximum power energy density **[LIU 2005]**. Kailiang et al. investigated the energy harvesting with an electrostrictive

polymer, possessing high electromechanical response and elastic energy density, which it possible to generate high electric energy density and attractive for the active energy harvesting scheme. It is shown that combining the active energy harvesting scheme and high electromechanical response of the polymer yields a harvested electric energy density of ~40 mJ/cm^3 with a 10% efficiency **[KAI 2007]**. Jean-Mistral *et al.* proposed the model based on a quasi-linear viscoelastic characteristic of polymer to predict the energy produced by electroactive membrane. The results are very promising for the supply of autonomous devices. A biaxial millimeter plate can produce a maximum of 600µJ at high electrical field of 150 MV/m **[JEA 2007]**. Furthermore, previous approaches, including a finite element method, represent the dynamic behavior by using the cantilever beam.

In parallel, since the past decade, a large development of energy harvesting devices has taken place, which raises the need for new electroactive materials **[ANT 2007][PER 2007]**. Thanks to their properties, as mentioned above, electrostrictive polymers can be considered as excellent candidates **[LAN 2006][LIU 2005]**.

Objectives of this work

The first objective of this study is to design an analytical modeling based on electrostrictive effect for predicting an harvested current. This model has been obtained for the first flexion mode of a beam on which the electrostrictive polymers have been glued and operated at low frequency, 20 Hz.

The second objective is to improve the efficient harvesting energy devices using nano charges in electroactive polyurethane polymers. The figure of merit of the harvested current relating the dielectric constant and young's modulus is used to predict the values of the harvested current and to point out solutions for the enhancement of energy harvesting. The dielectric, electrical and mechanical properties of the electrostritive polymers are investigated and the electromechanical properties of the electroactive polymers are also observed.

Thesis Outline

The thesis consists of six chapters. Chapter 1 devotes to describing the details of the different researches on the energy harvesting from different sources of energy.

Chapter 2 proposes the analytical modeling based on electrostrictive effect for predicting the harvested current. This model has been obtained for the first flexion mode of a beam based on Euler-Bernoulli bending. The analytical models are compared to the experimental data. Moreover, the power harvesting modeling for electrostrictive materials is also proposed.

Chapter 3 presents the material background of the electroactive polymer. The procedure used for the preparation and the fabrication of polyurethane thin films and composites filled with fillers are discussed. Measurements of the dielectric properties, mechanical properties and thermal DSC characterization are described and the obtained results are also discussed.

Chapter 4 devotes to the electrostriction of polymer. Electrostriction measurement is used to evaluate the electrostrictive coefficient of materials. The electrostrictive contribution of polymers is presented and discussed.

In Chapter 5, the effect of particle size on harvested current is investigated. Power harvesting for these composites is presented and discussed. Moreover, the enhancement of harvested current by using high permittivity terpolymer is also shown.

Chapter 6 summarizes of the main conclusions stated in various chapters of the present work and the prognosis for future investigation is given.

Chapter 1:

Literatures review and general concepts of different techniques of harvesting energy

1.1 Introduction

The history of energy harvesting dates back to the windmill and the waterwheel. People have searched for ways to store the energy from heat and vibrations for many decades. Renewable energy resources, such as water flow, wind energy or sun radiation, can also be exploited at miniature scale by energy harvesting. All almost analogous terms related to research and engineering activities aimed at extracting energy in electrical form from various ambient energy reservoirs. One driving force behind the search for new energy harvesting devices is the desire to power sensor networks and mobile devices without batteries. In addition to being wireless, batteries allow the sensor to be portable. Unfortunately all batteries have a finite amount of energy and wear out with time, after which they need to be either replaced or recharged. However, rechargeable batteries require portable power generation units to recharge them. Also, the battery would dominate the system volume and is the bulky dimension. The optimum solution is to have a power source co-located that uses the ambient energy

available at its location, whether this is solar, thermal or mechanical. Thus, a portable small scale power generation system (alternative methods of power) that can either replace batteries entirely or recharge them to extend their lifetime is of considerable interest. Then, this small, portable, and lightweight power generation systems are currently in very high demand in the commercial markets, due to a dramatic increase in the use of personal electronics and communications equipments.

Energy harvesting (also known as *Power harvesting* or *energy scavenging*) is the process by which energy is captured and stored. Frequently this term is applied when speaking about small autonomous devices, like those used in sensor networks. A variety of different methods exist for harvesting energy, such as solar power, ocean tides, piezoelectricity, magnetoelectricity, thermoelectricity, and physical motion. Scavenging energy from ambient vibrations, heat or light could enable smart sensors to be functional indefinitely. Over the past decade, the amount of literature published on the topic of energy harvesting has increased drastically due to renewed interest in alternative energy sources.

1.2 Energy Harvesting Principles

Energy harvesting, also referred to as “energy scavenging” or “energy extraction”, can be defined as “converting ambient energies such as vibration, temperature, light, RF energy, *etc*. to usable electrical energy by using energy conversion materials or structures, and subsequent storage of the electrical energy for powering electric devices”.

In other words, the general concept of energy harvesting is to convert energy from the environment that is in an otherwise unusable form or wasted form into a more useful form. Frequently the form of energy that is most useful in modern applications is electrical energy, where it can be stored in a battery or used to power electrical circuitry. The wasted or unused energy exits in various sources such as industrial machines, human activity, vehicles, structures and environment, as shown in table 1.1. **[SHA 2007]** The energy harvesting can be converted from the variety of initial energy form, which can originate from any number of energy domains, such as optical, thermal, mechanical, acoustical, fluidic, chemical, and biological. Transducer is required to convert ambient energy to a usable form of electrical energy.

Table 1.1 Sources of energy available in the surrounding.

Human body	Vehicles	Structures	Industrial	Environment
Breathing, blood pressure, exhalation, body heat	Aircraft, UAV, helicopter, automobiles, trains	Bridges, roads, tunnels, farm house structures	Motors, compressors, chillers, pumps, fans	Wind, solar, temperature gradient, daily temperature
Walking, arm motion, finger motion, jogging, swimming, eating, talking	Tires, tracks, peddles, brakes, shock absorbers, turbines	Control-switch, HVAC systems, ducts, cleaners, etc.	Conveyors, cutting and dicing, vibrating mach.	Ocean currents, acoustic waves, EM waves, RF signal

The solar power has the capability of providing power density of 15000 μW/cm^3 which is about two orders of magnitudes higher than other sources, however direct sunlight is not always available. Table 1.2 present the composition of power density of sources.**[MYK 2007]** Vibrational and acoustic energies are useful in places without sunlight which are available even though they are considerably lower than solar energy.**[ROU 2003]** Most of chemical energy sources are commonly employed today in the form of batteries and fuel cells.**[ROU 2003]** Used batteries must either be replaced or recharged and fuel cells require refueling for continual operation. By contrast, the harvested energy sources, such as heat, vibration, sun, and acoustic do not theoretically have a limited supply of energy, given the right operating environment.

Table 1.2 Comparison of energy sources.

	Power Density (μW/cm^3) 1 Year Lifetime	Power Density (μW/cm^3) 10 Year Lifetime	Source of Information
Solar (Outdoors)	15,000 . direct sun 150 . cloudy day	15,000 . direct sun 150 . cloudy day	Commonly Available
Solar (Indoors)	6 . office desk	6 . office desk	Roundy [3]
Vibrations	200	200	Roundy et al. [4]
Acoustic Noise	0.003 @ 75 dB 0.96 @ 100 dB	0.003 @ 75 dB 0.96 @ 100 dB	Theory
Daily Temp. Variation	10	10	Theory
Temperature Gradient	15 @ 10°C gradient	15 @ 10°C gradient	Stordeur and Stark 1997 [5]
Shoe Inserts	330	330	Starner 1996 [6]
Batteries (nonrecharge Lithium)	45	3,5	Commonly Available
Batteries (rechargeable Lithium)	7	0	Commonly Available
Fuel Cells (methanol)	280	28	Commonly Available
Nuclear Isotopes (Uranium)	6 x 10^6	6 x 10^5	Commonly Available

Compared to battery-powered sensors, the energy harvesting based sensors need an architecture to form energy harvesting modules. The module is composed of a harvesting device and an energy harvesting circuit. To better utilize the harvested energy, two additional submodules such as power switching and power management modules are required. Use of harvested energy modules are achieved with the wireless sensor node as shown Figure 1.1. **[WAN 2007]**

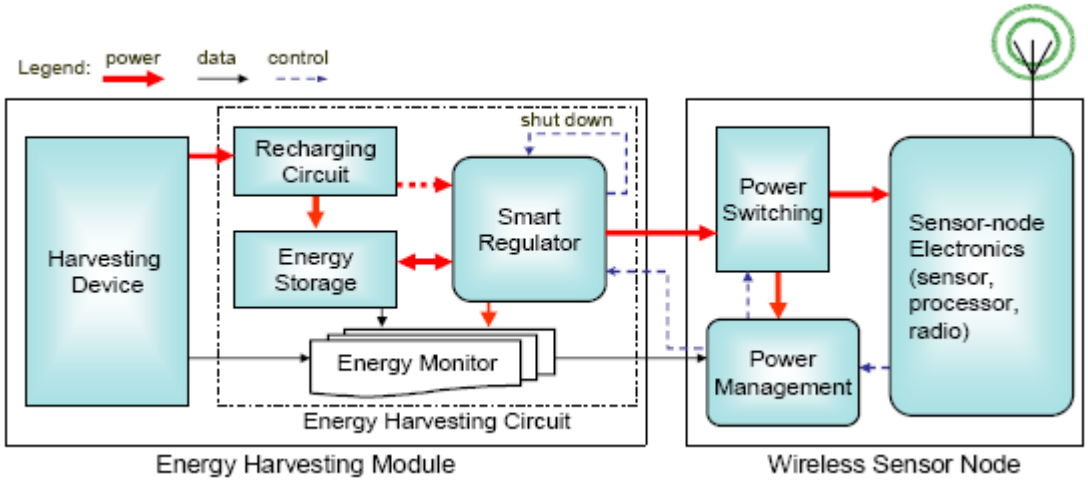

Fig. 1.1 General framework of an energy harvesting module and compatible wireless sensor nodes.

The *harvesting device* generates usable electrical energy from environment. It can be implemented by two mechanisms: one is based on materials for energy conversion such as piezoelectric material, electrostrictive material, pyroelectric material, solar cell, *etc*; the other relies on structures for energy conversion such as electromagnetic harvesters and electrostatic harvesters.

Unlike battery supply, which is simply characterized by the amount of residual and reliably available energy, the characterization of environmental energy is time-dependent and more complicated.

Also, the environmental energy has the potential to be used permanently. For the particular application considered in this dissertation, the initial energy is in the form of mechanical vibration, which usually uses ambient vibration around the energy harvesting device and then converts it into useful electrical energy by using electrostrictive material as harvesting material.

1.3 Summary of Potential Energy Sources

The potential ambient sources for energy harvesting include solar, vibration, and thermal gradient energy is discussed in this section.

1.3.1 Solar energy

Solar or other light energies can be converted into electrical power using solar cells, which are commercially mature and well characterized. Solar cells offer excellent power density of 15,000 μW/cm^3 in direct sunlight.**[MYK 2007]** The output energy depends on the material used. For example, crystalline materials such as silicon and gallium arsenide have moderated absorption efficiency and high conversion efficiency about 15% ~ 30%; while thin film materials such as cadmium telluride have high absorption efficiency and lower conversion efficiency (£10%). The choice of materials also relies on its spectral response and the light source of interest.**[BUL 2005]**

A thin film solar cell (hydrogenated amorphous silicon solar cell array) to power MEMS electrostatic actuators was developed.**[LEE 1995]** The array contained 100 single cells connected in series with total area of only 1 cm^2. They were able to produce 150 V on open circuit and 2.8 μA in short circuit condition under standard solar cell test light intensity. The device claims to be useful for any small device requiring voltages from tens to 100 V with currents in the nA to μA range. Under incandescent lighting situations, an area of 1 cm^2 produced power of around 60 μW.**[WOE 1998]** The current variation due to light intensity was overcome by a power converter integrated circuit. **[WOE 1998]**

The power converter integrated circuit is used to overcome the variation of current due to light intensity. In circuit design, the standard solar cell can be modeled as a voltage source in series with an internal resistor. A single solar cell has an open-circuit voltage of ~0.6 V, but panels with series and parallel combinations of such cells can generate any required voltage for circuit. Although the output voltage is fairly constant in the rated range, the current varies with light intensity.

The solar power at high performance is still more expensive than conventional methods. Typically solar power installations are small, generating 50W-5kW. Semi-conductor technology enabled the creation of solar cells which turn light energy into electrical energy. The conversion capability is dependant on the crystal structure and the electron bonds between neighboring atoms. The studies of solar power have been shown

that the average efficiency of commercially available solar power modules was 14.5% in 1994.**[ENG 1994]**

The commonly conversion efficiencies are between 10 to 30 percent. Then, the most efficient photovoltaic converters are costly, and these devices require clear, sunny days and sun tracking to insure optimal performance. Outdoor isolation levels offer approximately two to three orders of magnitude more electricity per unit area than indoor electric light sources. **[ROU 2003] [PAR 2005] [FAY 1997]**

Relative to other sources, solar devices can achieve high energy densities in direct sun, are shown in table 1.4.**[ROU 2003]** The photovoltaic cell under office lighting (a 100 mm^2) yields approximately 100 µW of power. **[PAR 2005] [FAY 1997]** Then, it has problem with indoor applications. Available solar power indoors, however, is drastically lower than that available outdoors. Measurements taken in normal office lighting show that only 6 $\mu W/cm^3$ can be converted by a solar cell **[FAY 1997]**, which is not nearly enough for the targeted application under consideration. If adequate light energy is available in the environment in which the node will operate, solar cells offer an attractive solution. However, in dim office lighting, or areas with no light, they are inadequate. Therefore using other techniques of harvesting energy such as vibration form and thermal form is suitable.

1.3.2 Thermal energy

Thermal gradients in the environment are directly converted to electrical energy through the Seebeck or thermoelectric effect. Temperature differential between opposite segments of a conducting material results in heat flow and consequently charge flow.

In 1826, the thermoelectricity phenomenon, a current would flow in a closed circuit made of two dissimilar metals or conductors at different temperatures, has been discovered by Thomas Johann Seebeck**[WAN 2007].** In 1834, Jean Charles Athanase Peltier observed that running an electric current through the junction of two dissimilar conductors could, depending on the direction of current flow, act as a heater or coolant. The heat absorbed or produced is proportional to the current, and the proportionality constant is known as the Peltier coefficient. Ideal thermoelectric materials have a high Seebeck coefficient, high electrical conductivity, and low thermal conductivity**[CAM 2004].**

After that in 1991, Kiely et al utilized silicon integrated circuit technology to fabricate a thermoelectric generator consisting of heavily implanted polycrystalline thermoelements on a quartz substrate. The generator had improved substrate qualities which allowed for better operation than previous designs.**[KIE 1991]**

Stordeur et al (1997) developed a low power thermoelectric generator to capable of generating tens of microwatts of power out of a device that had previously generated nanowatts out of the same device size. They offered a micro-thermoelectric harvester capable of producing 15 μW/cm^2 at 10 ^{o}C temperature differential. **[STO 1997]**

Thermopiles, a series-connected array of thermocouples, consisting of *n*- and *p*-type materials electrically jointed the high temperature junction, are therefore constructed, allowing heat flow to carry the dominant charge carriers of each materials to the low temperature end, establishing in the process a voltage difference across the based electrodes.

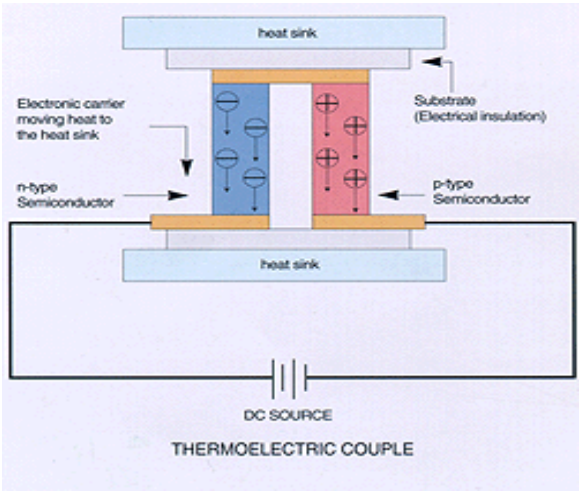

Fig. 1.2. Scheme of thermoelectric couple (www.inbthermoelectric.com)

Thermoelectric generators (TEGs) use the Seebeck effect, shown in Fig.1.3. which describes the current generated when the junction of two dissimilar metals experiences a temperature difference.

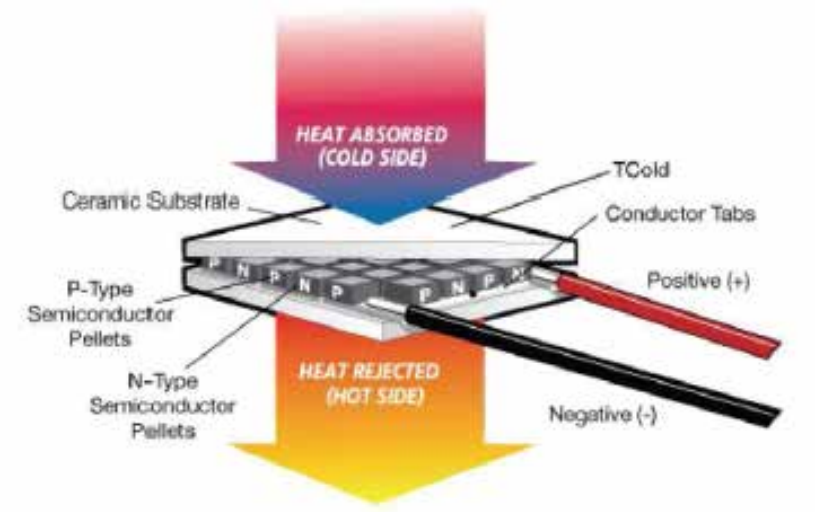

Fig. 1.3. Scheme of Thermoelectric generators (TEGs)

(http://www.tellurex.com/)

Zhang et al (2001) proposed and constructed a micromachined TEG with catalytic combustion chamber. Measuring only 2 mm x 8 mm x 0.5 mm, the combustion chamber ignited hydrogen and air and provided output power of up to ~1 μW per thermocouple. They reported that the proposed power output could be up to 10 μW per thermocouple when using the geometric modification at temperature differences of ~800K provided by the combustion chamber.**[ZHA 2001]**

In 2004, Fleming et al.**[FLE 2004]** investigated the use of TEG for powering microscale air vehicles. A TEG was mounted on the exhaust system of an internal combustion engine that was shown to generate 380 mW of power.

Several authors have studied the use of TEG for obtaining waste energy from the exhaust of automobiles. Birkholz et al.(1988) **[BIR 1988]** fitted a TEG unit around the exhaust pipe. The unit was experimentally tested and found to generate an open circuit voltage of 22 V and a total power of 58 W. Similarly, Matsubara (2002) **[MAT 2002]** constructed an exhaust system using ten TEG modules and a liquid heat exchanger to maximize the thermal gradient. The system was tested on a 2000 cc class automobile and shown to produce 266 W of power.

In 2006, Yang and Caillat looked at thermoelectric waste-heat recovery devices for use in the automotive industry. The motivation for the research was that only 25% of the combustion energy is actually used in an automobile, while up to 40% is lost to exhaust gases as waste. They start to design the radioisotope thermoelectric generators,

analyzing the existing technology that had been made in earlier decades for space vehicle applications. Specifically, the areas of device degradation over time and optimization of the figure of merit of thermoelectric devices within the specified operating temperature range are considered. The proposed benefits to automotive thermoelectric generation include eliminating secondary loads from the engine drive train and solid state, reliable and reversible air conditioning systems free from refrigerants. Challenges to such technology include difficulty of integrating with existing automotive electrical power systems and optimal operation over a broad range of temperatures.**[YAN 2006]**

Recently, Sodano et al (2007) proposed a novel approach to thermal harvesting using a small greenhouse device to capture thermal energy from solar radiation. The greenhouse was used in conjunction with a solar concentrator and a black body heat sink to harvest energy to recharge small nickel metal hydride batteries. The device was capable of recharging a 80 mAh and a 300 mAh nickel metal hydride battery in under 4 and 18 minutes, respectively. The study demonstrated that with relatively small thermal gradients and only conductive heat transfer, a thermoelectric generator can be used for energy harvesting applications.**[SOD 2007]**

1.3.3 Vibration Energy

Vibration energy harvesting techniques can rely on electromagnetic, electrostatic, piezoelectric, and magnetostrictive approaches. The current status of investigations on the energy harvesting techniques is briefly reviewed as below. Four common techniques will be discussed individually, and then a comparison table will be drawn to compare the features of different techniques.

1.3.3.1 Electromagnetic energy harvesting

In 1996, Williams and Yates proposed an electromagnetic energy harvesting device, which generated electricity when embedded in a vibrating source. Electromagnetic power conversion or electromagnetic energy harvesting device results from the relative motion of a conductor mass in a magnetic field. The electromagnetic systems based on Faraday's Law are composed of a coil and a permanent magnet attached to a spring. They reported that the amount of power generated was proportional to the cube of the vibration frequency. For a typical device the power generation was 1 μW at 70 Hz and 0.1 mW at 330 Hz. **[WIL 1996]**

In 1998, Amirtharajah and Chandrakasan developed a more complicated harvesting device with a test microchip, which demonstrate the possibility of running a digital signal processing (DSP) from the power generator by vibration in its environment. They was found that the electromagnetic generator was capable of supplying 400 µW of output power typical excitation similar to that of a human walking.**[AMI 1998]**

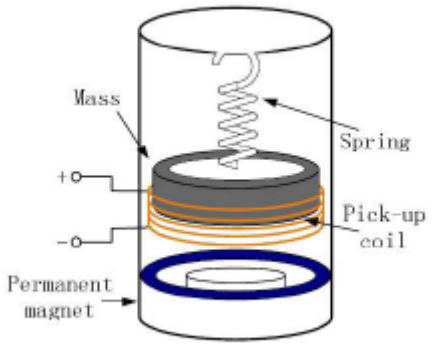

Fig. 1.4. Schematic of a typical electromagnetic harvester. **[AMI 1998]**

Recently an electromagnetic harvester was tested on a real automobile producing a peak power of 3.9 mW with a volume of 3.15 cm^3, however the average power was only 157 µW.**[GLY 2004]**

A micro-cantilever beam structure has been adopted to induce relative displacement between magnets and a coil bonded at free end of the beam.**[TOR 2005]** The silicon beam thickness was only 50 µm by using MEMS technique. At a 0.06g acceleration and 58.5 Hz resonant frequency, its maximum power and power density could reach 10.8 µW and 900 $\mu W/cm^3$, respectively.

In 2002, Ching *et al.* discussed a micro-harvester fabricated on a PCB (Printed Circuit Board) with total volume of ~1 cm^3 comprising a laser micro-machined spiral copper spring and an NdFeB magnet and a coil. The peak-to peak output voltage was up to 4.4 V and maximum power could reach 830 µW when driven by a 200 µm displacement at its resonant frequency at 110 Hz. **[CHI 2002]**

Yuen et al. developed an electromagnetic-based micro energy converter that can be placed into an AA battery-size container. The device was used as a power supply for

a wireless temperature sensing system. The converter is able to charge a capacitor up to a 1.6 V DC level in less than 1 minute.**[YUE 2004]**

In 2004, Poulin et al. presented a comparative study of electromagnetic and piezoelectric energy conversion systems. They suggested that the electromagnetic system is suitable to energy generation for medium-scale applications, while piezoelectric system appropriate to energy generation for microsystems because of a higher power density. **[POU 2004]** Recently, Ibrahim et al. presented a design, optimization and implementation of an electromagnetic type vibration-to-electrical micro energy harvester. The micro harvester generates voltage by virtue of the relative motion between the coils and a stationary magnet. The fabricated device occupies a volume of $9.5 \times 8 \times 6$ mm^3. The proposed harvester is carried out on a microscale which can generate a maximum voltage and power of 0.67 mV and 56 pW, respectively, at a vibration frequency of 3.4 kHz.**[IBR 2009]**

Above all, the energy conversion mechanism is simple without the need of smart materials, but it has relatively larger volume because of the required permanent magnets and pickup coil. Due to its inductive property, comparatively high output current levels are achievable at the expense of low voltage. Voltage multiplier may be a suitable solution to increase the voltage level. Wafer-scale systems, however, are quite difficult to achieve owing to the relatively poor properties of planar magnets, the limitations on the number of turns achievable with planar coils and the restricted amplitude of vibration.

1.3.3.2 Electrostatic energy harvesting

The electrostatic energy harvesting is one of vibration energy harvesting which relies on the changing capacitance of vibration-dependant varactors, or variable capacitors whose electrodes are moveable to each other and separated by a dielectric to form a capacitor as shown in Figure 1.5.**[ROU 2004]** By initially placing charge on the electrodes and moving the electrodes apart, mechanical motion can be converted into electrical energy. Energy density of the harvester can be increased by decreasing the capacitor spacing, facilitating miniaturization. However, the energy density is also decreased by reducing the electrode surface area.

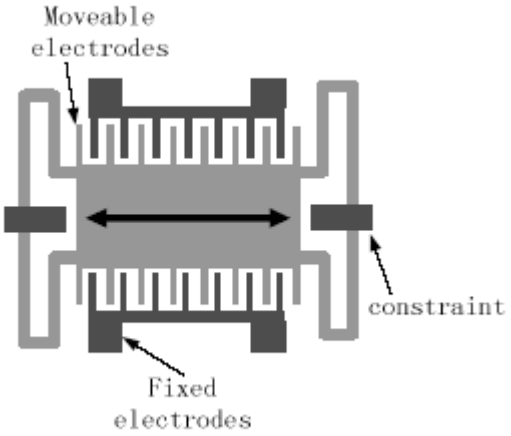

Fig. 1.5. Schematic of a typical electrostatic harvester vibrating horizontally.
[ROU 2004]

Meninger *et al.* proposed the use of the MEMS-scale variable capacitor transducer to convert meachanical vibrations into electrical energy for low power electronics. In theory slightly more power could be produced from a voltage constrained system. Furthermore, the electrostatic energy harvesting device attained power density of 0.23 μW/cm^3 at a vibration of 2.5 kHz.**[MEN 2001]** Roundy *et al*. optimized the electrostatic harvester and improved the output power density up to 110 μW/cm^3 at 120 Hz vibration.**[ROU 2004]**

The electrostatic energy harvesting does not require smart materials and is feasibly integrated with MEMS by relatively mature silicon micro-machining techniques. Due to capacitive-based device, it generates relative high voltage of 2~10 V and results in a limited current-supplying capacity.**[ROU 2004]** However, electrostatic harvesting requires an external voltage or charge source for initialization. Furthermore, mechanical constraints on the moving electrodes are indispensable to avoid electrode shorting.

1.3.3.3 Piezoelectric and Electrostrictive energy harvesting

One of the most popular methods of implementing an energy harvesting system to use mechanical vibration is to apply strain energy to a piezoelectric material due to reasonable electro-mechanical coupling coefficient. No bulky accessory (such as coil or permanent magnet) is needed, and feasibility of being deposited on substrates for MEMS applications has been shown.

Starner might be one of the first researchers realizing the potential of piezo-based energy harvesting and proposing possible storage methods. He proposed a survey of various power generation methods ranging from body heat and blood pressure.**[STA 1996]**

Umeda *et al.* proposed a piezoelectric transducer, using PZT, to transform mechanical impact energy of a falling steel ball into electric energy. The equivalent circuit model is used to predict the energy output power while modifying numerous parameters for energy harvesting.**[UME 2004]**

Kymissis *et al.* researched the concept of using a polyvinylidene fluoride PVDF and PZT piezoceramics as well as rotary magnetic generators to harvest energy inside of a shoe. The integrated PZT and PVDF with a running sneaker is shown in Fig. 1.6. Overall, average power generated from these PVDF and unimorph obtained roughly 1 mJ and 2 mJ per step, respectively. **[KYM 1998]**

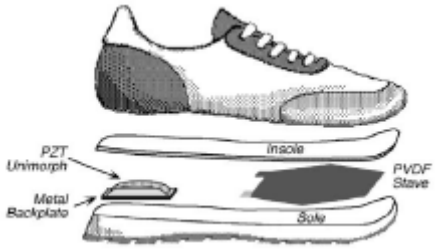

Fig. 1.6. Schematic and results of energy harvesting shoe.**[KYM 1998]**

Allen and Smits offered harvesting energy using the Karman vortex behind a bluff body from induced oscillations of a piezoelectric membrane. Four different membranes or “eels” were tested in the vortex street, and their behavior was successfully predicted by derived models. However, since this was only a feasibility study, no actual numbers were presented in terms of the amount of energy that could be harvested. **[ALL 2001]**

Fig. 1.7. Energy harvesting “eel” concept. (Source: Ocean Power Technologies, Inc.)

Elvin *et al.* used PVDF film attached to a simply-supported beam to generate electrical power. The goal of this conversion energy experiment was to generate sufficient power from the strain induced on this sample by a bending beam to provide the required energy to a telemetry circuit. A switch was added to the circuit to automatically discharge and charge the storage capacitor, which produced the output voltage range of 0.8~1.1 V for a RF transmitter.**[ELV 2001]**

To dynamically optimize the energy harvested from a vibrating piezoelectric device, an adaptive AC-DC rectifier with an output capacitor, rechargeable battery, and switch-mode DC-DC converter was introduced by Ottman *et al.***[OTT 2002]** A power density of 196 mW/cm^3 was obtained. However, if the voltage produced by the piezo-harvester was less than 10 V, then the power flow into the battery was reduced because of loss in the additional circuit components.

Sodano *et al.* investigated the possibility of using piezoelectric generators to recharge nickel metal hydride batteries. Two types of harvesters, a monolithic piezoelectric element (PZT) and a Macro Fiber Composite (MFC), were used for the experiment. While the MFC is much more flexible than the PZT, the use of interdigitated electrodes in the MFC limits the amount of current produced, and hence hinders its capabilities as a power harvesting device for charging batteries, except when relatively large disturbances are available. The PZT, however, was able to charge 40 mAh and 80 mAh batteries within two hours. It was also shown that charging a battery by vibrating the PZT at resonance typically took less time than by using a random input signal to the PZT.**[SOD 2003]** Roundy and Wright **[ROU 2004b]** presented an

equivalent electrical-mechanical circuit model to analyze the cantilever type of piezoelectric harvester; the maximum output power through a 300 kΩ resistor reached 375 μW/cm^3 subjected to a vibration of 2.5 m/s^2 at 120 Hz. To further improve the output power, the same theoretical model is also employed by Gao and Cui.**[GAO 2005]** The maximum output power density of a triangular beam could achieve 790 μW/cm^3 with 43.5 kΩ resistor under a frequency of 72 Hz; while the maximum output power density on a rectangular beam under the same scenario was 520 μW/cm^3.

Shashank Priya offered a model for electric power harvesting from wind energy using piezoelectric bimorph transducers. A piezoelectric windmill consisting of ten piezoelectric bimorphs was fabricated and characterized under the realistic environment to determine the power-wind speed relationship. The prototype piezoelectric windmill consisting of ten piezoelectric bimorph transducers was operated in the wind speed of 1–12 mph. A power of 7.5 mW at the wind speed of 10 mph was measured across a matching load of 6.7 kΩ.**[SHA 2005]**

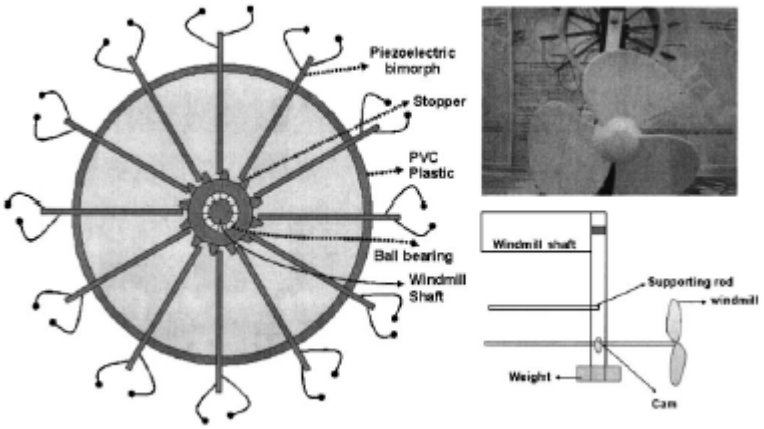

Fig.1.8. Schematic diagram of the piezoelectric windmill showing the arrangement of piezoelectric actuators.**[SHA 2005]**

Recently, Guyomar *et al.* 2005, Badel *et al.*, 2005, Lefeuvre *et al.*, 2005, investigate a new method of piezoelectric vibration energy harvesting system which called “Synchronized Switch Harvesting on Inductor” (SSHI) by using a self-adaptive power harvesting circuit. It was developed from a popular method of vibration suppression referred to as “synchronized switching damping on inductor” (SSDI). **[GUY 2005] [BAD 2005] [LEF 2005]** It adopted an electrical circuit containing an

inductor and an electrical switch to maximize charge extraction from PZT, and could enhance the output power four times**[BAD 2006a]** or even more **[BAD 2006b]**

In brief, piezoelectric vibration energy harvesting offers a straightforward and simple approach, whereby structural vibrations are directly converted into a voltage as output. There is no requirement for having complex geometries, external supply, and bulky accessories. Furthermore, its transduction principle is practically well suited to MEMS. However, most piezoelectric ceramics or crystals are very brittle, and this harvesting approach is required to be strained directly. Other disadvantages such as depolarization and charge leakage also exist in PZT. Thus their mechanical and physical properties limit overall performance and life time. Although PVDF film is flexible, it has low coupling efficiency. Due to the capacitive property, this method is capable of producing relatively high output voltage at the cost of low electrical currents.

1.3.3.4 Magnetostrictive energy harvesting

Magnetostrictive materials (MsM) are one of compounds which considered in applications of vibration energy harvesting. *Villari effect* utilized to explain the case, where vibration-induced strain of a MsM produces a change in the magnetization of the material. Upon dynamic or cyclic loading, this change in magnetization is converted into electrical energy using a pick-up coil or solenoid surrounding the magnetostrictive layer according to Faraday's law.

Staley and Flatau attempted to apply a Terfenol-D alloy in vibration energy harvesting. The Terfenol-D rod was operated in axial mode rather than flexural bending mode. It had bulky dimension because of 1000-turn pick-up coil and 1500-turn DC actuation coil for generating bias magnetic field. The maximum output power was up to 45 μW at resonant frequency of 45 Hz, and the amplitude of AC output voltage was less than 0.35 V which was inapplicable to voltage rectification. Due to the giant magnetostriction of Terfenol-D up to 2000 μm/m, Terfenol-D has been used as a medium to provide large extensional strains in a PZT layer for energy harvesting. A thin PZT layer sandwiched by two Terfenol-D layers is placed under time varying magnetic field. Since the outer Terfenol-D layers will induce higher strains than the traditional d_{31} bending mode in the PZT layer, the PZT layer will generate more charge. The time-varying magnetic field could be induced from ambient vibrations by a permanent magnet attached to either a cantilever beam or a spring.**[STA 2005]**

Huang *et al.* developed a Terfenol-D/PZT/Terfenol-D composite harvester which could achieve 1.2 mW of power at resonant frequency of 30 Hz at acceleration of 5 m/s^2. They claimed that more than 10 mW could be harvested from a volume of 1 cm^3 at acceleration of 5 m/s^2.**[HUA 2003]** Bayrashev *et al.* also fabricated a diameter of 0.5 mm thick PZT disc sandwiched between two Terfenol-D discs with thickness of 1.5 mm. When the laminate was exposed to low frequency (<100 Hz) varying magnetic field, the output power from PZT layer was found to be in a range of 10~80 μW.**[BAY 2004]**

Wang and Yuan first proposed the feasibility of using amorphous metallic glass (Metglas 2605SC) as MsM for harvesting energy from ambient vibrations. They introduced an equivalent electrical-mechanical circuit model to analyze the output performance of the harvester, and optimized the configuration of bias magnets and output performance.**[WAN 2006]** The max output power reached 200 μW. Lately they completed the system integration design and enhanced the output performance by utilizing transversely annealing treatment to Metglas.**[WAN 2007]** Compared to piezoelectric materials, the Metglas 2605SC offers advantages including higher energy conversion efficiency, longer life cycles, lack of depolarization and higher flexibility to survive in strong ambient vibrations. To enhance the energy conversion efficiency and alleviate the need of a bias magnetic field, Metglas ribbons are transversely annealed by a strong magnetic field along their width direction. According to the experimental results, the average power and power density during charging the ultracapacitor can achieve 576 μW and 606 $\mu W/cm^3$ (with respect to the active material volume) at high frequency, which compete favorably with piezoelectric vibration harvesters.**[WAN 2008]**

Compared to piezoelectric based harvesters, Metglas-based harvesters have high coupling efficiency (>0.9), higher Curie temperature, higher flexibility to be integrated with curved structures, and no depolarization problem. It is suitable to work in hash and high frequency environments. However, it has relatively large dimension, which is hard to be integrated with MEMS, because of the pick-up coil and permanent magnets.

1.3.3.5 Comparison of different techniques

Table 1.3 summarizes and compares the common vibration techniques.

Table 1.3 Summary of the comparison of the different type of mechanisms.**[WAN 2008]**

Type	Advantages	Disadvantages
Electromagnetic	• no need of smart material • no external voltage source	• bulky size: magnets and pick-up coil • difficult to integrate with MEMS • max voltage of 0.1V
Electrostatic	• no need of smart material • compatible with MEMS • voltages of 2~10V	• external voltage (or charge) source • mechanical constraints needed • capacitive
Piezoelectric	• no external voltage source • high voltages of 2~10V • compact configuration • compatible with MEMS • high coupling in single crystal (SiO_2)	• depolarization and aging problems • brittleness in PZT • poor coupling in piezo thin film (PVDF) • charge leakage • high output impedance
Magnetostrictive	• ultra-high coupling coefficient >0.9 • no depolarization problem • high flexibility • suited to high frequency vibration	• non-linear effect • pick-up coil • may need bias magnets • difficult to integrate with MEMS

1.4 Conclusions

There is abundant energy in our environment. Examples of energy sources are: solar light, vibration, thermal heat. The process of extracting energy from the environment or the surrounding system and converting it to useable electrical energy is known as Energy harvesting or scavenging energy. Energy harvesting from direct solar carried out high electrical power density but it is not always available. Harvesting energy from vibration is the most popular method as high available power density exists in the environment (machine vibration, human activities). The vibration harvesting energy using smart materials such as piezoelectric ceramics and electrostrictive polymers is of high interest due to the large amount of power that can be harvested and to the easiness of integration.

Chapter 2:

Energy harvesting using electrostrictive polymer

2.1 Introduction

This chapter deals with the analytical energy harvesting model at the first flexion mode of a cantilever beam. Background information is given for the governing equations of electrostrictive materials for energy conversion on this analytical model. The proposed model used for electrostrictive polymer will be constructed and validated. Experimental measurements of the harvested current will be compared to the theoretical behaviour predicted by the proposed model. The dielectric properties of polymer and how it affects harvested current and power will be also discussed.

2.2 Electrostrictive material constitutive equation

2.2.1 General principles of electrostrictive polymer generator mode

Electrostriction is generally defined as a quadratic coupling between strain, S and electric field, E (details will be shown in chapter 4). The constitutive equations for an electrostrictive material (including the elastic equation) can be written as

$$S_{ij} = s^{E}_{ijkl} T_{kl} + M_{mnij} E_m E_n \qquad (2.1)$$

The electric flux density D is expressed as independent variables of the electric field intensity and the stress T by the constitutive relation as:

$$D_m = e_{mn} E_n + 2M_{mnij} E_n T_{ij} \qquad (2.2)$$

where s^{E}_{ijkl} is the elastic compliance, M_{ijkl} is the electric-field-related electrostriction coefficient, and e_{mn} is the linear dielectric permittivity.

.

2.2.2 Energy harvesting cycles

In the energy harvesting cycle for electrostrictive polymers proposed by Y. Liu et al **[LIU 2005]**, the mechanical-to-electrical energy harvesting in electrostrictive materials is illustrated in the mechanical stress/strain and electric field/ flux density plots shown in Figure 2.1. Initially the material shown in Figure 2.1, has no applied stress, then stress is applied at constant E and the state travels along path A. The applied stress then is reduced at constant D. Due to the change in the electrical boundary conditions, the contraction path will not follow same path. Both in the mechanical and electrical planes, the material state traverses a closed loop. In the mechanical plane the rotation designates that the net energy flow is from the mechanical to the electrical. The area enclosed in the loop of the mechanical and electrical planes is equal and is the converted energy density in units of J/m^3.

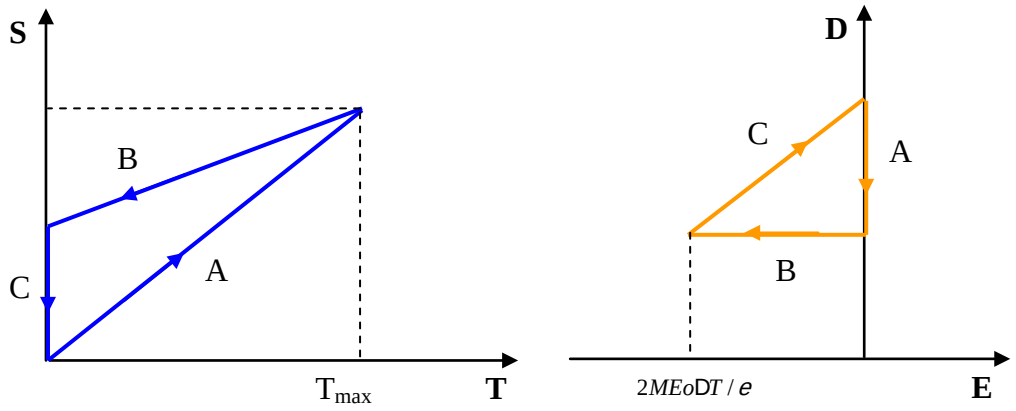

Fig. 2.1. Energy harvesting cycle

In order to adjust the mechanical boundary conditions, the design of a mechanical transformer such as a cantilever, bimorph are considered to modify the mechanical stresses applied to the material. Another approach is to control the electrical boundary conditions of the materials. Ideally the energy harvesting cycle consist of the largest loop possible, bounded only by the limitations of the material. Y. Liu et al. have analyzed electrical boundary condition that can be applied for optimized the energy harvesting.

They used the concept of coupling factor, as defined in the IEEE standard of piezoelectric **[IEEE 1988]**, is useful as a figure of merit for energy harvesting, and is given in equation (2.3):

$$k = \sqrt{\frac{W_1}{W_1 + W_2}} \qquad (2.3)$$

where W_1+W_2 is the input mechanical energy density, and W_1 is the output electrical energy density.

A constant electric field E_0 exists from state 1 to state 2 as the stress is increased to T_{max}. From state 2 to state 3 the electric field is increased from E_0 to E_1 until the stress is reduced from T_{max} to 0. At zero stress the electric field is reduced to E_0 (E_0=0), returning to state 1. In the dielectric-field plot, the path 1-2and 2-3 are not same path which is due to the stress dependence of the dielectric constant. The converted energy W_1 can be express by equation (2.4):

$$W_1 = T_{\max} M \left(E_1^2 - E_0^2 \right) \qquad (2.4)$$

The input mechanical energy density, $W_1 + W_2 = (1/2) s T_{\max}^2$ and the coupling factor, therefore, is given by equation (2.5):

$$k = \sqrt{\frac{M \left(E_1^2 - E_0^2 \right)}{\frac{1}{2} s T_{\max}}} \qquad (2.5)$$

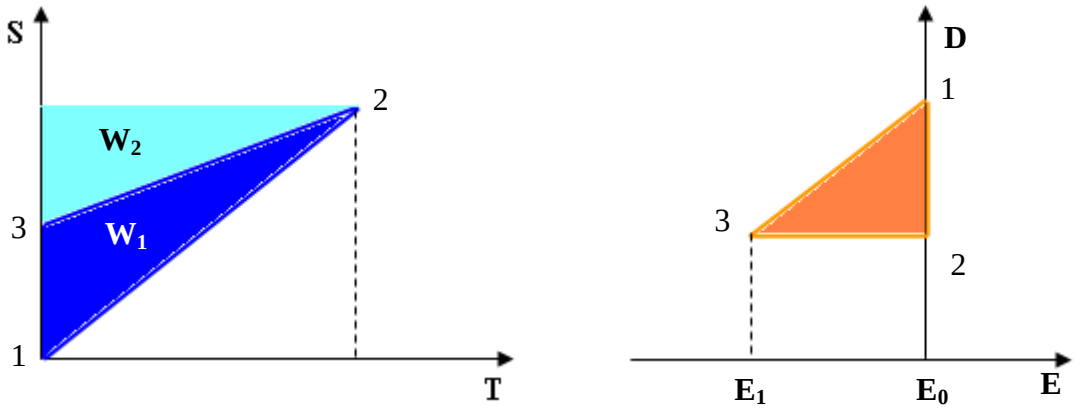

Fig.2.2. Energy harvesting cycle under constant electrical field condition (1-2) and open circuit (2-3) electrical boundary conditions.

2.3 Modeling analysis of the cantilever beam element

A. Euler-Bernoulli beam theory on the cantilever beam

The setup for the cantilever beam model is shown in Figure 2.3.

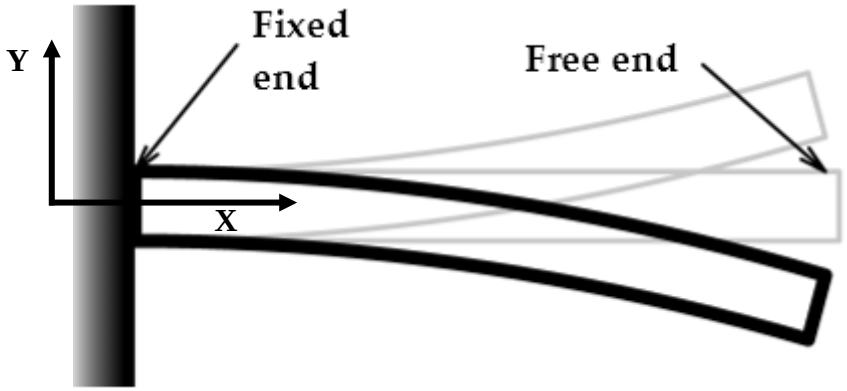

Fig. 2.3. Setup of cantilever beam model.

For cantilever beam, Euler-Bernoulli beam theory describes the relationship between the radius of curvature and the force applied, which is given by the following equation

$$r A \frac{\P^2 u(x,t)}{\P t^2} + Y_B I_m \frac{\P^4 u(x,t)}{\P x^4} = F(x,t) \qquad (2.6)$$

where u is the displacement of the beam, r is the density of the beam, A is the cross-sectional area, I_m is the moment of inertia and $F(x,t)$ is the applied force. If no external force is applied, then $F(x,t)$ is equal to 0 and the equation can be rewritten as:

$$\frac{\partial^2 u(x,t)}{\partial t^2} + c^2 \frac{\partial^4 u(x,t)}{\partial x^4} = 0 \qquad (2.7)$$

and $$c = \sqrt{\frac{Y_B I_m}{r A}}$$

A separation of variables solution is assumed to be

$$u(x,t) = \sum T_i(t) X_i(x) \qquad (2.8)$$

where T_i is the i-th model coordinate equation of the beam and X_i is the i-th mode shape of the beam. This is substituted into equation 2.7 which becomes:

$$c^2 \frac{X''''(x)}{X(x)} = -\frac{\ddot{T}(t)}{T(t)} = w^2 \qquad (2.9)$$

By rearranging equation 2.9, the spatial equation of the system can be found :

$$X''''(x) - \frac{w^2}{c^2} X(x) = 0 \qquad (2.10)$$

Defining,

$$b^4 = \frac{w^2}{c^2} = \frac{r A w^2}{Y_B I_m} \qquad (2.11)$$

And assuming a solution of the form

$$X(x) = Ae^{bx}$$

The general solution of equation (2.10) can be calculated as

$$X(x) = a_1 \sin(bx) + a_2 \cos(bx) + a_3 \sinh(bx) + a_4 \cosh(bx) \qquad (2.12)$$

The value of b and constant of integration can be determined by using boundary conditions. If a beam in transverse vibration is free at one end, the bending moment and shear force at that end must vanish:

$$Y_B I_m \frac{\partial^2 u}{\partial x^2} = 0 \qquad Y_B I_m \frac{\partial^3 u}{\partial x^3} = 0$$

If the end of the beam is clamped, the deflection and slope must vanish at that end:

$$u = 0 \qquad \frac{\partial u}{\partial x} = 0$$

Using these boundary conditions and substituting into equation 2.12, the mode shape of a cantilever beam becomes

$$X_i(x) = \cosh(\frac{\beta_i x}{L}) - \cos(\frac{\beta_i x}{L}) - \frac{\sinh(\beta_i L) - \sin(\beta_i L)}{\cosh(\beta_i L) + \cos(\beta_i L)}(\sinh(\frac{\beta_i x}{L}) - \sin(\frac{\beta_i x}{L})) \qquad (2.13)$$

Where L is the beam length, $\beta_i^4 = \frac{\omega_{ni}^2}{c^2}$ and ω_n is the natural frequency obtained by solving the transcendental equation:

$$\cosh(\beta_i L)\cos(\beta_i L) + 1 = 0 \qquad (2.14)$$

Table 2.1 lists the mode shape constants of β_i for a cantilever beam from the handbook **[BLE 1995]**. Figure 2.4. displays first five mode shapes of a cantilever beam.

Table 2.1 Mode shape constants of β_i for a cantilever beam.

Mode No. i	β_i
1	1.87510497
2	4.69409113
3	7.85475744
4	10.99554073
5	14.13716839
>5	$(2i - 1)\pi / 2$

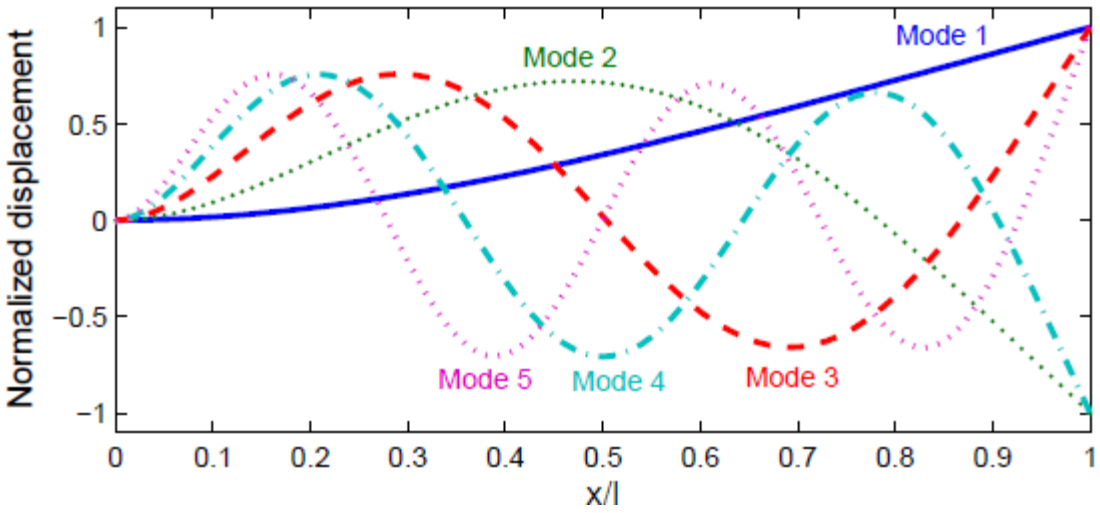

Fig. 2.4. First five mode shape of a cantilever beam.

The analysis for the cantilever beam shows that the natural frequencies can be found from: **[INM 2001]**

$$f_i = \frac{b_i^2}{2pL^2}\sqrt{\frac{Y_B I_m}{r A_c}} = \frac{b_i^2}{2p}\sqrt{\frac{Y_B I_m}{r A_c L^4}} \qquad (2.15)$$

where Y_B is Young's modulus of beam, I_m is area moment of inertia, L is the length of the beam, r is the density of the beam and A_c is the cross-section area of the beam.

2.4 Analytical energy harvesting model based on the electrostrictive polymer at the first flexion mode of a cantilever beam

A. Harvested Current Model

This paragraph describes the development of an analytical model of the current produced by polymers when the first flexion mode of a cantilever beam was excited with the help of an electromagnet. The cantilever beam is shown in Figure 2.5. The polymer film was glued to the metallic beam close to the clamped end, located at the maximum stress zone.

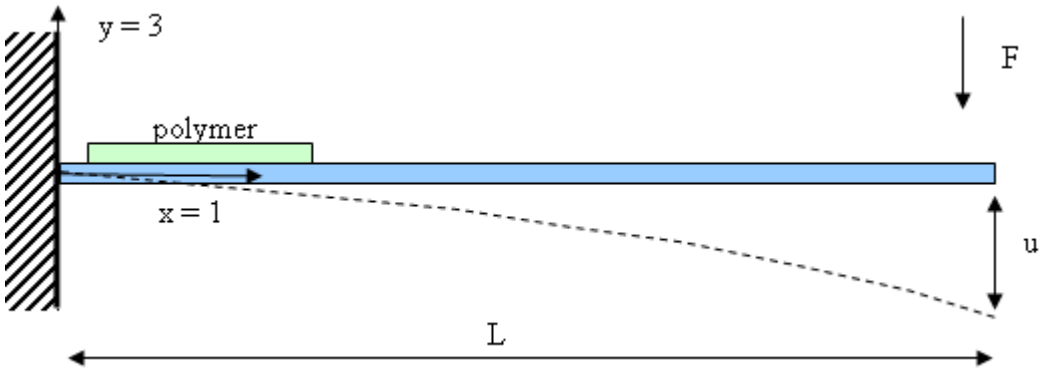

Fig.2.5. A schematic diagram of the electrostrictive-polymer cantilever beam.

An electromagnet was utilised to impose a given stress at the beam's free end in order to force it to vibrate in its first flexural mode.

The principle of the current modelling was based on the constitutive equations of electrostriction.

$$S_{ij} = s^{E}_{ijkl} T_{kl} + M_{mnij} E_m E_n \qquad (2.16)$$

The electric flux density, D, is expressed as independent variables of the electric field intensity and the stress by the constitutive relation**[LIU 2005]** as:

$$D_m = e_{mn} E_n + 2 M_{mnij} E_n T_{ij} \qquad (2.17)$$

For an isotropic electrostrictive polymer film contracting along its thickness direction and considering only the 31 lateral vibration mode coupling, then the constitutive equations may be written:

$$S_1 = s_{11}T_1 + M_{31}E_3^{\,2} \tag{2.18}$$

$$D_3 = e_{33}E_3 + 2M_{31}E_3T_1 \tag{2.19}$$

Here, e_{33} is the linear dielectric permittivity, s_{11} is the elastic compliance and M_{31} is the electrostriction coefficient. Equations 2.20 and 2.21 are obtained by derivation of equations 2.18 and 2.19:

$$\frac{\P S_1}{\P t} = s_{11}\frac{\P T_1}{\P t} + 2M_{31}E_3\frac{\P E_3}{\P t} \tag{2.20}$$

and

$$\frac{\P D_3}{\P t} = e_{33}\frac{\P E_3}{\P t} + 2M_{31}(E_3\frac{\P T_1}{\P t} + T_1\frac{\P E_3}{\P t}) \tag{2.21}$$

The electric field features an applied dc bias and an ac component ($E_3 = E_{dc} + E_{ac}$). Therefore, Equation (2.20) and (2.21) can be rearranged to

$$\frac{\P S_1}{\P t} = s_{11}\frac{\P T_1}{\P t} + 2M_{31}(E_{dc} + E_{ac})\frac{\P E_3}{\P t} \tag{2.22}$$

and

$$\frac{\P D_3}{\P t} = e_{33}\frac{\P E_3}{\P t} + 2M_{31}\left[(E_{dc} + E_{ac})\frac{\P T_1}{\P t} + T_1\frac{\P E_3}{\P t}\right] \tag{2.23}$$

Considering that the current is measured under short-circuit conditions with the help of current amplifier, we have $\frac{\P E_3}{\P t} = 0$ and $E_{ac} = 0$. Consequently, equations 2.22 and 2.23 can be rewritten as follows:

$$\frac{\P S_1}{\P t} = s_{11}\frac{\P T_1}{\P t} \tag{2.24}$$

and

$$\frac{\P D_3}{\P t} = 2M_{31}E_{dc}\frac{\P T_1}{\P t} \tag{2.25}$$

The harvested current, I_{sc}, and the electric displacement are related by:

$$I_{sc} = \int_A \frac{\partial D_3}{\partial t} dA$$

It is thus possible to calculate the harvested current from a polymer film as a function of the strain and the electric field, using the following formula:

$$I_{sc} = 2M_{31} Y E_{dc} \int_A \left(\frac{\partial S_1}{\partial t} \right) dA \qquad (2.26)$$

Here, I_{sc} is the harvested current, A is the area of sputtered electrode on the polymer film, $Y = \frac{1}{s_{11}}$ is the Young modulus of the polymer and M_{31} is the electrostrictive coefficient.

By assuming that the electrical field does not depend upon the x coordinate and by assuming that the strain along the x direction (S_1) on the upper surface of the cantilever is the same in the polymer - due to its very low Young modulus compared to this one of the blue steel – it then becomes possible to express the strain, S_1, as a function of the displacement, u, at the free end of the beam:

$$S_1 = - \frac{t_b}{2} \frac{\partial u^2}{\partial x^2} \qquad (2.27)$$

The stress, T_1, within the polymer is then equal to:

$$T_1 = \frac{Y}{1 - \upsilon^2} S_1 \qquad (2.28)$$

where S_1 is the strain, T_1 is the stress, υ is the Poisson ratio, t_b is the thickness of beam and u is the displacement of the beam. The theoretical expression for the displacement of the free end of a dynamic cantilever is **[GOU 2001]**:

$$u(x,t) = F\left[A_1.\cos(\Omega x) + A_2.\sin(\Omega x) + A_3.ch(\Omega x) + A_4.sh(\Omega x)\right]\cos(\omega t + \varphi) \qquad (2.29)$$

with $\Omega = \left(\frac{\rho S_c}{Y I_m} \right)^{\frac{1}{4}} \omega^{\frac{1}{2}}$ and $A_1 = - \frac{\sin \Omega L + sh \Omega L}{2\Omega^3 E I_m (1 + \cos \Omega L sh \Omega L)}$

$$A_2 = \frac{\cos WL + chWL}{2W^3 EI_m(1+\cos WL shWL)}$$

$$A_3 = - A_1$$

$$A_4 = - A_2$$

Here, r is the mass density of the beam material, S_c is the cross-sectional area, Y is the Young modulus, w is the angular frequency, F is the electromagnetic force and I_m is the second moment of the cross sectional area. For a rectangular cross-section of width w and of thickness d, I_m is given by $I_m = \frac{wd^3}{12}$.

B. Harvested Power Model

In this case, to measure harvested power, we cannot assume that the current is the short circuit condition current I_{sc}.

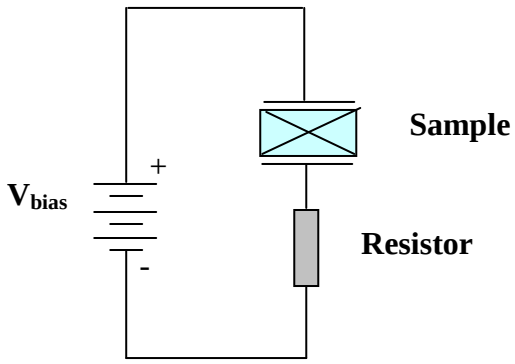

Fig. 2.6 Energy harvesting schematic

The constitutive equations for electrostrictive polymer are shown in eq. (2.18) and (2.19)

$$S_1 = s_{11}T_1 + M_{31}E_3^{\ 2} \qquad (2.18)$$

and

$$D_3 = e_{33}E_3 + 2M_{31}E_3T_1 \qquad (2.19)$$

Here, e_{33} is the linear dielectric permittivity, s_{11} is the elastic compliance and M_{31} is the electrostriction coefficient.

Assuming uniform strain and electric field over the sample allows expressing the macroscopic equation of the current, $I = \int_A \frac{\partial D_3}{\partial t} dA$ flowing out of the polymers as a function of the strain and electric field

$$I = A[e_{33} + \frac{2M_{31}}{s_{11}} S_1 - \frac{6M_{31}^2 E_3^2}{s_{11}}] \frac{\partial E_3}{\partial t} + \frac{2M_{31} A E_3}{s_{11}} \frac{\partial S_1}{\partial t} \qquad (2.30)$$

And the applied electric field features a dc bias and an ac component ($E_3 = E_{dc} + E_{ac}$), the current expression turns to

$$I = A[e_{33} + \frac{2M_{31}}{s_{11}} S_1 - \frac{6M_{31}^2 (E_{dc} + E_{ac})^2}{s_{11}}] \frac{\partial E_{ac}}{\partial t} + \frac{2M_{31} A (E_{dc} + E_{ac})}{s_{11}} \frac{\partial S_1}{\partial t} \qquad (2.31)$$

According to Fig.2.6 that presents the connection of the electrostrictive sample, the ac component of the electric field is generated by the load such as

$$E_{ac} = - \frac{RI}{t} \qquad (2.32)$$

with t the thickness of the sample. Therefore, the current expression turns to

$$I = - A \frac{R}{t} [e + \frac{2M_{31}}{s_{11}} S_1 - \frac{6M_{31}^2}{s_{11}} (E_{dc} - \frac{RI}{t})^2] \frac{\partial I}{\partial t} + \frac{2M_{31} A}{s_{11}} (E_{dc} - \frac{RI}{t}) \frac{\partial S_1}{\partial t} \qquad (2.33)$$

For realistic values of the current (less than 100μA), load resistance (less than 10 MΩ) and electric field (1-100 MV. m^{-1}), the ac component $E_{ac} = - \frac{RI}{t}$ can be neglected compared to the dc bias electric field. Additionally, the value of the coefficient $\frac{M_{31}}{s_{11}}$ is of the same order of magnitude than e_{33}, as well as the electric field component. Therefore, under low strain (a few percent), $\frac{M_{31}}{s_{11}} S_1$ and $\frac{M_{31}^2}{s_{11}} (E_{dc})^2$ can also be neglected compared to the permittivity. Hence, the current expression in term frequency is given by

$$I = \frac{2\frac{M_{31}}{s_{11}} AE_{dc}}{1 + j\frac{R}{t} Ae_{33} 2\pi f} j2\pi f S_1 \tag{2.34}$$

here j refers to the imaginary unit and f is vibration frequency. The associated power is then given by

$$P = \frac{2R(2\pi f \frac{M_{31}}{s_{11}} AE_{dc})^2}{1 + (\frac{R}{t} Ae_{33} 2\pi f)^2} S_M{}^2 \tag{2.35}$$

with S_M denoting the strain magnitude. Canceling the derivative of this expression with respect to R. Moreover, theoretical matching of optimum load can be approximated **[SHA 2005]** as

$$R_c{}^{Opt} = \frac{1}{\omega C} = \frac{1}{2\pi f . C} \tag{2.36}$$

Therefore, the maximum power output can be written as

$$P_{\max} = \frac{\omega M_{31}^2 Y^2 E_{dc}^2 S_M{}^2 A^2}{C} \tag{2.37}$$

where C is the capacitance of the composite and ω the pulsation of the beam vibration ($\omega = 2\pi f$). C could be calculated as a function of the dimensions of the composite (A: Area and t: thickness) and its permittivity using the following formula: $\frac{e_{33} A}{t}$.

As expected, in case of short circuit conditions (R=0), we build the previous established expression, $I_{sc} = 2M_{31} Y E_{dc} \int_A \left(\frac{\partial S_1}{\partial t}\right) dA$.

In case of optimal resistance, R_{opt} , the current is given by

$$I(R_{opt}) = \frac{2\frac{M_{31}}{s_{11}} AE_{dc}}{1 + j} j2\pi f S_1 \tag{2.38}$$

Thus, the current relationship between under resistance optimal load and under short circuit conditions can be written as

$$\left|I(R_{opt})\right|^2 = \frac{\left|I_{sc}\right|^2}{2} \tag{2.39}$$

Therefore, to calculated the power at R_{opt},

$$P_{\max} = R.I^2(R_{opt}) = R.\frac{I_{sc}^2}{2} \tag{2.40}$$

Consequently, the harvested power can be written as

$$P_{Harvesting} = 2\frac{t}{e_o e_r wLw}(M_{31}Y)^2.E_{dc}^2.\left[\int_A \left(\frac{\partial S_1}{\partial t}\right).dA\right]^2 \tag{2.41}$$

2.5 Measurement setup of harvested current for electrostrictive polymer

The experiment is performed in order to test the validity and accuracy of analytical current model of the cantilever beam. Figure 2.7 and 2.8 show a picture of the attached film on the beam. The test specimens constituted by films of neat PU in the shape of rectangular capacitors. They were prepared through a solution casting method (details will be shown in chapter 3). For the electrical characterisation, gold was sputtered on both sides of the films to form electrodes (1.8 × 4.0 cm^2). Furthermore, the beam, with a dimension of 0.5 *mm* × 142.7 *mm* × 0.2 *mm*, was fabricated in blue steel to determine the electrostrictive properties and the harvested power. The electrostrictive films were adhered on the cantilever beam after it was polished and cleaned with ethyl alcohol.

Measurements to determine the harvested current of the electrostrictive films were performed on the cantilever beam, as depicted in Figure 2.9(a) and Figure 2.9(b). The cantilever beam was excited by the electromagnetic force at the resonance frequency of its first flexural mode. Furthermore, the amplitude of the vibration of the beam was driven by an electromagnet. The electrostrictive film was rigidly glued to the clamped beam end in order to obtain the maximum possible stress for conversion energy. A dc electric field was applied to the film with the help of a generator

(Agilent,3220A) and a Trek Model 10/10 high-voltage power amplifier. The displacements at L (i.e., the free end of the beam) and at L/4 were measured with a gauge vibrator. As previously explained, the strain within the beam and within the active polymer were calculated from the measured displacement values.

The power output was estimated from the harvested current setup with addition of a resistant load (10 MΩ) between the film and current amplifier. Finally, the induced current and power harvesting under mechanical vibration was determined with a current amplifier (Keithley617) through a lock-in amplifier.

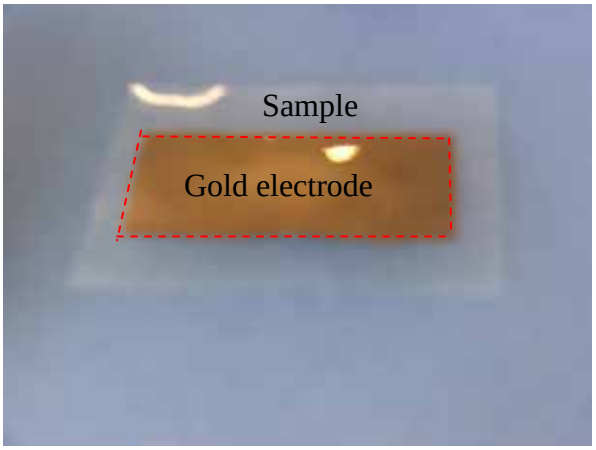

Fig. 2.7. The film polymer with electrode (1.8 cm x 4.0 cm) used in experiment

In our work, blue steel is used for the cantilever beam. Table 2.2 gives the beam parameters used in our work.

Table 2.2 Properties and dimensions for the beam.

Parameter of Beam	**Value**	***Units***
Young's Modulus	$2' 10^{11}$	*Pa*
density	7860	Kg / m^3
length	0.145	*m*
thickness	0.005	*m*
width	0.02	*m*

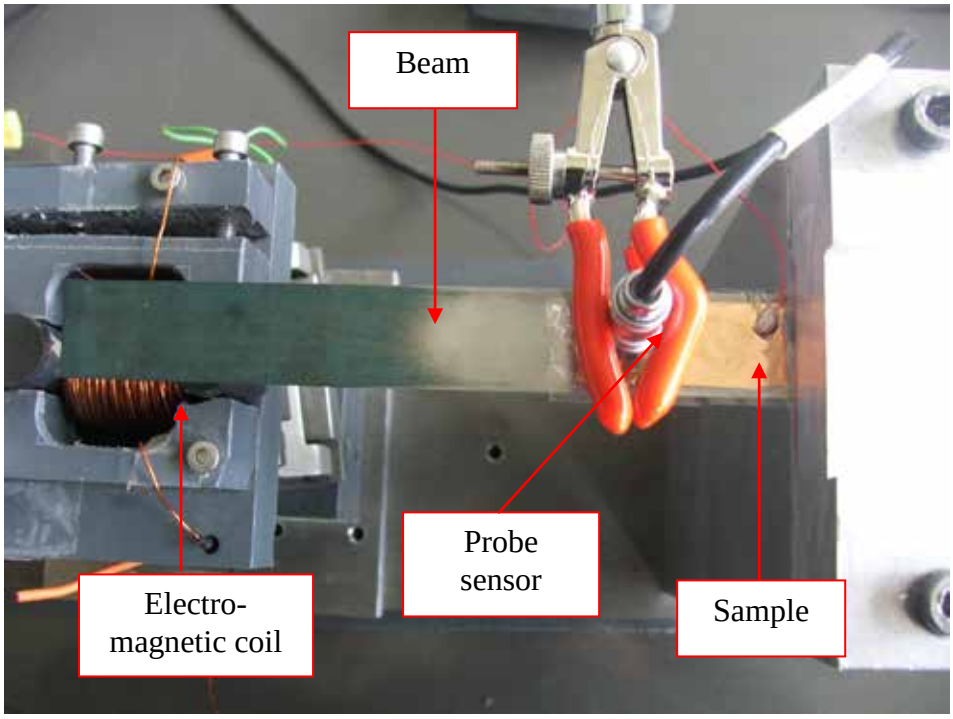

Fig. 2.8. The PU film is attached close to clamped end of the beam (top view).

(a)

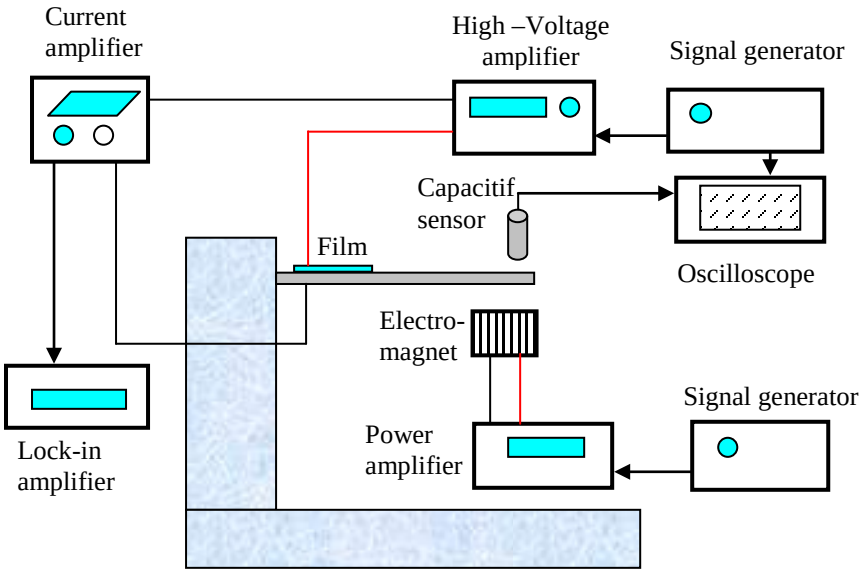

(b)

Fig. 2.9. A schematic (upper) and a picture (lower) of the experimental setup for measuring the harvested current in the electrostrictive polymers

2.6 Results and Discussion

2.6.1 Resonance frequency of cantilever Beam

The harvested current measurement of the electrostrictive films was performed on the cantilever beam at its resonance frequency. The natural frequency depends on the length of the beam can be calculated using equation (2.15), and data of table 2.2 as shown in Figure 2.10. For a 0.0145 m length beam, a value of 20.0 Hz is expected. The experiment data of the resonance frequency on the first flexion mode of the 0.0145 m length cantilever beam is shown in Figure 2.11. The experimental resonance frequency for this beam is about 19.8 *Hz*, which is in good agreement with the predicted value.

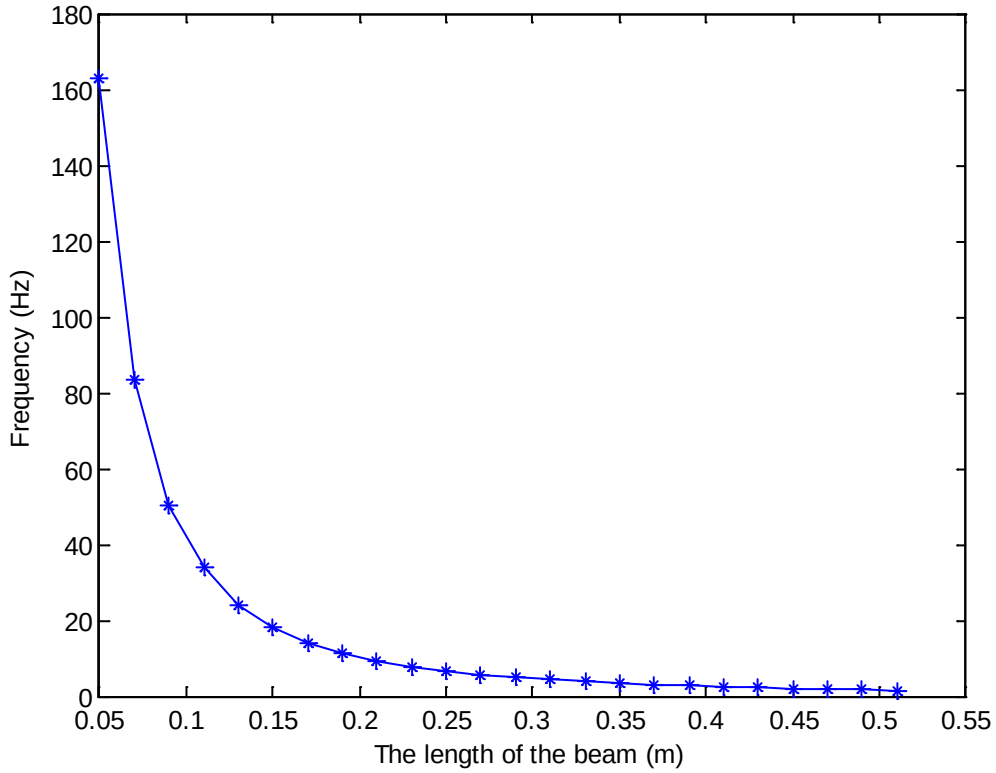

Fig. 2.10. The frequency as a function of the length of the cantilever beam using equation (2.15).

In addition, it is clearly shown that the polymer does not affect the resonance frequency of the beam and the displacement.

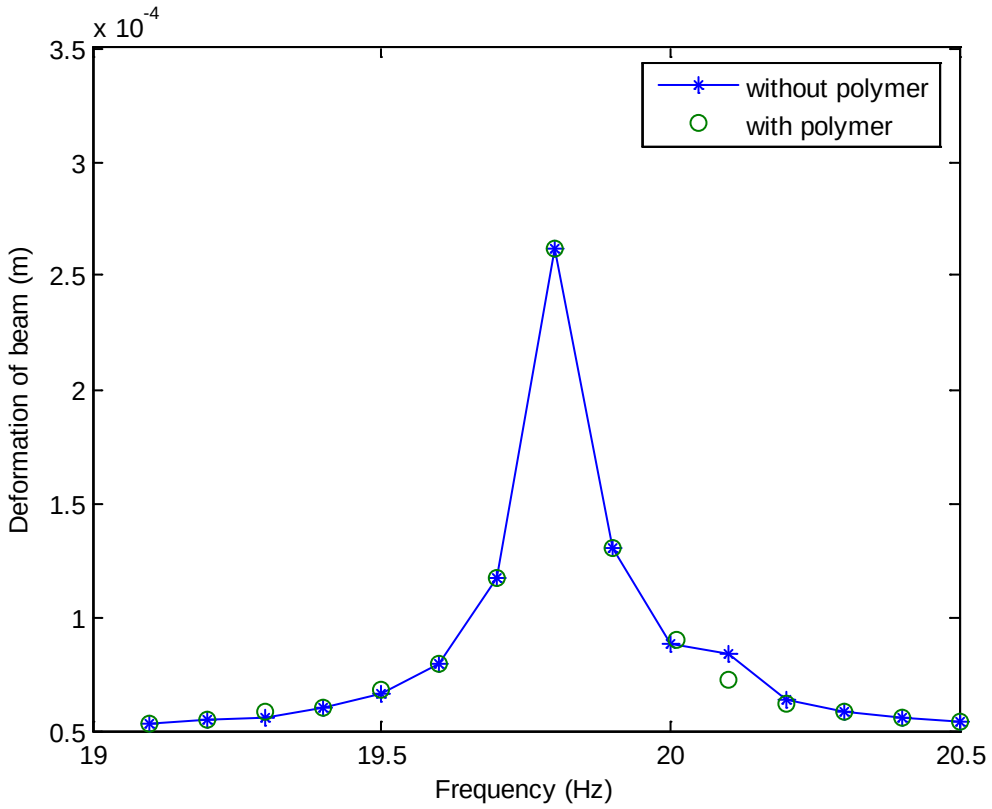

Fig. 2.11. Experiment data of resonance frequency of the cantilever beam with or without polymer.

2.6.2 The displacement and transverse strain of the cantilever beam

The bending behavior of the cantilever beam was investigated at its first flexural vibration mode. The displacement of the beam has been measured along three lines noted L_1, L_2 and L_3 on figure 2.12.

Figure 2.13 depicted the vibration behavior of the beam along L1. The experimental data have been fitted using a third order polynomial function. As expected for the first bending mode, an increase of the displacement is observed along L_1 with the lowest value (almost 0) at the clamped end and the highest one (almost $8x10^{-4}$m) at the free end of the beam. Figure 2.14 depicted the measured displacement along L_2 and

L_3. As expected the displacement along these two directions is constant indicating that no parasitic flexural mode exists within the structure.

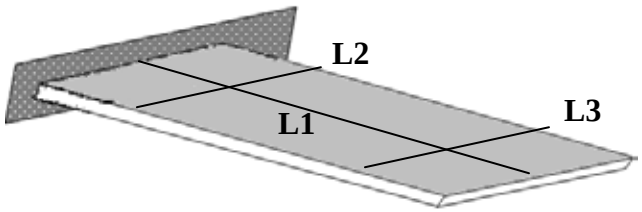

Fig. 2.12. Three featured lines along the top surface of the testing structure for observing the deformations.

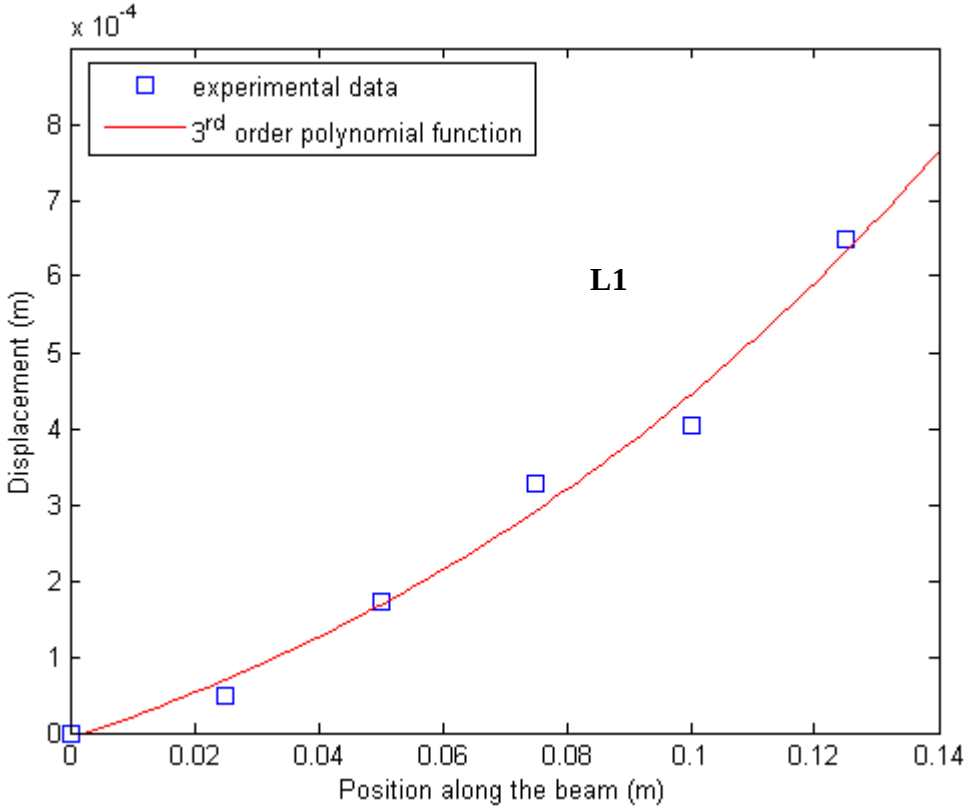

Fig. 2.13. The measured deformation configurations of the deformation along length at middle (L1) of the beam.

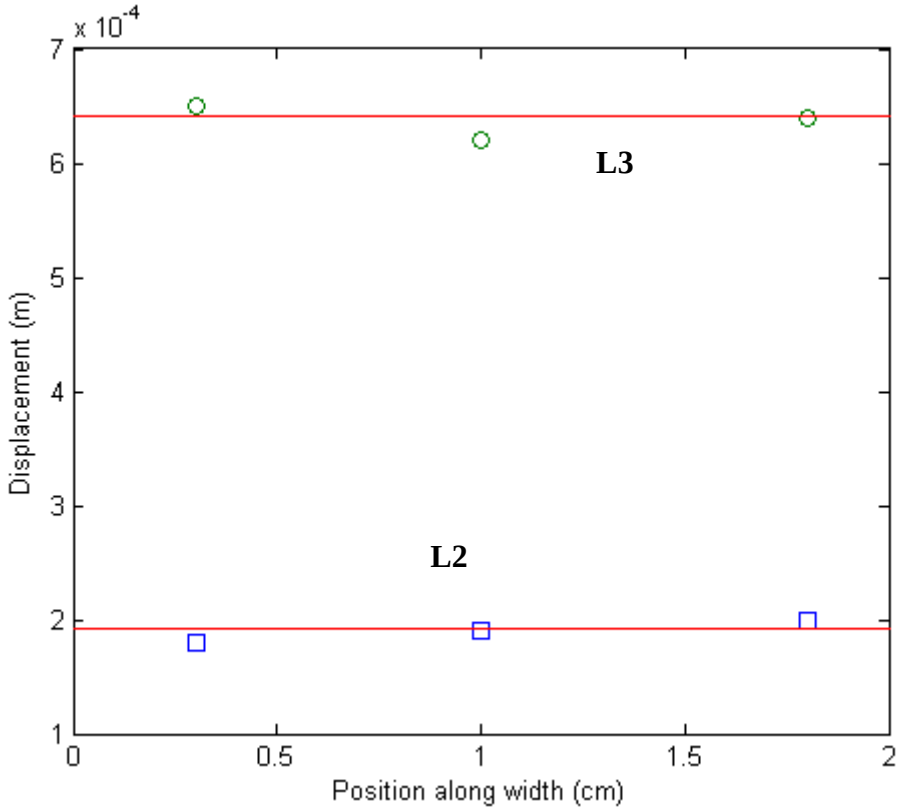

Fig. 2.14. The measured displacement configurations along beam width at the front end (L2) and the rear end (L3) of the beam.

The transverse strains on figure 2.15 have been calculated from the second derivative of the polynomial function following the equation (2.27) and from the theoretical calculation using the Euler Bernoulli expression in the equation (2.29), showing a good agreement between the two results.

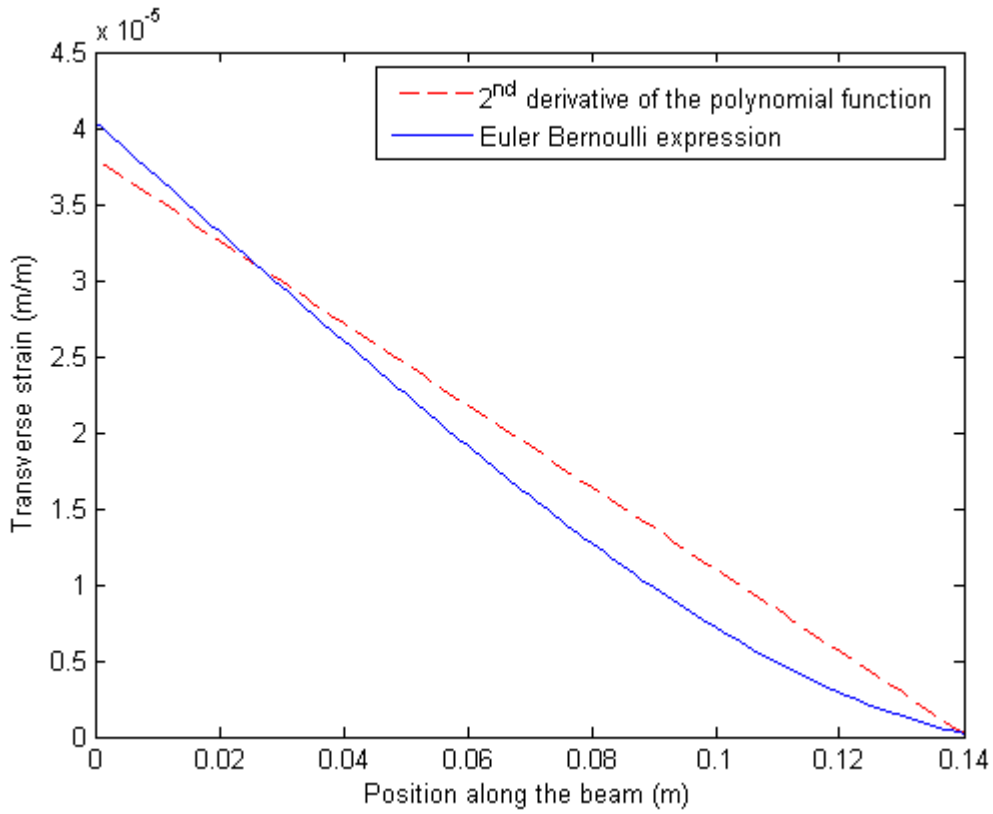

Fig. 2.15. Transverse strain along the beam length as a function of the position along the beam.

2.6.3 Validity of the harvested current model

The modelled harvested current was equal to $I_{sc} = 2M_{31}YE_{dc}\int_A \left(\frac{\partial S_1}{\partial t}\right) dA$. In order to verify the validity of the modelling, experimental measurements of the harvested current versus the area (A), versus the dc electrical field (E_{dc}) and versus the stress rate ($\frac{\partial S_1}{\partial t}$), were performed.

Figure 2.16 presents the electric field induced current (I - E) for two areas (i.e., A and 2A) of the polymer film. It is noteworthy that the experimental area values were chosen to maintain an almost identical average strain. As predicted by the modelling, the value of the current becomes twice as large when the area is doubled.

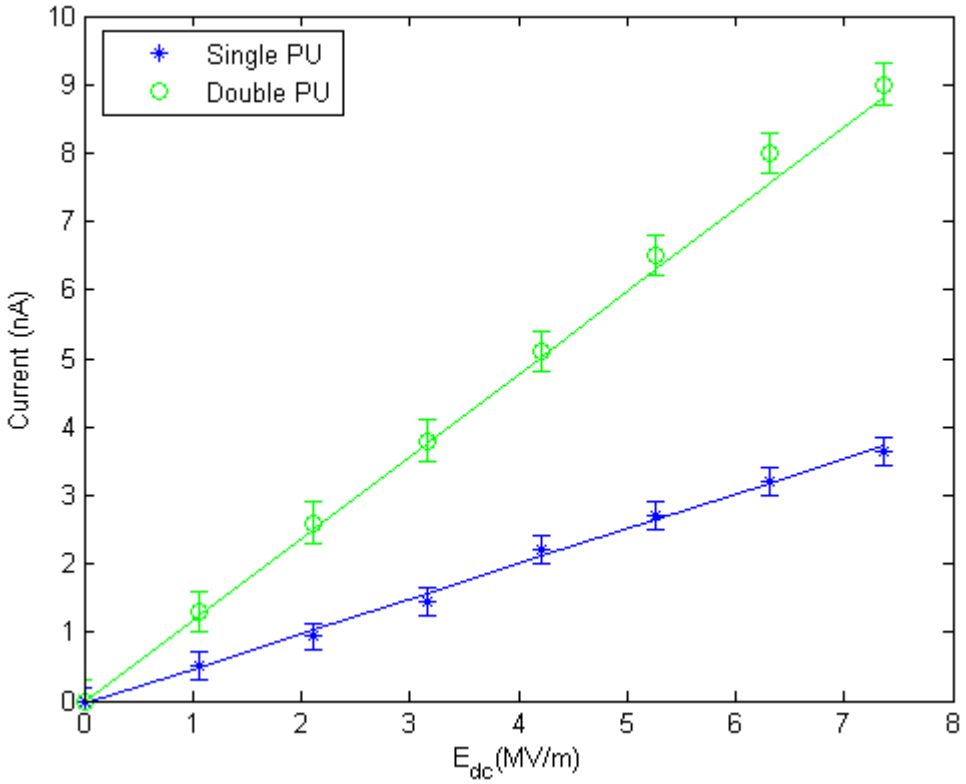

Fig.2.16. The induced current as a function of the dc electric field for two areas (i.e., A and 2A).

Figure 2.17 presents the induced current for a neat PU film measured at various strain rates and electric field values. As predicted, a linear variation of the induced current versus the strain rate was observed, regardless of the dc electric value.

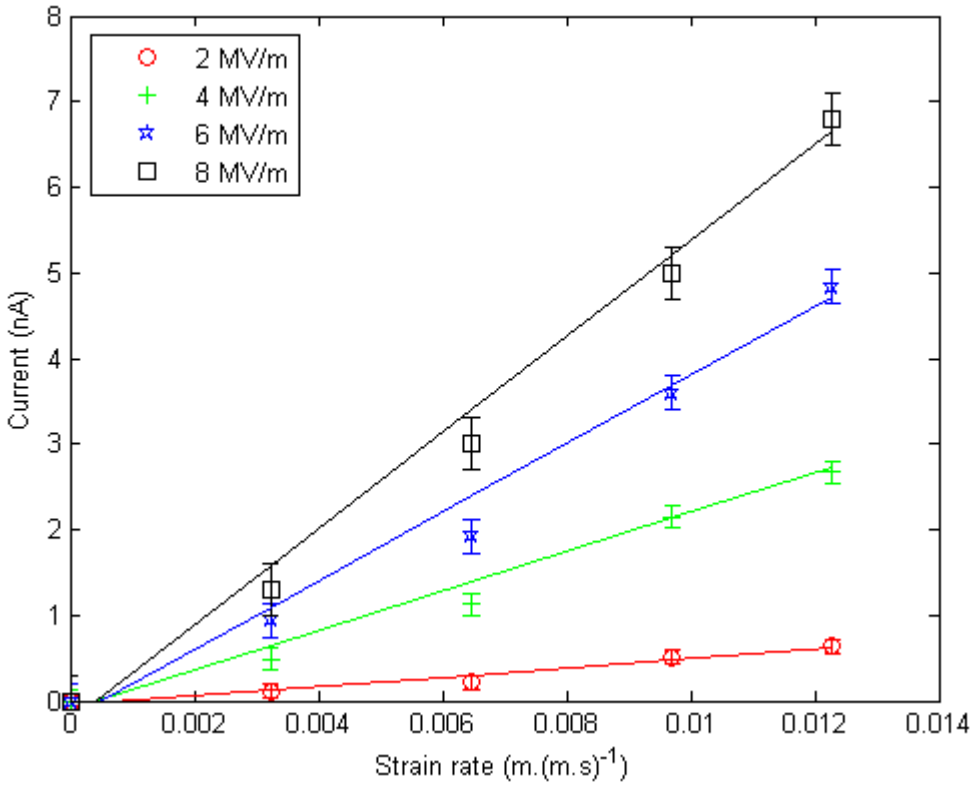

Fig. 2.17. The induced current as a function of the strain rate at various values of the applied electric field.

Figure 2.18 presents the induced current for the neat PU film under a dc electrical field at several displacement values of the free end of the beam. As predicted, a linear variation of I_{sc} versus the dc electrical field could be observed for all displacements. The results of these experiments clearly demonstrated the validity of the proposed model, along with its capability of providing the shape of the harvested current.

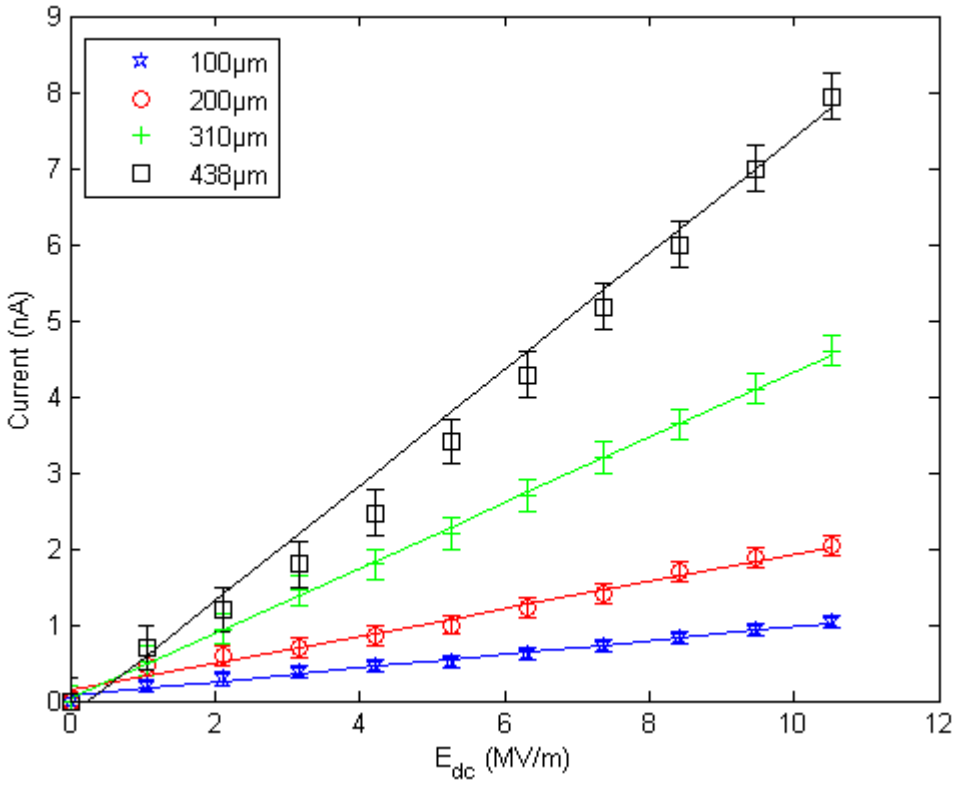

Fig. 2.18. The induced current as a function of dc electric fields for various displacements of the free end of the cantilever beam.

It is possible to calculate M_{31} from the analytical expression of the curves portraying the induced current versus the dc electrical field or the induced current versus the strain rate, provided that Young's modulus is known. For instance, neat PU film, with Young's modulus of 36 *MPa*, and from the slope of the curve of the induced current versus the strain rate, M_{31} is estimated to 8.9×10^{-19} m^2/V^2 at strain rate of 0.0079 $m.(m.s)^{-1}$.

Figure 2.19 presents the variation of M_{31} versus (a) the strain rate or versus (b) the dc electrical field for a PU film. The linear regression of the graph in figures 2.17 and 2.18 gives value of M_{31} from its slope. It was found that M_{31} is almost independent of the strain rate and dc electric field.

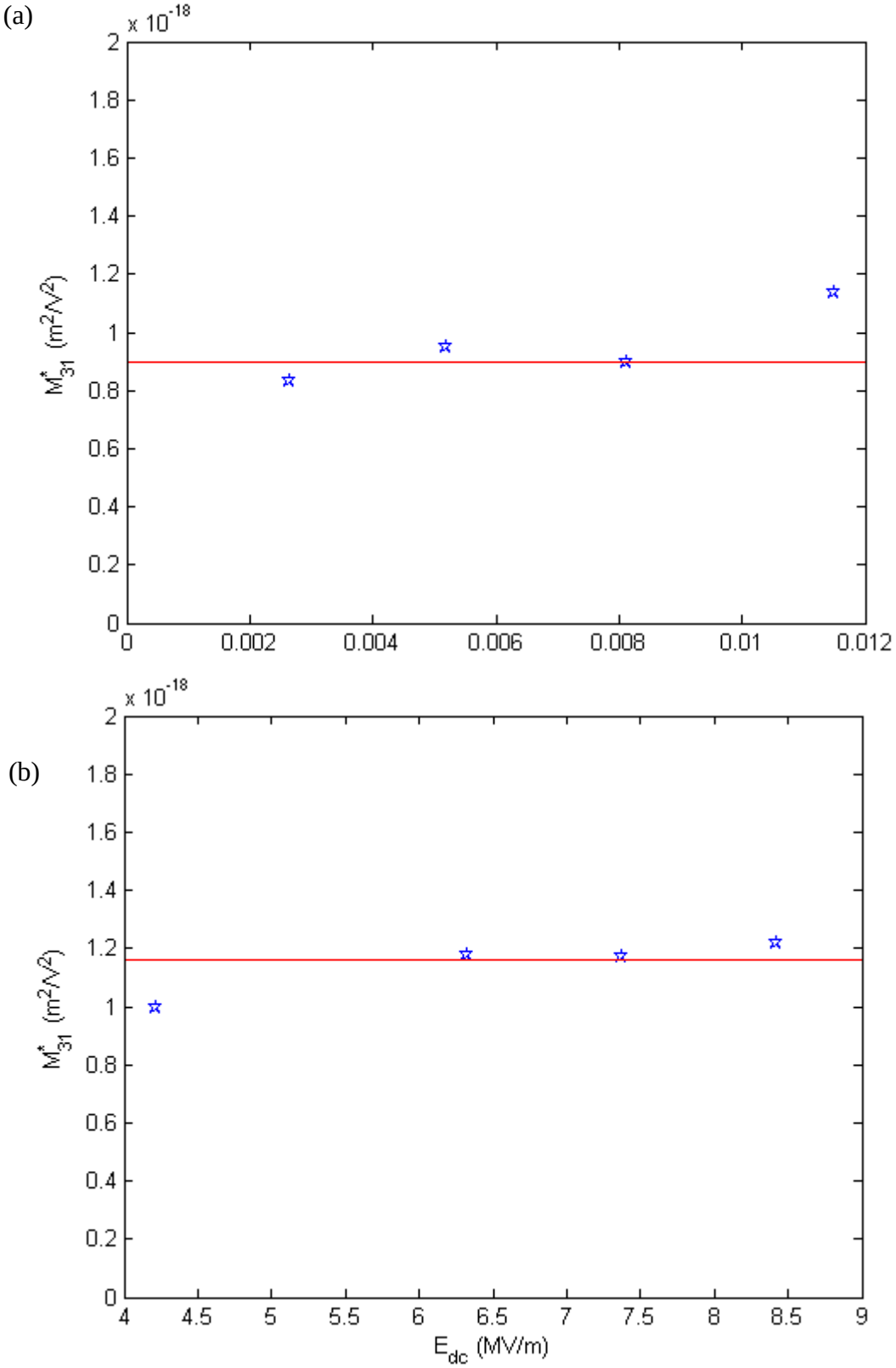

Fig. 2.19. M_{31} versus (a) the strain rate and (b) the electric field for a neat PU film.

2.6.4 Validity of the energy harvesting model on various polymers

Figure 2.20 shows the harvested current measured versus dc electric field for neat PU film and two other commercialized polymers (nylon® 6 and polyethylene). The highest value of harvested current is obtained for nylon film whereas the lowest one is obtained for polyethylene film. Comparisons of the values of the M_{31} coefficient of the electrostrictive materials are presented in Table 2.3.

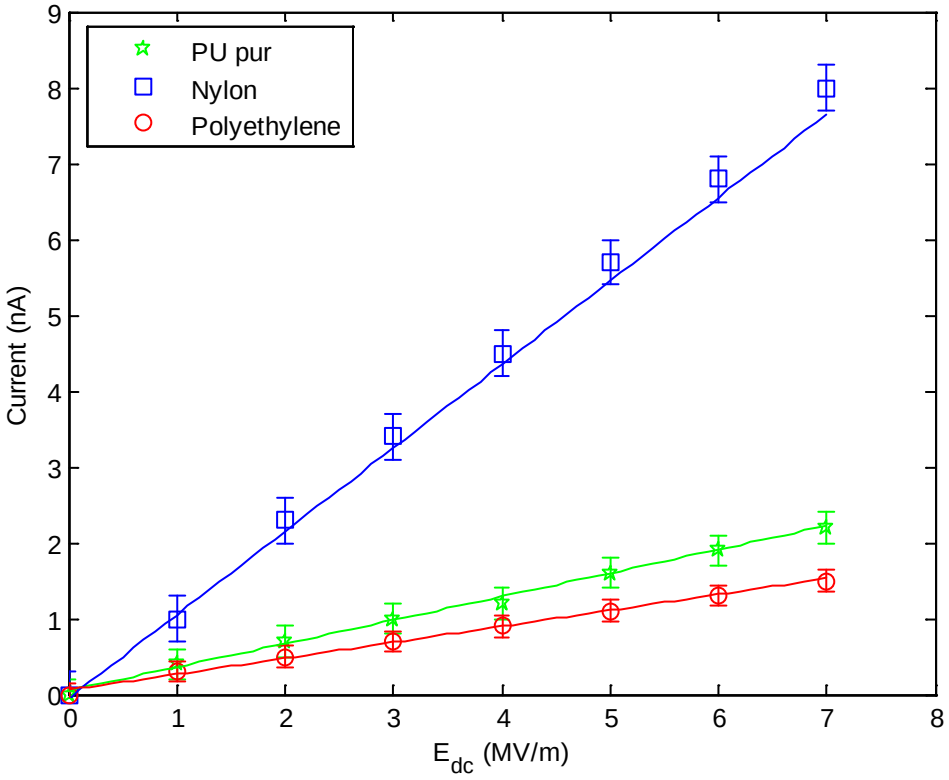

Fig. 2.20. The induced current as a function of the electric field for the neat and filled PU samples.

Table 2.3 Estimations of the strain coefficient of dielectric materials.

Materials	Thickness (µm)	e_r (1kHz)	Y (MPa)	M_{31} (x10^{-18}m2/V2)	$FoM = M_{31}Y$ (x10^{-10})	$\frac{e_o(e_r - 1)^2}{e_r Y}$
PU*	95	4.8	36	3.40	1.36	7.4´ 10^{-19}
Nylon®6*	100	12.0	2800	0.14	3.92	3.2´ 10^{-20}
Polyethylene*	100	2.2	260	0.34	0.88	2.2´ 10^{-20}

* Value of M_{31} measured at frequency 20 Hz in our work.

The polyurethane based films present higher electrostriction coefficient that the other films. As the electrostriction coefficient depends on thickness,**[GUI 2003]** it is speculative to conclude on the polyurethane based films performance using these data.

As previously reported,**[SU 1999][GUI 2003]** the apparent electrostriction coefficient of polymers is roughly proportional to $\frac{e_o(e_r - 1)^2}{e_r Y}$. Experimental values of this criterion are given in the last column of the table 2.3. This explains why PU films present the best M_{31} compared to nylon and polyethylene and why PU films will be the best material of the three for actuation.

The proposed modelling of the harvested current has lead to the following expression: $I_{sc} = 2M_{31}YE_{dc}\int_A \left(\frac{\partial S_1}{\partial t}\right) dA$. By assuming that M_{31} is almost proportional to $\frac{e_o(e_r - 1)^2}{e_r Y}$ and that $\int_A \left(\frac{\partial S_1}{\partial t}\right) dA$ is almost the same for all the tested films, it clearly appears that the Figure of Merit for the harvested current ($FoM = M_{31}Y$) is almost equal to the permittivity of the film in term of $\frac{e_o(e_r - 1)^2}{e_r}$. Figure 2.21 depicts the variation of the FoM calculated from the $I - E_{dc}$ slope versus calculated $\frac{e_o(e_r - 1)^2}{e_r}$ from experimental permittivity's measurement. As expected, a linear dependence is observed, confirming the assumed relationship in previous papers, **[SU 1999][WAN 1991] [GUI 2003].** Consequently, nylon films which have the highest permittivity have the best capability to convert mechanical energy into electrical energy. This experience also points out that actuation and energy harvesting do not have the same Figure of Merit but in both case, an increase of the permittivity is needed to increase the level of performance. The increase of the permittivity will be discussed in the following chapter.

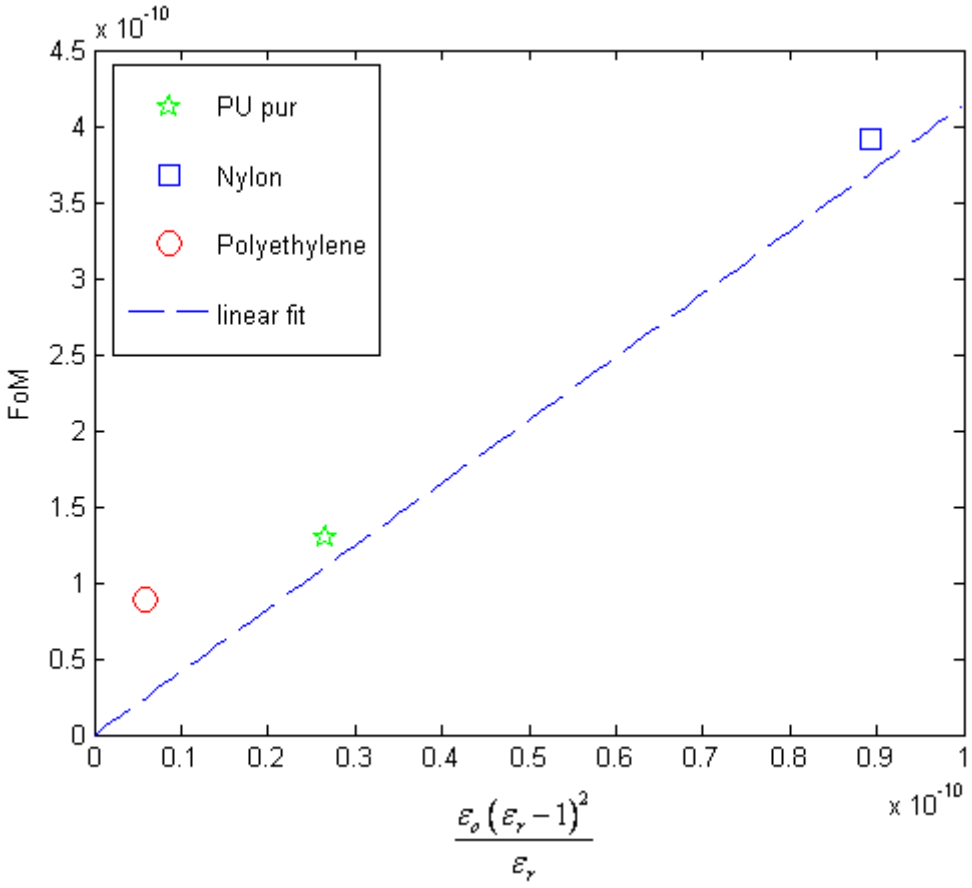

Fig. 2.21. The dependence of the $FoM = M_{31}Y$ on the dielectric constants.

After confirming the validity of harvesting current model with experimental results, we conclude that the current modelling can be used to predict the output power too. Figure 2.22 presents the output power of electrostrictive materials as a function of strain when the cantilever operates at its resonance frequency and for a fixed electric field. The relation between output power and strain shows the quadratic shape. The power harvesting generated by the electrostrictive polymers can be calculated by

$$P_{harvesting} = \frac{R.I_{sc}^{\ 2}}{2}$$

Here R is the resistor load, I_{sc} is the harvested current under short-circuit conditions. The harvested current from a polymer film as a function of the strain and the electric

field was given by equation (2.26). So the power harvesting for electrostrictive materials showed on equation (2.41), $P_{Harvesting} = 2\frac{t}{e_o e_r wLw}(M_{31}Y)^2.E_{dc}^2.\left(\int_A \frac{\partial S_1}{\partial t}\right).dA$.

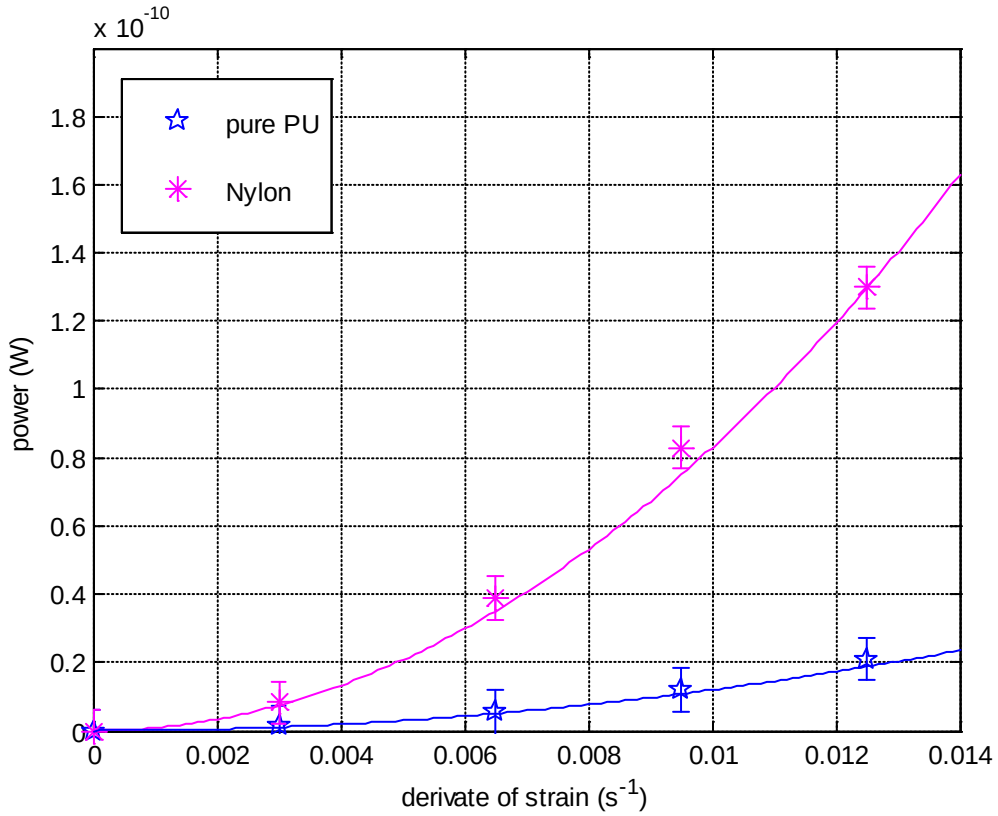

Fig. 2.22.The harvested power as a function of strain of strain at fixed 5MV/m and 20 Hz with an electric load of 10 MΩ.

2.7 Thickness and beam resonance frequency dependence on PU film energy harvesting capability

This paragraph is to complete our previous analytical modeling and our experimental data by studying how the polymer thickness and the resonance frequency of the beam affect its energy harvesting capability. It is well known that thickness of the film can affect the conversion properties of polymer. The study was carried out on

polyurethane films versus either the resonance frequency of the beam or the film thickness.

The expression of the harvested has been previously established: $I_{sc} = 2M_{31}YE_{dc}\int_A \left(\frac{\partial S_1}{\partial t}\right) dA$. The strain ($S_1$) as a function of the displacement (u) of the free end of a dynamic cantilever and beam thickness (t_b) is given by, $S_1 = -\frac{t_b}{2}\frac{\partial u^2}{\partial x^2}$. The integral of strain rate can be rewritten as:

$$\int_A \left(\frac{\partial S_1}{\partial t}\right) dA = wl\frac{t_b}{2}\int_x \frac{\partial^2 u}{\partial x^2} dx \qquad (2.42)$$

Therefore, the harvested current modeling in term on frequency (f) and on thickness polymer (t) is given by:

$$I_{sc} = M_{31}YE_{dc}wlt_b\int_{x_1}^{x_2}\left(\frac{\partial^2 u}{\partial x^2}\right) dx \qquad (2.43)$$

Here, I_{sc} is the harvested current, x is the area of sputtered electrode on the polymer film, $Y = \frac{1}{s_{11}}$ is the Young modulus of the polymer, M_{31} is the electrostrictive coefficient of the polymer, w is the angular frequency ($w = 2\pi f$), l is width of sputtered electrode on polymer film and t_b is the thickness of the beam.

2.7.1 Dependence of the harvested current versus the resonance frequency of the beam

Cantilever beams with three different lengths, 52 mm, 70 mm and 144 mm respectively have been prepared, which corresponds to a resonance frequency of the first flexural mode of 126 Hz, 78 Hz and 19 Hz. PU films of the same thickness (70 mm) have been glued on each beam and tested under the given $\int_x \left(\frac{\partial^2 u}{\partial x^2}\right) dx$ of 0.0065, at various E_{dc} fields.

From the analytical modeling of the current $I = M_{31} Y E_{dc} \left[w t_b \int_x \left(\frac{\partial^2 u}{\partial x^2} \right) dx \right]$, the ratio between the harvested currents for two frequencies f_1 and f_2 is equal to $\frac{I_2(f_2)}{I_1(f_1)} = \frac{M_{31}(f_2) Y(f_2) w_2}{M_{31}(f_1) Y(f_1) w_1} = \frac{M_{31}(f_2) Y(f_2) f_2}{M_{31}(f_1) Y(f_1) f_1}$ for a given E_{dc} field (2.44).

Based on Zhang et al.**[ZHA 1997]** results for the dependence of the Young's modulus of PU versus frequency, it can be assumed that Young's modulus will only exhibit small variation in the used frequency range. Moreover, it is assumed that the M_{31} coefficient dependence is also low within the frequency range. As a consequence, the ratio of harvested current on frequency can expressed by $\frac{I_2(f_2)}{I_1(f_2)} = \frac{f_2}{f_1}$ and appears to be in the ratio of the frequency.

Figure 2.23 presents the electric field induced current (I - E_{dc}) for the three investigated frequencies.

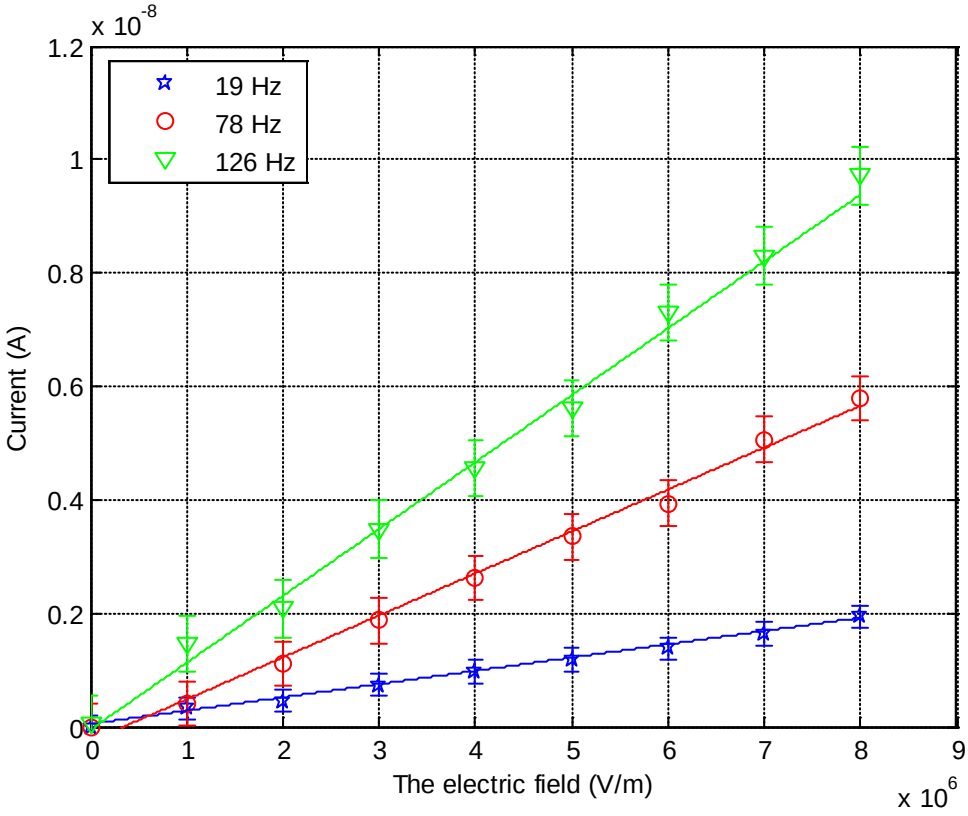

Fig. 2.23. The current as a function of the DC electrical field at three frequencies.

As expected from the modelling, a linear variation of I versus the dc electrical field is observed for all the three frequencies. From these experimental results, the slopes of harvested current versus electric field have been calculated for the three frequencies and reported in table 2.4. The ratio of the frequencies and the ratio of the slopes have been also presented in table 2.4.

Table 2.4 Comparison between the ratio of the I - E_{DC} slopes and of the frequencies.

harvested current	Frequency (Hz)	Slope of I - E_{DC} curve	Ratio of frequency $(\frac{f_i}{f_1})$	Ratio of slope of I - E_{DC} curve $(\frac{slope(f_i)}{slope(f_1)})$
I_{f1}	19	2.34e-16	1.00	1.00
I_{f2}	78	7.40e-16	3.97	3.16
I_{f3}	126	1.18e-15	6.40	5.06

The experimental ratios of the slopes are quite similar to the calculated ratio from frequencies, which validates the analytical modelling of the current and the independence of M_{31} and Young Modulus with frequencies in the used frequency range.

2.7.2 Dependence of the harvested current on PU thickness

Different polymer films of thickness from 30 microns to 250 microns have been respectively glued on cantilever beams of the same length (144 mm) to keep the resonance frequency constant (18.5 Hz). The harvested current has been measured for two given values of $\int_x \left(\frac{\partial^2 u}{\partial x^2}\right) dx$, respectively 0.0065 and (b) 0.0106, under various E_{dc} fields.

From the analytical modeling of the current $I = M_{31} Y E_{dc} \left[w t_b \int_x \left(\frac{\partial^2 u}{\partial x^2}\right) dx \right]$, the ratio between the harvested currents for two thickness t_1 and t_2 is equal to $\frac{I_2(t_2)}{I_1(t_1)} = \frac{M_{31}(t_2) Y(t_2)}{M_{31}(t_1) Y(t_1)}$ at a given E_{dc} field (2.45).

As previously reported **[DIA 2008][SU 1998]** the Young's modulus of the polyurethane depends on thickness. For this reason, the young's modulus of each polymer sample has been measured using a home-made bench working at the maximum frequency of 10 Hz. Figure 2.24 shows the Young's modulus as a function of the polyurethane thickness for three frequencies: 0.1 Hz, 5 Hz and 10 Hz respectively. It is observed that Young's modulus decreases when film thickness is increased and reaches a dwell for thickness above 100 microns, whatever the frequency is. Table 2.5 present the ratio of Young modulus for the three frequencies. It is worthwhile to note that this ratio is almost frequency independent and it is consequently reasonable to assume that it is kept at 20 Hz.

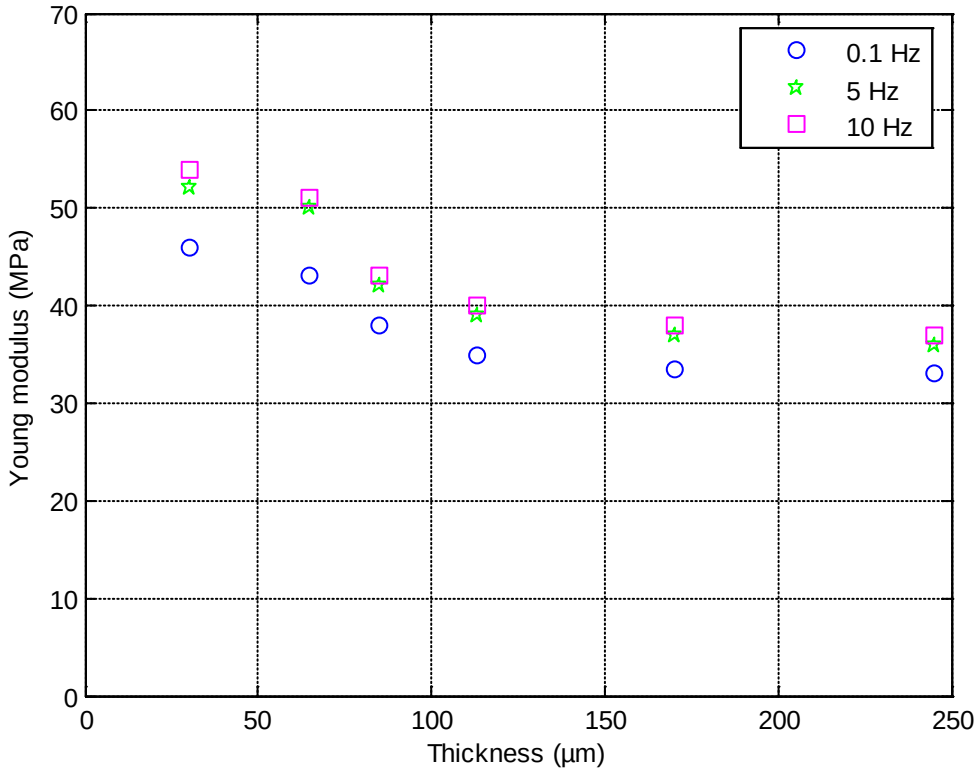

Fig. 2.24. Dependence of Young's modulus on film thickness for polyurethane.

Table 2.5. Young modulus versus thickness and frequency.

Thickness, t_i (μm)	Young modulus, $Y(t_i)$ (MPa)			Ratio of Young's modulus ($\frac{Y(t_i)}{Y(t_1)}$)		
	f_1 = 0.1 Hz	f_2 = 5 Hz	f_3 = 10 Hz	f_1 = 0.1 Hz	f_2 = 5 Hz	f_3 = 10 Hz
30	46	52	54	1.0000	1.0000	1.0000
65	43	50	51	0.9348	0.9615	0.9444
85	38	42	43	0.8261	0.8077	0.7963
113	35	39	40	0.7609	0.7500	0.7407
170	33.4	37	38	0.7261	0.7115	0.7037
245	33	36	37	0.7174	0.6923	0.6852

Figure 2.25(a) and 2.25(b) present the harvested current versus the dc electric filed (I - E_{DC}) for several thicknesses of the polymer film when the beam is excited at its resonance frequency (18.5 Hz) and $\int_x \left(\frac{\partial^2 u}{\partial x^2}\right) dx$ is kept constant at 0.0065 and 0.0106, respectively.

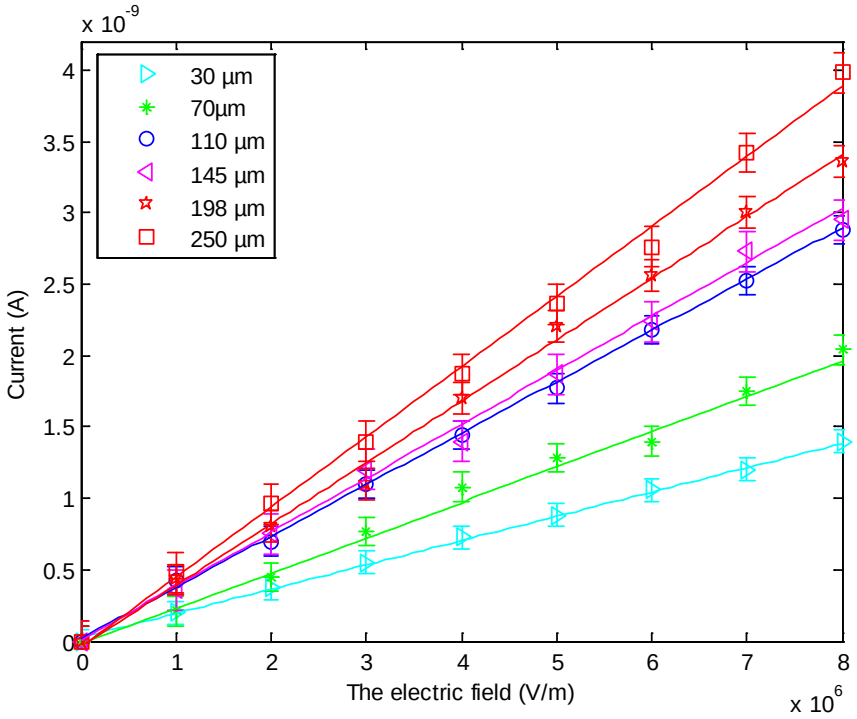

(a)

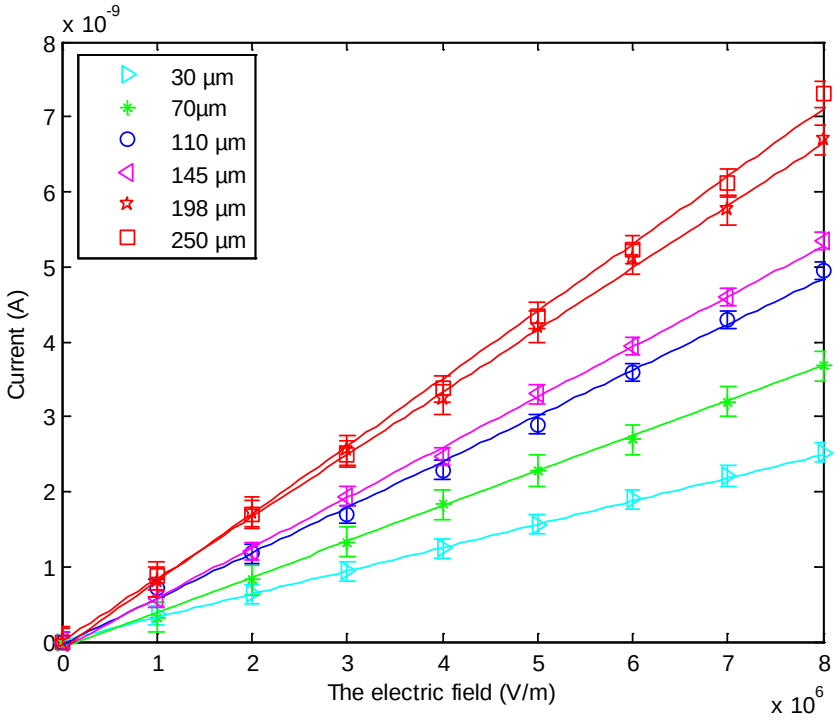

(b)

Fig.2.25. The induced current as a function of DC electric field for several thickness of film polymer at constant $\int_x \left(\frac{\partial^2 u}{\partial x^2}\right) dx$ as (a) 0.0065 and (b) 0.0106, respectively.

The harvested current continuously increases with the thickness of the PU film. As expected, the harvested current presents a linear dependence versus the dc electric field. It is then possible to calculate the slope of the curve and the ratio of the slopes. These results are summarized Table 2.6 and are also completed by the ratio of Young Modulus.

Table 2.6 Comparison of ratio of slope I - E_{DC} curve and ratio of Young's modulus.

Thickness (µm) (t_i)	Slope of I - E_{DC} graph ($\int \frac{\partial^2 u}{\partial x^2} dx = 0.0065$)	Ratio of slope I - E_{DC} curve ($\frac{slope(t_i)}{slope(t_1)}$)	Ratio of Young' modulus ($\frac{Y(t_i)}{Y(t_1)}$)
30	1.7×10^{-16}	1.00	1.00
70	2.5×10^{-16}	1.47	0.94
110	3.6×10^{-16}	2.12	0.74
145	3.8×10^{-16}	2.22	0.72
198	4.3×10^{-16}	2.53	0.70
250	4.9×10^{-16}	2.88	0.69

The slope of curve I - E_{DC} as a function of thickness of polymer is presented in figure 2.26 for the two values of the integration of the displacement 0.0065 and (b) 0.0106, respectively.

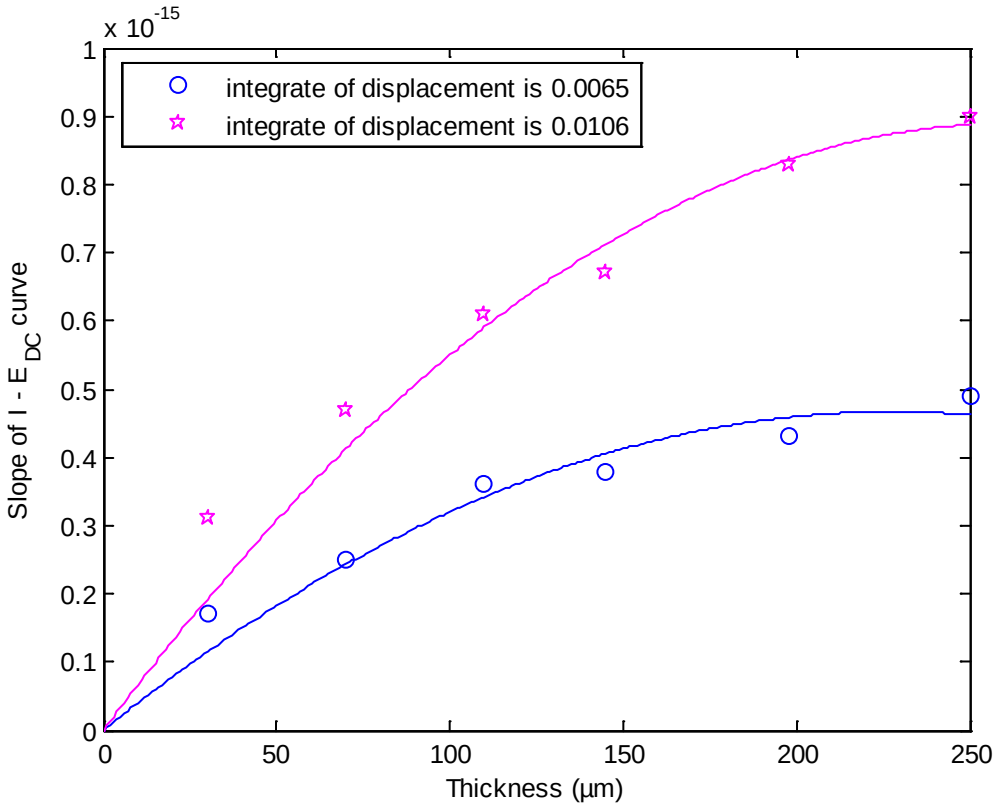

Fig. 2.26. Slope of curve I - E_{DC} versus thickness of polymer

In both cases, an increase of the slope of curve I - E_{DC} versus thickness is observed but it is worthwhile to note that the value of the increase begins to saturate for the thickness of 150 microns, which fixes the limit of the PU thickness which has to be used for such harvester.

From table 2.6, it can be seen that the ratio of the slopes is different from the ratio of the Young modulus. This is in good agreement with previous results **[DIA 2008][SU 1998]** that showed that M_{31} of PU films depends on thickness. As M_{31} measurements have usually been made on free films, it is unfortunately impossible to correlate the published results with these results or to predict them from electrical field induced S_{33} direct measurements due to the fact that the effect of clamping when the sample is glued on the beam cannot be easily known.

M_{31} can only be evaluated from the slope by $M_{31} = \frac{slope}{Y\left[w t_b \int_x \left(\frac{\partial^2 u}{\partial x^2}\right) dx\right]}$ by assuming that the value of the Young Modulus at 18.4 Hz is almost equal to this one at 10 Hz. Results are summarized table 2.7.

Table 2.7 Comparison of the ratio of harvested current at various thicknesses.

Sample	Thickness (µm)	Y (MPa)	M_{31} $\left(\int_x \left(\frac{\partial^2 u}{\partial x^2}\right) dx = 0.0065 \text{m}^{-1}\right)$	M_{31} $\left(\int_x \left(\frac{\partial^2 u}{\partial x^2}\right) dx = 0.0106\ \text{m}^{-1}\right)$
PU-A	30	54	4.65×10^{-19}	5.21×10^{-19}
PU-B	70	51	7.25×10^{-19}	8.36×10^{-19}
PU-C	110	40	1.33×10^{-18}	1.38×10^{-18}
PU-D	145	39	1.43×10^{-18}	1.56×10^{-18}
PU-E	198	38	1.70×10^{-18}	1.96×10^{-18}
PU-F	250	37	2.09×10^{-18}	2.21×10^{-18}

Figure 2.27 depicts the M_{31} coefficient as a function of film thickness. It shows that the apparent coefficient, M_{31} increases when the thickness of polymer increases. Moreover, the M_{31} coefficient does not depend on the value of $\int \frac{\partial^2 u}{\partial x^2} \text{dx}$, indicating that the behaviour of the beam is always linear up to 0.0106 m^{-1}. The values of the harvested current versus Pu film thickness cannot be predicted using this analytical modelling if the dependence of M_{31} versus thickness is unknown. For that, it will be necessary to find a relationship between the value of the M_{31} of free polymer film and the M_{31} of the same film when it is glued on the beam. This point is still under investigations.

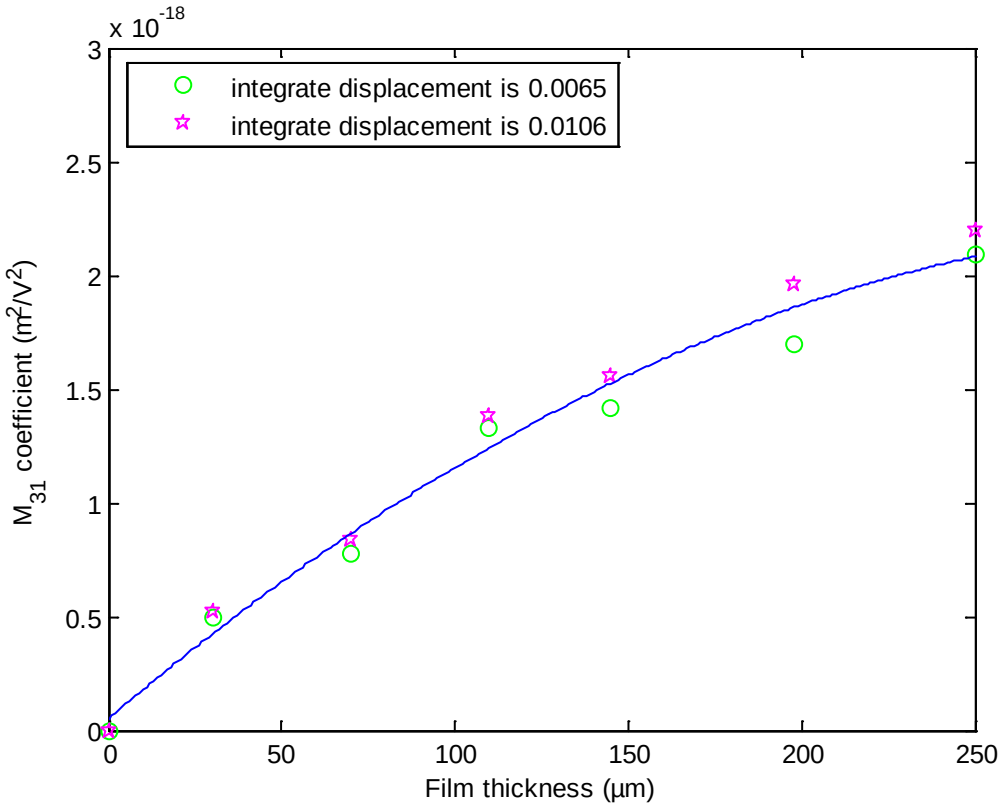

Fig. 2.27. The M_{31} coefficient as a function of film thickness.

2.8 Conclusions

The model proposed in this chapter, based on the electrostrictive behaviour, was able to predict the amount of the current power capable of being generated through the vibration of a cantilever beam to which films of neat polyurethane and two other commercialized polymers (nylon®6 and polyethylene) were attached. The model was verified based on experimental results with high accuracy. This model points out that in order to increase the energy harvesting capability, the dielectric permittivity needs to be increased but in case of actuators, it is also necessary to keep low the Young modulus. Moreover, the proposed model could be used to obtain the electrostrictive coefficient M_{31} of the materials, when they are stuck on a structure. In this sense, the developed model constituted an effective tool for accurately predicting the harvested energy.

Chapter 3:

Preparation and characterization of the electroactive polyurethane, terpolymer and composites

3.1 Introduction

In the previous chapter, it has been pointed out that a high permittivity is required to increase energy harvesting and also to increase the actuation capability if the Young modulus is kept low. Polyurethane is one of the promising full materials for actuation as its Young modulus is low and its relative permittivity is around 6. The main interest of this polymer is that it is also possible to synthesize films from commercialized granules with controlled properties at the laboratory scale. Another advantage is that the used process to prepare the polyurethane film is compatible with the filling of the polymer solution with micro or nano-objects. Previous studies in our laboratory have in particular shown that the actuation properties can be greatly enhanced by adding carbon nano-tubes or nanopowder within the polyurethane

matrix.**[GUI 2006]** In parallel, new formulations of terpolymers are now available.**[ZHI 2004][NEE 2009]** These materials presents high relative permittivity (higher than 40) and should be good candidates for energy harvesting purpose. These formulations can also be prepared in our laboratory from commercialized powders and as for polyurethane, it is also possible to incorporate micro or nano-objects within the matrix.

This chapter firstly presents a short presentation of the various electroactive polymers which can be used as actuator materials, with a focus on terpolymer and polyurethane. Secondly, the process used in our laboratory to prepare neat polyurethane films, neat terpolymers films and filled composites films is described in details. Finally, the influence of fillers on microstructure, dielectric permittivity, Young Modulus and thermal behaviour using **D**ifferential **S**canning **C**alorimetry is studied.

3.2 Material background for the electroactive polymer

During the last decade, among of technological advancements, conventional materials such as metals and alloys are being replaced by polymers in such fields as automobiles, aerospace, biological muscles, and electronics device because the shape properties can be easily modified.

Polymers have many attractive characteristics. They are lightweight, inexpensive, fracture tolerant, and pliable, and easily processed and manufactured. Further, they can be configured into almost any complex shape and their properties can be tailored to suit a broad range of requirements.

For several decades, it has been known that certain polymers show change in shape or size in response to electrical simulation and are emerging as a new class of actuation material. These polymers have been referred to Electroactive Polymers or EAPs. This progress has added an important capability to these polymers. This capability of the EAPs attracted the attention of engineers and scientists from many different disciplines. Initially, EAP's received relatively little attention due to their limited actuation capability. However, in the last decade the potential capability of these materials have emerged which large displacement response. Table 3.1 shows comparison of performance of EAP's with that of biological muscle and other actuator technologies.

Table 3.1 Comparison of EAP's with other actuator technologies.**[KOR 2004]**

	Actuator Type (specific example)	Typical (Max.) Strain (%)	Typical (Max.) Stress (MPa)	Typical (Max.) Specific Elastic Energy Density (J/g)	Typical (Max.) Elastic Energy Density (J/cm^3)	Typical (Max.) Avg. Specific Power Density at 1 Hz (W/g)	Peak Strain rate (%/s)	Elastic Modulus (MPa)	Est. Max. Efficiency (%)	Relative Speed (full cycle)
NATURAL MUSCLE	Mammalian Skeletal Muscle	20 (40)	0.1 (0.35)	0.041 (0.08)	0.041 (0.08)	0.041 (0.08)	> 50	10–60	20%	Medium
ELECTROACTIVE POLYMER	Dielectric elastomer	25 (> 300)	1.0 (7.0)	0.1 (3.4)	0.1 (3.4)	0.1 (3.4)	> 450	0.1–10	60–90	Med. - Fast
	Electrostrictive Polymer	3.5 (7.0)	20 (45)	0.17 (> 0.53)	0.3 (> 1.0)	0.17 (> 0.53)	> 2000	400–1200	60–90	Fast
	Electrochemo-mechanical Conducting Polymer	2 (20)	5 (200)	0.1 (1.0)	0.1 (1.0)	0.1 (1.0)	1	200–3000	< 5	Med. -Slow
	Ionic Polymer Metal Composite	0.5 (3.3)	3 (15)	(0.004)	(0.006)	0.004	3.3	50–100	1.5–3	Med. - Slow
	Mechano-chemical Polymer/Gels (Polyelectrolyte)	> 40	0.3	0.06	0.06	< 0.06	< 1	?	30	Slow
	Piezoelectric Polymer (PVDF)	0.1	4.8	0.0013	0.0024	0.0013	?	450	60–90	Fast
OTHER	Liquid Crystal Elastomer (Thermal)	19 (45)	0.12 (0.45)	0.003 (0.06)	0.003 (0.06)	< 0.003	37	0.3 – 4	< 5%	Slow
	Shape Memory Polymer	100	4	2	2	< 0.2	?	?	< 10	Slow
NONPOLYMER ACTUATORS	Electromagnetic									
	Direct (Voice Coil)	50	0.10	0.003	0.025	0.003	> 1000	NA	> 80	Fast
	Motor/transmission	50	NA	NA	NA	0.5	< 200	NA	> 50	Medium
	Piezoelectric									
	Ceramic (PZT)	(0.2)	(110)	(0.013)	(0.10)	(0.013)	> 1000	25,000–70,000	> 90	Fast
	Single Crystal (PZN-PT)	(1.7)	(131)	(0.13)	(1.0)	(0.13)	> 1000	9000	> 90	Fast
	Shape Memory Alloy (TiNi)	> 5	> 200	> 15	> 100	< 15	300 (one direction only)	20,000–80,000	< 10	Slow
	Thermal (Expansion)	1	78	0.15	0.4	< 0.15	Depends on heat transfer	> 70,000 (varies)	< 10	Slow
	Magnetostrictive (Terfenol-D, Etrema Products)	0.2	70	0.0027	0.025	>0.0027	>1000	40,000	60	Fast

The application of these materials as actuators to drive various manipulation, mobility and robotic devices involves multidiscipline including materials, chemistry, electromechanics, computers, electronics, etc. Consequently, they are used in a large number of applications. The pie chart of figure Fig. 3.1 shows the approximate distribution on various applications. **[LAN 2006]**

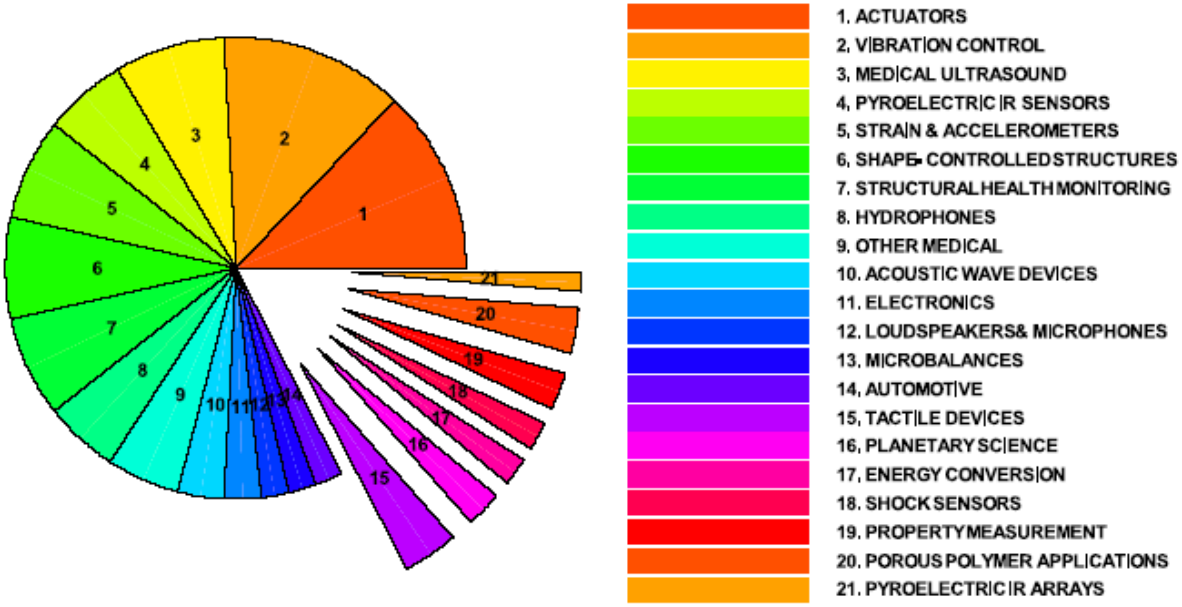

Fig. 3.1. The application of EAPs during the year from 1999 to 2004.**[LAN 2006]**

3.3 Electroactive polymers (EAPS)

As mentioned before, polymers that respond to electrical stimulation with a significantly shape and size change have emerged. These polymers are called electroactive polymers (EAPs) and are classified primarily into two groups, depending on the mechanism responsible for actuation. Electronic EAPs for which the change of range is due to the driven electric field. Ionic EAPs for which change of shape is due to mobility or diffusion of ions and their conjugated substances. A list of leading electroactive polymers is presented in table 3.2

Table 3.2 List of leading EAP materials

Electronic EAP	**Ionic EAP**
Ferroelectric polymers	*Ionic polymers gels (IPG)*
Dielectric EAP	*Ionic polymer metal composite (IPMC)*
Electroviscoelastic elastomers	*Conducting polymer*
Electrostrictive graft elastomers	*Carbon nanotubes (CNT)*
Electrostrictive paper	

3.3.1 Electronic EAP's

Based on the mechanism of actuation, EAPs that are driven by electric field or coulomb forces are called electronic EAPs. They are capable of performing energy conversion between electric and mechanical form and hence can be used as solid-state electromechanical actuators and motion sensors. Different types of electronic EAPs are discussed in this section.

Ferroelectric Polymers

Ferroelectric materials are used in analogy to ferromagnets, where the application of an electric field aligns polarized domains in the material. Permanent polarization exists even after the removal of the electric field.**[MAD 2004]** Moreover, phenomenons of a spontaneous electric polarization of a material that can be reversed by the application of an external electric field are called ferroelectricity. Poly (vinylidene difluoride) (PVDF or PVF2) and its copolymers are commonly exploited ferroelectric polymers. These polymers that show a semi-crystalline structure have a Young's modulus of nearly 1-10 GPa, which offers high mechanical energy density. Strains of nearly 2% have been reported in PVDF at large applied AC fields (~200MV/m). Electric field- induced strains of almost 5% have been reported for P(VDF-TrFE) copolymer at low frequency drive fields of about 150 MV/m.**[ZHA 1998]** Ferroelectric polymers can be operated as actuator in air, vacuum and water. Polymers performed as actuator in air are shown in Fig. 3.2.

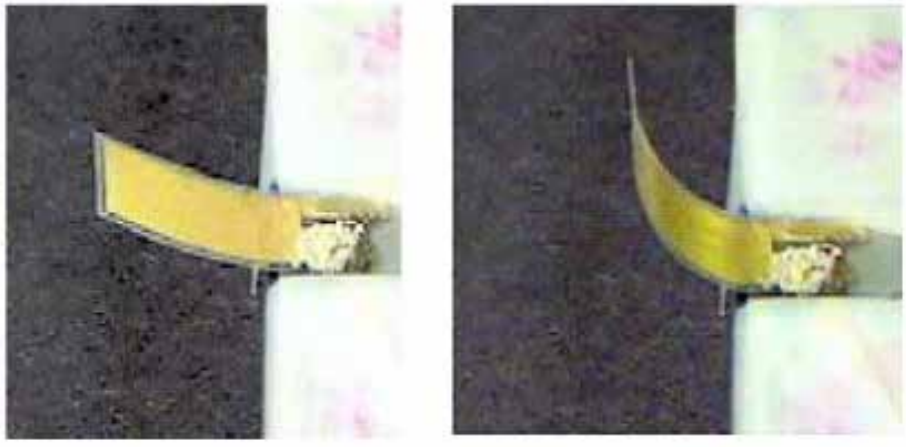

Fig. 3.2. Ferroelectric polymer in the reference state (left) and in its actuated state (right), where actuation is performed in air. **[ZHA 1998]**

Dielectric EAPs

Dielectric elastomers consist of a polymer film sandwiched between two compliant electrodes as well as a parallel plate capacitor. A large actuation strain of these polymers with low elastic stiffness and high dielectric are induced by applied electrostatic field, causing compression in thickness and stretching in area of the polymer. The actuation of a circular dielectric elastomer is shown in Fig.3.3.

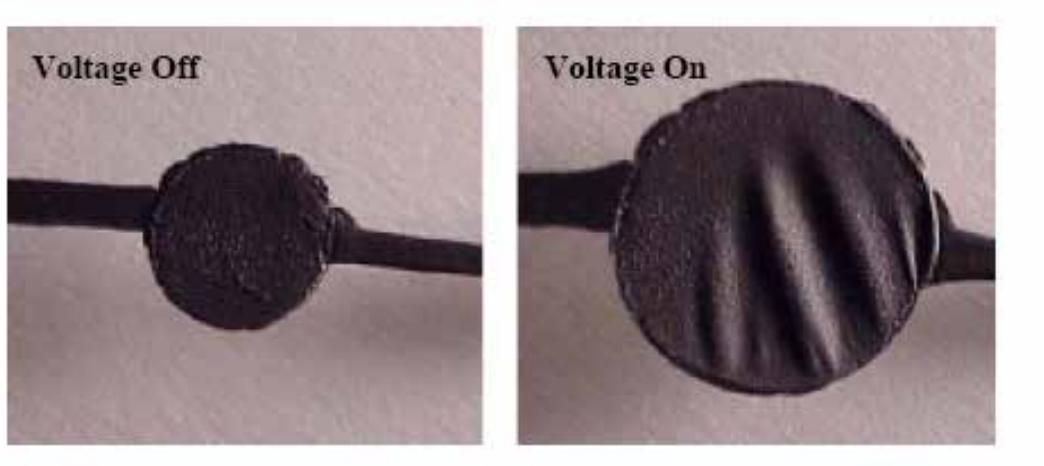

Fig. 3.3. Circular strain test of a dielectric elastomer with carbon grease electrodes, in its reference (left) and actuated (right) states.**[KOF 2001]**

Electroviscoelastic Elastomers

Electroviscoelastic elastomers are the solid form of an electrorheological fluid (ER), which is a suspension of dielectric particles. When these ER fluids are subjected to an electric field, the induced dipole moments cause the particles to form chains in the directions of the field. This material behaves as electro-rheological fluids before cross linked in first uncured state. The orientation and fixture of the position of a polar phase are observed after applied electrical field during the time of curing. These particles tend to move toward each other, creating stress which causes deformation of elastomer when the electric field is applied. Electro-rheological (ER) fluids can be also transformed from a liquid state into a solid state in same milliseconds by applying an external electric field. Similar to electrorheological effects can be induced in elastomers using magnetic fields and as much as 50% change in shear modulus can be induced.**[DAV 1999][ZRI 1999]**

Liquid Crystal Elastomer (LCE)

LCEs are composite materials that consist of monodomain nematic liquid crystal elastomers and conducting polymers distributed within their network structure.**[SHAH 2000]** They can be activated by electrical energy through inducing Joule heating. LCEs consist of long chains of molecules that can slide past each other and so allow the material to be stretched with little effort. The result of changes in order and alignment of crystalline side chains generate stress in polymer. The actuation mechanism of these materials involves phase transition between nematic and isotropic phases that exist in their crystal structure. Contractions strain of 45% have been reported for LECs sample consisting of monodomain of 50-200µm.**[COH 2001b]** These materials have a low stiffness and tensile strength so a small change in load can result in a large change in length.

Electrostrictive Graft Polymers

Electrostriction is defined as the change in shape of a body due to rearrangement of its molecules in presence of an external electric field. The actuation mechanism of these polymers is based on development of Electrostriction and Maxwell contribution. Electrostrictive polymers will be discussed in detail in Chapter 4.

3.3.2 Ionic EAP's

EAPs that known shape changes because of movement or diffusion of ions are called ionic EAPs. Some of the most commonly used ionic EAPs are discussed below.

Ionic Polymer Gels (IGL)

Polymer gels are multi-phase materials consisting of a cross-linked polymer network and interstitial fluid. These materials show actuation by contracting or swelling up in response to an electric field or pH stimuli.**[OSA 1993]** For example, Polyacylic acid gel is used as IGL actuation due to movement of hydrogen ions in or out of this gel. The planar expansions and bending motions have been generated with ionic diffusion rates in the polymeric gels which are shown in Fig 3.4. Bending being Planar expansions of 300% **[CAL 1998][LUI 2000]** and bending motions of greater than 90 deg have been reported. **[HIR 1999]**

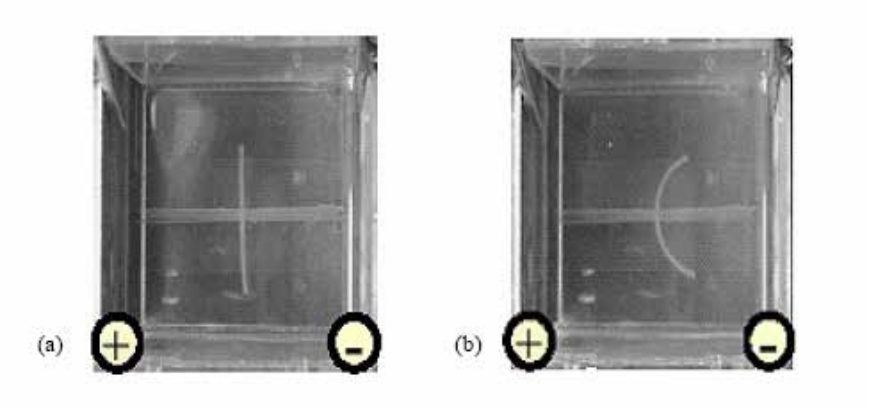

Fig. 3.4. Ionic gel at reference state (a) and activated state (b) where the gel bends with a concave negative side

Ionomeric Polymer-Metal Composites (IPMC)

IPMCs are a variety of EAPs, which typically produce a bending motion under the application of an external electric field. The bending motion is produced due to the mobility of cations in the fixed polymer network of negative ions on interconnected clusters when the electric field is applied. An IPMC consists of a polymer membrane sandwiched between layers of thin metal plated electrodes. Two commonly used polymers are Nafion® (perfluorosulfonate, made by DuPont) and Flemion® (perfluorocarboxylate, made by Asahi Glass, Japan)**[COH 2001c].** These polymer films produced net charge from anions covalently fixed to the polymer chains, which is balanced by an amount of externally introduced ions. The bending response of IPMC depends on the ionic content which induced a large deformation at low voltage and frequencies below 1Hz. The bending deformation of IPMC decreases with the increase of frequency. In recent years, the gold metallization is used to enhance the bending displacement of IPMC causing the higher electrode conductivity.**[OGU 1990]**

Conducting Polymers

Conducting polymers are electronically conducting organic materials. Actuation is produced in these polymers due to the electronically change of oxidation state. The flux of ions into and out of these polymers backbone causes deformation of conducting polymers. Conducting polymers with appropriate dopant, such as hydrogen chloride or sulphuric acid, exhibit chemically and electrochemically controllable electronic conductivities. Doping is done in order to have ions that can flow across the covalently

bonded conjugated polymer chain. The bending of a conducting polymer sandwich is presented in Fig. 3.5.**[SCHR 2000b]** When an electric field is applied to doped conducting polymers with appropriate electrolyte, a reversible exchange of ions takes place between the conducting polymer and the electrolyte. Exchange of ions leads to oxidation or reduction reactions in the conducting polymer, which leads to significant changes in its volume.**[COH 2001c]** These ions are transferred into and out of the polymer and electrolyte to balance the charges.

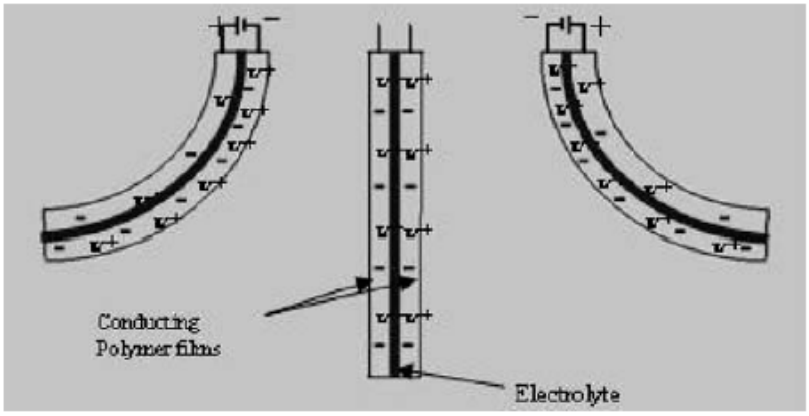

Fig. 3.5. Schematic representation of three states during the electromechanical cycle of a rocking-chair type of bimorph-conducting polymer actuator. Both electrodes have the same concentration of dopant (K^+) when the cantilever is undistorted, and electrochemical transfer of dopants between electrodes causes bending either to the right or to the left. **[SCHR 2000b]**

Carbon Nanotubes Actuators

Carbon nanotubes (CNTs) emerged as a class of EAP that can be thought of as a hexagonal network of carbon atoms that has been bundled to make a cylindrical form. Nanotubes are categorized as single-walled nanotubes (SWNTs), which is the fundamental cylindrical structure and multi-walled nanotubes (MWNTs), which consist of multi rolled layers. The response of actuation mechanism of a carbon nanotube depends on a change in bond length of the carbon-carbon bond due to repulsion between similar charges developed on carbon atoms forming the nanotube. The carbon-carbon bond is suspended in an electrolyte changes length as a result of net charge injection causing the ionic charge balance between the nanotubes and the

electrolyte.(Fig. 3.6)**[BAU 1999]** The repulsion between similarly positive charged adjacent carbon nuclei results in increase in the C-C bond length, which leads to the increase of the length and diameter of the nanotube. **[COH 2001c]** Isotonic strains greater than 0.2% have been reported in bimorph cantilever actuators fabricated using single wall nanotube sheets in 1M NaCl solution.**[BAU 1999]**

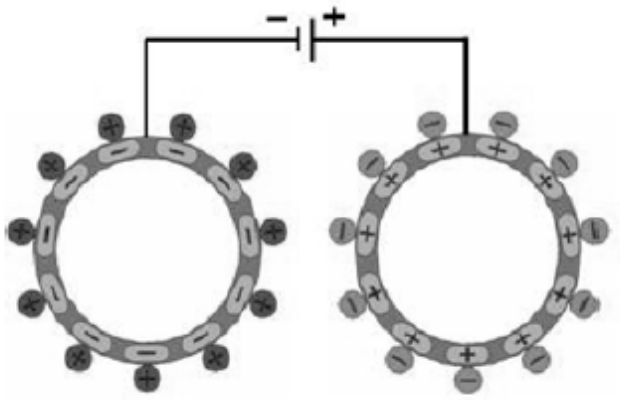

Fig. 3.6. Schematic illustration of a charge injection in a nanotube-based electromechanical actuator.**[BAU 1999]**

3.4 Polyurethane and P(VDF-TrFE-CFE) Terpolymers

As mentioned in earlier, Electrostrictive polymers exhibit very attractive characteristics, and as a result, they have been widely studied either for the purpose of understanding the electrostriction phenomenon or in view of practical applications.**[YIM 1999][SUN 1996][GUI 2003]** Numerous reports are devoted to the characterization of the electrostrictive behavior versus applied electric fields.**[SU 1998][WAN 1991][GUIF 2006]** Under moderate electric fields, electrostrictive polymers have been found to produce large strains of >10%, and for this reason they are considered as good candidates for actuation. **[BHA 1999]**

As an example, polyurethane (PU) elastomers are of great interest for a wide range of transducer and actuator applications when considering their significant electrical-field-induced strains, high specific energy, and small response. In addition, it has recently been shown that the incorporation of nanofillers such as carbon nanotubes

into a polymer matrix can greatly enhance the expected strain versus electric field. **[PAR 2008]**

The recent discovery of high electromechanical performance in P(VDF-TrFE-CFE) based terpolymer opens a new avenue for developing high performance electroactive polymers. From basic materials consideration, it is expected that one can achieve high electromechanical performance by means of electrostriction approach, such as introducing ter-monomer to form PVDF based terpolymer. The basic requirement for the ter-monomer is discussed in order to achieve a high electromechanical performance in P(VDF-TrFE-CFE) based terpolymer. This terpolymer is reported that exhibits high electrostrictive strain (>7%) with relatively high modulus (>0.3GPa). It has been also observed that the large electrostrictive strain is nearly constant in the temperature range from 20 to 80 ^{o}C. The high room temperature relative dielectric constant (~50), which is the highest among all the known polymers), high induced polarization (~0.05 C/m^2), and high electric breakdown field (>400 MV/m) lead to very high volume efficiency for the electric energy storage operated under high voltage (~10 J/cm^3) **[BAU 2006]**

In this thesis, the Polyurethane elastomers (TPU 58 888) and P(VDF-TrFE-CFE) terpolymer which was filled with nano-charges are prepared to study the electromechanical effect and the energy harvesting based on the electrostriction phenomenon.

3.4.1 Polyurethane matrix

The polyurethane – general structure

Polyurethane is the general name of polymer consisting of a chain of organic units joined by urethane links. Polyurethane polymers are formed through step-growth polymerization by reacting a monomer containing at least two isocyanate functional groups with another monomer containing at least two hydroxyl (alcohol) groups in the presence of a catalyst.

Polyurethanes or urethane linkage is produced by reacting an isocyanate group, -N=C=O with a hydroxyl (alcohol) group, -OH, (Figure 3.7). Polyurethanes are produced by the polyaddition reaction of a polyisocyanate with a polyalcohol (polyol) in the

presence of a catalyst and other additives. In this case, a polyisocyanate is a molecule with two or more isocyanate functional groups, R^1-$(N=C=O)_{n \geq 2}$ and a polyol is a molecule with two or more hydroxyl functional groups, R^2-$(OH)_{n \geq 2}$. The reaction product is a polymer containing the urethane linkage, -$R^2NHCOOR^1$-. Isocyanates will react with any molecule that contains active hydrogen.

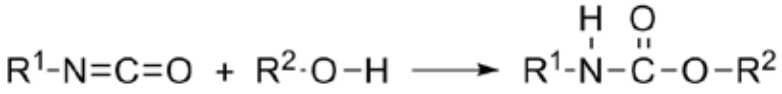

Fig. 3.7. Generalized polyurethane reaction.

The first essential component of a polyurethane polymer is the isocyanate. Molecules that contain two isocyanate groups are called diisocyanates. These molecules are also referred to as monomers or monomer units, since they themselves are used to produce polymeric isocyanates that contain three or more isocyanate functional groups. Isocyanates can be classified as aromatic, such as diphenylmethane diisocyanate (MDI) or toluene diisocyanate (TDI); or aliphatic, such as hexamethylene diisocyanate (HDI) or isophorone diisocyanate (IPDI). An example of a polymeric isocyanate is polymeric diphenylmethane diisocyanate, which is a blend of molecules with two-, three-, and four- or more isocyanate groups.

The second essential component of a polyurethane polymer is the polyol. Molecules that contain two hydroxyl groups are called diols, those with three hydroxyl groups are called triols, and so on. In practice, polyols are distinguished from short chain or low-molecular weight glycol chain extenders and cross linkers such as ethylene glycol (EG), 1,4-butanediol (BDO), diethylene glycol (DEG), glycerine, and trimethylol propane (TMP). Polyols formed by polyesterification are polyester polyols. The choice of initiator, extender, and molecular weight of the polyol greatly affect its physical state, and the physical properties of the polyurethane polymer. Important characteristics of polyols are their molecular backbone, initiator, molecular weight, percent of primary hydroxyl groups, functionality, and viscosity.

The polyurethane-Estane 58 888

The studied PU is a commercial material, Estane 58888-NAT021 provided by Noveon. The structure of PU 58888 is depicted in figure 3.8. This PU is based on MDI

(4,4’ methylene bis(phenyl isocyanate), BDO (1,4-butanediol) as hard segments (HS) and poly(tetramethylene oxide) as soft segments (SS). The HS content is about 46 wt% and the physical properties depend partially on the phase separation degree between hard and soft phases which are shown in figure 3.9.

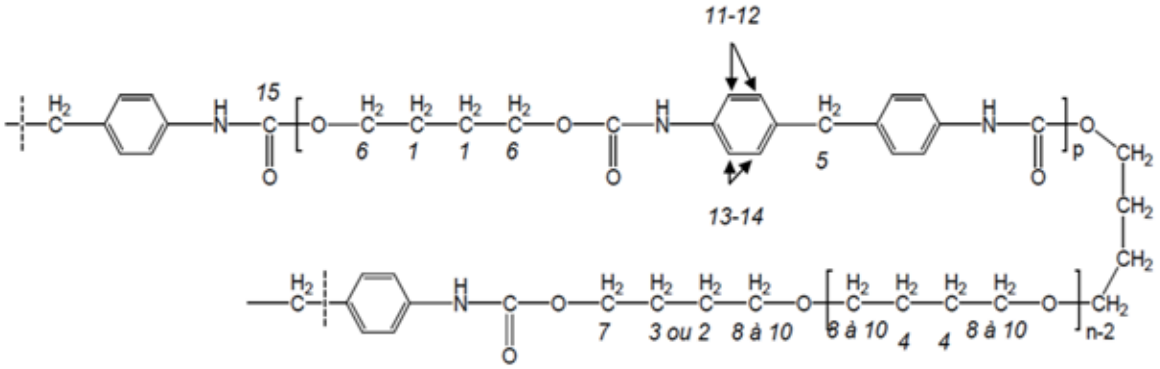

Fig. 3.8. Structure of Polyurethane- Estane 58 888.

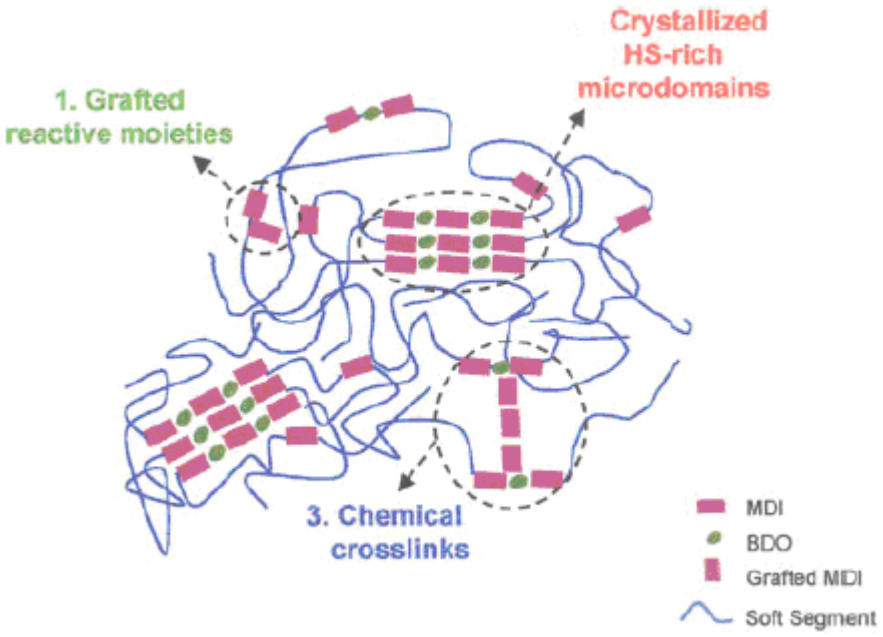

Fig. 3.9. Schematic representation of chains urethane and micro-separation of rigid segments.**[LAP 2007]**

Linear, segmented polyurethanes (PUs) that consist of alternating soft segments (SSs) and hard segments (HSs) offer unique possibilities for tailor-made polymers through the variation of the block length and composition. The SSs are typically polyether or polyester and provide the flexible character of the polymers. These segments are connected by HSs formed from the reaction of diisocyanates with diol chain extenders. Thermodynamic immiscibility between HSs and SSs induces phase separation and generates a two-phase morphology in these segmented block copolymers. Several physical and chemical properties of PU –Estane 58 888 are listed in Table 3.3

Table 3.3. Physical and chemical properties of PU –Estane 58 888

Characterization	Polyurethane (TPU 58 888)
Molecular Weight ($g.mol^{-1}$)	1000
Density ($g.cm^{3}$)	1.13
Melting temperature (^{o}C)	160
Breaking stress (MPa)	38
Breaking elongation	640%

3.4.2 P(VDF-TrFE-CFE)Terpolymers

Ferroelectric materials like Poly(vinylidene fluoride) (PVDF) and its copolymer with trifluoroethylene P(VDFTrFE) are intrinsically multifunctional. In the copolymer with TrFE these ferroelectric polymers will exhibit a Curie transition, where a phase transition between the ferroelectric and paraelectric phases occurs with increasing temperature. Figure 3.10 shows the molecular conformations for PVDF based polymer.**[NEE 2009]**

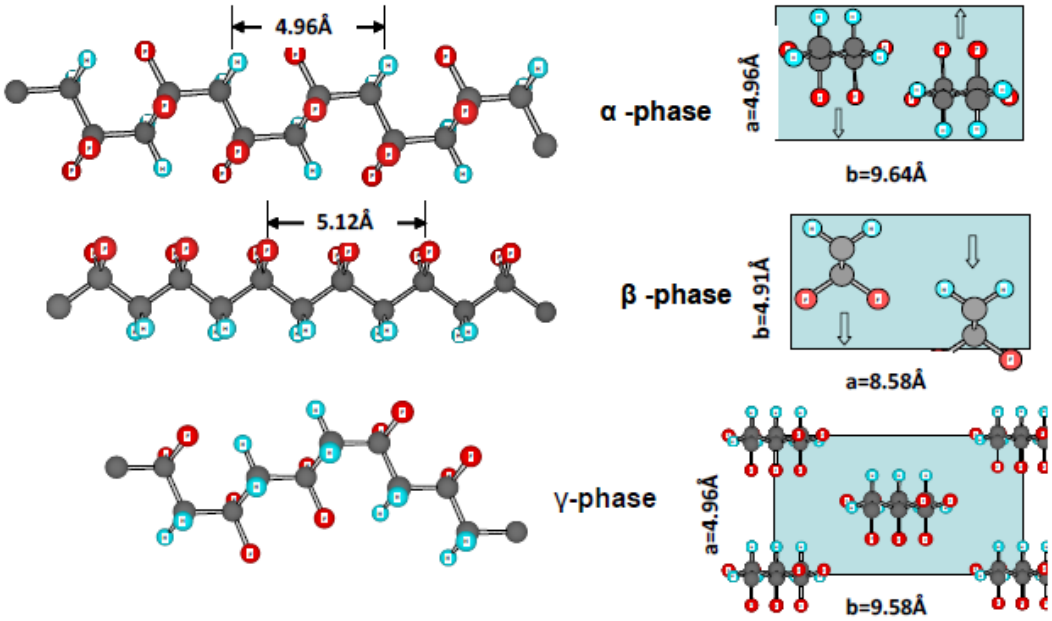

Fig. 3.10. The conformations of the different phases of PVDF.

The most common, thermodynamically stable, and easily obtainable phase is the α-phase (also commonly referred as phase II), which has a trans-gauche (TGTG') conformation and does not show a net lattice polarization due to its antiparallel chain arrangement, i.e., the dipoles oppose each other. The β-phase (phase I) crystallizes with the molecules being configured in an all-trans (TTTT) zig-zag conformation, giving this phase polarity due to the parallel packing of polymer chains, i.e., the C-F dipoles are all aligned in the same direction. This gives the β-phase crystals a spontaneous lattice polarization which is necessary to observe ferroelectricity in PVDF. The γ phase (phase III) is intermediate between the α and β-phases, consisting of a (T3GT3G') conformation. A fourth polymorph of PVDF is the δ-phase (phase IIp), which is a polar

version of the α-phase, with essentially the same unit cell parameters but a varying symmetry.

The development of P(VDF-TrFE)

The discovery of piezoelectricity and pyroelectricity in PVDF sparked many studies on altering the chemical structure of PVDF in order to enhance and make practical use of the ferroelectric properties.**[FAR 1972]** One of the draw back of utilizing PVDF as a ferroelectric material is the fact that it does not easily crystallize into the ferroelectric β-phase without some specialized processing such as uniaxial drawing. This problem was addressed with investigations on how to alter the stereochemistry of the PVDF chain such that it could naturally crystallize into the polar phase. The monomer units of VDF have directionality, meaning that CH_2 is considered as the head and CF_2 is considered as the tail. When PVDF is synthesized and the monomers are linked together they are often linked up head-to-head and tail-to-tail, creating an irregularity in the polymer structure in which the amount of these defects can be controlled in the synthesis. Farmer et.al first predicted the effect of these defects on the polymorphism of PVDF, using potential energy calculations based on adding tetrafluoroethylene (TFE) as a comonomer to simulate the defects.**[FAR 1972]** They found that the addition of head-head-tail-tail (HHTT) defects can cause the TTTT conformation to become a lower energy state than the TGTG' conformation. These calculations confirmed experimental evidence of Lando and Doll that showed copolymers of P(VDF-TFE) and P(VDF-TrFE) can more easily crystallize in the β-phase, even when directly cooled from the melt state. **[NEE 2009]**

The development of P(VDF-TrFE-CFE)

A new class of ferroelectric polymers, i.e., the terpolymers of P(VDF-TrFE-CFE), was developed from the normal ferroelectric PVDF polymer by employing proper defect modifications which eliminate detrimental effects associated with a normal first order F-P transition while maintaining high material responses.**[BAU 2004][XIA 2002][HUA 2004]** The introduction of the third monomer into the polymer chain serves to interrupt the ferroelectric domains, thereby reducing their size.**[HUA 2004]** Random defect introduction, as in the irradiated copolymer samples**[ZHA 1995]**, broadens the ferroelectric transition and reduces the ferroelectric-paraelectric transition

temperature. The random incorporation of the bulky third monomer into the polymer chains forces a conformation change from the all-trans (Tm≥4) or conformation to the transgauche (TG) and T3G conformations.**[BOB 2003]**

Addition of defects in the form of chemical monomers, in this case 1, 1-chlorofluoroethylene (CFE) which are copolymerised with the VDF-TrFE, eventually favor the TG conformation and eliminate the normal ferroelectric phase, leading to a relaxor ferroelectric with electromechanical strain greater than 7% and an elastic energy density of 0.7 J/cm^3 at 150 MV/m.**[ZHA 2004]** It is the change in conformation from the disordered TG and T3G to the all trans conformation that leads to the observed large electrostrictive strain. This high electrostrictive strain coupled with relatively high modulus (>0.3GPa) makes the polymers suitable as a structure component in addition to the electroactive functions (actuators and sensors). This relaxor ferroelectric terpolymer P(VDF-TrFE-CFE) exhibits a room temperature dielectric constant greater than 50.**[BAU 2004][HUA 2004]**

It has been shown that the amount of CFE added to the P(VDF-TrFE) strongly affects the strain response and the polarization hysteresis by changing the spontaneous polarization, the crystallinity, the Young's modulus, the dielectric properties, and the structural conformations.

3.5 Dielectric and Mechanical behavior of EAPs

The electromechanical effect of EAPs relates on the dielectric properties and mechanical behavior. Several reports previously mentioned that the electromechanical effect on electrostriction materials depends on the electrostrictive and Maxwell stress effect. Both two effects (are presented in chapter 4) relate on the dielectric properties and mechanical behavior.

A prediction of the likely size of the electrostrictive and Maxwell stress effect require knowledge of dielectric constant and modulus of the film. For this reason, the dielectric constant and modulus for each film was studied.

3.5.1 Dielectric properties

A dielectric material is an electrical insulator that may be polarized by the action of an applied electric field. However, the exact response of a certain material to an applied electric field is quite hard to predict. When dielectric is placed in electric field,

electric charges do not flow through the material, like in conductor, but only slightly shift from their average equilibrium positions causing dielectric polarization, positive charges are displaced along the field and negative charges shift in the opposite direction. This creates an internal electric field which partly compensates the external field inside the dielectric. If a dielectric is composed of weakly bonded molecules, those molecules not only become polarized, but also reorient themselves so that their symmetry axis aligns to the field. If the material is conducting, the electric field will give rise to charge transport, due to which the effects of polarization will be obscured. The remainder of this chapter considers insulating, non-conductive materials.

The dielectric constant

A typical model of an insulating material regards the material as composed of small dipoles, which are electrically neutral, but possess internal charge separation. When exposed to an external electric field, the tendency of a single dipole is to align itself with the electric field, such that the positive end points toward lower potential, and the negative end points toward the higher potential.**[FRO 1950]** When all the dipoles in a material align in this way to an applied electric field, the material is known as a dielectric. Figure 3.11(a) depicts the situation when a constant voltage is applied to a set of juxtaposing capacitor plates. Electric field lines may only begin on free positive charges, and end on free negative charges. Thus, surface charge concentration builds up on the capacitor plates. The charge build up continues, until the voltage drop over the capacitor plates matches that of the voltage source. The relation between the amount of free charge, Q, and the voltage drop, V, is $Q = CV$, where C is the capacitance of the sample. The dielectric constant ϵ_r can be calculated, by assuming that the sample approximated to a simple parallel plate capacitor:

$$\epsilon_r = \frac{Ct}{\epsilon_o A} \qquad (3.1)$$

A is the area of the plates, and t is the distance between them. ϵ_o is the vacuum permittivity, $8.854' 10^{-12}$ F/m. The density of the field lines is known as the electric flux density, or just flux density, for vacuum and is given by

$$D = \epsilon_o E \qquad (3.2)$$

where E are the components of the electric field between the plates. When a piece of dielectric material is inserted between the plates, figure 3.11(b) and figure 3.11(c), the dipoles in the material will reorient such that the positive end of the dipole points toward the negative potential. The flux density is also known as the electric displacement, because it is a measure of the displacement of the dipoles in the material.

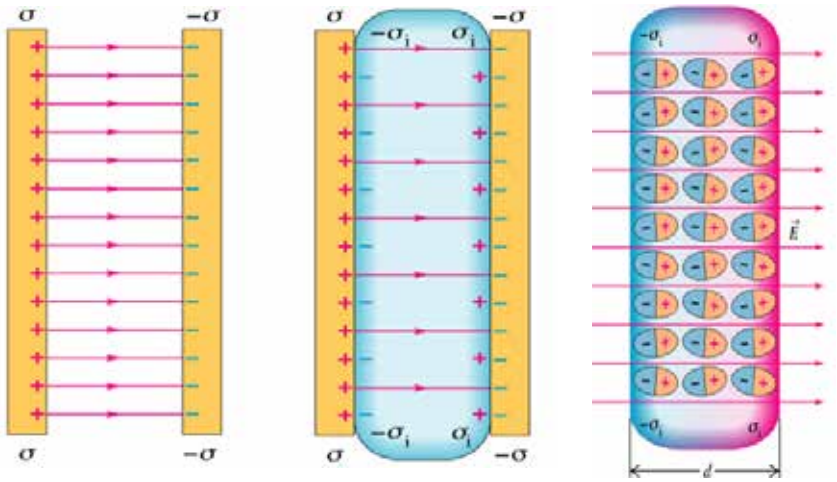

Fig. 3.11. (a) Electric field lines with vacuum between the plates. (b) The induced charges on the faces of the dielectric decrease the electric field (c) Polarization of a dielectric in an electric field gives rise to thin layers of bound charges on the surfaces, creating positive and negative surface charge densities. The sizes of the molecules are greatly exaggerated for clarity. (www.physics.sjsu.edu)

Part of the electric displacement, originates from the vacuum displacement, the other part from actual polarization of the dielectric. The electric displacement D is related to the polarization density P by

$$D = \varepsilon_o E + P \tag{3.3}$$

and the electric susceptibility χ is the part of the relative dielectric constant caused by the material,

$$\chi = (\varepsilon_r - 1)\varepsilon_o \tag{3.4}$$

So, if the dielectric is linear, the polarization can write as

$$P = \varepsilon_o(\varepsilon_r - 1)E = \chi E \tag{3.5}$$

The flux density in the material has increased, and is now

$$D = \varepsilon E = \varepsilon_o \varepsilon_r E \tag{3.6}$$

where ε is the dielectric of the material.

In this thesis, ε_r is referred to as the dielectric constant. In general, the dielectric constant is a complex parameter, so by definition the complex dielectric constant is

$$\varepsilon^*(\omega,T) = \varepsilon'(\omega,T) - i\varepsilon''(\omega,T) \tag{3.7}$$

where ε' is the real part of the dielectric constant and ε'' is the imaginary part of the complex dielectric constant. ω is the angular frequency and T is the temperature. The ratio of the imaginary to the real parts ($\varepsilon''/\varepsilon'$) is the ''dissipation factor'' which represented by $\tan\delta$, which $\frac{\pi}{2} - \delta$ is the angle between the voltage and the charging current. The angle, δ is known as ''loss angle''.

At the interface of two dielectric materials having different dielectric constant and/or conductivities, charges are accumulated according to simple electrodynamic considerations. Thus, a layer of dipoles induced by the external electric field is formed at interface, resulting in an increase of the total polarization field, i.e., an increase of the dielectric constant, often up to very high values.

In these arguments the ohmic conductivity is included in the complex permittivities as

$$\varepsilon^*(\omega,T) = \varepsilon'(\omega,T) - i\left[\varepsilon''(\omega,T) + \frac{\sigma(T)}{\varepsilon_o \omega}\right] \tag{3.8}$$

where σ is the conductivity arising from charge transport, which is usually not dependent on the angular frequency and increases exponentially by increasing temperature.**[NAL 1995]**

In the case of the metal-polymer composites, the dielectric constant of the two phase composites were enhanced by applying the percolation phenomenon. The

increase in the dielectric constant was small until the metal particle concentration became close to the percolation threshold. This is explained by the power law variation of dielectric permittivity.**[DEV 2006]**

$$e = e_i \left| (f_c - f) / f_c \right|^{-q} \tag{3.9}$$

where e_i is the dielectric constant of the base polymer. f_c is the percolation threshold volume fraction of loading, and f is the volume fraction of loading in the composite. q is the dielectric constant critical exponent.

3.5.2 Mechanical behavior of polymer

The nonlinear elastic behavior of materials such as polymers (fig. 3.12) has also been exploited in composite structure. In the natural vulcanized rubber or elastomer, the strain obtained saturates as stress is increased in the low megapascal range. Elastomers are materials of a very high molecular weight, generally composed of one or more monomers polymerised or co-polymerised together to form a polymer (or copolymer). In a process known as *cross-linking*, molecules are used to bind two different polymer chains together. When all polymer chains are linked together, they can not flow past each other. Such a cross-linked polymer is known as an *elastomer*. Elastomers have very little mechanical loss, and are capable of sustaining very high stretches. Fig 3.13(a) and (b) show high randomness of all polymer chains are linked together, (b) aligns the molecules – some parts of it now begin to resemble the crystallites.

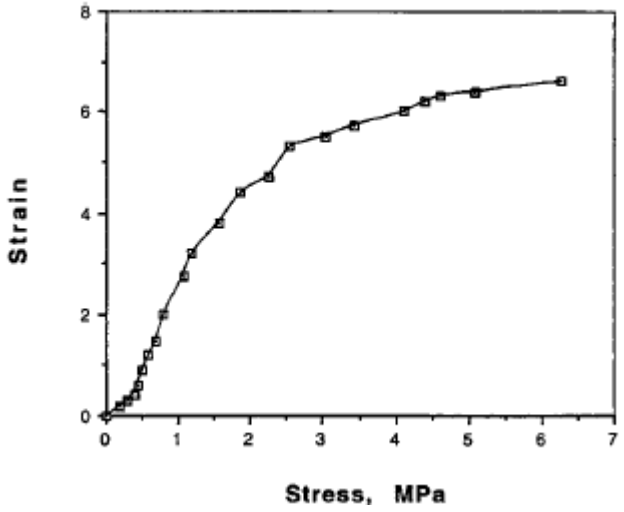

Fig. 3.12. Nonlinear strain vs stress behavior of a typical natural vulcanized rubber.**[NEW 1997]**

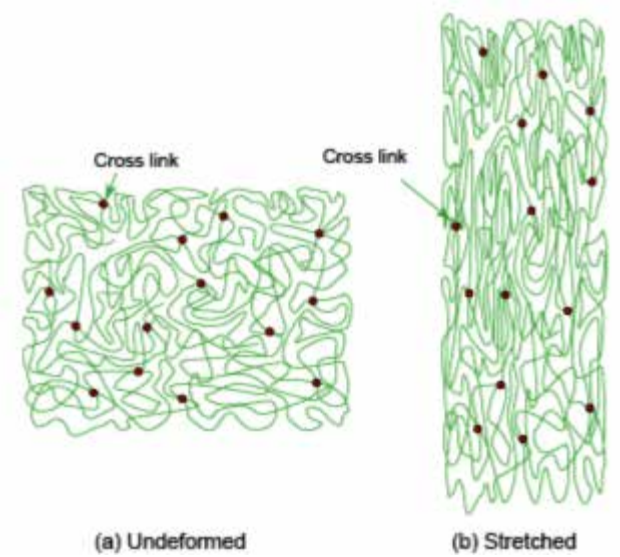

Fig. 3.13. The stretching of an elastomer causes alignment, producing crystal-like regions. (http://www.grantadesign.com/education/sciencenote.htm)

Linear stress- strain behavior conforming to Hook's law is observed only in regions of low stress. In the linear region, the strain S_{ij} is related to the stress T_{ij} by the relation $S_{ij} = s_{ijkl}T_{kl}$. Nonlinear elastic behavior in general may be described by the equation

$$S_{ij} = s_{ijkl}T_{kl} + s_{ijklmn}T_{kl}T_{mn} + \ldots \qquad (3.10)$$

where s_{ijkl} is the elastic compliance and s_{ijklmn} the higher order elastic compliance.

A number of experimental studies were conducted to investigate the relationship between mechanical properties and material morphology. This special niche of TPUs among other polymers and elastomers imparts high elasticity combined with high abrasion resistance.

Thermoplastic polyurethanes are randomly segmented copolymers composed of hard and soft segments forming a two-phase microstructure (fig. 3.14).**[HEP 1982]** Generally, phase separation occurs in most TPUs due to the intrinsic incompatibility between the hard segments and soft segments: the hard segments, composed of polar materials, can form carbonyl to amino hydrogen bonds and thus tend to cluster or aggregate into ordered hard domains, whereas the soft segments form amorphous

domains. Phase separation, however, is often incomplete, i.e., some of the hard segments are isolated in the soft domains as illustrated schematically in Figure 3.14(b).**[PET 1991]** In many TPUs, the hard domains are immersed in a rubbery soft segment. Depending on the hard segment content, the morphology of the hard domains changes from one of isolated domains (Figure 3.14(a), to one of interconnected domains (Figure 3.14(b)). **[EST 1971] [PET 1991]**

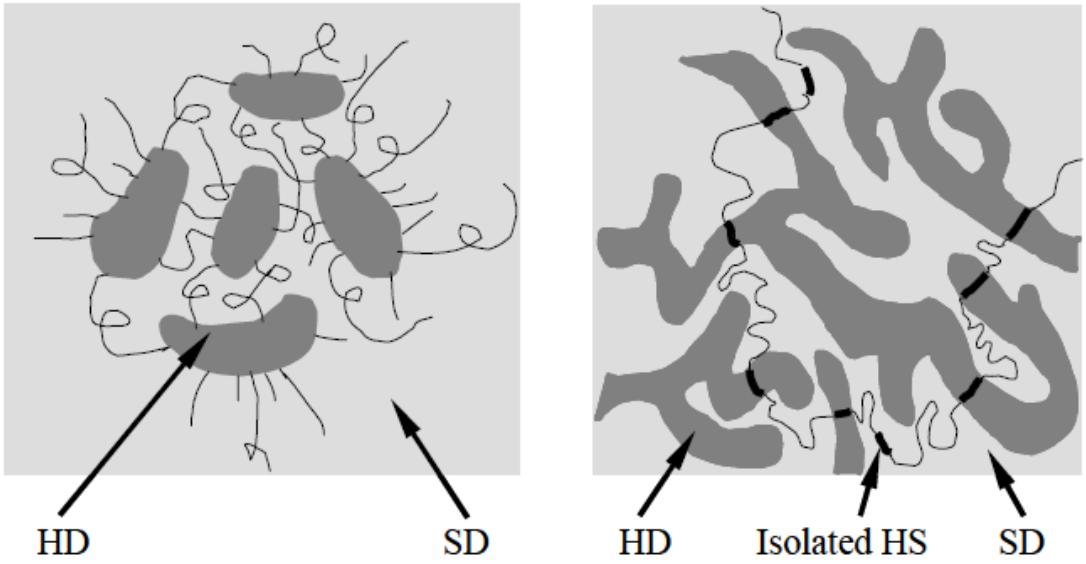

Fig. 3.14 Hard domains (HD) and soft domains (SD) of TPUs with (a) a low hard segment content **[PET 1991]**; (b) a high hard segment content.**[EST 1971]**

The presence of hard domains in segmented polyurethanes is very important to the mechanical properties. In segmented polyurethanes, hard domains act as physical crosslinks, playing a role similar to chemical crosslinks in vulcanizates and imparting the material's elastomeric behavior. Since hard domains also occupy significant volume and are stiffer than soft domains, they also function as effective nano-scale fillers and render a material behavior similar to that of a composite.**[PET 1991]** At room temperature, soft domains are above their glass transition temperature and impart the material its rubber-like behavior; hard domains are below their glassy or melt transition temperature and are thought to govern the hysteresis, permanent deformation, high modulus, and tensile strength. The domain structure also imparts TPUs' versatility in mechanical properties. A wide variety of property combinations can be achieved by varying the molecular weight of the hard and soft segments, their ratio, and chemical type.

As previously reported **[GUIF 2006]**, the carbonblack nanopowder (C) and silicon carbide nanotubes fillers (SiC) are used to enhance the electrostrictive properties. The optimal fraction volume for polyurethane (elastomer 58 888) filled with carbonblack nanopowder and silicon carbide nanotubes fillers shown at 1% and 0.5% by volume, respectively.

Moreover, to improve the energy harvesting and the actuation capability, the metal filler is one of attached choices. The concentration of the metal fillers has shown to be a significant parameter, governing the electrical behaviour of the metal-polymer composites. The increase of dielectric constant of metallic fillers in the insulating matrix e has been predicted to follow the power law (equation 3.9). **[DEV 2006] [QI 2006]**

For electrostriction use, the insulating behavior of the composite needs to be maintained and it is the main reason why the studied composites have been designed with low metallic fillers content, typically less than 5% in volume, to be far from the percolation threshold.

The dielectric properties of the composites depend on the volume fraction, size and shape of metal fillers including preparation method, interface either between the fillers and matrix or between the conductive and non-conductive phases.**[QUR 2008] [HUN 2007] [MIT 2004]** The composites with different metallic fillers, e.g., Fe, Ag, W, Zn, Cu and Ni, are also reported for increased electric properties. Cu is attractive because of its low density (8.94 g/cm^3) and low price. Especially, Qureshi et al. found that the dielectric constant of Cu filled composites is higher than Al filled into either PVC or PMMA composites.**[QUR 2008]**

In this chapter, the dielectric behaviour of the PU composites filled with SiC nanowire, CB nanopower and metallic fillers of Cu has been studied over a broad range of frequency (0.1 Hz-1MHz). The effect of fillers size on dielectric properties of composites has been also investigated. In addition of dielectric measurements, SEM imaging and glass temperature and melting temperature measurements with the help of Differential Scanning Calorimetry (DSC) have also been performed to visualize the fillers distribution and to investigate how it affects the microstructure of the composite. Moreover, their mechanical property has been also investigated by using Dynamic mechanical analysis (DMA). The table 3.4 shows the average particle size and density of filler.

Table 3.4 The density and size of fillers.

Type of filler	Density ($g.cm^3$)	Average particle size
Carbonblack nanopowder (C)	2.20	30 nm
Silicon carbide nanotubes (SiC)	0.60	diameters of 30 nm and lengths of 100 µm
Copper nanopowder (n-Cu)	8.94	100 nm
Copper micropowder(m-Cu)	8.94	10 µm

3.6 Experimental procedure

3.6.1.1. Preparation of the Polyurethane and composites filled with carbon black nanopowers and Silicon carbide nanotubes

The Estane 58888-NAT021 ether based thermoplastic polyurethane was selected as high level of hard segments. PU films were prepared through a solution casting method **[GUIF 2006]**. Films with fillers in addition to neat PU were also prepared by solution casting.

The PU granules were first dissolved in *N*,*N* dimethylformamide (DMF) under mixing at 80 °C (during 45 min) until the PU solution became homogeneous. Silicon carbide nanotubes fillers (with average diameters and lengths of 30 nm and 100 µm, respectively) or carbonblack nanopowder (with an average particle size is less than 50 nm, Aldrich 633100) was added to the solution and stirred at 80°C for 60 min until the mixture became homogeneous and had a suitable viscosity. An ultrasonic probe (Hielscher UP400S) was first used for 20 min to disperse the filler into the DMF before to be added to the solution. The procedure of the preparation of PU is shown in Fig. 3.15.

3.6.1.2. Preparation of Cu powder/polyurethane composites

The Noveon Estane 58888-NAT021 ether-based thermoplastic polyurethane was used as the polymer matrix with addition of either a copper nanopowder (Aldrich, 99.8%, <100nm) or a copper micropowder (Aldrich, 99%, <10μm) as fillers. The two types of composites were denoted MPU, when the copper micropowder was used, and NPU, when the copper nanopowder was employed.

The volume fraction of fillers varied from 0 to 4% vol. within the composites. The calculation of the volume fraction was based on the solid densities of the constituents. The filled polymer matrixes were prepared by a solution casting method, where N, N–dimethylformamide (DMF) was used as a solvent to dissolve the polymers. An ultrasonic probe was first used for 20 min to disperse the filler into the DMF. Then the mixture of polymers and fillers was stirred at 80^{o}C for 50-60 min.

Thin film fabrication

Fig.3.16 shows the steps for thin films preparation. 10ml of the obtained PU solutions were deposited on glass disc using a spin coating technique. The PU solution was dropped onto the glass and spun with the following conditions first step 200 rpm for 10s and second step 300 rpm for 20s. After deposition, the film was dried at 60 ^{o}C for 24 hr. After removing from the glass, the films were annealed at 130 ^{o}C for 3hr, for a complete elimination of the solvent. Gold electrodes were sputtered on both sides of the samples for dielectric measurements. The film samples were used for dielectric coefficients and energy harvesting densities measurement.

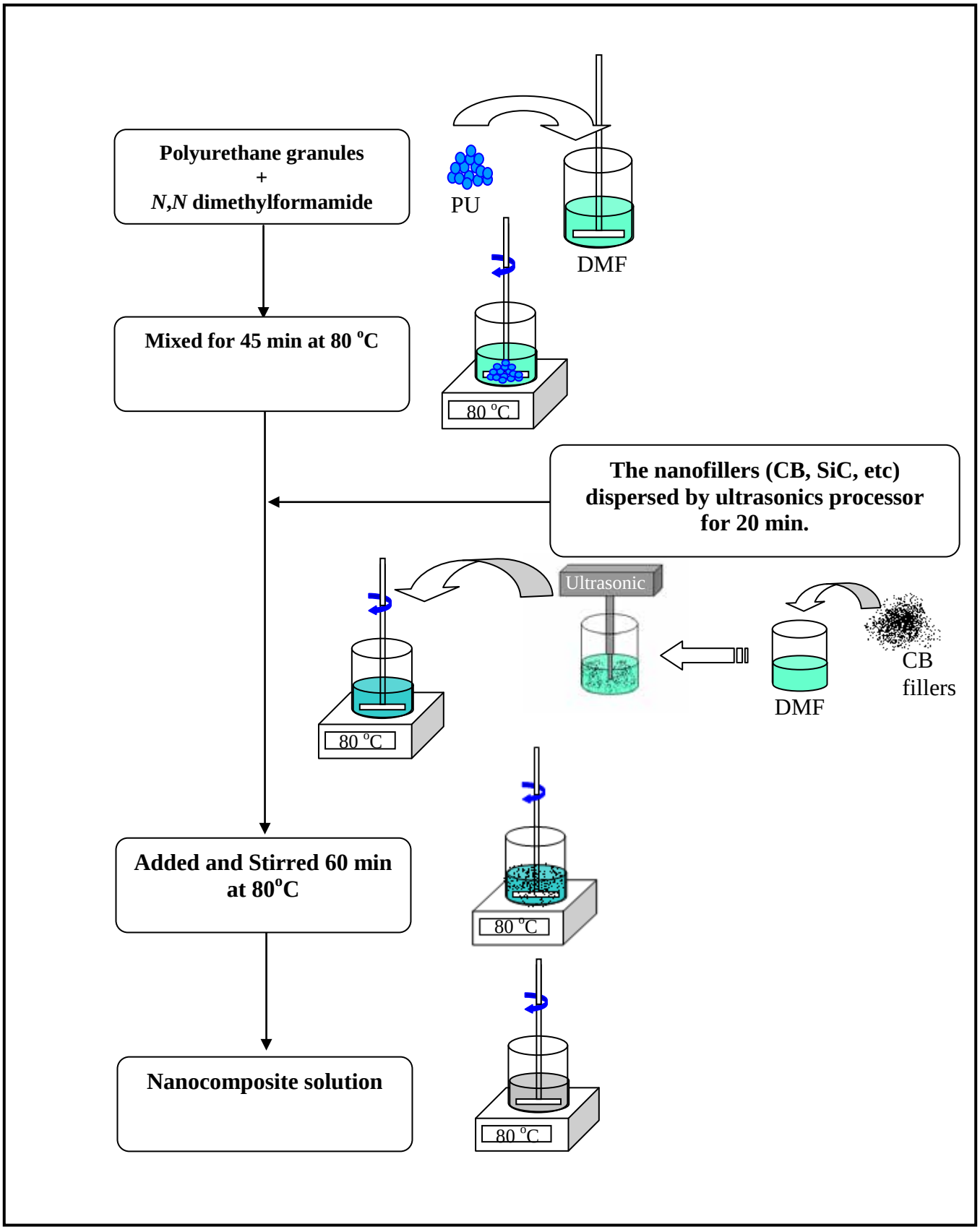

Fig. 3.15. Flow chart of the PU composites solution process.

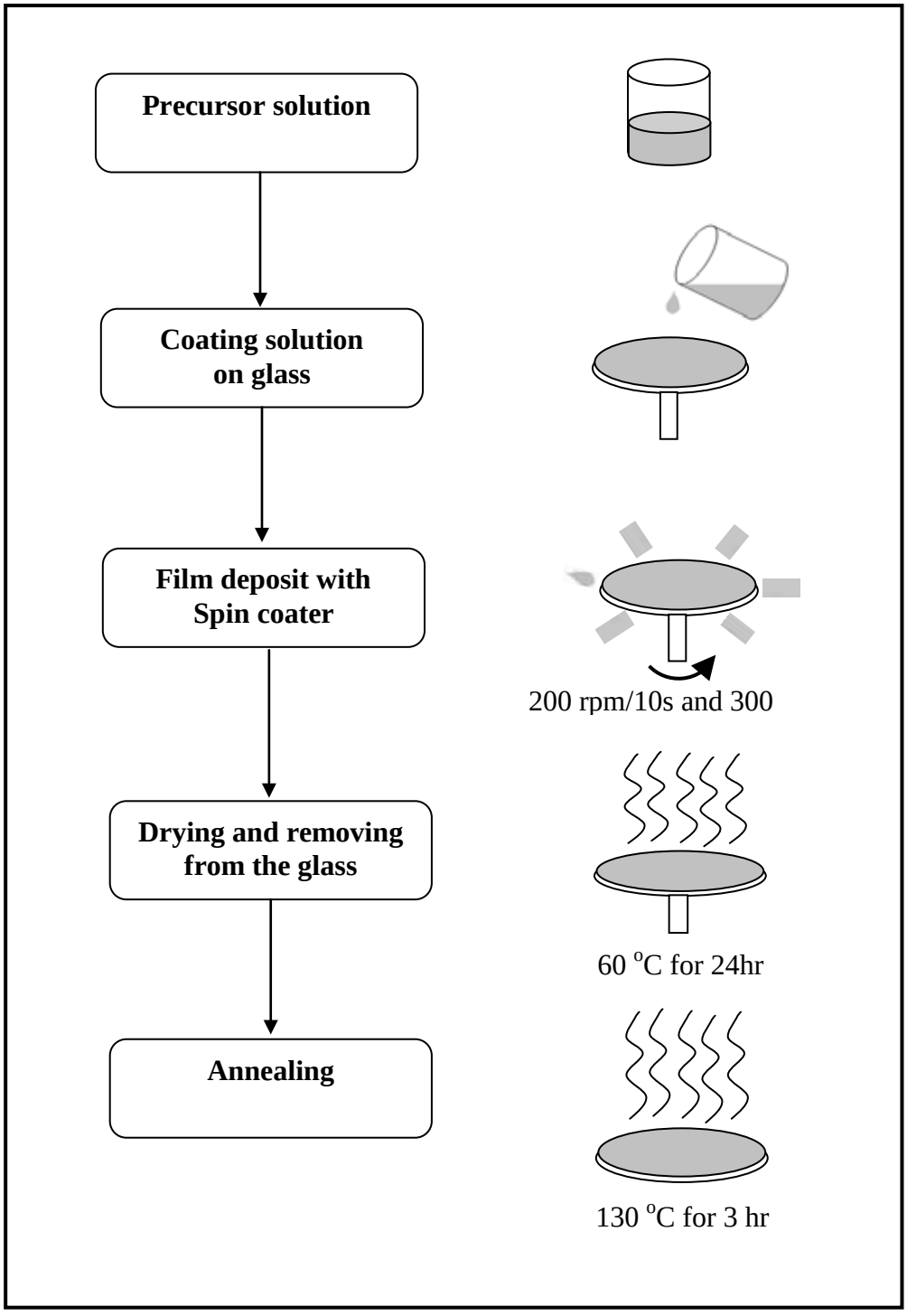

Fig. 3.16. Flow chart of the PU composites films fabrication.

3.6.2. Preparation of the P(VDF-TrFE-CFE) and composites filled with nano charges.

A P(VDF-TrFE-CFE) terpolymers, Ter22 (piezo tech S.A.S.), was selected as the working matrix, and P(VDF-TrFE-CFE) films were prepared through a solution casting method. In addition to P(VDF-TrFE-CFE) samples, films of filled polymer were prepared also by solution casting.

At first, the P(VDF-TrFE-CFE) solution was prepared by dissolving the granules in an appropriate solvent.

For composites filled with nano-charges, carbonblack nanopowder (Aldrich, 633100) was added to the P(VDF-TrFE-CFE) solution. An ultrasonic processor (Hielscher UP400S) was used for 30 min to disperse the filler into the solution, then was stirred for 30 min until the mixture became homogeneous.

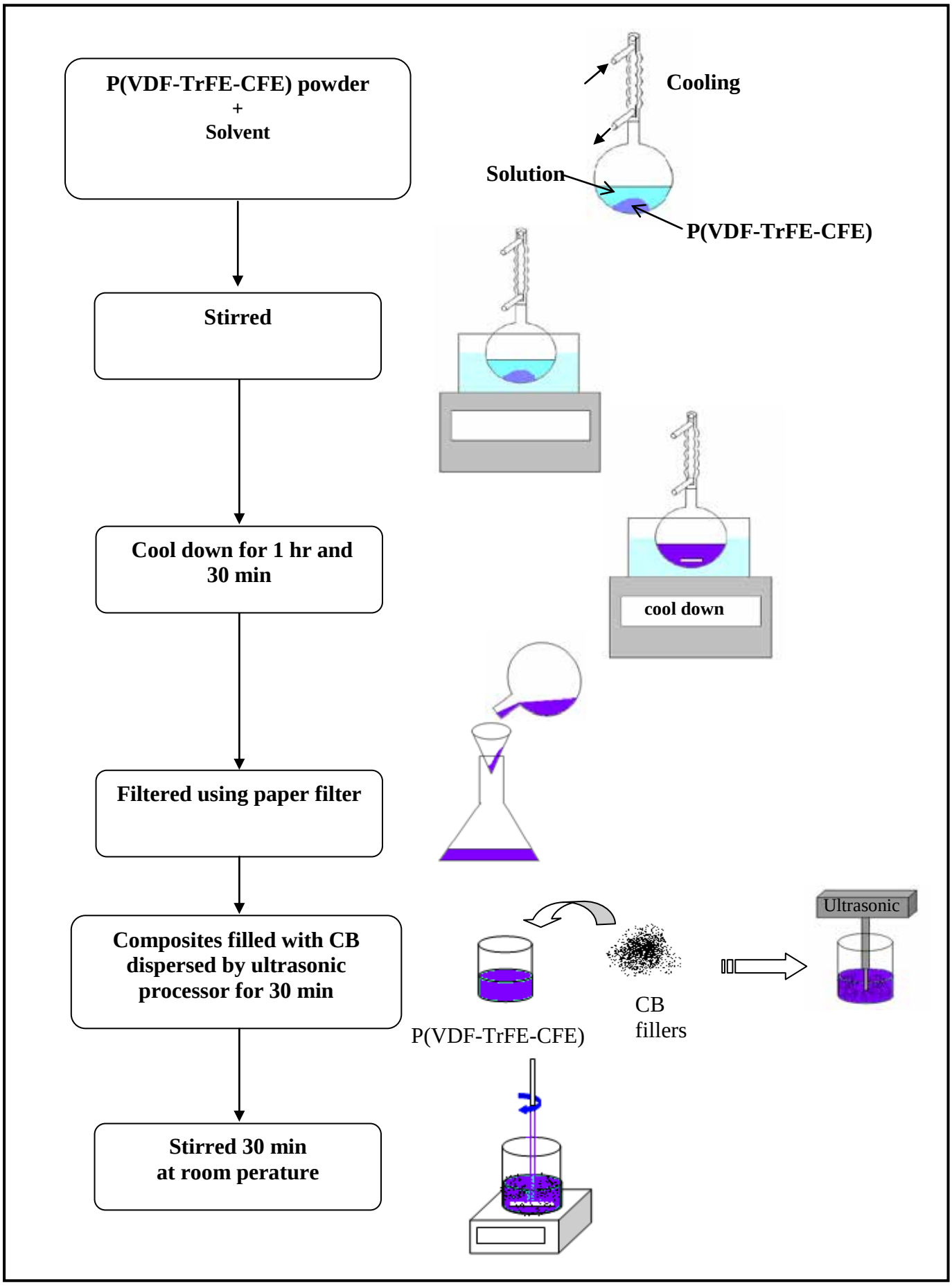

Fig. 3.17. Flow chart of the P(VDF-TrFE-CFE) composites solution process.

3.6.3 Dielectric characterization

For the dielectric characterization, gold was sputtered on both sides of the films to form electrodes (diameter of electrodes of 20 mm). The capacitances of the films were measured using a HP 4284A *LCR* meter over a broad range of frequencies (from 0.1 Hz to 1 MHz) at room temperature. At extra low frequency (0.1 Hz), the dielectric constant and dielectric loss of all specimens were obtained using a lock-in amplifier (SR 830) combined with a current amplifier (Keithley 428). The lock-in amplifier measures both amplitude and phase of the current of the specimen under low field dielectric properties. Samples thickness is 100 +/- 5 µm in all case. The dielectric constant ε_r can be calculated using equation, $\varepsilon_r = \frac{Ct}{\varepsilon_o A}$.

3.6.4 Mechanical tensile measurement

The Uniaxial tensile tests (nominal rates of 10^{-1} s^{-1}) were performed using a load sensor setup under conditions of constant nominal strain rate, as depicted in Fig. 3.18(a). The deformation and strain rate of sample was driven by a function generator through the controlled Newport and computer. The force sensor was used to estimate the stress during an elongation. The specimen was clamped both on the two sides with aluminum bar, as shown in Fig 3.18(b). Sheets of specimen of about 70 mm in thickness were cut into rectangular of about 1cm ´ 3cm. Specimens were subjected to constant true strain rate loading-unloading cycles and the true stress vs. true strain curve cycle was documented for each test.

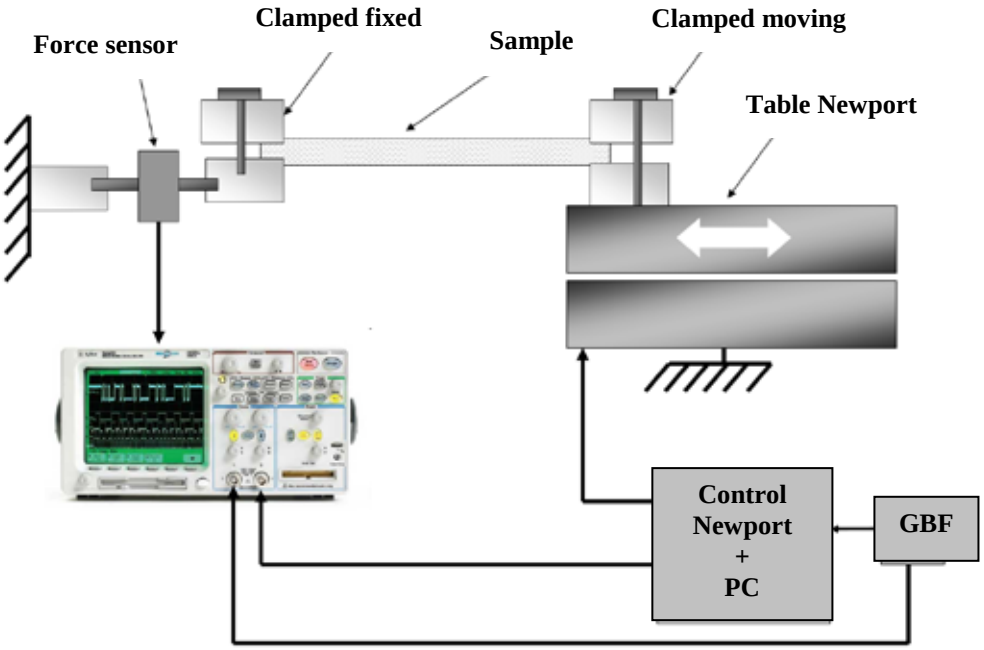

(a)

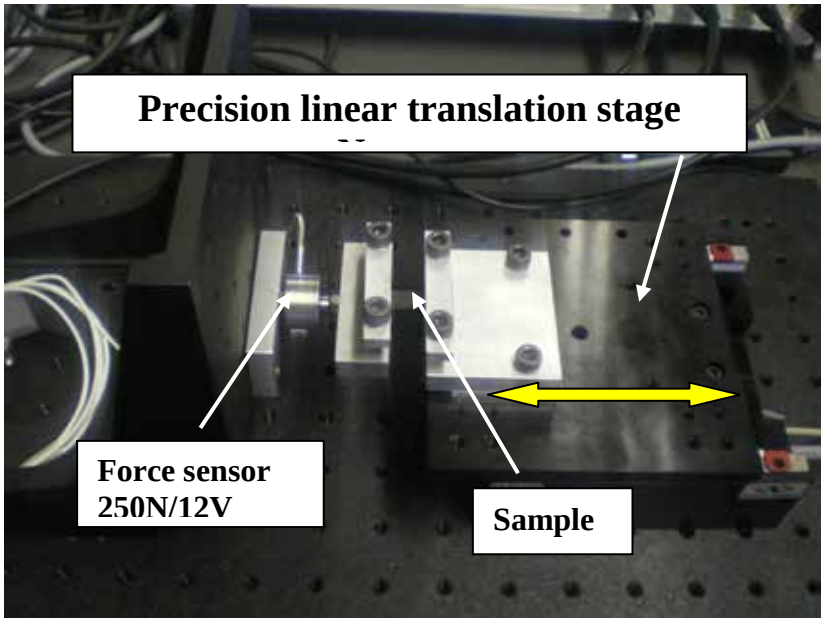

(b)

Fig. 3.18. (a) Schematic and (b) photo of the Uniaxial tensile tests setup.

3.6.5 Thermal DSC measurement

The Thermal analyse was performed by Differential Scanning Calorimetry with DSC 131Evo (SETARAM, France) under an argon atmosphere. The specimens (~22mg) were placed in a closed aluminium pan and were cooled from ambient temperature down to -100^{o}C then heated to 210^{o}C (10^{o}C/min heating rate) and finally cooled to 25^{o}C (10^{o}C/min cooling rate).

3.7 Results and discussions

Previous studies in our laboratory have in particular shown that the actuation properties can be greatly enhanced by adding carbon black nanopowder and SiC naowires incorporation in polyurethane matrix.**[GUI 2006][GUI 2009]** It is possible that this addition can also enhance the energy harvesting capability of composites. Therefore, carbon black nanopowder and SiC nanowires are firstly utilized as incorporation in polyurethane matrix. The results of dielectric properties, which is crucial parameter for energy harvesting, and Young modulus, which relates to the strain response for actuator material, are shown in 3.7.1.

3.7.1 Experimental results on PU, PU-C and PU-SiC composites

3.7.1.1 Microstructure characterization for PU and composites filled with C nanopowder and SiC nanowire.

Scanning electron microscopy images of the fracture surface of the PU-C nanopowder and PU-SiC nanowire composites are presented in Figure 3.19 and 3.20, respectively.

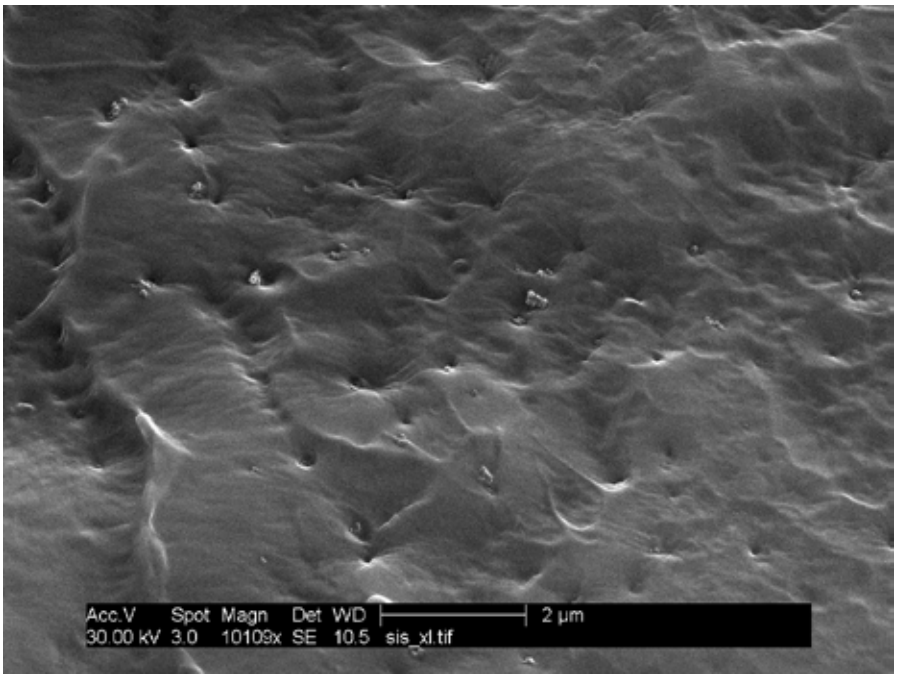

Fig. 3.19. SEM fracture surface of the PU filled with C nanopowder.

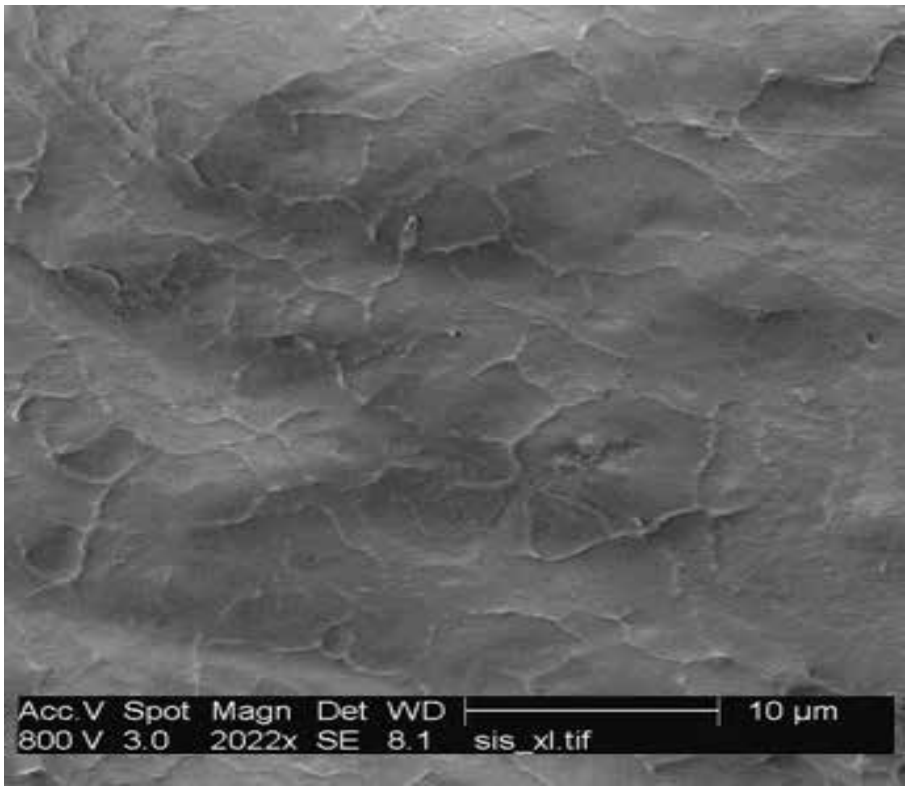

Fig. 3.20. SEM fracture surface of the PU filled with SiC nanowire.

The degree of filler dispersion in the polymer matrix and the binding between nano-charges and matrix determine the properties of the composite materials. Fig. 3.19 and Fig. 3.20 respectively depicted carbon black nanopowder at 1% by volume and SiC nanowires at 0.5% by volume dispersion within the PU matrix. They showed a rather good dispersion of the both fillers in good agreement with the non conduction state observed on composites.

3.7.1.2 Dielectric constant for PU and composites filled with C nanopower and SiC nanowire.

The variation of dielectric constants for a pure PU composite and filled composites versus frequency is shown in Figure 3.21. The frequency dependence of the effective loss tangent for a pure PU composite and filled composites is shown in Figure 3.22. The capacitance of these films is performed over the frequency range from 0.1 Hz to 1 MHz.

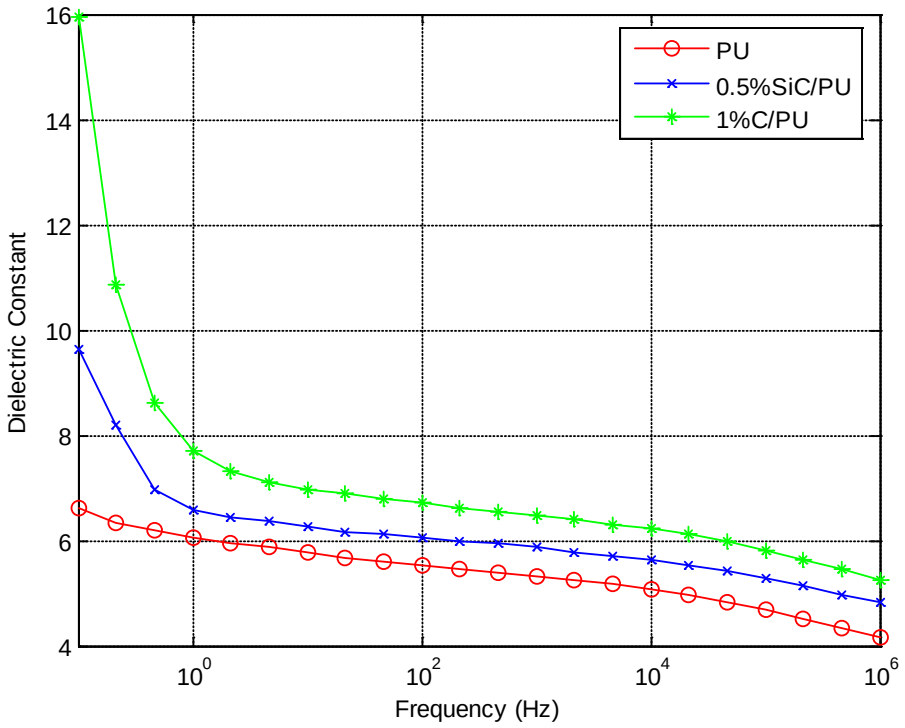

Fig. 3.21. Variation of the dielectric constant for a pure PU composite and filled composite versus frequency.

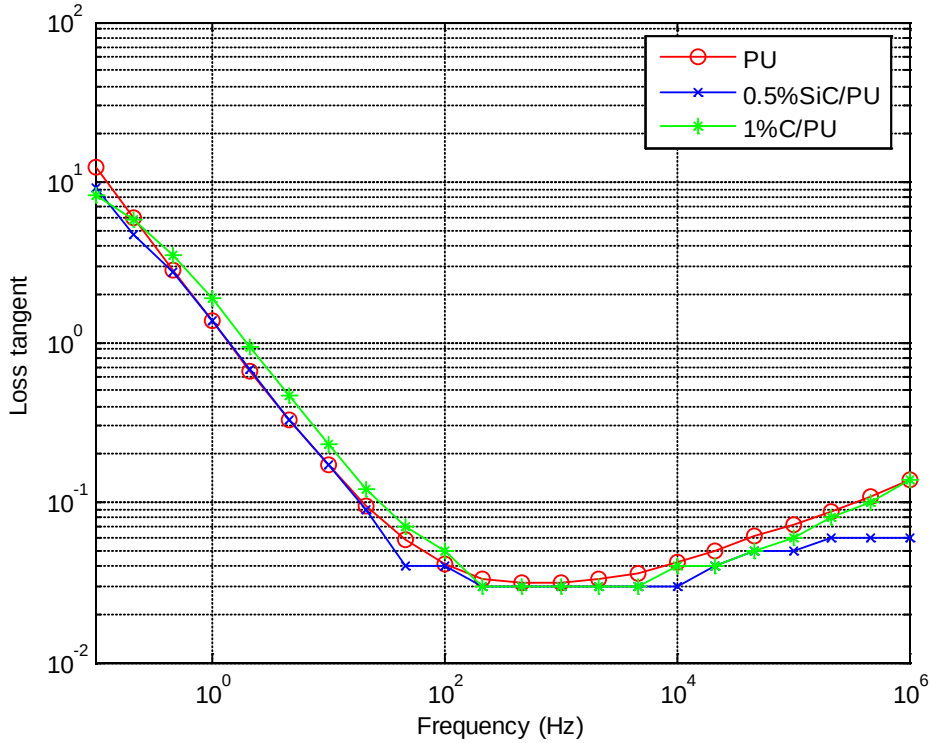

Fig. 3.22 Variation of the dielectric loss for a pure PU composite and filled composite versus frequency.

Figure 3.21 shows the variation of dielectric constants for a pure PU composite and filled composites versus frequency. A large decrease of the dielectric constant is observed around 1 Hz for both composites when the frequency increases. Such behaviour is known to be due to the loss of one of the polarization contribution (interfacial polarisation, orientation polarisation, electronic polarisation, atomic polarisation…) of the dielectric constant value.**[MIT 2004]** Considering the value of the frequency, this decrease can be unambiguously attributed to the loss of the space charges induced interfacial polarization contribution and it can been seen that the contribution of the space charge can be neglected for frequencies higher than tens of Hertz.

As shown on figure 3.21, the dielectric constant of the C nanofilled and SiC nanofilled composites is always higher than this one of the pure PU composite. As expected, at higher frequencies, the gap between the values of the dielectric constant for pure PU and nano filled composites is not so high, which confirms the fact that the fillers content is low compared to the threshold value. Moreover, the space charge

mechanism does not contribute to the dielectric constant. At lower frequencies (less than 1 kHz), the gap between the values of the dielectric constant for pure PU composites and the composites with C fillers is a bit higher that this one observed at 20 Hz. The incorporation of conductive charge has also probably increased the space charge density in addition to these intrinsically induced by the existence of soft and hard segments within the matrix. Similar observations have been reported by Z M Dang et al., who assumed an additional contribution to the quantity of accumulated charge when fillers are used.**[DAM 2004]**

As previously reported **[NUR 2006]**, the percolation threshold not only depends on the size, shape, and spatial distribution of the fillers within the polymeric matrix but also on the processing. It is clear that the percolation threshold must be different for the SiC nanowires and the carbon black powder used as the fillers for the studied composites. This remark can explain the slight difference observed between the permittivity of the two composites in addition to the fact that the two fillers have not been incorporated with the same content.

Figure 3.22 shows the variation of dielectric loss for a pure PU composite and filled composites versus frequency. Wherever, the value of dielectric loss for the composites filled with nano-charges is closely equal the value of the polyurethane.

3.7.1.3 Mechanical behaviour for PU and composites filled with C nanopower and SiC nanowire.

The uniaxial tensile tests stress-strain behavior of polyurethane and composites was examined using the techniques described in Section 3.6.4. The true stress-train curves cycle for PU and composited filled with SiC and C fillers are presented in Fig.3.23.

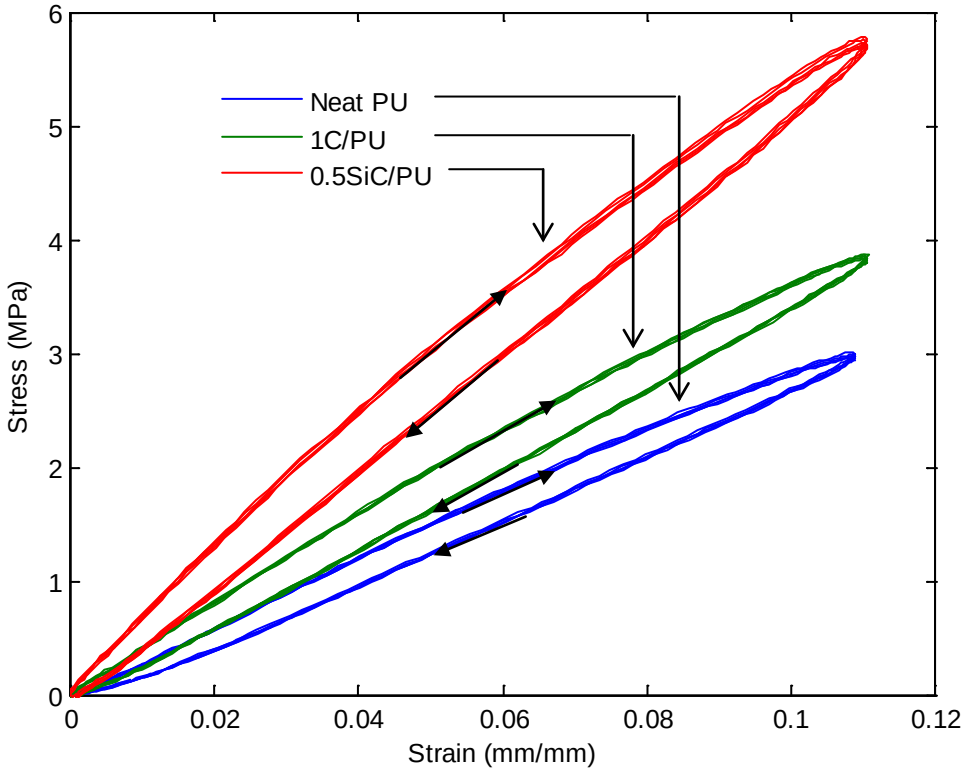

Fig. 3.23. Stress-Strain behavior of PU and composite filled with SiC and C nano-fillers at strain rates of 10^{-1} s^{-1}.

The uniaxial tensile stress-strain behaviour is observed to be non-linear and fillers dependent. The cycles show an initially relatively stiff behavior followed by a rollover to a more compliant behavior at low strains, with the stress magnitude depending on fillers. The highest stress for a given strain was observed on composites filled with SiC nano-wire. Previously, Nurazareena *et al.* reposted that the shape of fillers and fillers distribution might influence the tensile strength of the composites materials.**[NUR 2006]** In agreement with Nurazareena paper, Rusu et al. also reported that the tensile strength of the composites which is larger than that of neat, may be explained by change of crystalline polymer degree and polymer crystalline structure.**[RUS 2001]** The increased tensile stress may be due to good interaction and interfacial adhesion between PU and filler, which seems that the inclusion restricting molecular motion.

3.7.2 Experimental results on pure PU and composites filled with Cu loading

Polyurethane-based metal-filler composite was also prepared by incorporating copper filler in order to improve the energy harvesting and the actuation capability. Previous, Qureshi et al. found that the dielectric constant of Cu filled composites is higher than Al filled and dielectric loss is lower than Al into either PVC or PMMA composites.**[QUR 2008]** The dielectric properties of the composites depend on the volume fraction, size and shape of metal fillers.**[QUR 2008]** Therefore, copper filler is choice because spherical powders was available at the micron and nanoscale. The effect of copper fillers size (micro and nanopowders) on microstructure, dielectric constant, Young modulus and thermal behaviour using DSC is investigated.

3.7.2.1 Microstructure characterization for PU and composites filled with Cu loading

Scanning electron microscopy images of the fracture surface of the PU filled with the copper micropowder, MPU and the PU filled with the copper nanopowder, NPU composites are presented in Figure 3.24 and 3.25, respectively.

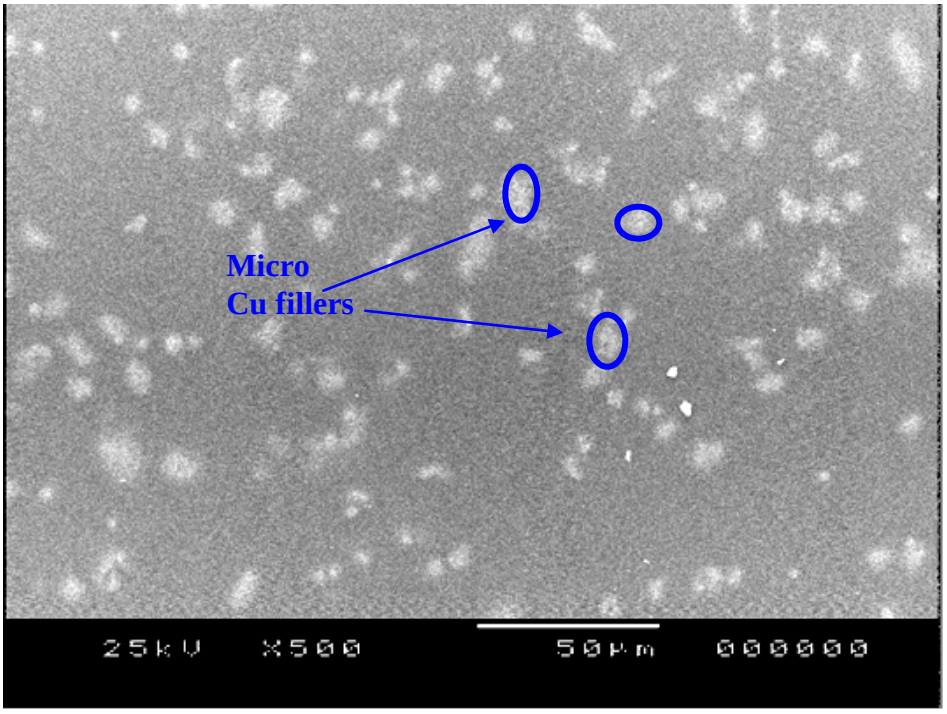

Fig. 3.24. SEM micrograph of micro Cu fillers at 3 % by volume in PU matrix.

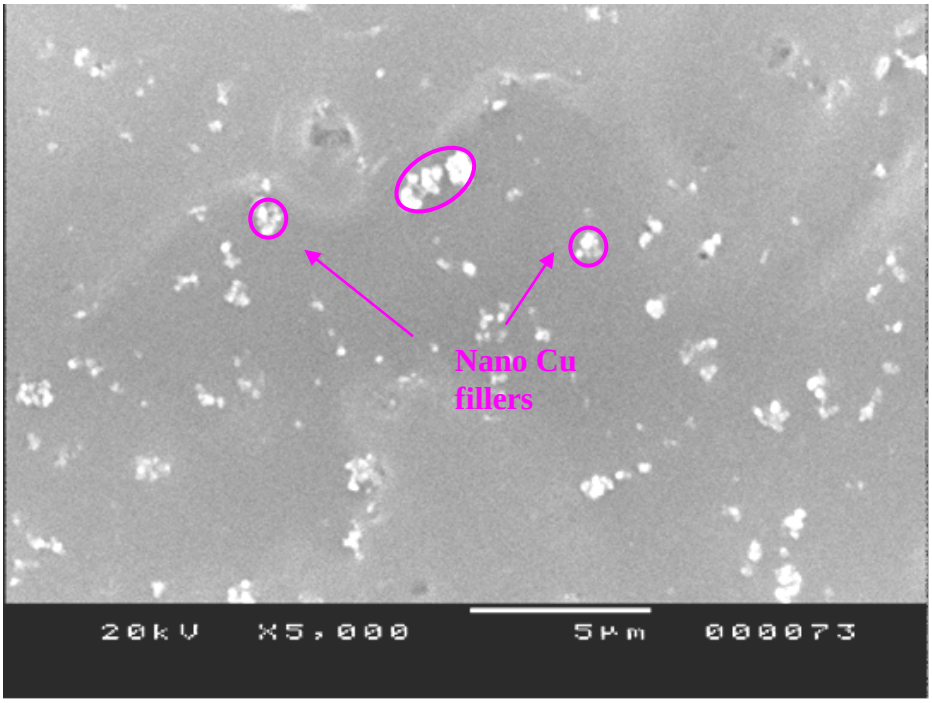

Fig. 3.25 SEM micrograph of nano Cu fillers at 3 % by volume in PU matrix.

Scanning electron microscopy images of the fracture surface of MPU and NPU composites are respectively presented in figure 3.24 and figure 3.25. Figure 3.24 shows that the micron-sized copper fillers including a small amount of their agglomerated particles homogenously dispersed in the matrix. A similar manner was shown in figure 3.25 for the case of the copper filler of nano-size with, however, tiny clusters..

3.7.2.2 Dielectric constant for PU and composites filled with Cu loading

Dependence of the dielectric constant on the frequency at room temperature for MPU and NPU composites is shown in Figure 3.26 and 3.27, respectively.

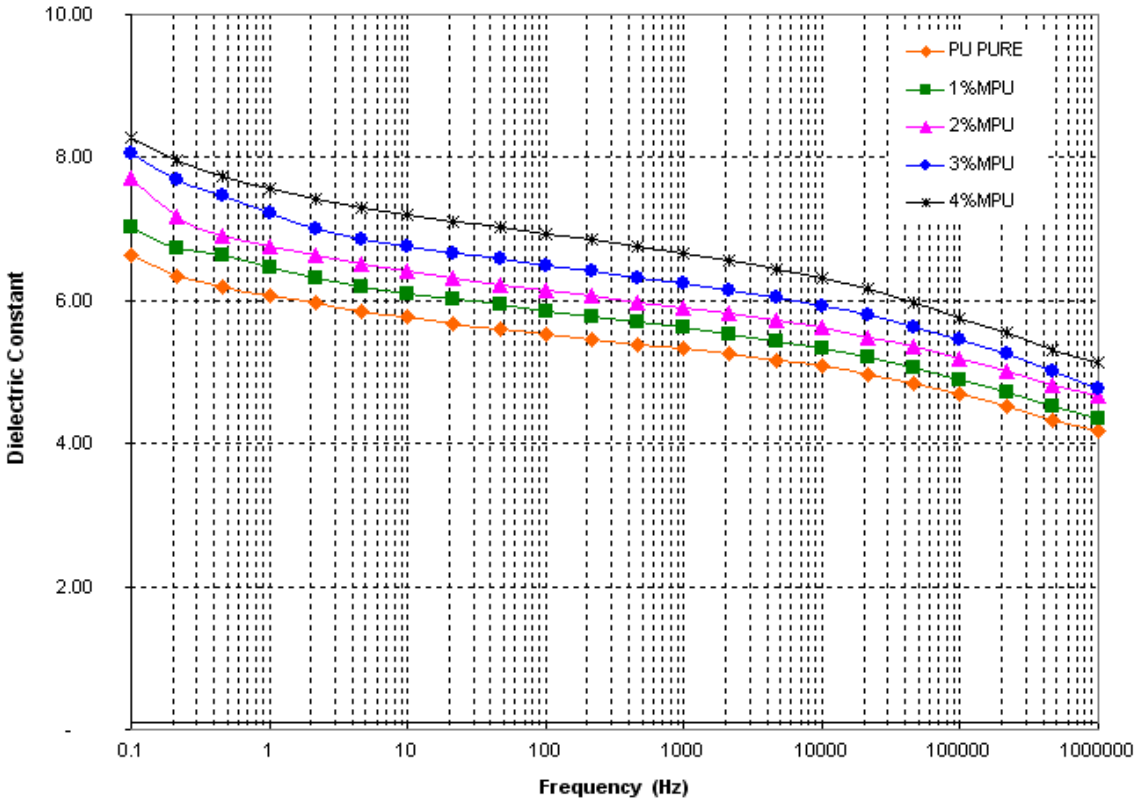

Fig. 3.26. Frequency dependences of dielectric constant for composites with micro Cu fillers at room temperature.

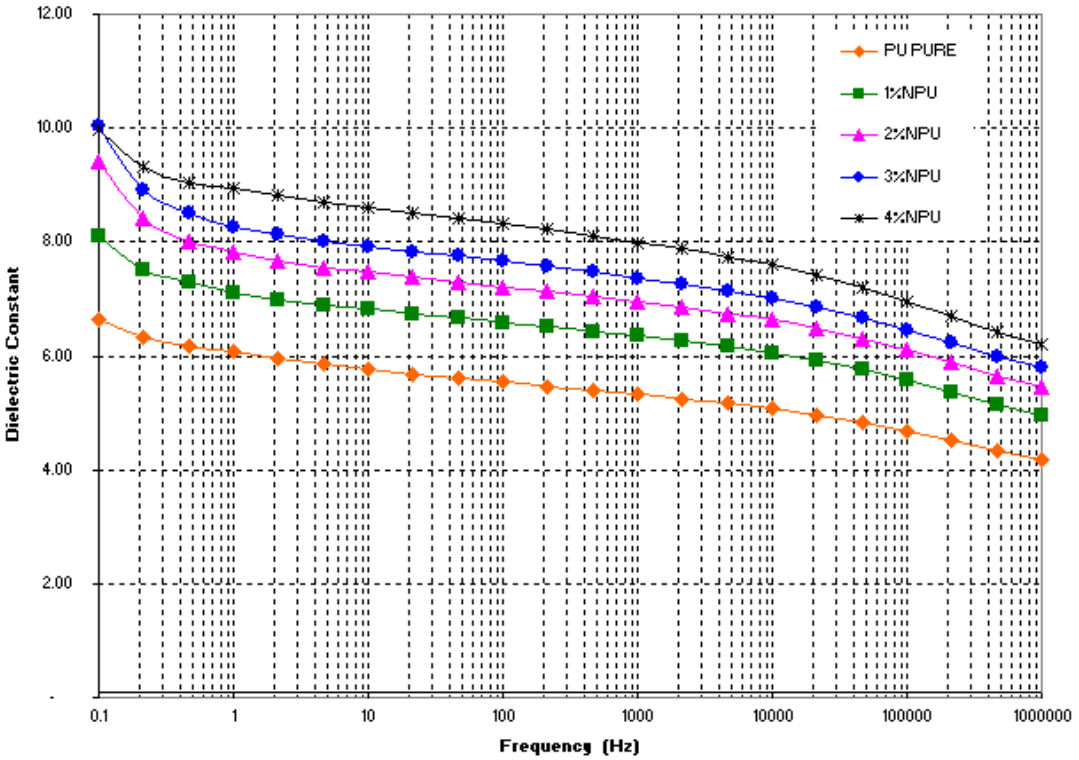

Fig. 3.27. Frequency dependences of dielectric constant for composites with nano Cu fillers at room temperature.

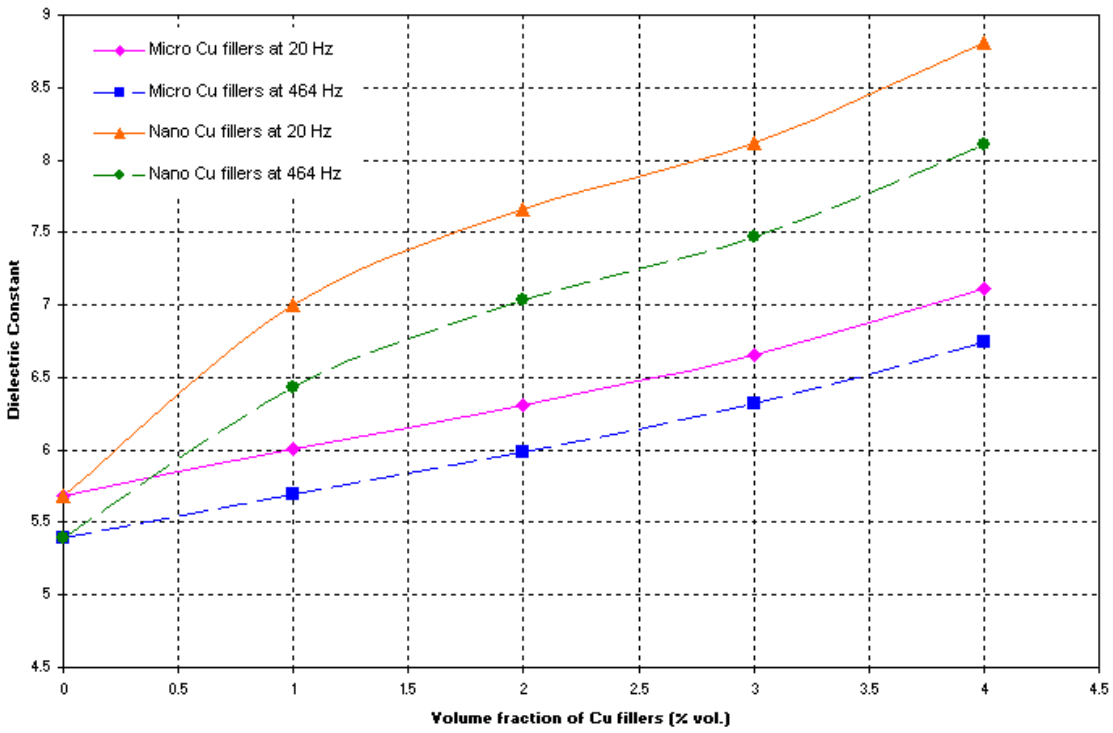

Fig. 3.28. Plot of dielectric constant versus volume fraction of filler at frequency of 20 Hz and 464 Hz.

Figures 3.26 and 3.27 depict the frequency dependence of the dielectric constant of the MPU and NPU composites versus the volume content of fillers.

For all composites, the dielectric constant slowly decreases when the frequency is increased. Moreover, it is noted that dielectric constant increases with increasing fillers concentration whatever the frequency is.

As the same behaviour is observed whatever the frequency is and in order to increase the readiness, figure 3.28 depicts the dielectric constant of both MPU and NPU composites versus content only for two frequencies.

As previously reported on figures 3.26 and 3.27, the dielectric constant increases when the filler content is increased. At a given frequency, the increase of the dielectric constant versus content is higher for the NPU composites than for the MPU composites.

Due to the fillers and to the two types of segments which exist in PU, the composite can be considered as an heterogeneous material. Consequently, an interfacial Maxwell-Wagner type polarization exists within the sample and its effect increases as the filler content is increased. This polarization contributes to the increase of the permittivity constant value versus filler content. This observation is also in good agreement with the assumed power law $\varepsilon = \varepsilon_i \left| (f_c - f) / f_c \right|^{-q}$ frequently published for composite filled with conductive particles. This law predicts an increase of the dielectric constant when the filler content (f) is increased.

Mechanisms of polarization strongly depend on the frequency and tend to disappear when the frequency is increased. Maxwell-Wagner type Polarization is known to be active at the lowest frequency that explains why a decrease of the dielectric constant is observed when the measurement frequency is increased.

The percolation threshold depends on the size and on the dispersion of the fillers within the matrix. This threshold decreases when the filler size decreases. This is why the dielectric constant of NPU composite is always higher than the dielectric constant of MPU composites, for a given content.

Dependence of the dielectric loss on the frequency at room temperature for MPU and NPU composites is shown in Fig. 3.29 and 3.30, respectively.

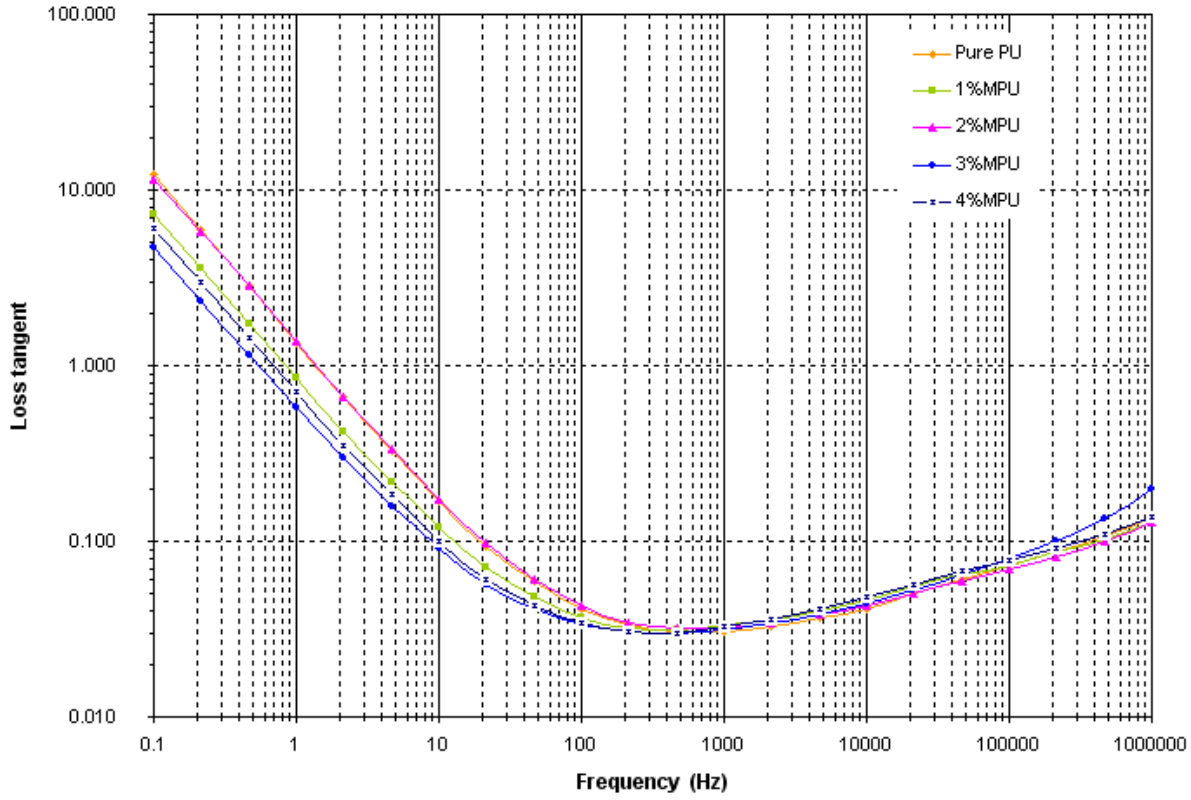

Fig. 3.29. Frequency dependences of dielectric loss for composites with micro Cu fillers at room temperature.

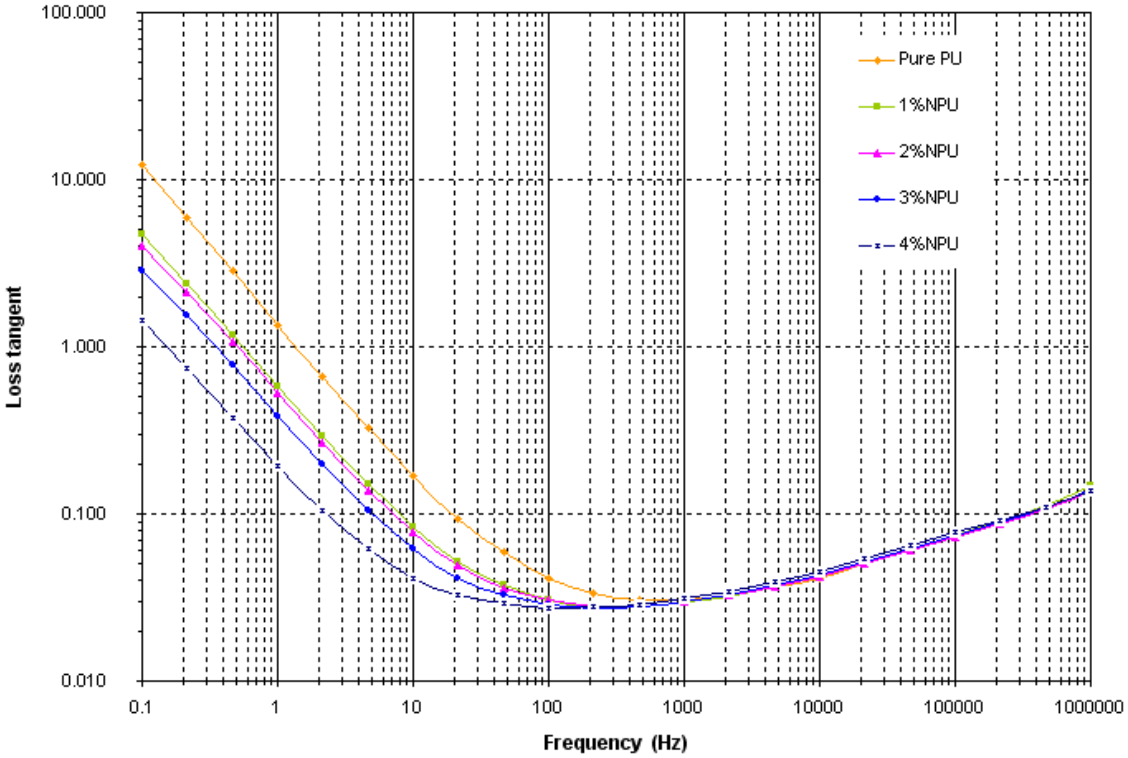

Fig. 3.30. Frequency dependences of dielectric loss for composites with nano Cu fillers at room temperature.

Fig. 3.29 and 3.30 depict the frequency dependence of the effective loss tangent for NPU and MPU composites. For both MPU and NPU composites, a minimum of the effective loss tangent is observed when the frequency is increased, starting from very high values at the lowest frequency (0.1 Hz) and reaching almost the same lowest value (0.030) at around 100 Hz, whatever the composites are. In addition, for NPU composites, the effective loss tangent decreases when the filler content is increased, from 0 to 4%vol., whatever the frequency is. For MPU composites, the difference of effective loss tangent values versus fillers content is smaller even at the lowest frequency. In addition, the effective loss tangent does not regularly vary with the filler content.

By assuming that $\tan\delta = \frac{\varepsilon''}{\varepsilon'} + \frac{\sigma}{\omega\varepsilon_0\varepsilon'}$, the contribution of the conductivity σ to the effective losses tan δ clearly decreases when the frequency increases leading to a decrease of tan δ versus frequency.

The observed decrease of the effective losses of NPU versus fillers content is not yet clearly understood. Due to the low contents of fillers used to prepare the composite,

it is reasonable to assume that the studied compositions are far away from the percolation and as a consequence that the conductivity σ does not change a lot. In this case, as ε' slightly increases with filler content (cf. for example figure 3.28), then $\frac{\sigma}{\omega\varepsilon_0\varepsilon'}$ decreases. However, it is not possible to predict the evolution of $\frac{\varepsilon''}{\varepsilon'}$ as the single contribution of ε'' cannot be determined but it can be assumed that if the effective area of the active interfaces (particles/matrix) decrease due to the agglomeration of the nanoparticles (Hung et al), the contribution to the dielectric losses (ε'') will also decrease. In this case, the observed decrease of the effective losses for NPU composites could also be attributed to an increase of nanoparticle of copper agglomerates as the content is increased. Unfortunately, the agglomerates versus content cannot be accurately quantified with the help of SEM.

3.7.2.3 Dielectric properties as a function of temperature

The dielectric constant is the key parameter for energy harvesting. It is important to study their behaviour versus frequency and temperature because they are one of the extrinsic parameter that changes with the targeted application. The dielectric constant at various content of PU composites as a function of temperature are depicted in Figure 3.31. There is a significant change of the dielectric constant of the sample with increasing temperature from 25 ^{o}C to 125 ^{o}C and returning to same rate condition. The dielectric constant decreases with increasing the temperature, then increases when the temperature is cooling. The changing of the dielectric constant with increasing and decreasing the applied temperature does not follow the same path.

For each frequency, the dielectric constants while increasing the temperature are larger in value than that while decreasing temperature. It is also of interest to see that the dielectric constant value decreases after a temperature cycle.

Furthermore, as shown in Figure 3.31, the dielectric constant at a constant temperature also changes with frequency. The dielectric constant decreases significantly when the measuring frequency increases from 100 Hz to 100 kHz. The gradually trend is similar for the dielectric loss tangent (as shown in Figure 3.32). At each measuring frequency, the dielectric loss tangent increases with increasing the temperature and then slightly increases when the temperature is cooling. The dielectric loss tangent is also

found to increase a little bit after a temperature cycle. Champa et al. reported that hydrogen bonding (H=N) of polyurethane can be formed in the amorphous and crystalline phases.**[CHA 1997]** Davis et al., reported that the reduction of dielectric constant is due to the changes in crystalline phase and dipole orientation.**[DAV 1982]** Moreover, Champa et al also presented that the net dipole orientation from the crystal and amorphous regions was reduced with an increase in temperature. Due to these effects, the dielectric constant can be decreased when the temperature of the samples was increased. In addition, it may be attributed that the amorphous phase crystallized and the dipoles of the crystallized phase are fixed by the hydrogen bonding. Therefore, the dipole polarization in the samples should be decreased in the cooling process compared with the heating process. It can also explain the dielectric loss peak shift to the higher temperatures in cooling process.

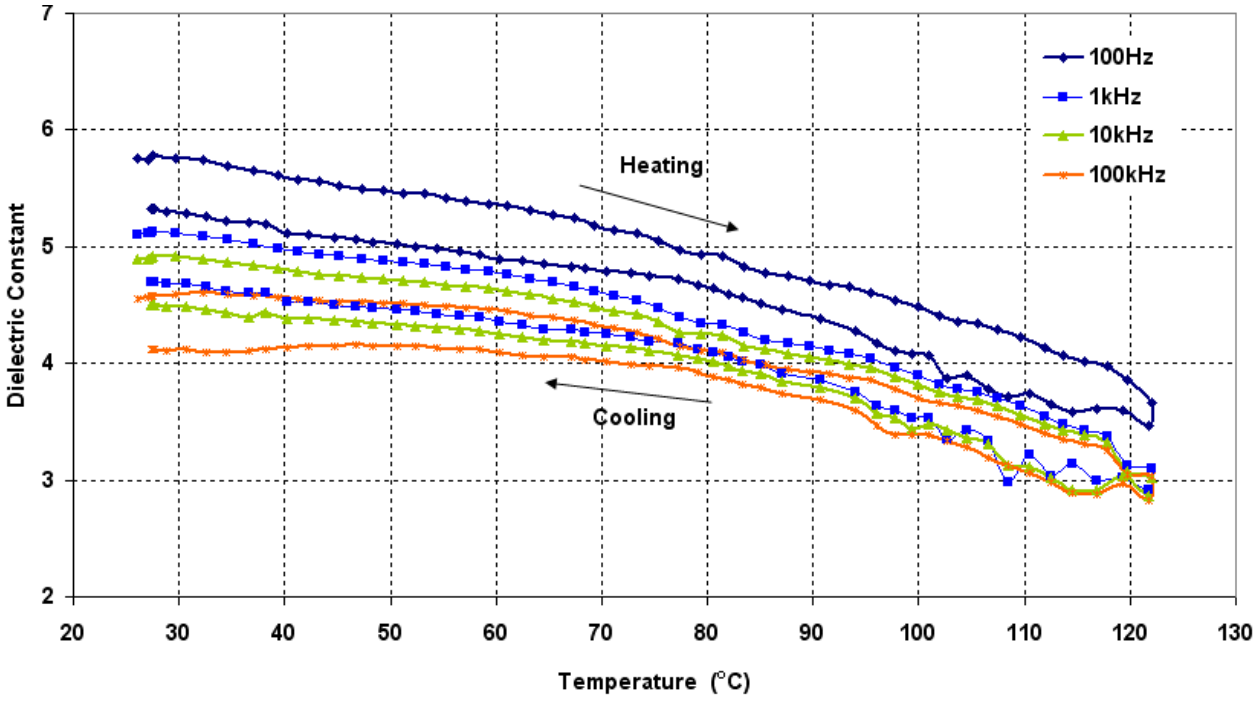

Fig. 3.31. Dielectric constant as a function of temperature for neat PU at various frequencies.

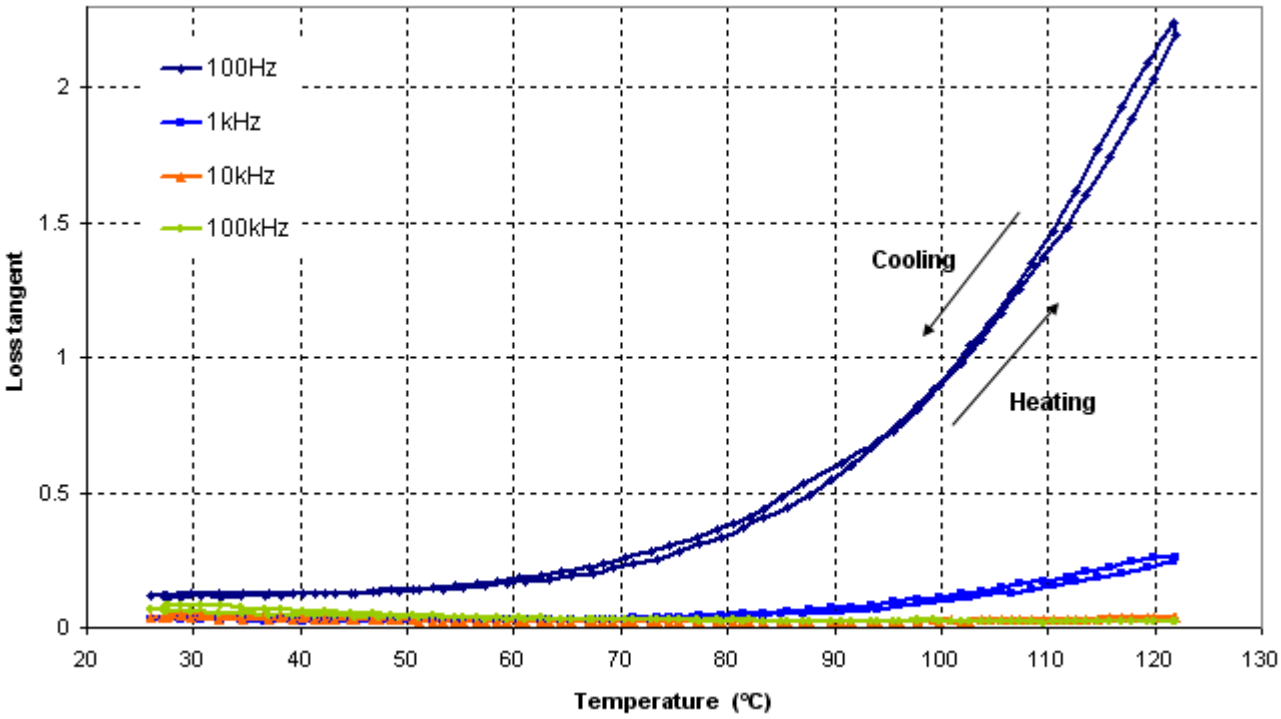

Fig. 3.32. Loss tangent as a function of temperature for neat PU at various frequencies.

Figure 3.33 and 3.35 show the dielectric constant at various contents of MPU and NPU composites as a function of temperature, respectively. The dielectric constant decreases monotonically with the increasing of the temperature, then increases only slightly when the temperature is gradually decreased. For all composites, the dielectric constants with increasing the temperature are as well as with decreasing temperature when contents are increased. The value of dielectric constant at constant temperature increases when content is increased. The trend is opposite for the dielectric loss tangent of MPU(as shown in Figure 3.34). The loss tangent of NPU composites (Figure 3.36) significantly decreases with increasing content at high temperature.

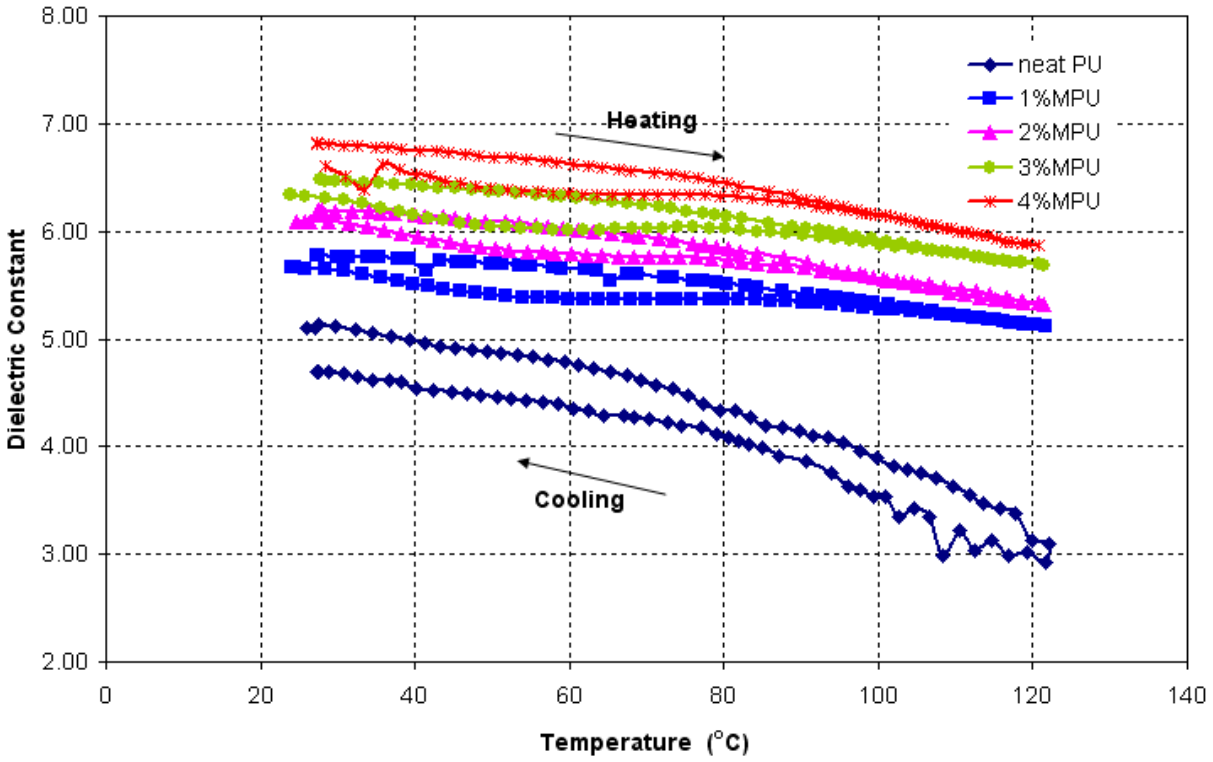

Fig. 3.33. The dielectric constant as a function of temperature at various contents for MPU composites at 1 kHz.

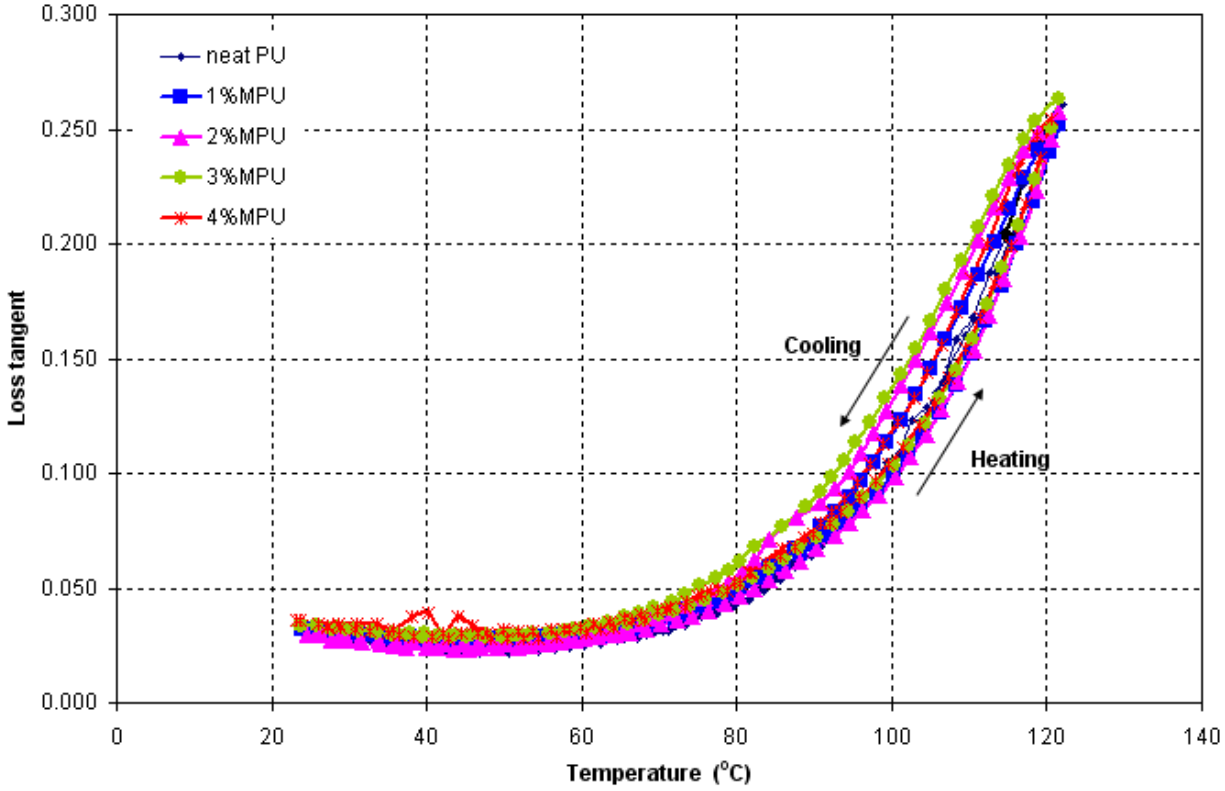

Fig. 3.34. Loss tangent as a function of temperature at various contents for MPU composites at 1 kHz.

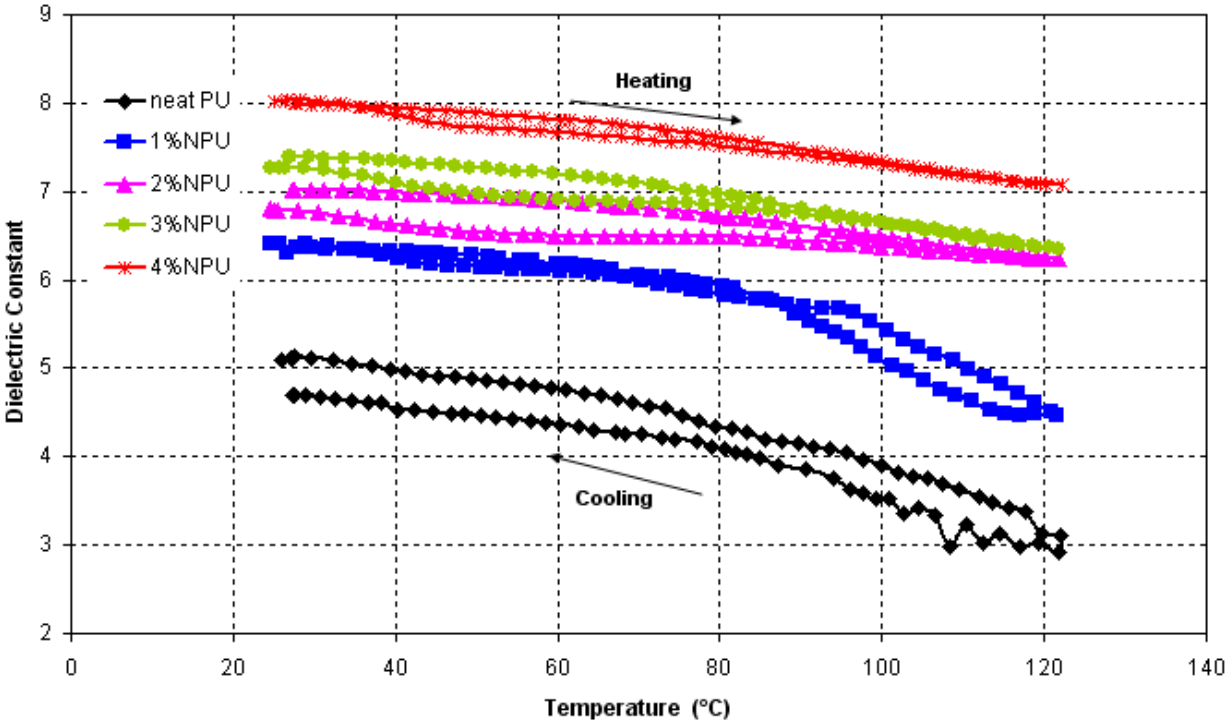

Fig. 3.35. The dielectric constant as a function of temperature at various contents for NPU composites at 1 kHz.

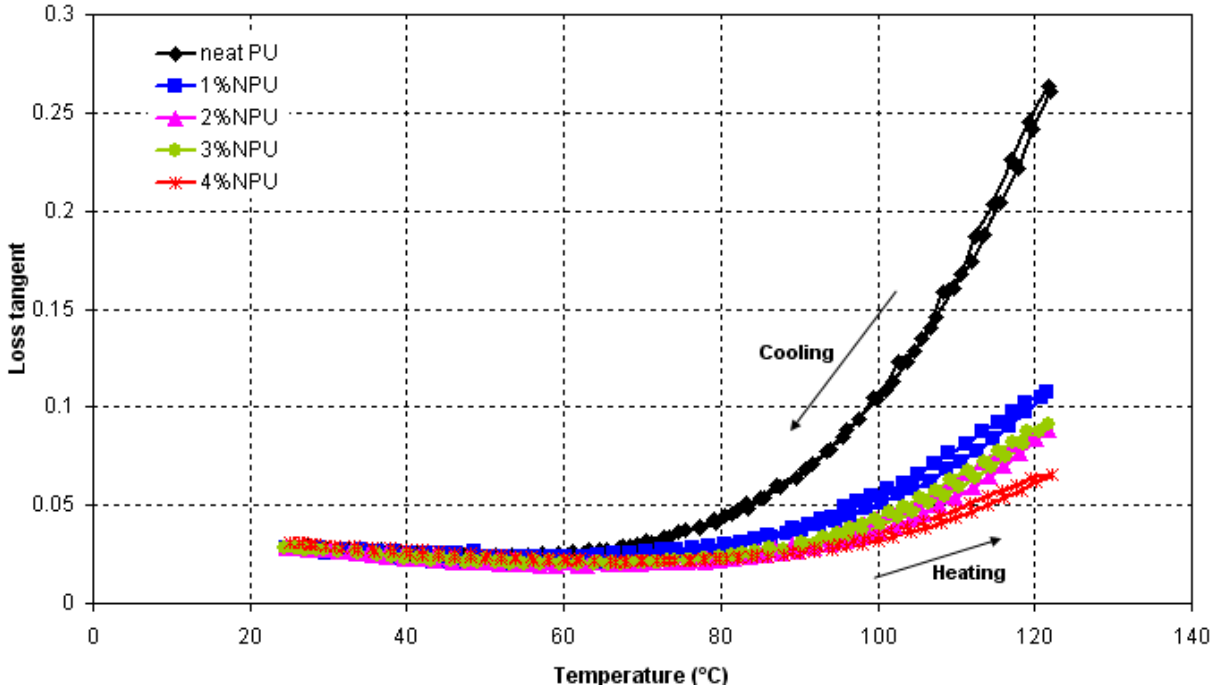

Fig. 3.36. The loss tangent as a function of temperature at various contents for NPU composites at 1 kHz.

3.7.2.4 Mechanical behavior for PU and composites filled with Cu loading

Fig. 3.37 shows the Stress-Strain behavior of PU and composite filled with (a) micro Cu and (b) nano Cu powders at strain rates of 10^{-1} s^{-1}.

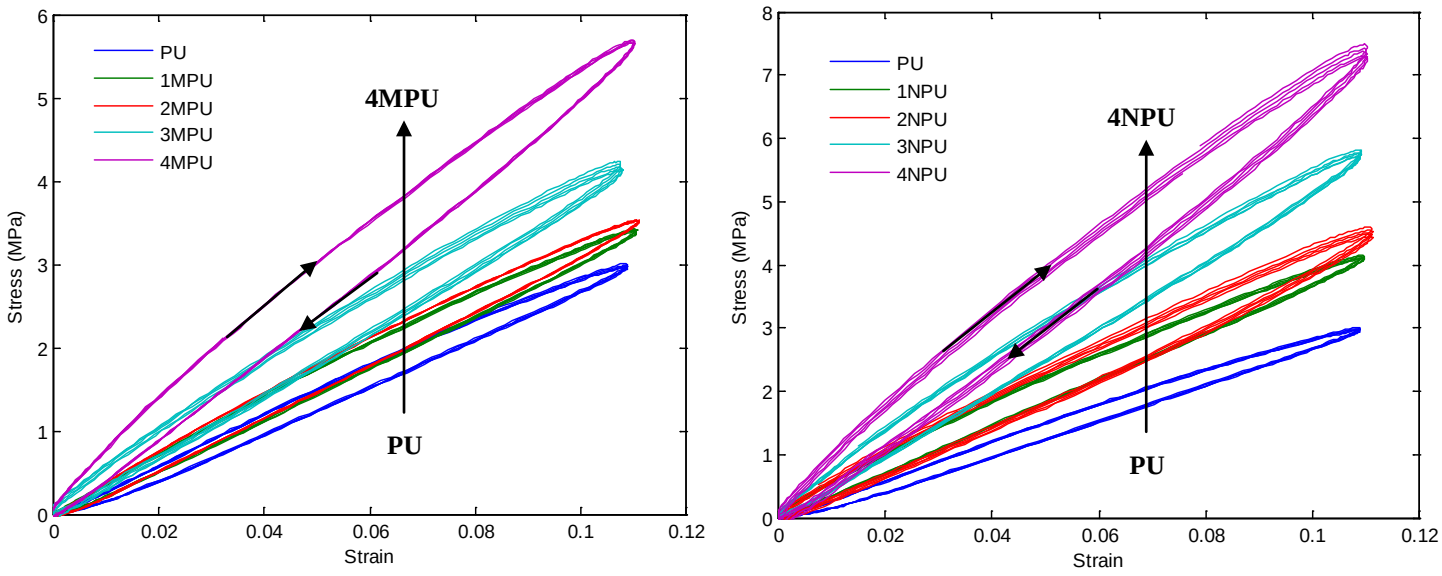

Fig. 3.37. The Stress-Strain behavior of PU and composite filled with (a) micro Cu and (b) nano Cu powders at strain rates of 10^{-1} s^{-1}.

It is noted that the true stress increases with increasing fillers concentration regardless of strain. At applied strain, the increase of the stress versus content is higher for the NPU composites that for the MPU composites. The compressed stress-strain cycle between the PU and composites filled with micro Cu fillers (4MPU) and nano Cu fillers (4NPU), as presented in Fig 3.38. The addition of Cu powder on PU induces an increase of the Young's modulus which is calculated from the slope of stress-strain curve, as shown in Table 3.5. In general, all composite systems showed an increase in Young's modulus follows the normal trend of the effect of the filler in a polymeric matrix, where Young's modulus increases with increasing the amount of filler and size of filler loading.

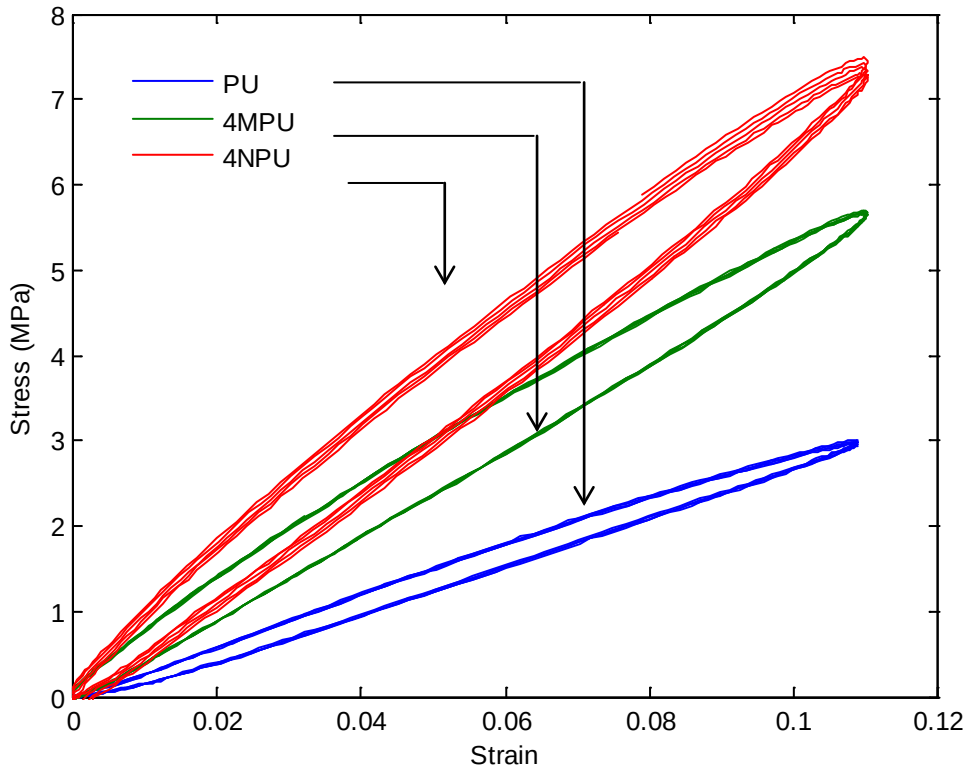

Fig. 3.38 A comparison of the stress versus strain for PU and 4MPu composite and 4NPu composite.

Table 3.5 Comparison of value of Young's modulus of PU filled with Cu loading by using load sensor technique.

% content of loading	Young's modulus (MPa) for MPU composite	Young's modulus (MPa) for NPU composite
Neat PU	31	31
1%	33	37
2%	36	42
3%	42	49
4%	48	59

3.7.2.5 DSC measurement of PU and composites filled with Cu loading

The DSC curves of pure PU and composites for 4%MPU and 4%NPU are shown in Figure 3.39. The glass transition temperature (T_{gSS}), melting temperature (T_m), recrystallization temperature (T_c) of MPU and NPU filled composite are presented in table 3.6.

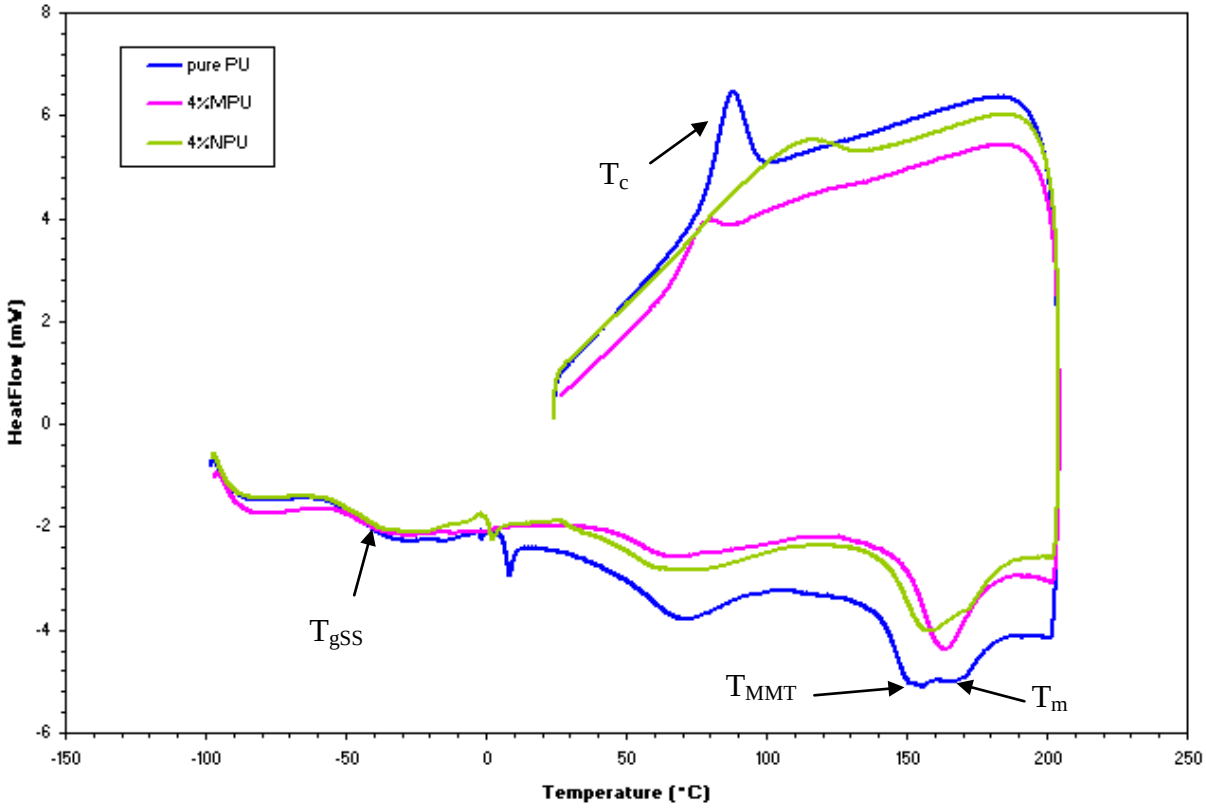

Fig. 3.39. DSC thermogram of neat PU and composites filled with nano and micro Cu charge at 4 wt%

Table 3.6 The parameters obtained from the DSC thermograms of pure PU and MPU and NPU composites.

Samples	$T_{g\ SS}$ (^oC)	T_{MMT} (^oC)	T_m (^oC)	ΔH_m (J /g)	T_c (^oC)
Pure PU	-45.0	154.0	160.0	10.6	87.5
1% **micro** Cu filled composites	-45.3	156.0	179.0	9.9	80.1
2% **micro** Cu filled composites	-46.9	157.3	-	10.4	79.3
3% **micro** Cu filled composites	-45.6	156.1	174.0	10.8	82.0
4% **micro** Cu filled composites	-46.8	163.4	-	8.6	77.6
1% **nano** Cu filled composites	-44.9	156.3	167.0	11.0	84.1
2% **nano** Cu filled composites	-45.0	158.9	170.2	9.2	81.8
3% **nano** Cu filled composites	-46.0	159.6	170.0	8.8	107.8
4% **nano** Cu filled composites	-48.9	157.4	172.0	10.5	114.8

The DSC technique was used to study the effect of the size of the two Cu filler types on the morphological structure of the polyurethane films. The DSC curves of the pure PU and the composites filled with 4% of either micro- or nano-Cu fillers are presented in Figure 3.39, and a summary of the features of all materials is provided in Table 3.6.

Regardless of the filler size, the same thermal events were observed. Thermal studies were rendered complicated by the complex morphology of the polyurethane. The studied PU was a commercial material, Estane 58888-NAT021 provided by Noveon. This PU was based on 4,4’ methylene bis(phenyl isocyanate) (MDI) and 1,4-

butanediol (BDO) as hard segments (HS), and poly(tetramethylene oxide) as soft segments (SS). The HS content was approximately 46 wt% and the physical properties depended partially on the degree of phase separation between the hard and soft phases. The first observed thermal event at around -45 ^{o}C was related to the glass transition temperature of the soft segments ($T_{g\ SS}$). The following thermal event near 70 ^{o}C was attributed to relaxation effects within the hard domains (i.e., to the influence of the degree of soft and hard segment ordering on the morphology and mechanical behavior of semicrystalline segmented polyurethanes). **[KOR 2006]** An endotherm was finally observed between 140 and 180^{o}C. The first peak could be attributed to the disruption of the structure that occurred at the microphase mixing transition (T_{MMT}), and the second endotherm corresponded to the melting of the microcrystalline HS. **[LAP 2007]** The two phenomena (MMT and HS melting) interacted and demonstrated a strong dependence on the thermal history. During cooling, these two phenomena could not be distinguished. Nevertheless, the corresponding temperature was named the "re-crystallization temperature" (T_c).

The glass transition temperature of pure PU occurred at approximately -45 ^{o}C and the addition of micro-sized fillers did not affect either the glass transition temperature or the crystallization temperature. The glass transition temperature of all composites filled with nano-sized fillers decreased very slightly as the filler volume fraction was raised. It was difficult to determine an influence of the fillers on the T_{MMT} and T_m. Most samples displayed the two phenomena, i.e., both the microphase mixing transition and melting of the microcrystalline HS, whereas the endotherm of certain samples consisted of only the phenomenon of melting (in the case of 2% MPU and 4% MPU). During cooling, for the samples with micro Cu fillers, there occurred no change of the crystallization temperature, whereas for the nano Cu samples, T_c increased with the nano Cu content.

It could thus be concluded that there occurred no interaction between particles and the PU matrix for micro Cu fillers. For the nano-fillers, on the other hand, a slight increase in T_g and an almost more important raise in T_c were observed. The T_g was indicative of the relative purity of the SS domains: a slight increase in T_g could indicate that the incorporation of nano Cu fillers improved the degree of phase mixing between hard and soft segments. The degree of microphase separation was thus lower. The

increase in T_c for the composites filled with nano Cu fillers showed a modification of the crystallinity and was coherent with the increase of hard segments.

Finally, results of the dielectric properties and mechanical properties of all polyurethane composites filled with C and SiC loading (3.7.1) and filled with copper loading (3.7.2) are compared in table 3.7.

Table 3.7 Comparison of the dielectric constant and Young's modulus of all composites.

Sample	*Dielectric constant (20Hz)*	*Young's modulus (MPa)*
PU	4.8	31
PU-0.5%SiC	5.3	60
PU-1%C	6.8	35
PU-1%MPU	5.2	33
PU-2%MPU	5.5	36
PU-3%MPU	5.7	42
PU-4%MPU	6.0	48
PU-1%NPU	5.9	37
PU-2%NPU	6.2	42
PU-3%NPU	6.7	49
PU-4%NPU	7.5	59

Table 3.7 shows the dielectric constant and Young's modulus of composites filled loading are always higher than the pure PU. For PU filled with copper composites, it is noted that dielectric constant increases with increasing fillers concentration. At a given content, the increase of the dielectric constant is higher for the NPU composites than for the MPU composites. Composite filled with copper needs to maintaine the insulating behaviour for electrostriction on energy harvesting. It is the

reason why the studied this composites have been designed with low metallic fillers content, to be far from the percolation threshold.

However, high permittivity material is required to increases the energy harvesting. P(VDF-TrFE-CFE) terpolymers are now available. These materials presents high relative permittivity (higher than 40) and should be good candidates for energy harvesting purpose. These formulations can also be prepared in our laboratory from commercialized powders and as for polyurethane, it is also possible to incorporate micro or nano-objects within the matrix.

3.7.3 Experimental results on P(VDF-TrFE-CFE) and composites filled with nano C loading

3.7.3.1 Dielectric constant for P(VDF-TrFE-CFE) and composites filled with nano C loading

Figure 3.40 and 3.41 show the behaviors of the dielectric constant and dielectric loss tangent as a function of frequency for P(VDF-TrFE-CFE),(TP) and composites filled with C nanofiller concentrations, respectively.

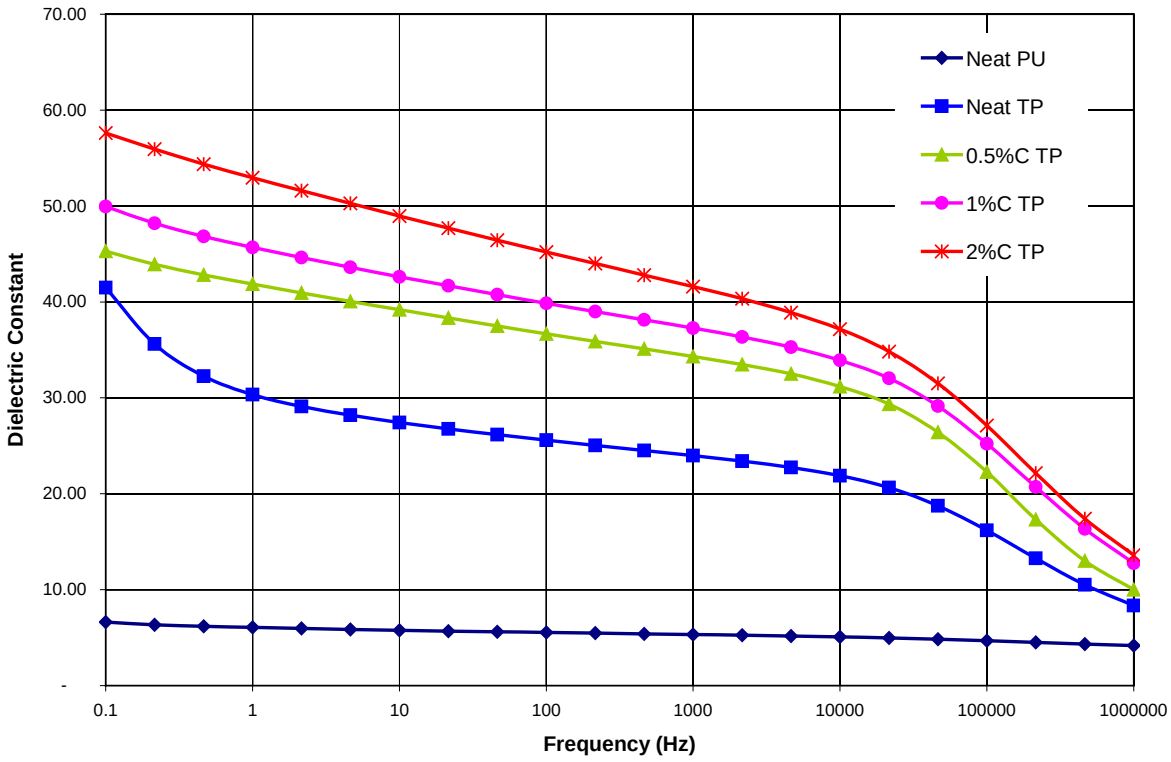

Fig. 3.40. Dependence of dielectric constant of P(VDF-TrFE-CFE) terpolymer filled with C fillers on frequency.

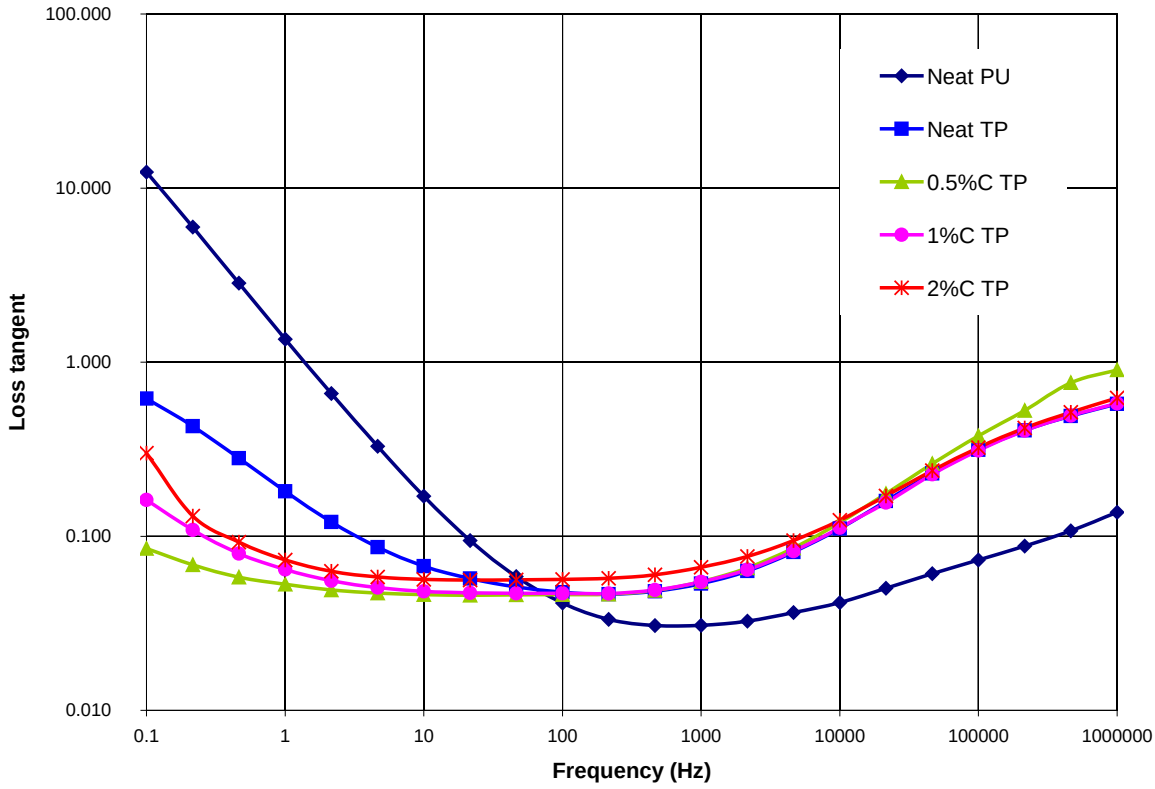

Fig. 3.41. Dependence of loss tengent of P(VDF-TrFE-CFE) terpolymer filled with C fillers on frequency.

As can be seen figures 3.40 and 3.41, for all samples, the values of the dielectric constant and loss tangent for P(VDF-TrFE-CFE) filled with C nanofillers depend both on measuring frequency and the nanofiller concentration. The dielectric constant slowly decreased when the frequency was raised. The values of dielectric constant of P(VDF-TrFE-CFE) terpolymers are distinctly higher than neat PU regardless of the frequency. Moreover, it can be noted that the dielectric constant increased with an increasing filler concentration regardless of the frequency. In place of P(VDF-TrFE-CFE) terpolymers filled by the C fillers, the quantity of the accumulated charge will increase because the polarization of the P(VDF-TrFE-CFE)/C interfaces. The polarization makes an additional contribution to the charge quantity. As a consequence, the dielectric constant of the composites will be higher than that of the P(VDF-TrFE-CFE) terpolymer.

Otherwise, the loss tangent of PU is higher than terpolymer at low frequency. Figure 3.41 depicts the frequency dependence of the effective loss tangent for P(VDF-TrFE-CFE) terpolymer filled with nano CB fillers. The value of loss tangent of PU was obviously higher than P(VDF-TrFE-CFE) terpolymer when the frequency was increased, however was lower after frequency of 100 Hz.

3.7.3.2 Mechanical behavior for P(VDF-TrFE-CFE) and composites filled with nano CB loading

Stress-Strain behavior of *P(VDF-TrFE-CFE)* and composite filled with CB nanofillers at strain rates of 10^{-1} s^{-1} was shown in Figure 3.42. The value of Young's modulus was calculated as the slope of stress-strain and the values are given in Table 3.8. The addition of content resulted in increase in Young's modulus at 2% volume. Young's modulus is quit constant at low content (0-1%).

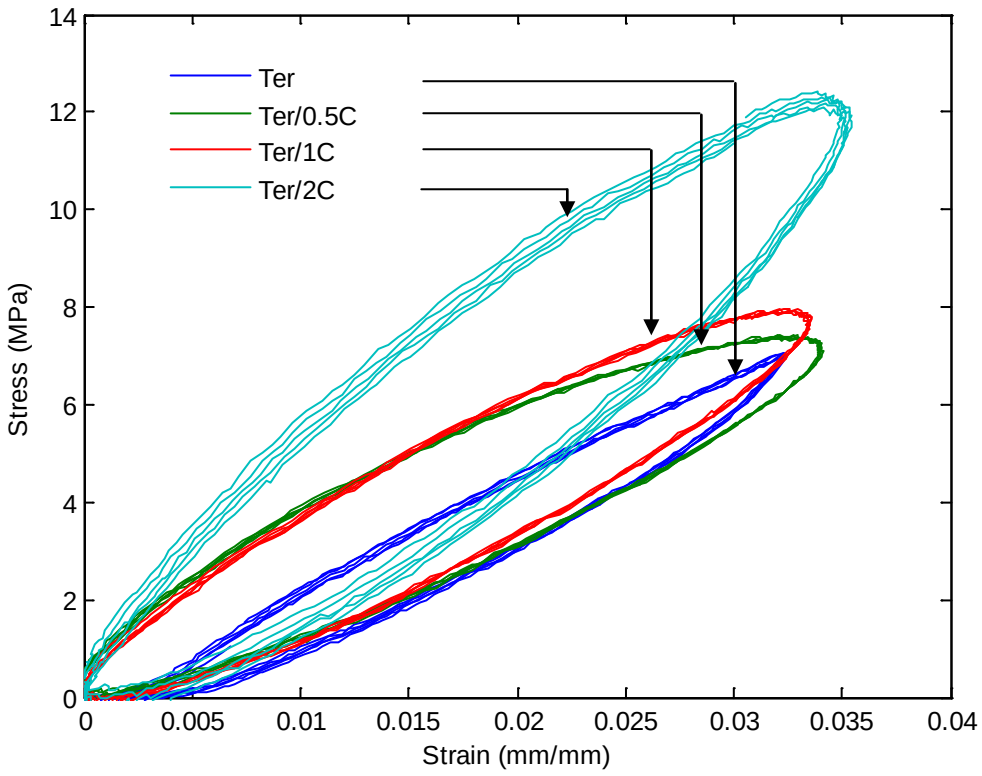

Fig. 3.42. Stress- strain behavior for P(VDF-TrFE-CFE) filled with nano CB fillers.

Table 3.8. Summary of mechanical properties for P(VDF-TrFE-CFE) filled with nano CB fillers.

Samples	Young's modulus (MPa)
Neat Ter	240
0.5%C Ter	250
1%C Ter	280
2%C Ter	330

It is noted that the stress increases with increasing fillers concentration regardless of strain. Due to increasing Young's modulus that follows the normal trend of the effect of the filler in a polymeric matrix, where Young's modulus increases with increasing the amount of filler and size of filler loading.

3.8 Conclusions

Thermoplastic polyurethane films (the elastomer 58888 TPU Estane) were prepared through a solution casting method. In addition to neat PU samples, films of filled polymer were prepared also by solution casting. SEM was performed on the composites and results showed a rather good dispersion of the both C nanofillers and SiC fillers in good agreement with the non conduction state observed on composites. Moreover, results of SEM for composites filled with copper fillers also showed a rather good dispersion of the fillers within the matrix when the microsized fillers were used. When the nanofillers were employed, some agglomerates could be observed, but the dispersion remained homogeneous.

Based on DSC runs, no modification of the thermal events occurred for the MPU composites as compared to the neat polyurethane, whereas a slight increase in T_g and a significant rise in T_c were observed for NPU. It seemed that the nano-sized particles interacted to a larger extent with the polymer matrix as opposed to their micro-sized counterparts.

The dielectric constant of the composites with fillers was studied over a broad range of frequencies. It is shown that the dielectric constant of the all composites are higher than that the pure PU. The dielectric properties of the MPU and NPU composites

were studied over a broad range of frequencies and a varying volume fraction of fillers. For both composites, the dielectric constant decreased slowly with an increasing frequency. Regardless of the size of the fillers, an increase of the permittivity as compared to the neat polymer took place, but the effect was more pronounced when nano-sized copper particles were used. This was in good agreement with the fact that the percolation threshold was lower for the nano-sized fillers than for their micro-sized analogs. The slight enhancement of the permittivity versus fillers content can be explained by the incorporation of conductive charges in the polymer matrix. This effect is small due to the fact that the contents are very low compared to the critical content for which percolation appears. Nano fillers affect the dielectric properties of P(VDF-TrFE-CFE) on the same manner than for PU composites. Higher permittivity is achieved with P(VDF-TrFE-CFE) composite than with PU composite. In addition, this effect seems to be kept on a larger frequency range.

The results of the tensile setup demonstrate on mechanical behaviour that the addition of fillers on either PU or P(VDF-TrFE-CFE) matrix induces an increase of the Young's modulus. At low concentration, the Young's modulus slowly increases with increasing content. In case PU filled with Cu fillers, Young's modulus for NPU is larger than MPU due to its size effect of inclusion restricting molecular motion. Moreover, the highest young's modulus was observed on P(VDF-TrFE-CFE) terpolymer.

Chapter 4:

Electrostrictive effect of polyurethane, P(VDF-TrFE-CFE) and composites

4.1 Introduction

In chapter 3, it has been shown that the use of nanofillers can greatly increase the permittivity especially at low frequencies. These fillers also increase the Young's modulus. The objective of the chapter is to detect how the fillers affect the electrostriction properties.

The development of new materials with large strains results in several applications that take advantage of the electrostrictive materials as actuators or as tunable transducers.**[CRO 1995][SUN 1996]** Electrostriction is a quadratic coupling of strain and field, which is present in all materials, including gases and liquids. Interest in the phenomenon of electrostriction has been increased significantly since the introduction of PMN as a prototype electrostrictive material. **[JAN 1979]** The advantage that electrostrictors have over other actuator materials include low hysteresis of the strain field response, no remnant strain, reduced aging and creep effects, a high response speed, and substantial strains at realizable electric fields. Zhang et al. reported

the large electrostrictive strain in electron-irradiated poly(vinylidene fluoride-trifluoroethylene), P(VDF – TrFE) copolymers, investigations of the actuator and transducer applications of the polymers are underway. Recently, the ceramics are replaced with polymers for electrostriction.**[ZHA 1998]**

Electrostrictive polymers exhibit very attractive characteristics, and as a result, they have been widely studied either for the purpose of understanding the electrostriction phenomenom**[YIM 1999][GUI 2003][SUN 1996]** or in view of practical applications. **[HER 1982][COH 2001d]** Numerous reports are devoted to the characterisation of the electrostrictive behaviour versus applied electric fields. **[SU 1997][WAN 1991][GUIF 2006]** Under moderate electric fields, electrostrictive polymers have been found to produce large strains of >10%, for this reason they are considered as good candidates for actuation.**[BHA 1999]** As an example, polyurethane elastomers are of great interest for a wide range of transducer and actuator applications when considering their significant electrical-field-induced strains, high specific energy and small response. Furthermore, these materials are lightweight, very flexible, presenting low manufacturing costs and can be readily moulded into any desirable shape. In addition, it has recently been shown that the incorporation of nanofillers such as carbon nano-tubes into a polymer matrix can greatly enhance the expected strain versus electric field.**[PAR 2008]**

The electrostriction effect can be measured either by using the direct effect (mechanical data versus electrical data) or an inverse effect (electrical data versus mechanical data). In the first case, small strains are determined by techniques including capacitance dilatometer**[CHE 1999]**, strain gauge measurements**[UCH 1980]** and laser-based interferometer. **[GUY 1999][LAM 2005]** In the second case, the change in dielectric permittivity is measured as a function of an applied mechanical stress.**[YIM 1990b] [EUR 1999]** The main issue is to accurately determine very small displacements, in the case of the direct effect, or very small variations in permittivity, for the converse effect. Moreover, in addition to the true electrostrictive effect as described by the M_{mnij} and Q_{mnij} coefficients , other influences such as the electrostatic attraction between the electrodes (Maxwell effect) and space charge effects can greatly enhance the apparent electrostriction coefficient.**[SU 1997][GUI 2003]**

4.2 Electrostrictive Polymers

Electrostriction is defined as the change in shape of a body due to rearrangement of its molecules in presence of an external electric field. Materials showing actuation due to electrostriction are called electrostrictive materials. Electrostrictive graft elastomers are polymers consisting of two components, a flexible macromolecule backbone and a grafted polymer that can be produced in a crystalline form. Fig. 4.1 shows the grafts on the backone that can crystallize to form physical cross linking sites network and to generate electric field responsive polar domains.**[SU 2000]** This polymer exhibits high electric field induced strains (~5%) with a relatively large force and a response speed in the region of milliseconds due to electrostriction.**[CRO 2004]** Typically the combination of electrostrictive-grafted elastomer with a piezoelectric poly(vinylidene fluoride-trifluoro-ethylene) copolymer can be operated both as sensor and an electrostrictive actuator that yields several compositions of a ferroelectric-electrostrictive molecular composite system.**[SU 1999]**

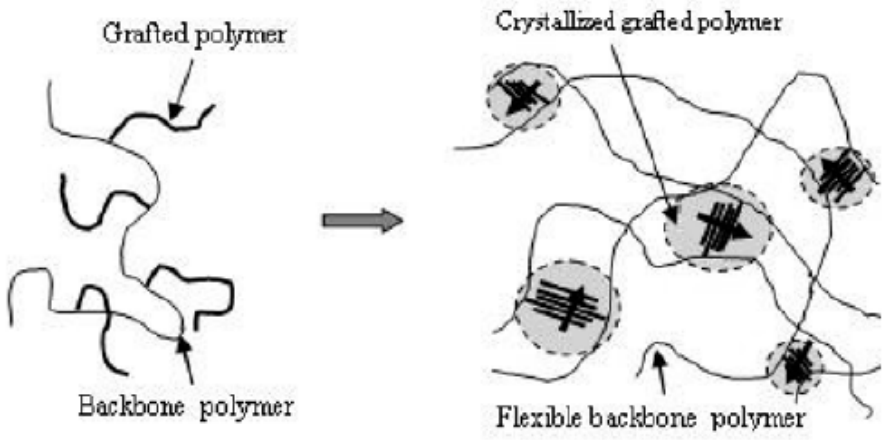

Fig. 4.1. Schematic showing (a) molecular structure and (b) morphology of a grafted elastomer

Kim et al., presented on electrostrictive paper which behaves like an actuator. An electrostrictive paper is composed of a multitude of discrete particles, which are mainly of a fibrous nature forming a network structure.**[KIM 2000]** For example, silver laminated paper, whereby two silver laminated pieces of paper with silver electrodes are placed on the outside surfaces, shows bending motion upon application of electric voltage to the electrodes and its performance depends on the stimulation such as electric

field, type of adhesive and of host paper. Application of these material concerns sound absorbing materials, flexible speakers, and smart shape control devices.

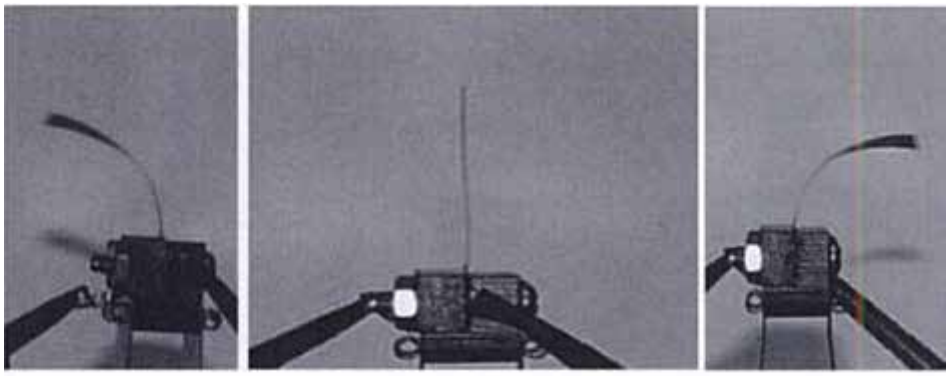

Fig. 4.2. An electrostrictive grafted elastomerbased bimorph actuator in an unexcited state (middle), one direction excited state (left), and opposite direction excited state (right).**[SU 1999]**

4.2.1 Principle of Operation

The operation of the electrostrictive polymers is similar than a DEA (Dielectric Elastomer Actuators) which can be represented by a parallel plate capacitor, with the conducting electrodes as the two plates and electrostrictive elastomer as the dielectric medium, as shown figure 4.3. Moreover, the stress and the corresponding induced strain response of these polymers is typically proportional to the square of the applied electric field, as shown in Fig. 4.4.

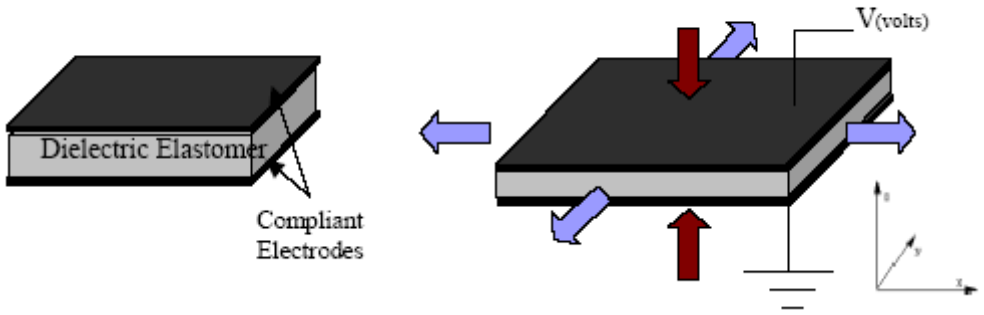

Fig. 4.3. Schematic representation of operation of a DEA.

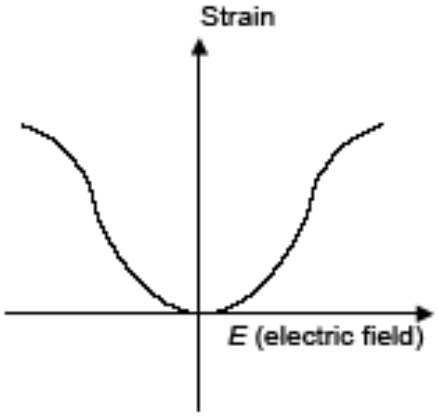

Fig. 4.4. Typical strain – electrical field for electrostricive material.

Electrostriction exists in all dielectric materials and corresponds for instance to a strain induced by an electrical field. Electrostrictive materials have been widely utilised in actuators, transducers and electromechanical devices.**[HER 1982][SUN 1996]** From the Devonshire formalism of the thermodynamic phenomenology, the elastic Gibbs function G for the free energy of the a material may be expressed as **[UCH 2000][NEW 1997]**

$$G = \frac{1}{2}\beta_{mn}P_mP_n - \frac{1}{2}s_{ijkl}T_{ij}T_{kl} - Q_{ijmn}T_{ij}P_mP_n + \ldots \tag{4.1}$$

where T_{ij} and P_m are the stress, and polarization, respectively, and s_{ijkl} and Q_{ijmn} are called the elastic compliance and the electrostrictive coefficient, respectively. This leads to the strain, S_{ij} and electric field, E_m as equation 4.2 and 4.3

$$S_{ij} = -\left(\frac{\partial G}{\partial T_{ij}}\right) = s_{ijkl}T_{ij} + Q_{mnij}P_m^{\,2} \tag{4.2}$$

and

$$E_m = -\left(\frac{\partial G}{\partial P_m}\right) = \beta_{mn}P_m - 2Q_{ijmn}P_mT_{ij} \tag{4.3}$$

Properties relating derived variables such as S_{ij} and E_m to fixed variables of state such as T_{ij} and P_m are obtained by taking the second derivation of this free energy

function. For example, the first-order terms for inverse dielectric susceptibility β_{mn} and elastic compliance s_{ijkl} may be expressed as

$$\beta_{mn} = \left(\frac{dE_m}{dP_n}\right)_{T,T_T} = \left(\frac{d^2G}{dP_m dP_n}\right)_{T,T_T} \tag{4.4}$$

and

$$s_{ijkl} = \left(\frac{dS_{ij}}{dT_{kl}}\right)_{P,T_T} = \left(\frac{dG}{dT_{ij}dT_{kl}}\right)_{P,T_T} \tag{4.5}$$

Cross-coupled properties can be derived by changing the differentiation variable for the second differential. The properties that introduce strain in a material are derived by differentiating the elastic Gibbs function with respect to stress. The tensor properties associated with these effects are elastic constants, linear and nonlinear thermal expansion, linear piezoelectric constants (d_{ijm} and g_{ijm}) and quadratic (M_{ijmn} and Q_{ijmn}) electrostriction constants. These electromechanical interactions can be expressed in a power series to the second order (fixed T) and (fixed P) as

$$S_{ij} = g_{ijm}P_m + Q_{ijmn}P_mP_n + \ldots \tag{4.6}$$

and

$$S_{ij} = d_{ijm}E_m + M_{ijmn}E_mE_n + \ldots \tag{4.7}$$

Electrostriction may be thus defined as the quadratic coupling between strain and electric field, or between strain and polarization. It is a fourth-rank tensor defined by the following relationship:

$$S_{ij} = M_{ijmn}E_mE_n \tag{4.8}$$

and

$$S_{ij} = Q_{ijmn}P_mP_n \tag{4.9}$$

Here M_{ijmn} are elements of the fourth-rank electric field related electrostriction tensor and Q_{ijmn} are elements of the fourth-rank polarization related electrostriction tensor.

Considering the coupling between dielectric and elastic properties of solids, electrostriction is a fourth rank tensor property relating the mechanical strain, S, to an applied electric field, E, or to the polarisation, P, expressed by the following relationships.**[SUN 1996][YIM 1999]**

$$S_{ij} = s^{E}_{ijkl} T_{kl} + M_{mnij} E_m E_n \tag{4.10}$$

and

$$T_{ij} = c^{E}_{ijkl} S_{kl} + m_{mnij} E_m E_n \tag{4.11}$$

where s^{E}_{ijkl} and c^{E}_{ijkl} is the elastic compliance and the stiffness tensor under appropriate boundary conditions for constant electric field, T_{kl} is the elastic stress component, and M_{mnij} and m_{mnij} are the electrostriction coefficients.

If polarization is used as the independent electrical variable, the equations became

$$S_{ij} = s^{P}_{ijkl} T_{kl} + Q_{mnij} P_m P_n \tag{4.12}$$

$$T_{ij} = c^{P}_{ijkl} S_{kl} + q_{mnij} P_m P_n \tag{4.13}$$

From the constitutive equations listed above, it is seen that there are four electrostrictive coeffcients; M, m, Q and q. There coefficients are not all independent which gives $M = - sm$, or $m = - cM$ by combining equations (4.10) and (4.11). Similarly, from equations (4.12) and (4.13), $Q = - sq$, or $q = - cQ$.

The M and Q coefficient are equivalent and form the basis of most of literature. The field-polarization relationship is used to converse between the two coefficients.**[YIM 1999]**

$$P_n = \chi_{nm} E_m \tag{4.14}$$

$$E_m = \beta_{nm} P_n \tag{4.15}$$

where χ_{nm} is the dielectric susceptibility tensor and β_{nm} is the inverse dielectric susceptibility or dielectric stiffness tensor.

Since dielectric permittivity ε_{mn} is generally used as the variable instead of the dielectic susceptibility, χ_{nm} and the dielectric stiffness, η_{nm}.

χ_{nm} is expressed by

$$\chi_{mn} = \varepsilon_{mn} - \varepsilon_o = \left[(\varepsilon_r)_{mn} - 1\right]\varepsilon_o \tag{4.16}$$

and by substitution into the constitutive equations, the relationship between M and Q coefficients became,

$$M_{mnij} = \chi_{im}\chi_{jn}Q_{mnij} = \varepsilon_o^2\left[(\varepsilon_r)_{im} - 1\right]\left[(\varepsilon_r)_{jn} - 1\right]Q_{mnij} \tag{4.17}$$

where ε_r is the dielectric constant, and ε_o is the dielectric permittivity of vacuum (ε_o =8.854´ 10^{-12} F/m).

Q values for soft elastomers are as high as 10^6 m^4/C^2 while they are only about 10^{-2} m^4/C^2 for ferroelectric relaxors. Other insulators are in between with the Q coefficients roughtly proportional to $\frac{1}{Y\varepsilon}$, (Y: the Young's modulus and ε: dielectric permittivity). This can be rationalized in the following way. Since $S_{ij} = Q_{ijmn}P_mP_n$ (equation (4.9)), and S_{ij} is large when the material deforms easily (such an elastomer). Since both the strain and the polarization are proportional to ε, the Q coefficient will be propertional to $1/\varepsilon$. Hence Q varies as $\frac{1}{Y\varepsilon}$, and M coefficient as $\frac{\varepsilon}{Y}$.**[EUR 1999]** Guillot et al also suggests that M_{33} coefficient is proportional to $\frac{\varepsilon_0(\varepsilon_r - 1)^2}{\varepsilon_r Y}$ in case of polyurethane.**[GUI 2003]**

4.2.2 Crystal symmetry and Electrostrictive coefficient

While the electrostrictive coefficients are fourth rank tensors, their symmetry means that they can be described using the reduced matrix notation. There are three symmetry groups: cubic single crystals in point group m3m, alumina single crystals in point group $\bar{3}m$, and isotropic materials, made of ceramics, glasses and polymers. The matrix forms of the electrostriction M_{mnij} tensors of these three groups are shown here. The first and last two subscripts are combined into one, using the convention described by the rules.**[NYE 1985]** The full notations are shortened by using the abbreviated forms: 11® 1, 22® 2, 33® 3, 23 and 32® 4, 13 and 31® 5, 12 and 21® 6. The matrix element M_{mnij} is obtained from the tensor component M_{mnij}. For electrostriction tensor,

$M_{mn} = M_{mnij}$, when both n and m = 1, 2, 3

$M_{mn} = 2M_{mnij}$, when either n or m = 4, 5, 6

$M_{mn} = 4M_{mnij}$, when both n and m = 4, 5, 6

By these conventions, the complete electrostriction matrices for the three groups of these materials are written as follow:

i) Cubic single crystals in point group m3m

$$\begin{matrix} M_{11} & M_{13} & M_{13} & 0 & 0 & 0 \\ M_{13} & M_{11} & M_{13} & 0 & 0 & 0 \\ M_{13} & M_{13} & M_{11} & 0 & 0 & 0 \\ 0 & 0 & 0 & M_{44} & 0 & 0 \\ 0 & 0 & 0 & 0 & M_{44} & 0 \\ 0 & 0 & 0 & 0 & 0 & M_{44} \end{matrix}$$

ii) Trigonal single crystals in point group $\bar{3}m$

$$\begin{matrix} M_{11} & M_{12} & M_{13} & M_{14} & 0 & 0 \\ M_{12} & M_{11} & M_{13} & -M_{14} & 0 & 0 \\ M_{13} & M_{13} & M_{33} & 0 & 0 & 0 \\ M_{14} & -M_{14} & 0 & M_{44} & 0 & 0 \\ 0 & 0 & 0 & 0 & M_{44} & 2M_{14} \\ 0 & 0 & 0 & 0 & M_{14} & 2(M_{11}-M_{12}) \end{matrix}$$

iii) Isotropic materials and Curie groups $\infty\infty m$ and $\infty\infty$

$$\begin{matrix} M_{33} & M_{13} & M_{13} & 0 & 0 & 0 \\ M_{13} & M_{33} & M_{13} & 0 & 0 & 0 \\ M_{13} & M_{13} & M_{33} & 0 & 0 & 0 \\ 0 & 0 & 0 & 2(M_{33}-M_{12}) & 0 & 0 \\ 0 & 0 & 0 & 0 & 2(M_{33}-M_{12}) & 0 \\ 0 & 0 & 0 & 0 & 0 & 2(M_{33}-M_{12}) \end{matrix}$$

So, three independent electrostrictive cofficients (M_{11}, M_{13} and M_{44}) are needed to describe the effects in cubic single crystals in point group m3m, while there are five independent coefficients ($M_{11}, M_{12}, M_{13}, M_{14}$ and M_{44}) for electrostrictive descrition of trigonal crystals in point group $\bar{3}m$. On the other hand, only two (M_{33} and M_{13}) are needed for isotropic materials.

4.2.3 Electrostriction measurement

The electrostriction effect can be measured either by using the direct effect (mechanical data versus electrical data) or an inverse effect (electrical data versus mechanical data). In the first case, small strains are determined by techniques including capacitance dilatometer**[CHE 1999]**, strain gauge measurements**[UCH 1980]** and laser-based interferometer.**[GUY 1999] [LAM 2005] [EUR 1999]** In the second case, the change in dielectric permittivity is measured as a function of an applied mechanical stress.**[YIM 1999][EUR 1999]** In our work, the interferometer technique is used to investigate the M_{33} coefficient for electroactive polymer, since $S_3 = M_{33}E_3^2$ (equation

(4.8)). Measuring technique and results for electroactive polymers will be now discussed in details.

4.2.4 Other quadratic effects

If the response is dominated by the field-induced reorientation of a crystalline or semicrystalline structure inside polymer, this phenomena is said to be electrostrictive while if the response is dominated by the interaction of the electrostatic charges on the electrodes, it is called Maxwell stress.

Maxwell stress

When an electric field is applied to a sample, then the electrostatic attraction between the electrodes generates a stress in the material. The strain which results from this stress varies quadratically with the field and also depends on the mechanical compliance of the material.

The strain S^M, resulting from the Maxwell stress, is given by equation (4.18).**[KRA 1999]** If all fields and strains are in the same direction, it is possible to simplify the expression by omitting the tensor notation.

$$S^M = - \frac{1}{2Y} e_o e_r E^2 (1 + 2u) \qquad (4.18)$$

where e_o is the permittivity of free space, e_r is the dielectric constant, Y is the Young' modulus and u is the Poisson's ratio of the material.

Thermal expansion

When a voltage is applied to a material, current flows in the material and heating results. The amount of heating varies quadratically with the applied voltage. This heating leads to thermal expansion, which will also vary quadratically with the applied voltage. An exact calculation of the magnitude of this effect becomes difficult, because of the heat losses involved, however a rough estimate is readily made.

It is assumed that the heat dissipated in each half-cycle of the applied voltage goes entirely into heating the sample, This energy is

$$DQ = \frac{V_o^2}{2R} \frac{t}{2} = \frac{V_o^2}{4Rf} \qquad (4.19)$$

where V_o is the peak value of the applied voltage, R is the sample resistance, t is the period and f is the frequency.

The resulting change in temperature will be

$$\Delta T = \frac{\Delta Q}{mc} = \frac{V_o^2}{4Rfmc} \tag{4.20}$$

where c is the specific heat capacity and m is the mass of the sample. If the thickness of the sample is t and the thermal expansion coefficient is α, then the expansion resulting from the heating will be

$$\Delta t = \frac{\alpha t V_o^2}{4Rfmc} \tag{4.21}$$

This calculation will over-estimate the expansion, since heat losses to the surroundings will reduce the amplitude of the temperature fluctuations.

Therefore, the true electrostriction coefficient M must be replaced in the equation by the apparent electrostriction coefficient, M_{33} in order to take into account all the contributions to the strain, $M_{33} = M + M_M + M_T$ Here, M_M represents the contribution of the Maxwell effect and M_T represents the contribution of the thermal effect. When considering the behavior of isotropic materials, the contribution of the true electrostriction can be expressed as $M = \varepsilon_o^2(\varepsilon_r - 1)^2 Q$. Moreover, the Maxwell effect for the transverse strain is obtained with $M_M = -\frac{1}{2Y}\varepsilon_o\varepsilon_r$. The temperature range used in the present experiment was low enough to neglect the thermal effect.

4.3 Measurement setup

4.3.1 Interferometer setup

The electric field-induced strain was measured with a double-beam laser interferometer (Agilent 10889B with a precision on the order of 10 nm). The tested samples were placed on a horizontal strain less steel disc (20 mm in diameter) in order to avoid measuring a parasitic flexure motion and a second brass disc is placed on the upper side of the sample, which are shown in Fig. 4.5 (b). The experiments were preformed on bipolar electric field at several frequencies. The applied voltage was

supplied by a function generator (Agilent 33250A) amplified through a high-voltage lock–in amplifier (Trek 10/10B). The induced strain can be calculated from these deformation measurements.

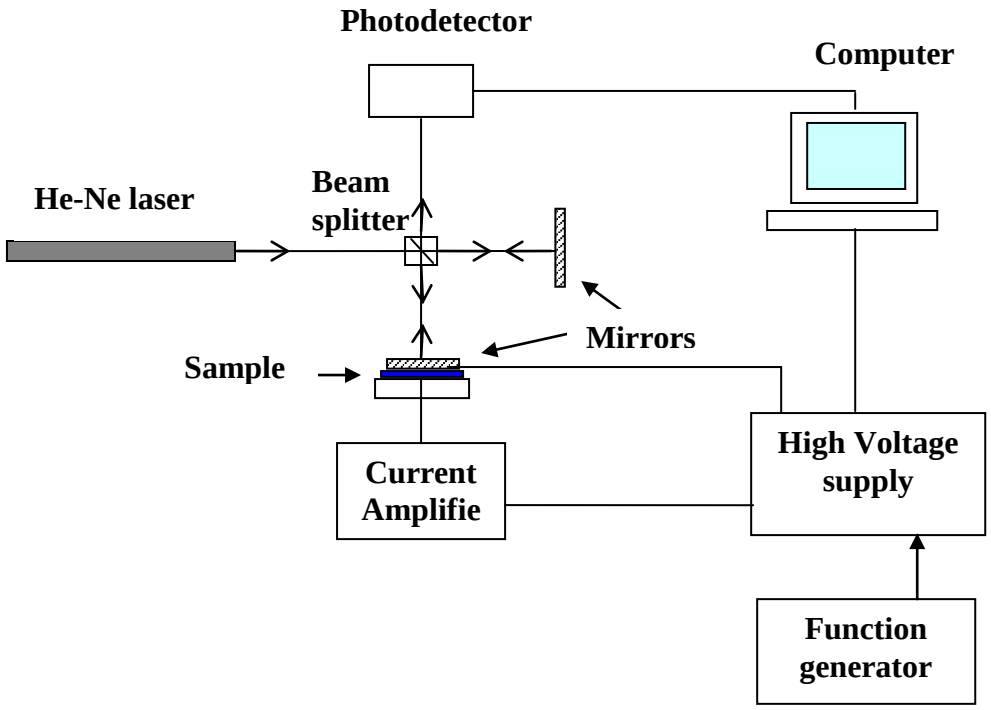

Fig. 4.5 (a) Schematic diagram of the interferometer setup.

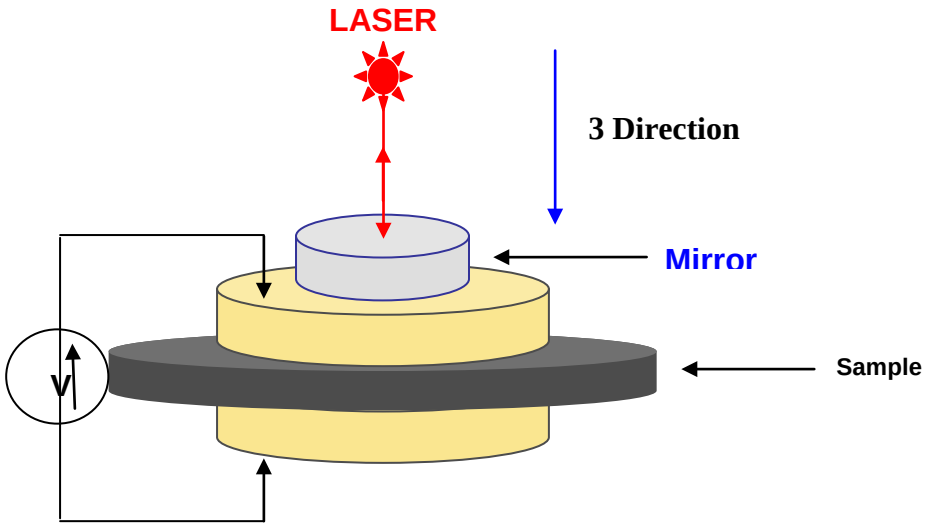

Fig. 4.5 (b) Illustration of the orientation of the sample relative to the laser beam in the interferometer.

4.3.2 Gauge displacement sensor setup

The setup developed for characterizing longitudinal strain response of polymer films is schematically shown Fig. 4.6. The test specimens were placed between substratum, brass disc (fixed) and a rear brass disc which is placed on the upper side of the sample. When the polymer film is subjected to the electric field, its expansion and contraction cause the rear brass disc to move, which can be detected using gauge displacement technique. In the current setup, a displacement probe sensor is employed. The gauge sensor with the displacement probe (Fogal nanotech MC 940) has a sensitivity range of 10V/mm. All the measurements were conducted at ac mode. The applied voltage was supplied by a function generator (Agilent 33250A) amplified through a high-voltage lock – in amplifier (Trek 10/10B). The output signal of the displacement sensor was measured and recorded through a digital oscilloscope (Agilent, DSO7034A). The induced strain can be calculated from these deformation measurements.

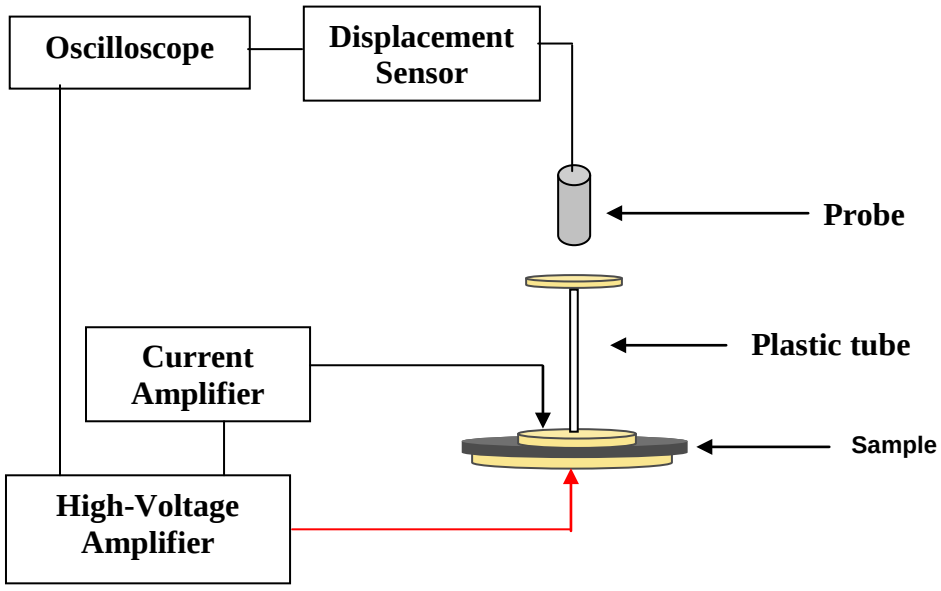

Fig. 4.6. Schematic of the displacement gauge setup.

4.4 Experimental Results and Discussions

4.4.1 Results of frequency effect and thickness on electrostrictive polyurethane polymers

The interferometer setup is employed to investigate the thickness strain versus frequency and thickness of films. Fig. 4.7 presented the longitudinal strain (parallel to the applied electric field) as a function of the electric field, for various frequencies (0.1 to 1 kHz), for pure PU with a thickness of 105 µm. The used driving electric fields were in a range of 0 to 15 V/µm. It is shown that the thickness strain decreases when the frequency is increased regardless of the electric field. Fig 4.8 depicts the longitudinal strain as a function of the electric field for various thickness (15 to 250 µm) for pure PU at frequency of 0.1 Hz.

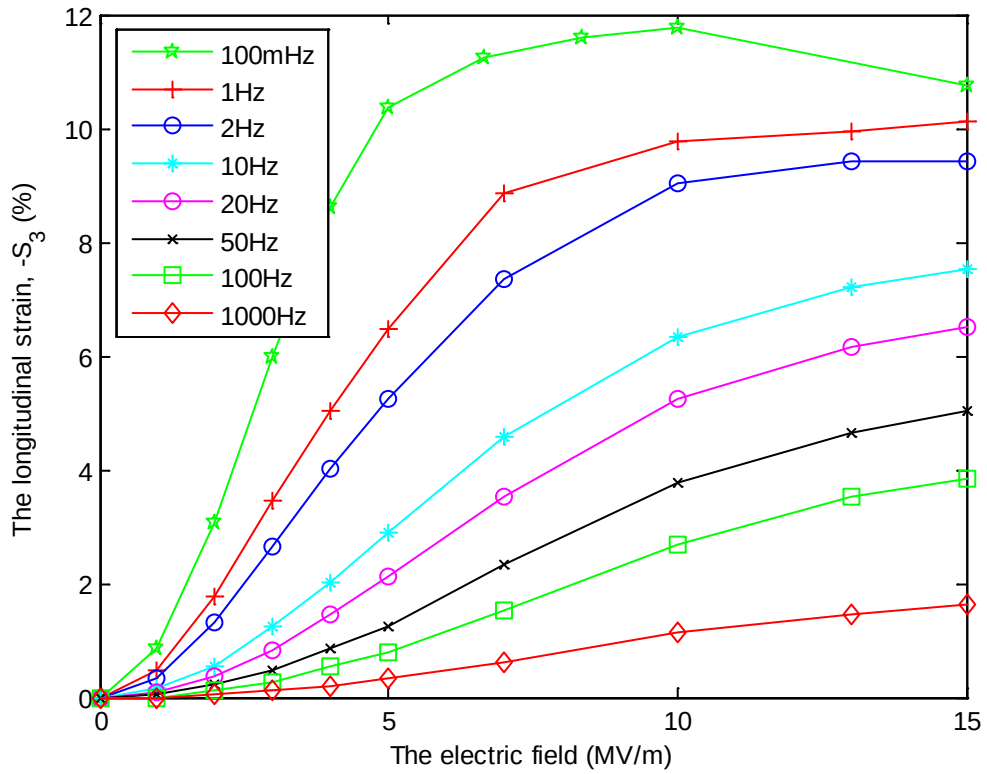

Fig. 4.7. Variations of the longitudinal strain with the electric field verified frequency for pure PU at room temperature.

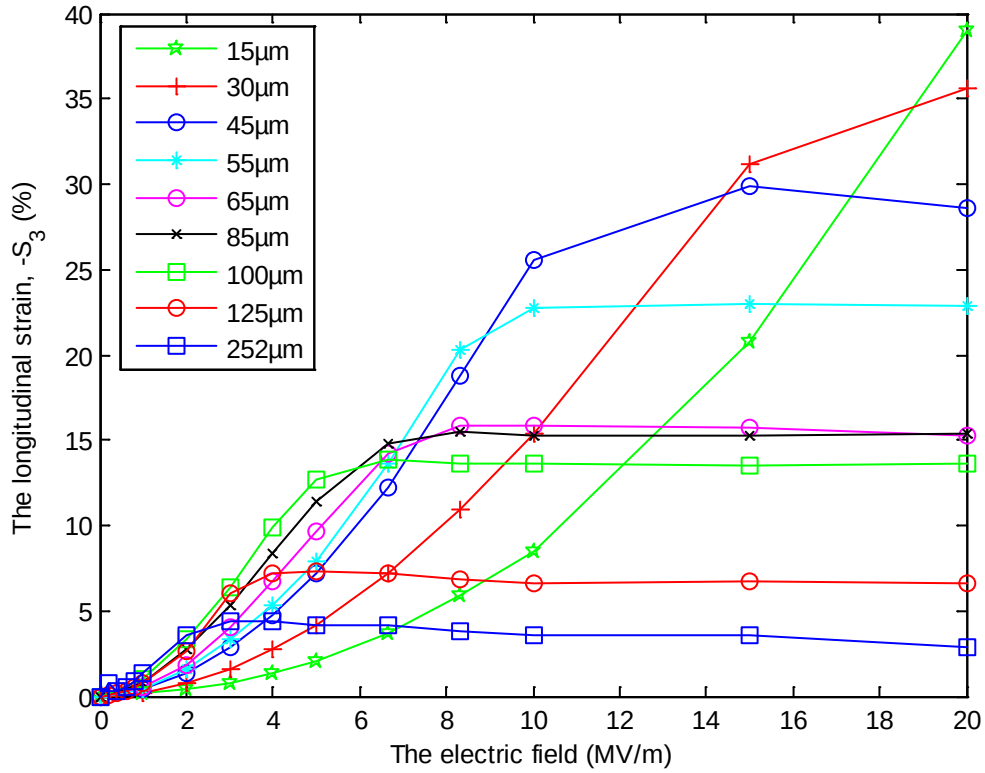

Fig. 4.8. Variations of the longitudinal strain with the electric field verified thickness for pure PU at 0.1 Hz.

The electrostrictive response of pure PU versus electric field mainly obeys a quadratic relation at low electric field, in good agreement with equation 4.8, $S_3 = - M_{33} E_3^{\,2}$. M_{33} is the electrostrictive coefficient and can be calculated from slope of the electrostrictive strain, S_3 versus the square of the electric field, $E_3^{\,2}$. The negative sign indicates a contraction response of the polymer. At higher electric field, saturation of the strain is observed and could be explained by the saturation of the electric field induced polarization. This saturation is also thickness dependent. Fig. 4.9 presented the M_{33} coefficients versus the frequency. It is shown that the M_{33} coefficient decreases with increasing frequency.

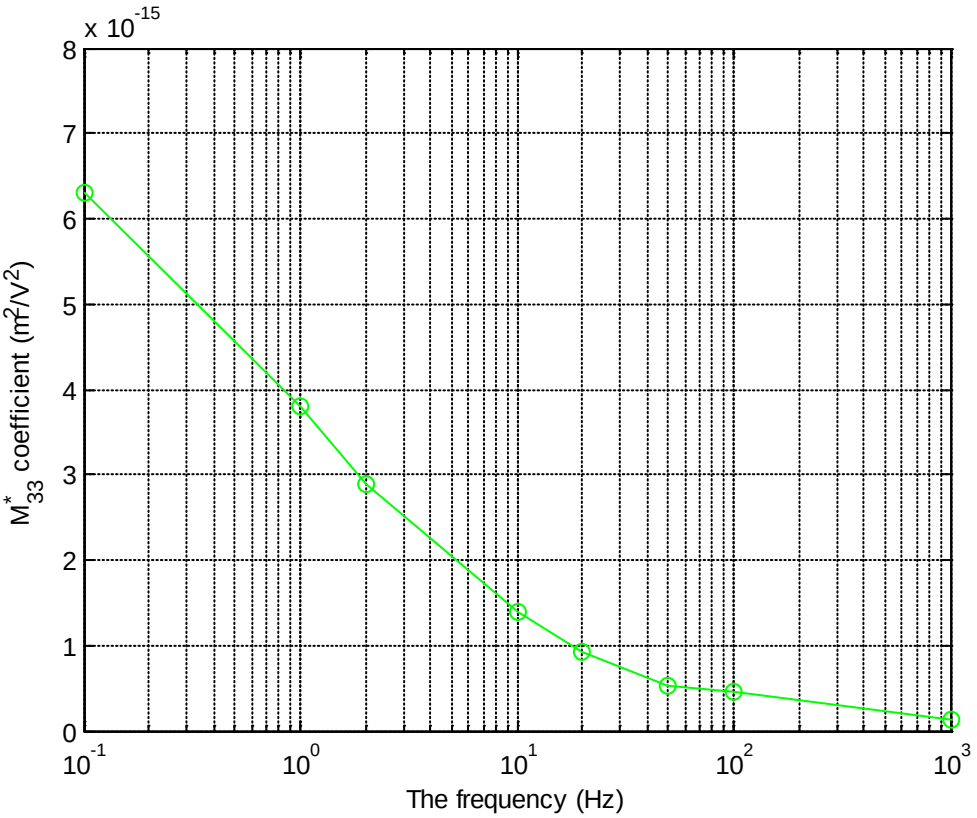

Fig. 4.9. The M_{33} coefficient as a function of the frequency for PU.

Eury et al. proposed that the hydrostatic electrostriction coefficient (Q_h) is linearly related to the ratio of the elastic compliance s, to the dielectric constant ε_r, $\frac{s}{\varepsilon_o \varepsilon_r}$ or $\frac{1}{Y \varepsilon_o \varepsilon_r}$ where Y is Young's modulus ($s = \frac{1}{Y}$).**[EUR 1999b]** As a consequence, M_{33} should be proportional to $\frac{\varepsilon_o (\varepsilon_r - 1)^2}{Y \varepsilon_r}$, due to the following relationship between the electrostriction coefficients M and Q, $M = \varepsilon_o^2 (\varepsilon_r - 1)^2 Q$.**[GUI 2003]**

In fact, the dielectric permittivity decreases when the frequency is increased while the Young's modulus increases with increasing frequency. Moreover the relaxation time also influences on the electrostrictive polymers behaviour. Previously, Diaconu et al. reported that the thickness strain decreases when the relaxtion time is decreased as shown Fig. 4.10. Therefore, the M_{33} coefficient decreases when the frequency is increased.**[DIA 2005]**

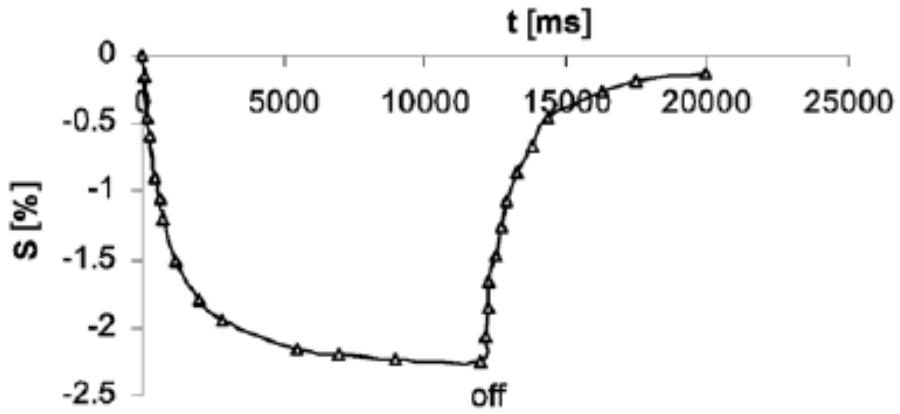

Fig. 4.10. Time response of relaxation for polyurethane.**[DIA 2005]**

As previously reported, the thickness strain increases at low electric field when the thickness is increased. The M_{33} coefficients as a function of thickness (PU samples at frequency of 20 Hz) are shown in Figure 4.11. The values of M_{33} increase when the thickness is increased and a saturation occurs for thicknesses higher than 100 µm. The dielectric constant as a function of the film thickness is shown figure 4.12.

Figure 4.13 shows Young's modulus as a function of thickness for PU samples. The dielectric constant is thickness independent in the thickness range whereas the Young's modulus decreases and saturates when the thickness is higher than 100µm. The increase of M_{33} is fully explained by the decrease of Y as M_{33} is roughly proportional to $\frac{e_o(e_r - 1)^2}{Ye_r}$.

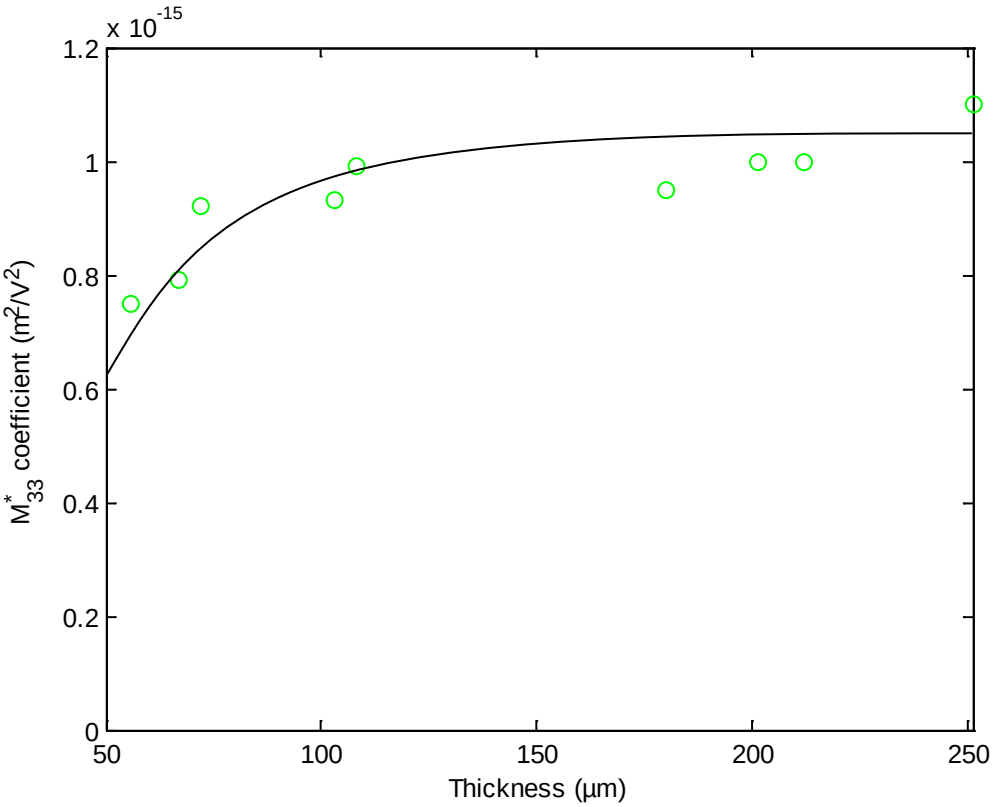

Fig. 4.11 The M_{33} coefficient as a function of the thickness of PU sample at 20 Hz.

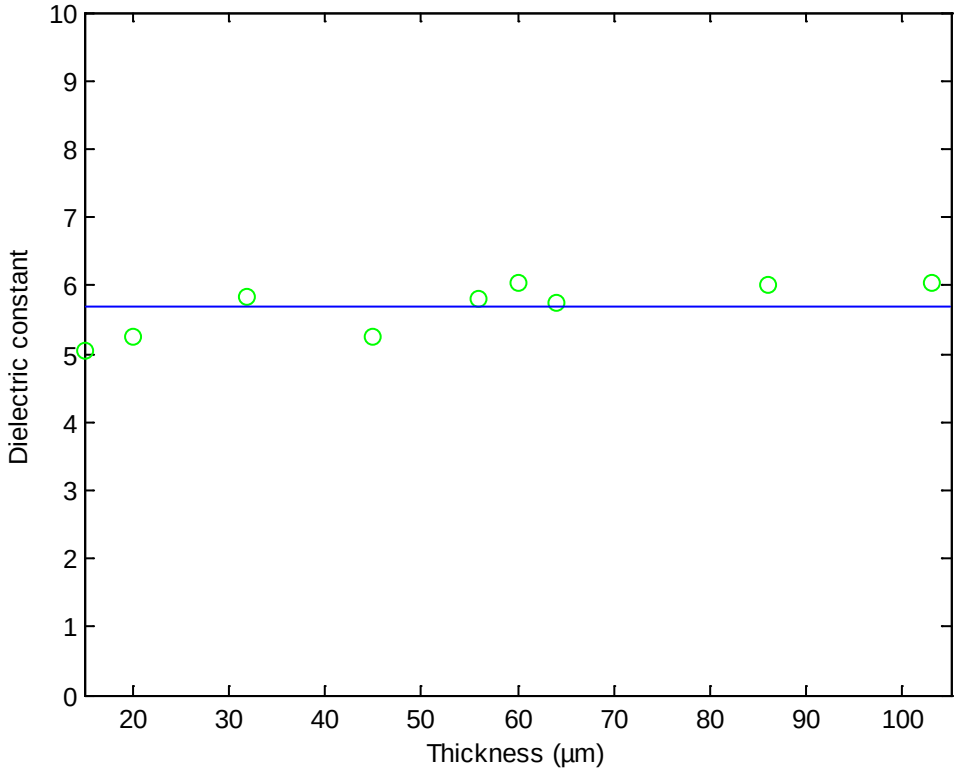

Fig. 4.12 Dielectric constant as a function of film thickness for polyurethane at 20 Hz.

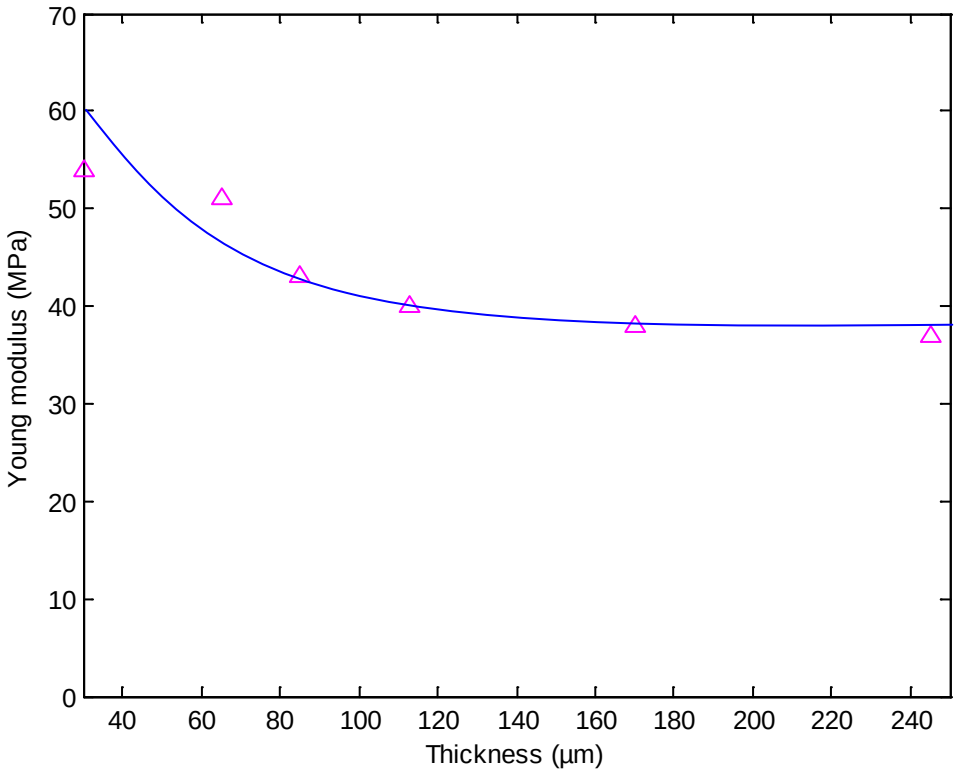

Fig 4.13 Dependence of Young's modulus on film thickness for polyurethane.

4.4.2 Experimental results of fillers effect on electrostrictive coefficient M_{33}

Figure 4.14 shows the induced strain as a function of the electric field for Nylon®6, Polyethylene, pure PU and composites filled with C nanopowder and SiC nanowire fillers. The operating frequency for all measurements was 0.1 Hz, and the driving electric fields used were in a range of 0 to 5kV/mm measured by using interferometer setup. The strain response of all the polymer films followed the quadratic equation $S_3 = - M_{33} E_3^2$ at low electric field (0-7 MV/m).

As previously reported, M_{33} can be calculated from the slope of S_3 versus E_3^2 at low electric field. The values are reported table 4.1. As various polymers are tested, it is important to calculate the Maxwell contribution to the measured strain.

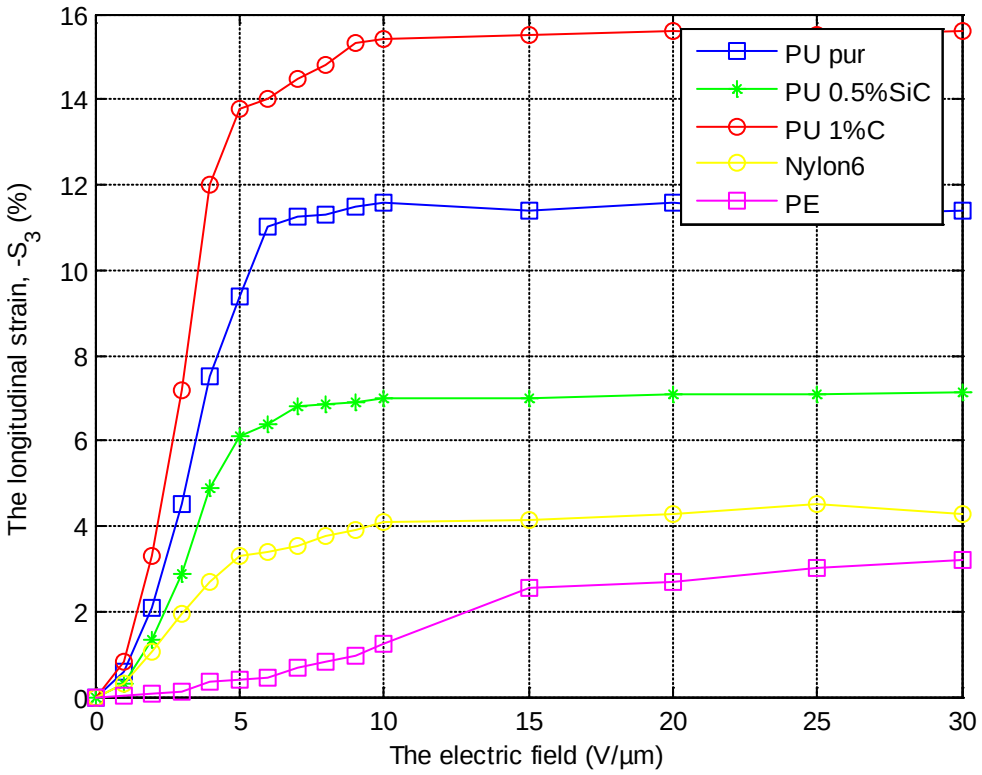

Fig. 4.14 Electric field dependence of the longitudinal strain measured at room temperature and frequency of 0.1 Hz.

The value of dielectric constants and Young's modulus for PU and composites are already indicated in section 3.7.1. Table 4.1 gives the Maxwell stress contribution to M_{33} for each of the materials, calculated directly from equation ($M_M = -\frac{1}{2Y}\varepsilon_o\varepsilon_r(1+2\upsilon)$) where υ is the Poisson ratio assumed to be equal to 0.5 for all the polymers.

Table 4.1 Estimations of the Maxwell stress contribution to the strain coefficient of dielectric materials.;

Samples	Thickness (μm)	e_r	Y (MPa)	M_{33} (m^2/V^2)	M_M (m^2/V^2)
PU	95	4.8	36	4.7E-15	1.3E-18
PU0.5%SiC	100	5.1	80	3.2E-15	7.5E-19
PU1%C	100	8.3	40	7.5E-15	2.0E-18
Nylon® 6	55	12.0	640	2.1E-15	1.5E-19
PE	95	2.3	2833	2.0E-15	6.6E-21
PVDF[a]	-	16	2381	2.2E-18	5.3E-20
PVDF/TrFE[a]	-	11	2500	9.8E-19	3.5E-20
PVC[a]	-	3.4	3003	4.7E-20	9.2E-21

[a] reference from **[SU 1999b]**

The experimental M_{33} values presented in table 4.1 can be explained if we assume that for these polymers, M_{33} is roughly proportional to $\frac{e_o(e_r - 1)^2}{Ye_r}$.

For example, the M_{33} of PU1%C is almost double compared to the M_{33} of the neat PU due to the ratio between their permittivity and due to the fact these two polymers have very closed Young's modulus. On the contrary, the relative low value of M_{33} observed for PU0.5%SiC is caused by its relative high value of Young's modulus. For the same reason, Nylon and PE exhibit low M_{33} due to their high Young's modulus.

Finally, as previously reported, the use of nanofillers increases the actuation capability if it only increases the permittivity **[DAN2004]** and not the Young's modulus.

4.4.3 Experimental results for fillers effect on high permittivity P(VDF-TrFE-CFE)

Fig. 4.15 presented the longitudinal strain versus the electric field for high permittivity polymers P(VDF-TrFE-CFE) either without filler or filled with C nanopowder, and the comparison with neat PU. All samples measurements are performed at 0.1 Hz for a film thickness of almost 65µm.

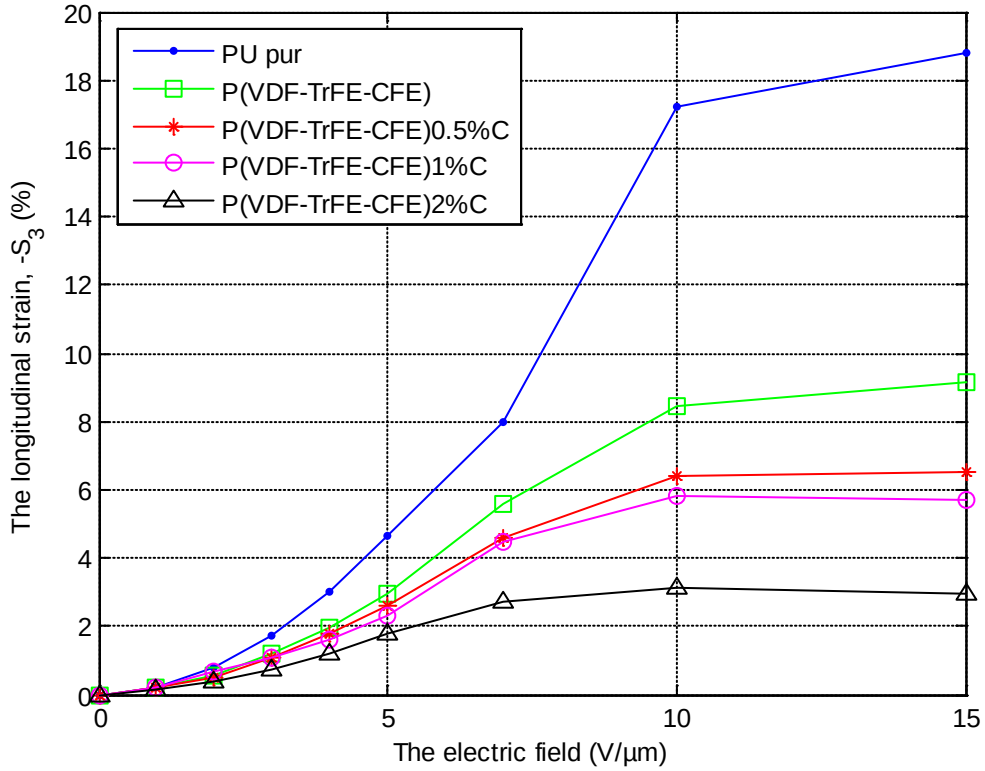

Fig. 4.15. Electric field dependence of the longitudinal strain measured at room temperature and frequency of 0.1 Hz.

The Maxwell contribution to the strain can be neglected. The values of the M_{33} coefficient of high permittivity polymers P(VDF-TrFE-CFE) and composites filled with nano C powders are presented in Table 4.2. These values have been calculated as previously from slope of S_3 versus E_3^2 at low electric field.

Table 4.2 Estimations of the M_{33} contribution to the strain coefficient of P(VDF-TrFE-CFE) and composites.

Samples	Thickness (μm)	e_r (0.1 Hz)	Y (MPa)	M_{33} (m^2/V^2)
PU	67	6	31	1.9E-15
P(VDF-TrFE-CFE)	64	42	250	1.2E-15
P(VDF-TrFE-CFE) 0.5%C	63	45	250	1.1E-15
P(VDF-TrFE-CFE)1%C	65	50	260	9.8E-16
P(VDF-TrFE-CFE)2%C	67	57	340	7.5E-16

This comparison is shown in table 4.2. It is seen that the value of M_{33} coefficient of high permittivity P(VDF-TrFE-CFE) is less than neat PU. Moreover, the measured M_{33} coefficient of P(VDF-TrFE-CFE) decreases with increasing content. This decrease was attributed to the increase of the Young's modulus versus content even if the dielectric constant of composites increases a little bit.

4.4.4 Results of effect of electrode on electrostriction polyurethane

Fig. 4.16 depicts the thickness strain versus the electric field for pure PU with and without the electrode. For this characterization, gold was sputtered on both of the films to form electrodes (diameter of 20 mm). This result is more pronounced for PU without electrode. For PU with electrode and electrode stuck with glue on substrate compared to PU without electrode, a gain of almost 0.09 and of almost 0.04 is respectively observed on the thickness strain.

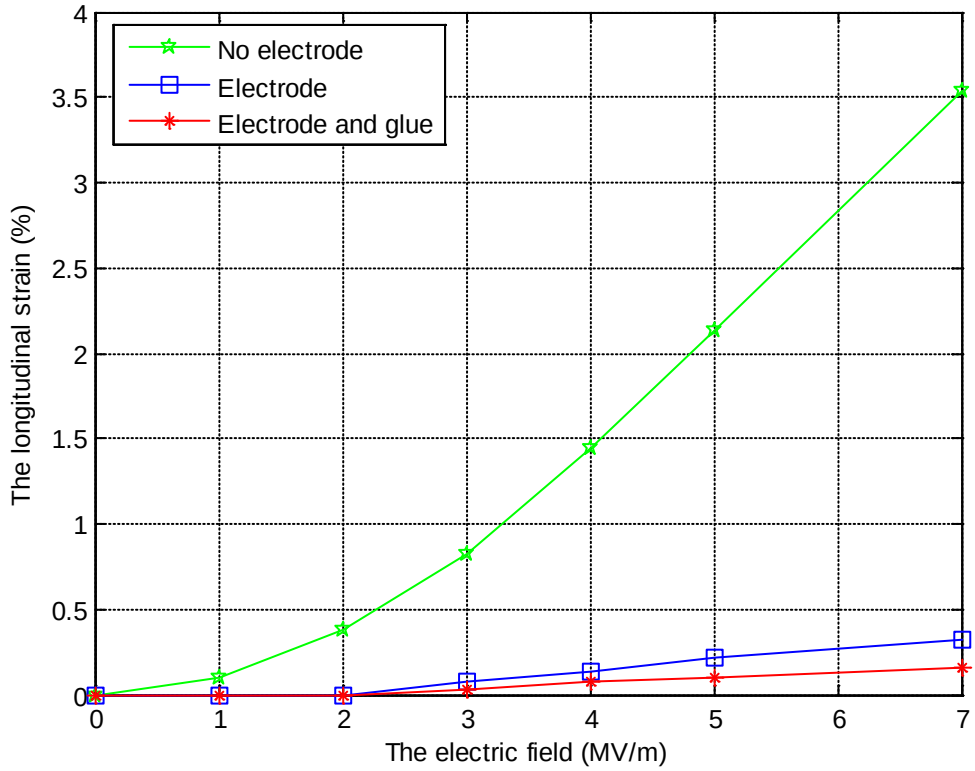

Fig. 4.16. Effect of electrode on electric field induced longitudinal strain measured at room temperature.

The stretching and compressing are mechanically coupled to the volume incompressibility of the polymer. If the polymer is sputtered by rigid electrodes (i.e. gold electrode), these electrodes can only compress closer together with the film. Therefore the thickness strain significantly decreases due to clamping effect of electrodes and glue on the film. Zhenyi et al. proposed a model of the thickness strain electrostriction with electrode.**[ZHE 1994]** The thickness strain, under the lateral strain

on electrodes and film was equal and the modulus and Poisson's ratio of the gold electrodes and film were independent of field, is given by:

$$S = - \frac{s}{E_1} K_{\text{constraint}} \qquad (4.25)$$

and

$$K_{\text{constraint}} = 1 - \frac{4u_1^2}{2(1 - u_1) + (1 - u_2)\frac{t_1 E_1}{t_2 E_2}} \qquad (4.26)$$

where E_1, u_1 and t_1 are the elastic modulus, Poisson's ratio, and thickness of the polymer film, E_2, u_2 and t_2 are the corresponding values for the gold electrodes and s is the electrostriction stress. Assumed parameter values for these constants (gold electrode on PU film) are summarized Table 4.3.

Table 4.3 Parameter of electrostriction PU films and electrode.

Parameter	**PU film**	**Electrode**[a]
Poisson's ratio	0.5[a]	0.42
Elastic modulus (Pa)	38 x 10^6	7.89x 10^{10}
Thickness (m)	90 x 10^{-6}	20 x 10^{-9}

[a] reference from**[ZHE 1994]**

$K_{\text{constraint}}$ is a correction factor produced by the surface constraint. Value of $K_{\text{constraint}}$ was calculated using parameter on table 4.3 and is equal to 0.56.

4.4.5 Experimental Results for size effect of Cu loading on Polyurethane.

The strain response for PU filled with micro Cu powder (MPU) and nano Cu powder (NPU) can be obtained by using gauge displacement technique. Figures 4.17 and 4.18 showed the obtained electrostrictive strain as a function of the applied field for MPU and NPU at room temperature and frequency of 0.1 Hz, respectively.

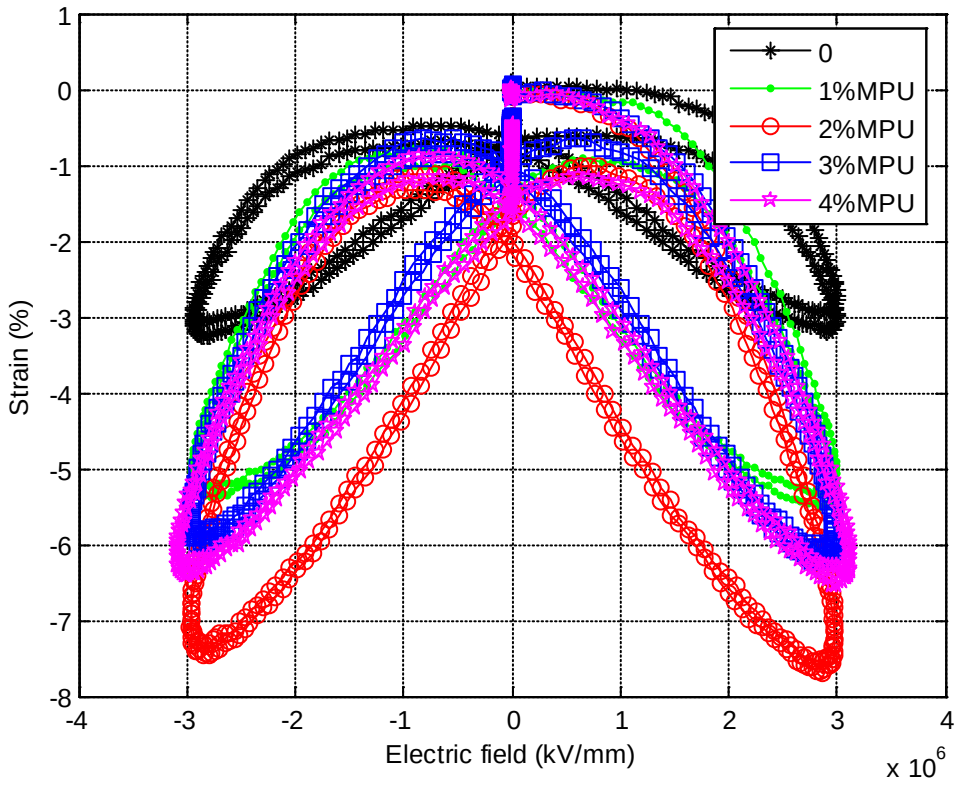

Fig. 4.17 The obtained strain as a function of the applied field for MPU composites at frequency of 0.1 Hz.

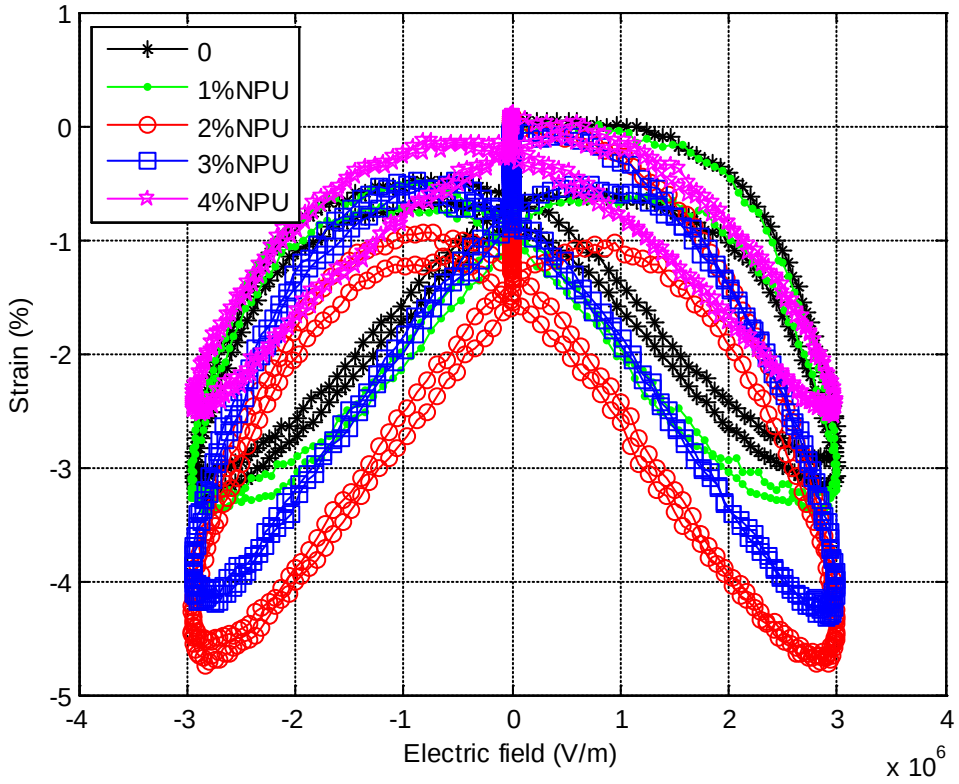

Fig. 4.18 The obtained strain as a function of the applied field for NPU composites at frequency of 0.1 Hz.

Hysteresis of S versus E is observed. An alternative electric field used for all samples was two cycles in a range of -3 to 3 V/μm. As expected for electrostriction, all samples show symmetry in the detected strain for positive and negative alternative field. In addition, the curves measured for the first cycle and the second one do not superimpose exactly. It may be attributed to electric and/or mechanical losses. The electrostriction coefficient for all samples was calculated on the first cycle by approximation the loop to a straight line.

Table 4.4 The electrostriction coefficient for MPU and NPU composites.

Content	e_r (0.1 Hz)		Y (x10^7 Pa)		M_{33} coefficient (x 10^{-15} m^2/V^2)			
					0.1 Hz		1 Hz	
	MPU	**NPU**	**MPU**	**NPU**	**MPU**	**NPU**	**MPU**	**NPU**
0	6.6	6.6	3.10	3.10	2.76	2.76	1.13	1.13
1%	7	8.1	3.30	3.72	6.20	3.00	1.43	2.57
2%	7.7	9.4	3.60	4.29	7.67	4.10	3.14	3.14
3%	8.1	9.6	4.20	4.99	6.16	3.50	2.73	2.20
4%	8.3	9.9	4.78	5.89	6.14	2.90	2.58	1.50

The obtained electrostriction coefficient of both MPU and NPU is higher than this one of PU regardless of frequency. The optimal volume fraction which corresponds to the highest M_{33} for all composites is found to be 2%. Content dependence of the M_{33} coefficient and Young's modulus for MPU composites are presented figure 4.19. Even if the permittivity also increased with content, this increase is not so large than this one of Young's modulus. This is why M_{33} decreases after the optimal content.

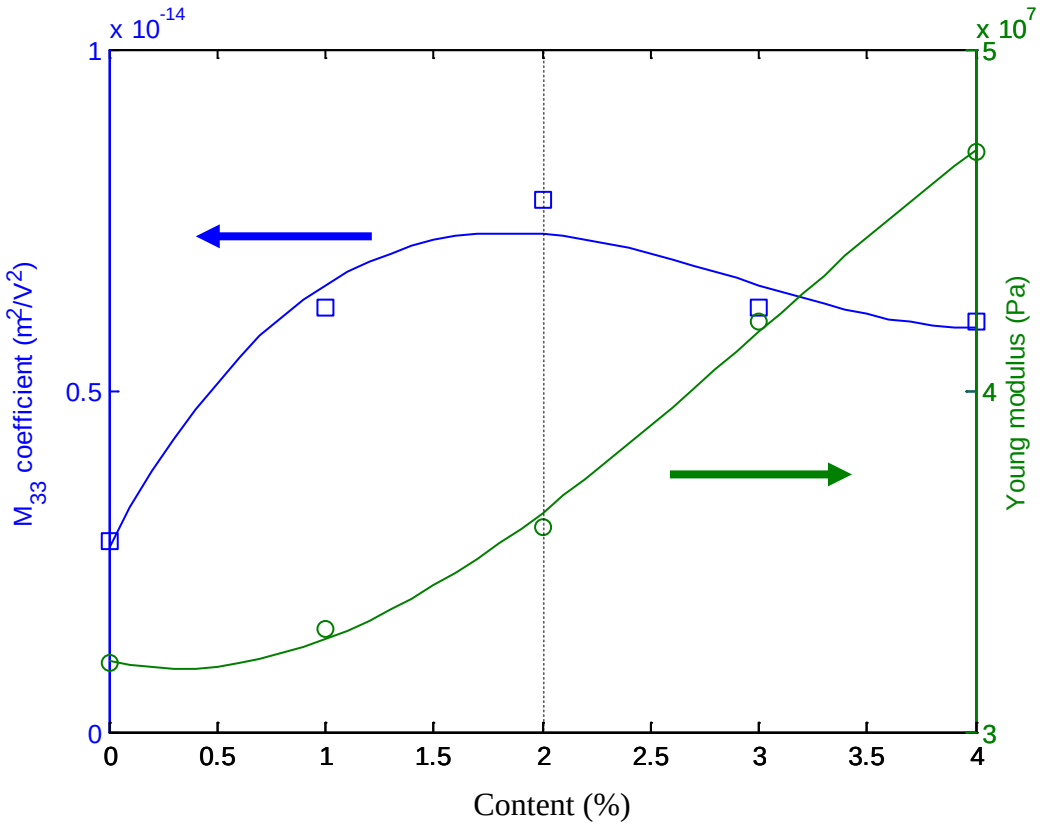

Fig. 4.19 Comparison of the M_{33} coefficient and Young's modulus for MPU composites as a function of content at 0.1 Hz.

Size effect of fillers content affects dielectric constant and mechanical behavior of matrix. Regardless of the size of the fillers, an increase of the dielectric permittivity as compared to the neat polymer, but the effect was more pronounced when nano-sized copper particles were used. This was in good agreement with the fact that the percolation threshold was lower for the nano-sized fillers than for their micro-sized analogs. Furthermore, the addition of Cu fillers on PU induces an increase of the Young's modulus of composites. Young's modulus for NPU is high than MPU composites. Therefore, the values of M_{33} coefficient for MPU composite is higher than NPU composites.

4.5 Conclusions

As expected for electrostriction, the electromechanical response of all materials, neat PU, high permittivity P(VDF-TrFE-CFE) and composites filled with nano charges, follows a simple quadratic relation with the applied electric field at low electric field. The two other possible mechanisms, named Maxwell stress and thermal effects have been shown to be too small to explain the observed response. The M_{33} coefficients of those materials were measured by either interferometer setup or gauge displacement sensor setup.

The influence of frequency and thickness affected the electrostriction behavior of polymer because it was mainly governed by the dielectric and elastic properties of those materials. The M_{33} coefficient decreases when increasing frequency due to dependence of dielectric properties on frequency and time relaxation of these materials. The M_{33} coefficient increases when increasing thickness due to dependence of elastic properties on thickness in particular because the Young's modulus decreases when the thickness of film is increased.

The electrostriction coefficient, M_{33} for PU composites filled with SiC nanowire is lower than composites filled with C nanopower. It is the reason why SiC nanofilled PU with the highest *Y* has the lowest M_{33} coefficient, almost in the ratio of the Young modulus, when compared to the neat PU and the C nanofilled PU. It also explains why C nanofilled PU and neat PU exhibit closed values of M_{33} coefficient. This behavior is also observed on P(VDF-TrFE-CFE) terpolymer. The value of M_{33} coefficient for high permittivity P(VDF-TrFE-CFE) terpolymer is lower than PU due to its very large Young's modulus.

Consequently, these results point out that both the dielectric and modulus are linked. In case of actuation, the composites need a high permittivity but Young's modulus should not be too large in order to enhance actuator capability.

Chapter 5:

Improving efficiency of the energy harvesting

5.1 Introduction

This chapter is to evaluate the energy harvesting efficiency of, either nonpercolated composites based on polyurethane (PU) filled with copper (Cu) powders of varying sizes or high permittivity P(VDF-TrFE-CFE) terpolymer filled with C nanofillers and to discuss the obtained results using data from chapter 3. Dielectric constant of composite can be improved with increasing fillers concentration and consequently it will increase the harvested energy. In this chapter, experimental values of the harvested current and power have been compared to the calculated data obtained from analytical modeling - using the constitutive equations of electrostriction - of the first flexural mode of the beam.

5.2 Improving the efficiency of harvested current by filling PU with metallic particles or by high permittivity terpolymer

From earlier chapter 2, it has been shown that the increase of the dielectric permittivity of EAPs is one of the key factors for increasing the energy conversion. Among the various ways to raise the dielectric permittivity, the development of polymeric composites filled with conductive nanofillers is of interest. Moreover, such metal-composites are very interesting because it is possible to tune their electrical properties by choosing a suitable concentration. The electrical properties are directly related to the permittivity and conductivity, which strongly depend on the dispersion of

the fillers throughout the polymer as well as on the effective microstructure of the composite.

The concentration of the metal fillers has proven to be a significant parameter, governing the electrical behavior of the metal-polymer composites. In chapter 3, the dielectric constant of composites filled loading is always higher than the pure PU. For PU filled with copper composites, it is noted that dielectric constant increases with increasing fillers concentration. At a given content, the increase of the dielectric constant is higher for the PU filled with copper nanopowder (NPU) than for the PU filled with copper micropowder (MPU). Composite filled with copper needs to be maintained the insulating behaviour for electrostriction on energy harvesting. It is the reason why the studied this composites have been designed with low metallic fillers content, to be far from the percolation threshold.

The effect of the filler size on the harvested current of the composites has also been investigated. Moreover, experimental values of the harvested current and power have been compared to the calculated data obtained from analytical modeling - using the constitutive equations of electrostriction - of the first flexural mode of the beam.

5.3 Experimental results

5.3.1 Effect of filler content and filler size to improve energy harvesting

As mentioned in 2.4, the harvested current measurement of the electrostrictive composites was performed on the cantilever beam at its resonance frequency (20 Hz) and for $\iint_A \frac{\partial S_1}{\partial t} dA$ kept constant (7.5×10^{-7} m.(m.s)$^{-1}$). Figures 5.1(a) and 5.1(b) present the harvested current as a function of the DC electric field for the MPU and NPU composites, respectively. As expected by the modeling a linear dependence of I versus E_{dc} is observed. From these curves, one could subsequently determine YM_{31} by measuring the slope of the I-E_{dc} curves.

(a)

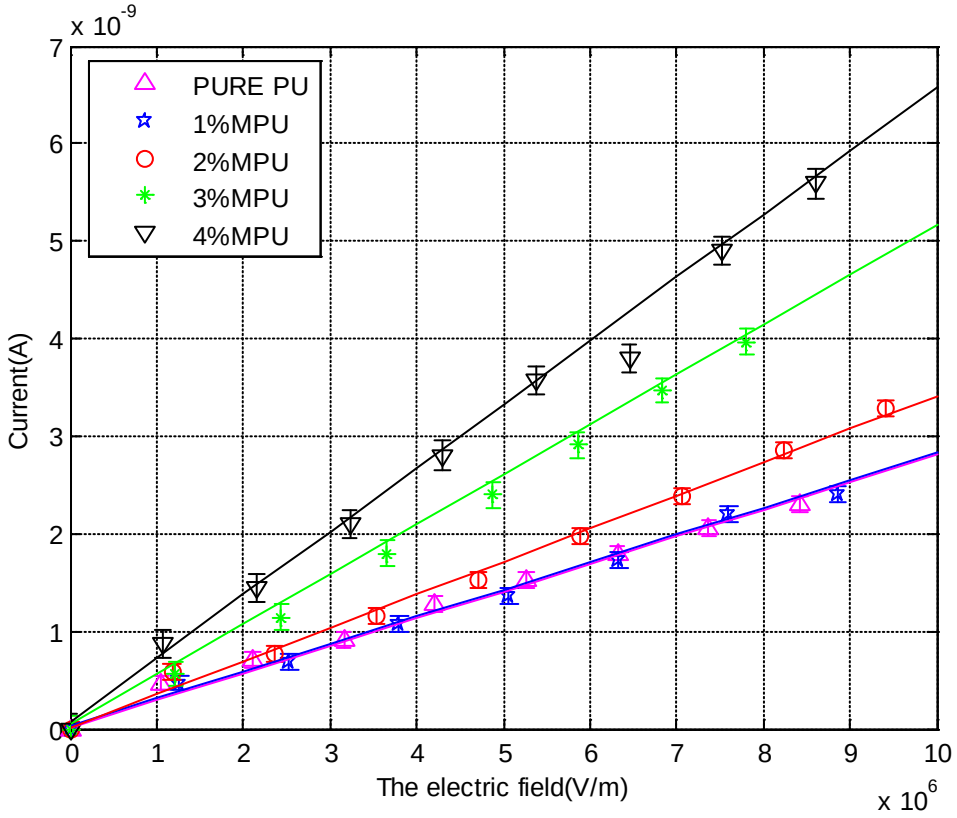

(b)

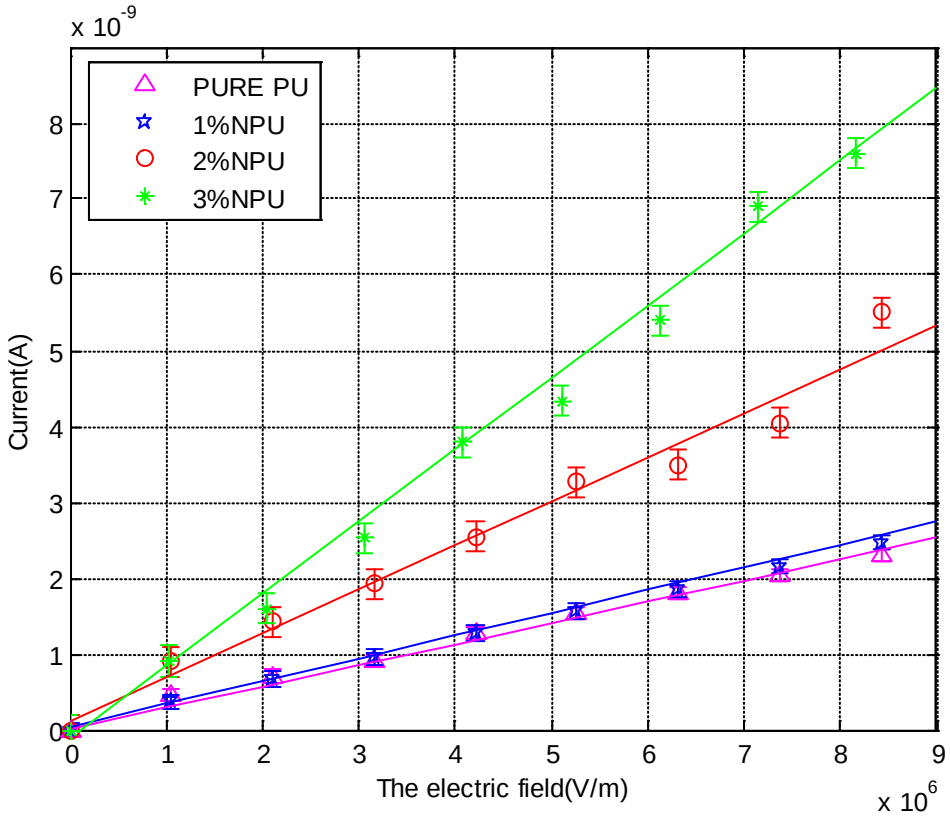

Fig. 5.1. The induced current as a function of the electric field for the neat and (a) MPU and (b) NPU composites at an electric filed (6 MV/m) and a kept strain rate (7.5´ 10^{-7} m.$(m.s)^{-1}$).

Table 5.1 summarizes the values of e_r, Y and YM_{31} ($YM_{31} = \frac{slope}{2\int_A \frac{\partial S_1}{\partial t} dA}$) versus the filler content for both the MPU and NPU composites. The harvested current increased for increasing values of YM_{31}. For both the MPU and NPU materials, an increase of the harvested current were observed when the content of fillers was raised, leading to the observed increase of the YM_{31} values in Table 5.1.

Table 5.1 Estimation of the strain coefficient of neat PU, MPU and NPU composites

Samples	**Thickness (μm)**	e_r **(20Hz)**	Y **(MPa)**	YM_{31} **(x10^{-10} m^2/V^2.Pa)**
Pure PU	95	5 .68	31.2	1.82
1% **micro** Cu filled composites	90	6.03	33.0	1.87
2% **micro** Cu filled composites	91	6.34	36.0	2.27
3% **micro** Cu filled composites	91	6.70	42.0	3.27
4% **micro** Cu filled composites	93	7.11	46.8	3.89
1% **nano** Cu filled composites	107	6.70	37.2	2.03
2% **nano** Cu filled composites	96	7.35	42.9	3.87
3% **nano** Cu filled composites	95	7.80	50.4	6.33

In a previous paper **[GUI 2003]**, it has been reported that Q is proportional to $\frac{1}{Ye_oe_r}$. As a consequence, M_{31} should be proportional to $\frac{e_o(e_r - 1)^2}{Ye_r}$ and YM_{31} to $\frac{e_o(e_r - 1)^2}{e_r}$. In this case, the increase of the harvested current was induced by an augmentation of the permittivity.

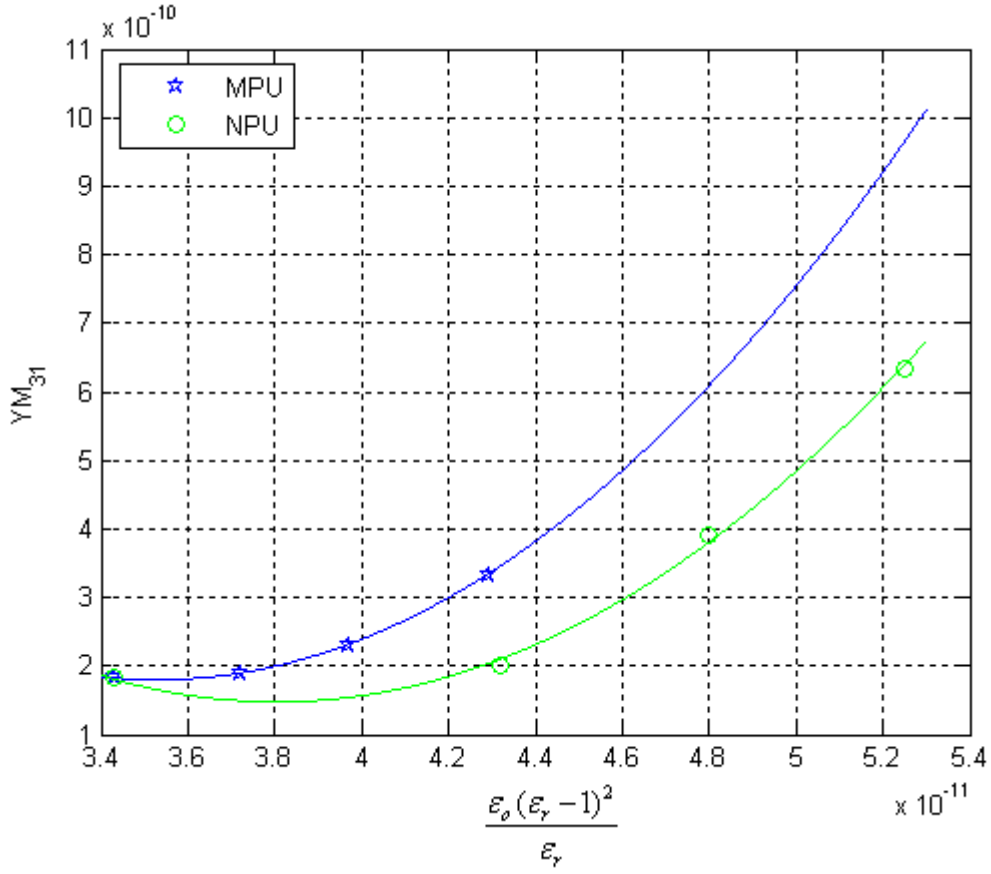

Fig. 5.2. The YM_{31} as a function of $\frac{e_o(e_r - 1)^2}{e_r}$ for MPU and NPU composites at 20 Hz.

Figure 5.2 depicts YM_{31} versus $\frac{e_o(e_r - 1)^2}{e_r}$ and clearly shows that the assumed proportionality was not valid for the composites in the present study. However, the increase of the harvested current corresponds to an increase of the permittivity and could be related to the use of metallic particles as fillers, which enhanced the

performance. The dependence of M_{31} versus e_r and Y for these new composites is still under investigation.

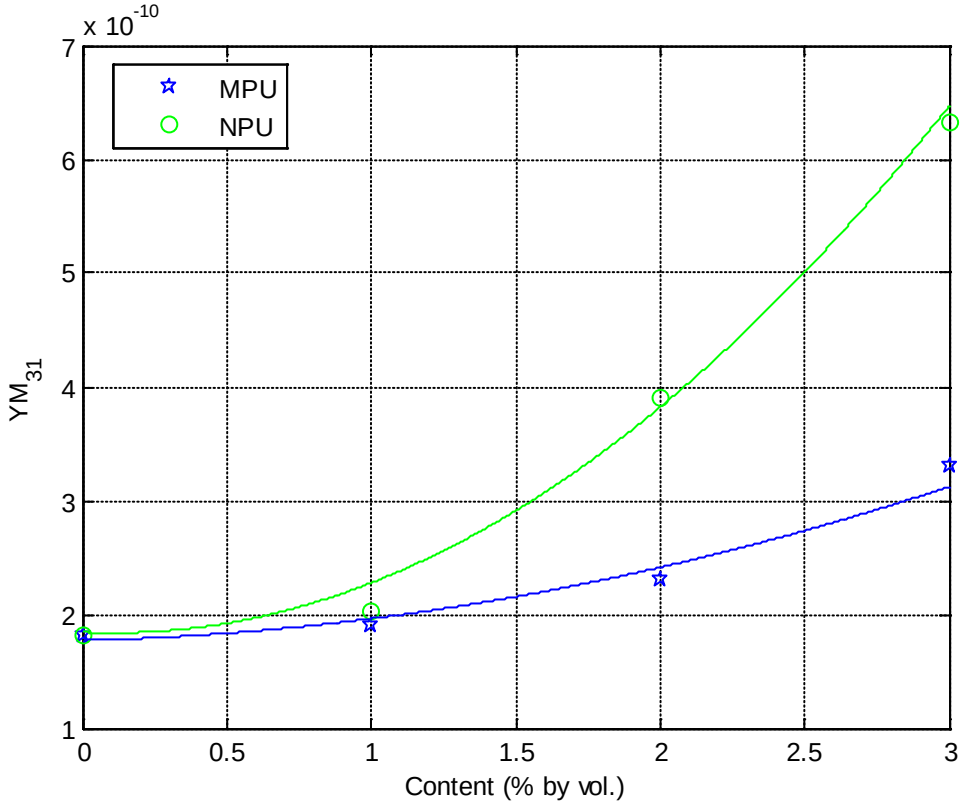

Fig. 5.3. The YM_{31} as a function of the volume content of fillers for MPU and NPU composites at an electric field (6 MV/m) and a kept strain rate ($7.8´ 10^{-7}$ m.(m.s)$^{-1}$).

Figure 5.3. depicts the variation of YM_{31} versus the concentration of filler. The harvested current was measured at E_{DC} = 6 MV/m for both MPU and NPU composites. An increase in YM_{31} was observed when the filler content was raised. The NPU composites presented a more significant enhancement of YM_{31} as opposed to the MPU composites. In both cases, the shape of the curves followed a quadratic law. The observed results can be explained by the fact that the Young modulus and the permittivity of an NPU composite with a given filler content was consistently higher than that of its MPU counterpart (cf. Table 5.1).

5.3.2 Measurement of the harvested power by using a resistive load

The variation of power calculated using $P = \frac{R.I_{sc}^{2}}{2}$ as a function of load at frequency 20 Hz for neat PU, 2%MPU and 2%NPU is shown in Fig. 5.4. It shows that the power rapidly increase and then searches maximum. Experimentally the magnitude of power for neat PU, 2%MPU and 2%NPU using the above expression at frequency of 20 Hz and its optimal load was found to be $8.4' 10^{-3}$, $1.5' 10^{-2}$and $3.9' 10^{-2}$ nW, respectively.

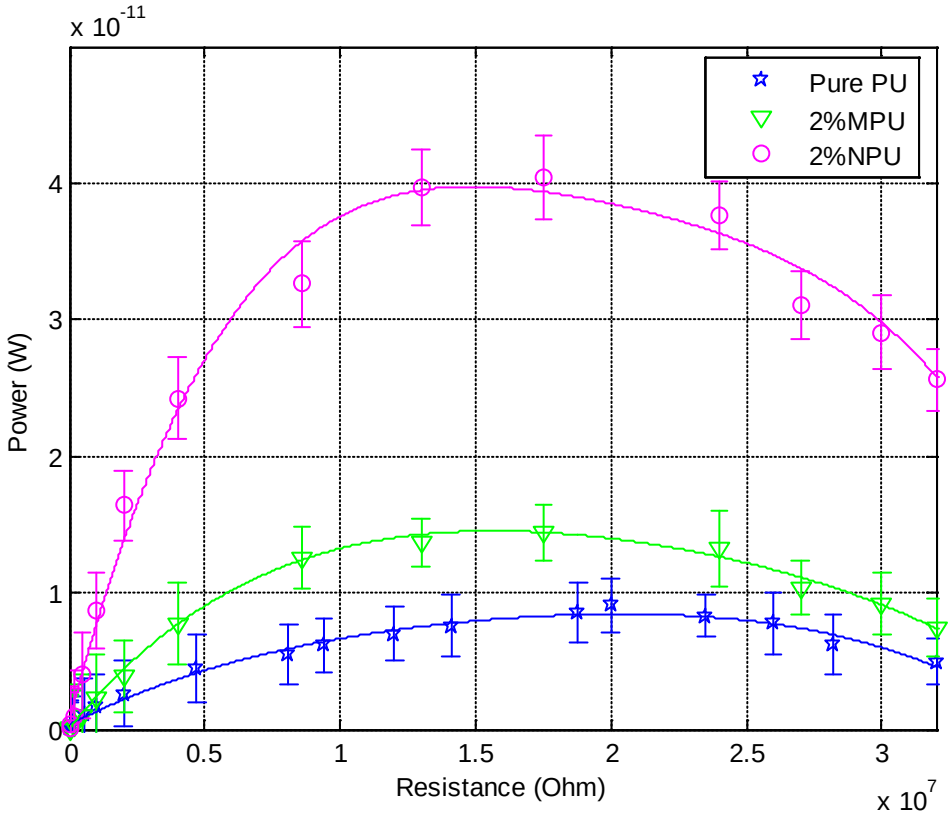

Fig. 5.4. Variation of the power as a function of the load for neat PU, 2%MPU and 2%NPU.

The power reaches maximum at an optimum load or matched load (R_c^{Opt}) which for the equivalent circuit shown in figure 5.5 is given as

$$R_c^{Opt} = \left| R_s + \frac{1}{j\omega C} \right|$$

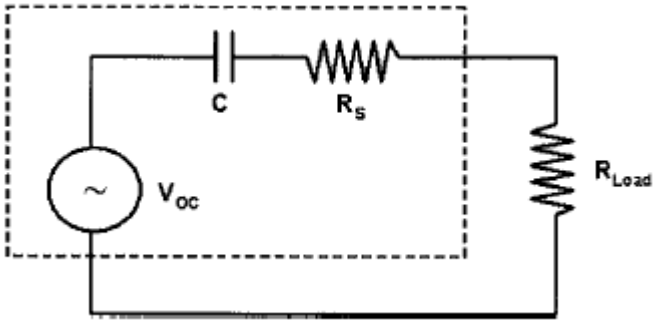

Fig.5.5. Equivalent circuit representation of the generator.

It is evident from this figure that power depends on C is the damped capacitance and R_s is the series resistance of generator. Which, generally $R_s << \frac{1}{j\omega C}$

So theoretical matching of optimum load can be approximated **[SHA 2005]** as

$$R_c^{Opt} = \frac{1}{\omega C} = \frac{1}{2\pi f.C} \qquad (5.1)$$

Table 5.2 The comparison of power and optimal load.

Samples	Thickness (μm)	ε_r (20Hz)	$\tan\delta$ (20Hz)	C (pF) (20Hz)	R_{Thoery}^{Oti} (W)	$R_{experiment}^{Oti}$ (W)	P_{Max} (nW)
Neat PU	95	4.9	0.0690	295	2.7×10^{7}	2.4×10^{7}	8.4×10^{-3}
2%NPU	95	6.3	0.0986	380	2.0×10^{7}	1.7×10^{7}	1.5×10^{-2}
2%NPU	93	7.0	0.1024	426	1.8×10^{7}	1.6×10^{7}	3.9×10^{-2}

Table 5.2 presents the comparison of power and optimal load for neat PU, 2%MPU and 2%NPU composites. It shows that the value of optimum load resistance for composites is closely with neat PU due to its capacitance and dielectric constant is not far away. S. Priya explained that the magnitude of the matching load or optimum land depends on the damped output capacitance, dielectric loss factor.

5.3.3 Validation of the power energy harvesting

The harvested power could be calculated from the harvested current using $P_{harvesting} = \frac{R_c . I_{sc}^{\ 2}}{2}$ (5.2), where R_c is the matched load. In this case, R_c is equal to $\frac{1}{C_p w}$, where C_p is the capacitance of the composite and w the pulsation of the beam vibration. C_p could be calculated as a function of the dimensions of the composite (L: length, w: width and t: thickness) and its permittivity using the following formula: $\frac{e_0 e_r L w}{t}$.

Consequently, the power can be written as

$$P_{Harvesting} = 2\frac{t}{e_o e_r w L w}(M_{31}Y)^2 . E_{dc}^2 . \left[\int_A \left(\frac{\partial S_1}{\partial t}\right) . dA\right]^2 \qquad (5.3)$$

Figure 5.6 depicts the harvested power ($P_{Harvesting}$) calculated from equation 5.3 by using the data from Table 5.1. E_{DC} was kept constant at 6 MV/m (6 V/mm), which corresponded to an applied voltage of 600 V, and $\int_A \frac{\partial S_1}{\partial t} dA$ = 5.5×10^{-7} m.($m.s^{-1}$), which corresponded to an average strain of 0.86×10^{-5} (m/m) (dotted lines). The figure also presents the measured harvested power, under equivalent conditions, versus the content (squares for the MPU composite, triangles for the NPU composite).

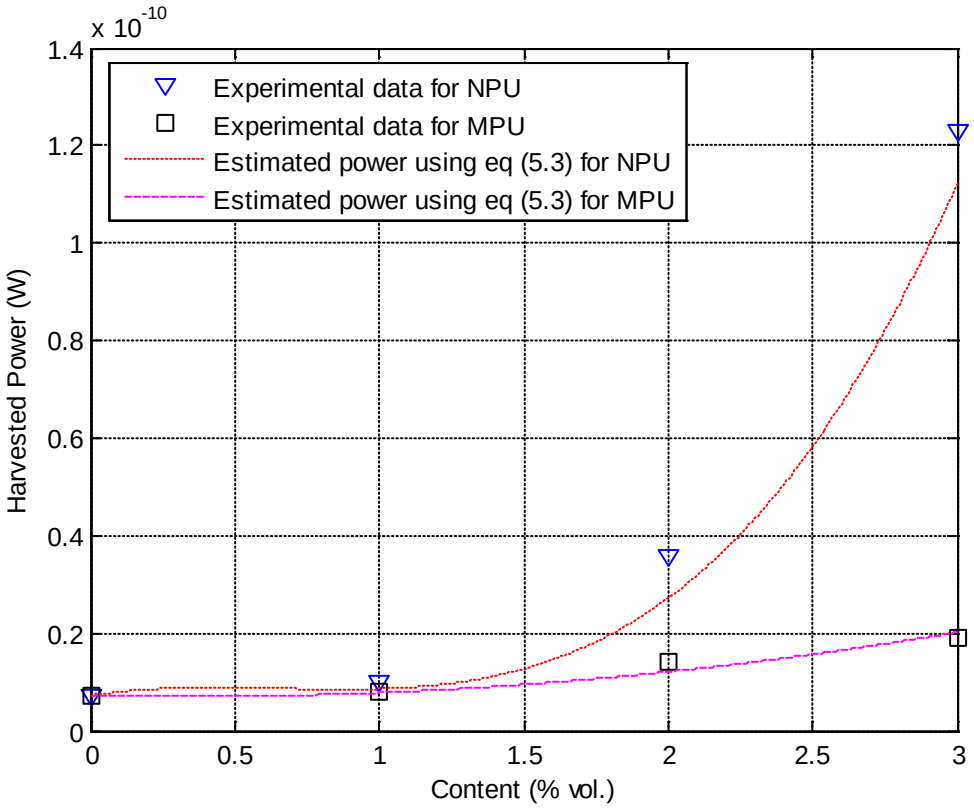

Fig. 5.6. The experimental harvested power and the estimated harvested power (dotted lines) versus the content for MPU and NPU composites at an electric filed (6 MV/m).

The calculated power was in good agreement with its measured counterpart, which validates the model proposed herein. In addition, it could be shown that nanofillers led to a higher enhancement of the power as opposed to microfillers.

5.3.4 High permittivity terpolymer to improve energy harvesting

Figure 5.7 presents the induced current as a function of the electric field for P(VDF-TrFE-CFE) terpolymer, (TP) and C nanofilled P(VDF-TrFE-CFE), (C TP) to compare with neat PU. The experimental is performed at kept constant $\int_A \frac{\partial S_1}{\partial t} dA$ of 6.4×10^{-7} m.(m.s^{-1}) and 19 Hz. The figure of merit for harvested current, YM_{31} for P(VDF-TrFE-CFE) terpolymer and C nanofilled P(VDF-TrFE-CFE) terpolymer is shown in table 5.3.

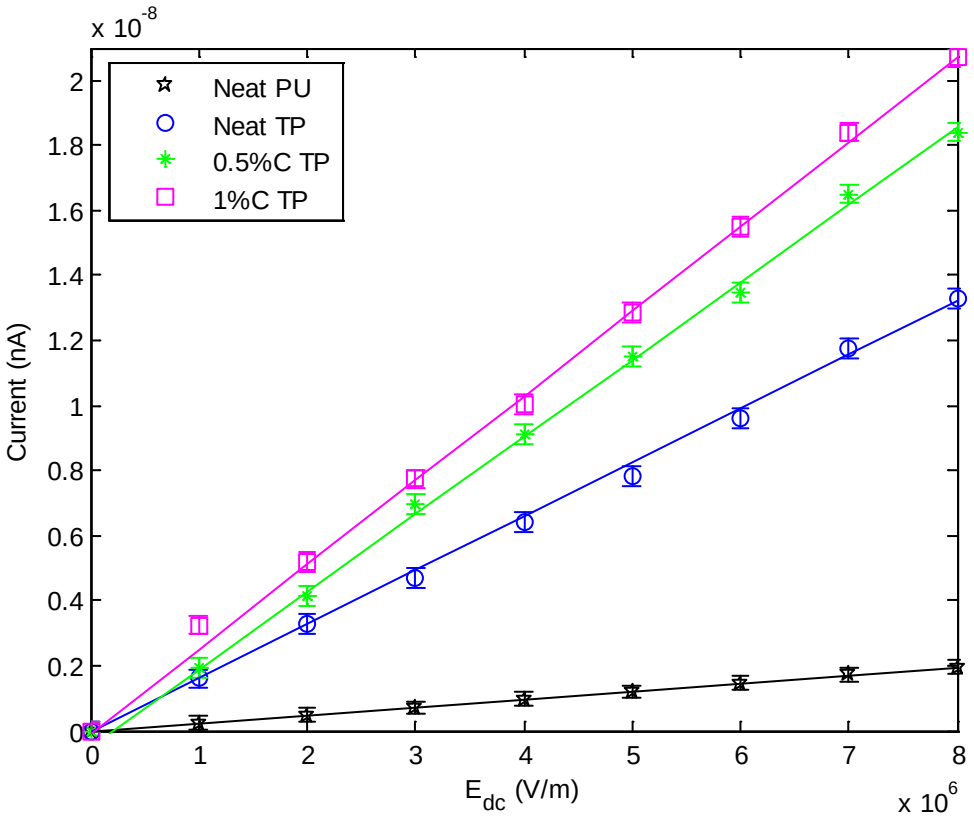

Fig. 5.7. The harvested current as a function of the electric field for the neat and filled P(VDF-TrFE-CFE) terpolymer to compare with neat PU.

An increase in the figure of merit $M_{31}Y$ was observed when the filler content was raised. The ratio between the $M_{31}Y$ for neat PU and P(VDF-TrFE-CFE) terpolymer is equal to 7.1 and terpolymer filled with C nanocharge is more than 10 which is shown in table 5.3. These results give that the enhanced harvested current and figure of merit for electrostrictive material is a consequence of the permittivity of sample, but M_{31} is not proportional to $\frac{e_o(e_r - 1)^2}{e_r Y}$ for filled composites.

Table 5.3 Estimations of the figure of merit for high permittivity terpolymer.

Samples	t (μm)	e_r	Y (MPa)	$M_{31}Y$	Ratio of figure of merit $(M_{31}Y)_i/(M_{31}Y)_{PU}$
Neat PU	68	5.9	35	1.94´ 10-10	1.0
Neat P(VDF-TrFE-CFE)	67	27.3	250	1.43´ 10-9	7.1
P(VDF-TrFE-CFE)filled with 0.5% C nano-fillers	68	38.3	250	2.42´ 10-9	11.7
P(VDF-TrFE-CFE)filled with 1% C nano-fillers	65	41.6	280	2.67´ 10-9	13.2

Finally, the obtained output power for high permittivity P(VDF-TrFE-CFE) terpolymer will be examined. Figure 5.8. presents the output power of electrostrictive materials as a function of strain rate for P(VDF-TrFE-CFE) terpolymer, neat PU and C nanofilled composites at its resonance frequency and a fixed electric field (5 MV/m).

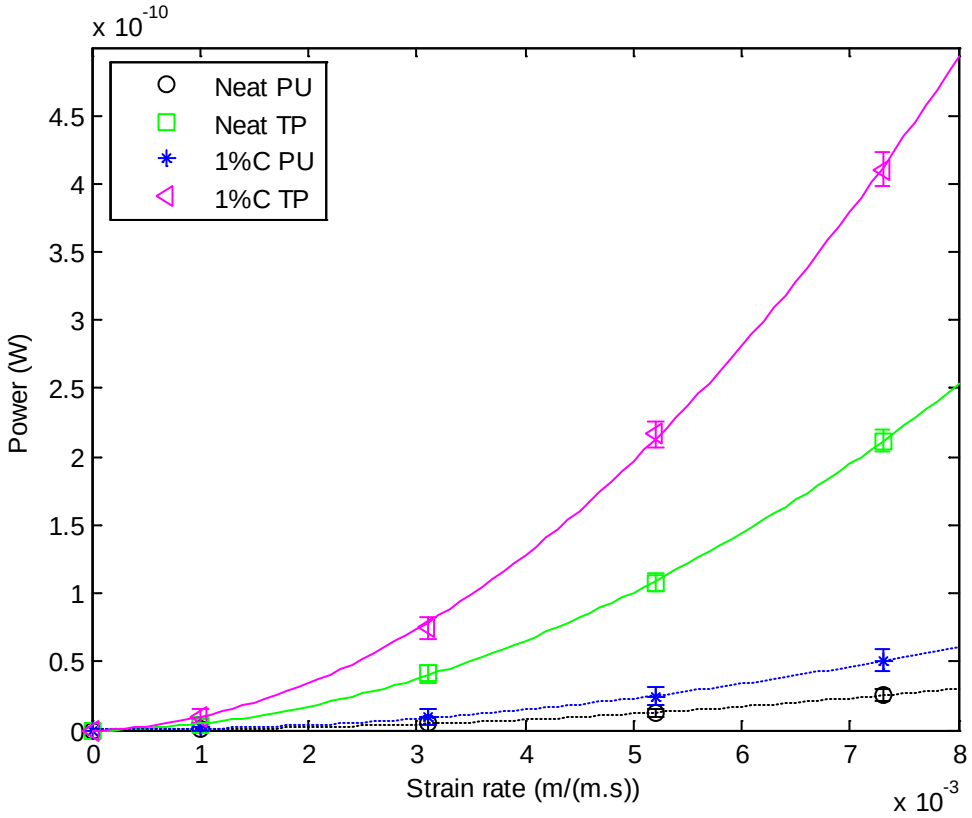

Fig. 5.8. The output power as a function of strain rate for terpolymer and filled with C nanocharge.

The output power of the terpolymer, the terpolymer with C nanofillers, neat PU and PU filled with C nanofillers under 5 MV/m and at 18 Hz is estimated to be 1.72 nW/cm^3, 3.06 nW/cm^3, 0.20 nW/cm^3 and 0.50 nW/cm^3, respectively. The ratio between the estimated harvesting power for neat PU film and nanofilled composites is, respectively, equal to 8.6 for terpolymer, 15.3 for terpolymer filled with nanofillers and 2.5 for PU filled with nanofillers.

5.4 Conclusions

In this chapter, the value of harvested current and harvested power can be improved by using nanofilled polymers. An increase of the harvested current as well as of the output power was experimentally observed for NPU and MPU composite when the filler content was raised. Moreover, the high harvested current and harvested power is observed for high permittivity P(VDF-TrFE-CFE) terpolymer. The ratio between the $M_{31}Y$ for neat PU and P(VDF-TrFE-CFE) terpolymer is equal to 7.4-fold and compared with terpolymer filled with C nanocharge is more than 10-fold. The use of fillers enhances the harvested current and the power due to the increase of the permittivity. For composites, the proportionality between M_{31} and $\frac{e_o(e_r - 1)^2}{e_r Y}$ is not observed as it has been previously reported for neat polymers.

Chapter 6:

Conclusions and Future work

6.1 Main Conclusions

In this study, analytical model that attempt to predict mechanical energy harvesting from a vibrating cantilever beam have been designed, developed and tested. Experimental measurements of the harvested current have been compared to the theoretical behaviour predicted by the proposed model. A good agreement was observed between the two sets of data, which consequently validated that the modelling can be used to optimise the choice of materials. A method for performing energy conversion was developed, and consisted in employing polyurethane and polymers loaded with nanofillers since such materials can convert the ambient vibration energy that surrounds them into an electrical energy.

Specific contributions of this study to mechanical energy harvesting are summarized as follows:

· Analytical modelling based on the constitutive equations of electrostriction to estimate the harvested current of electrostrictive polymer is developed and examined. The proposed model was verified based on experimental results with high accuracy. In order to verify the validity of the modelling, experimental measurements of the harvested current versus the area (A), versus the dc electrical field (E_{dc}) and versus the stress rate ($\frac{\P S_1}{\P t}$), and various the resonance frequency and thickness films were performed. The results of these experiments clearly demonstrated the validity of the proposed model, along with its capability of providing the shape of the harvested current. It has been in particular shown that the harvested current not only increased

when the first resonance frequency is increased in good agreement with the analytical modelling but also when the thickness of the polymer film is increased.

· The model proposed, based on the electrostrictive behaviour, was able to predict the amount of the current power capable of being generated through the vibration of a cantilever beam to which films of neat and composites were attached. The composites loaded with nanofillers demonstrated enhanced results of current harvesting and energy conversion due to increase the permittivity of the composites and consequently its capabilities to harvest electrical energy on mechanical virbraions. In this sense, the developed model constituted an effective tool for accurately predicting the harvested energy.

· The proposed model could be used to obtain the electrostrictive coefficient (M_{31}) of the materials. It has been shown that the electrostirctive coefficient, M_{31} is not depend on the dc electric field and strain rate but depends on the frequency and thickness of polymer. The electrostriction coefficient of polymers is roughly proportional to $\frac{e_o(e_r - 1)^2}{Ye_r}$.

· The Figure of Merit for the harvested current ($FoM = M_{31}Y$) is almost equal to the permittivity of the film in term of $\frac{e_o(e_r - 1)^2}{e_r}$ by assuming that M_{31} is almost proportional to $\frac{e_o(e_r - 1)^2}{e_r Y}$. Consequently, composite which has the highest permittivity leads to the highest current whereas neat polyurethane which has the lowest one leads to the lowest value of current. Therefore, in order to increase the power of conversion of the composites, it is necessary to increase the dielectric constant.

· The development of these new composites to improve the available current in case of energy harvesting are performed by either filling PU with metallic particles or high permittivity terpolymers. Moreover, those metal-composites are of great interest because their performances can be adapted by a suitable choice of concentration. It is shown that the dielectric constant of the all composites are higher than that the pure PU. The slight enhancement of the permittivity versus fillers content can be explained by the incorporation of conductive charges in the polymer matrix. Regardless of the size of the fillers, an increase of the permittivity as compared to the neat polymer took place, but

the effect was more pronounced when nano-sized copper particles were used. This was in good agreement with the fact that the percolation threshold was lower for the nano-sized fillers than for their micro-sized analogs. The value of dielectric constant of P(VDF-TrFE-CFE) terpolymers are distinctly higher than neat PU regardless of the frequency. Moreover, it can be noted that the dielectric constant increased with an increasing filler concentration regardless of the frequency.

· In case of actuation, the experimental results insist on the fact that the both the dielectric and modulus are linked and need a high permittivity but Young's modulus should be not too large in order to enhance actuator capability.

· An increase of the harvested current as well as of the output power was experimentally observed for NPU and MPU composite when the filler content was raised. This increase corresponded to the increase of the figure of merit for the harvested current (YM_{31}) and of the power harvesting ($\frac{(M_{13}Y)^2}{e_o e_r}$), and the result was more pronounced for the NPU composites. Moreover, the high harvested current and harvested power is observed for high permittivity P(VDF-TrFE-CFE) terpolymer. The ratio between the $M_{31}Y$ for neat PU and P(VDF-TrFE-CFE) terpolymer is equal to 7.4-fold and compared with terpolymer filled with C nanocharge is more than 10-fold. These results gives that the enhanced harvested current and figure of merit for electrostrictive material is a consequence of the permittivity of sample.

· Consequently, the proposed model was able to predict the energy harvesting and provide a good description of the experimental results and could thereby aid in the choice of the best material., higher values of the harvested current could be obtained with increasing permittivity of the electrotrictive polymer.

6.2 Future work

Future work may focus on the following issues to further improve the performance of the current design.

· The energy harvesting using cantilever beam needs to increase the strain of sample to enhance the harvested current. With double clamp structure, it is possible to enhance harvested power from vibrating structures.

· An analytical model that properly predicts power generation for an arbitrary substrate shape can be established. Plates, disks, and membranes are all shape that are used in industry and that could provide a base for power generation.

· The storage of the generated power should be designed and examined for electrostrictive polymer. Storing a charge in a capacitor or recharging a battery is possible options. Applications for the use of the output power for electrostrictive polymer can be determined.

· To improve the harvest power, the permittivity of electrostrictive polymer should increase. The development of these new composites such as P(VDF-TrFE-CTFE) terpolymer with conductive polymer, polyaniline (PANI) should be studied and investigated. Moreover, the concentration, shape of fillers or conductive polymers are of great interest how to get the giant permittivity composite while kept as non-conductive polymers because their performances can be improved the harvest power.

· The used dispersion of fillers is homogenous and in volume in this study, the next step will concern the organization of the fillers with the matrix, for example in a 1.D and 2.D distribution in order to increases the content and consequently the Maxwell-wagner interfacial polarization.

List of figures

List of tables

List of published

1. L.Lebrun, D.Guyomar, B. Guiffard P.-J. Cottinet and **C. Putson**, *The Characterisation of the harvesting capabilites of an electrostrictive polymer composite*, Sensors and Actuators A 253, 251-257 (2009).
2. D.Guyomar, L.Lebrun, **C. Putson**, P.-J. Cottinet, B. Guiffard and S. Muensit, *Electrostrictive energy conversion in polyurethane nanocomposites*, J. Appl. Phys. 106, 014910 (2009).
3. P.-J. Cottinet, D.Guyomar, B. Guiffard, **C. Putson** and L.Lebrun, *Modeling and Experimentation on an Electrostrictive Polymer Composite for Energy harvesting*, IEEE Transactions on Ultrasonics Ferroelectrics and Frequency Control. 57(4), 774-784 (2010).
4. **C. Putson,** L.Lebrun, D.Guyomar, N. Muensit,, P.-J. Cottinet, L. Seveyrat and B. Guiffard, *Effects of copper filler sizes on the dielectric properties and the energy harvesting capability of nonpercolated polyurethane composites*, J. Appl. Phys. (in press)
5. **C. Putson,** L.Lebrun, P.-J. Cottinet, D.Guyomar and N. Muensit, *Frequency and thickness dependence of the energy-harvesting capability of polyurethane by mechanical vibration*, Sensors and Actuators A. (in press)

International conferences

6. **C. Putson,** L.Lebrun, S. Muensit, and D.Guyomar, *Conversion Energy in Electrostrictive Nano-Charged/Polyurethane composite thin*, ^{2nd} Thailand Nanotechnology Conference, Phuket , August13-15 (2008).
7. **C. Putson,** L.Lebrun, D.Guyomar, B. Guiffard, P.-J. Cottinet and S. Muensit, *Vibration energy conversion of nano-filled electrostrictive polyurethane composites*, The 3rd Thailand Nanotechnology Conference: Health, Energy, Enviroment, Bangkok, December 21-22 (2009).

References:

[ALL 2001] J. Allen and A. Smits, *Energy Harvesting Eel*, Journal of Fluids and Structures. 15, 629-640 (2001).

[AMI 1998] R. Amirtharajah, and A. P. Chandrakasan, *Self-powered signal processing using vibration-based power generation*, IEEE Journal of Solid-State Circuits. 33(5), 687-695 (1998).

[ANT 2007] S. R. Anton and H. A. Sodano, *A Review of Power Harvesting Using Piezoelectric Materials (2003-2006)*, IOP: Smart Mater. Sruct. 16**,** R1-R12 (2007).

[BAD 2005] A.Badel, D.Guyomar, E. Lefeuvre, and C. Richard, *Efficiency enhancement of a piezoelectric energy harvesting device in pulsed operation by synchronous charge inversion*. Journal of Intelligent Material Systems and Structures. 16(10), 889-901 (2005).

[BAD 2006] A.Badel, D.Guyomar, E.Lefeuvre and C.Richard, *Piezoelectric energy harvesting using a synchronized switch technique*, Journal of Intelligent Material Systems and Structures.17(8-9), 831-839 (2006).

[BAD 2006b] A.Badel, A.Benayad, E.Lefeuvre, L.Lebrun, C.Richard and D.Guyomar, *Single crystals and nonlinear process for outstanding vibration-powered electrical enerators*, IEEE Transactions on Ultrasonics Ferroelectrics and Frequency Control. 53(4), 673-684 (2006).

[BAY 2004] A. Bayrashev, W. P. Robbins, and B. Ziaie, *Low frequency wireless powering of microsystems using piezoelectric-magnetostrictive laminate composites*, Sensors and Actuators A: Physical. 114(2-3), 244-249 (2004).

[BAU 1999] R.H. Baughman, C. Cui, A.A. Zakhidov, Z. Iqbal, J.N. Barisci, G.M. Spinks, G.G. Wallace, A. Mazzoldi, D. De Rossi, A.G. Rinzler, O. Jaschinski, S. Roth, and M. Kertesz, *Carbon nanotube actuators*, Science. 284, 1340–1344 (1999).

[BAU 2004] F. Bauer, E. Fousson, Q. M. Zhang and L. M. Lee, *Ferroelectric Copolymers and Terpolymers for Electrostrictors: Synthesis and Properties*, IEEE Trans. on Dielec. and Elec. Insul. 20, 293-297 (2004).

[BAU 2006] F .Bauer, E. Fousson, and Q. M. Zhang, *Recent Advances in Highly*

Electrostrictive P(VDF - TrFE - CFE) Terpolymers, IEEE Transactions on Dielectrics and Electrical Insulation. 13(5), 1149 - 1154 (2006).

[BIR 1988] Birkholz, E. Grob, M. Riffel, H. Roth, and U. Stohrer, *Conversion of Waste Exhaust Heat in Automobile Using FeSi2 Thermoelements*, Proceedings of 7th International Conference on Thermoelectric energy conversion, University of Texas, March 16-18, 124-128 (1988).

[BHA 1999] V. Bharti, Z. Y. Cheng, S. Gross, T. B. Xu, and Q. M. Zhang, *High electrostrictive strain under high mechanical stress in electronirradiated poly(vinylidene fluoride-trifluoroethylene) copolymer*, Appl. Phys. Lett. 75, 2653 (1999).

[BLE 1995] R. D. Blevins, *Formulas For Natural Frequency and Mode Shape*, (Malabar, FL: Krieger, 1995).

[BOB 2003] V. Bobnar, B. Vodopivec, M. Kosec, A. Levstik, B. Hilczer, and Q. M.Zhang, *Dielectric Properties of Relaxor-like Vinylidene Fluoridetrifluoroethylene- base Electroactive Polymers*, Macromolecules 36, 4436-4442 (2003).

[BUL 2005] N. Bulusu, and S. Jha, Wireless sensor networks, Artech House, Boston, MA. 2005.

[CAL 1998] P. Calvert, J. O'Kelly, and C. Souvignier, *Solid freeform fabrication of organicinorganic hybrid materials*, Material Science and Engineering. C6, 167-174 (1998).

[CAM 2004] Edward Camacho, *MEM's Optical Pyrometer*, 22nd Annual Microelectronic Engineering Conference, May 2004.

[CHA 1997] A. Champa jayasuriya, Shigeru Tasaka and Norihiro inagaki, *Drawing and poling effects on dielectric properties of an aromatic polyurethane*, Eur. Polym. J. 33(10-12), 1645-1649 (1997).

[CHE 1999] Z. Y. Cheng, V. Bharti, T. B. Xu, S. Wang, and Q. M. Zhang, *Transverse strain respones in electrostrictive poly(vinylidene fluoride-trifluoroethylene) films and development of adilatometer for the measurement*, J. Appl. Phys. 86, 2208 (1999).

[CHI 2002] N. N. H. Ching, H. Y. Wong, W. J. Li, P. H. W. Leong, and Z. Y. Wen, *A laser-micromachined multi-modal resonating power transducer for*

wireless sensing systems, Sensors and Actuators A-Physical. 97-8, 685-690 (2002).

[COH 2001] Y. Bar-Cohen, *Electroactive Polymers as Artificial Muscles – Reality and Challenges*, Proceedings of the 42nd American Institute of Aeronautics and Astronautics, Gossamer Spacecraft Forum (GSF), held in Seattle WA, April 16-19 (2001).

[COH 2001b] Y. Bar-Cohen, *Electroactive Polymer (EAP) Actuators as Artificial Muscles (Reality, Potential, and Challenges)*. SPIE Press, Bellingham, Washington, USA (2001).

[COH 2001c] Yoseph Bar-Cohen, *EAP actuators as Artificial muscle*, SPIE-International Society or Optical Engine, October 2001.

[COT 2009] P.-J Cottinet, D. Guyomar, B. Guiffard, C. Putson and L. Lebrun., IEEE UFFC (manuscript accepted).

[CRO 1995] L.E. Cross, *Ferroelectric Materials for Electromechanical Treansducer Applications*, Jpn. J. Appl. Phys. Part I, 34(5B), 2525 (1995).

[CRO 2004] L.E. Cross and W. Ma, *An electromechanical investigation of electromechanical response in a dielectric acrylic elastomer*, Appl. Phys. A 78:1201–1204 (2004).

[DAM 2004] Z. M. Dang, Y. H. Zhang, and S. C. Tjong, *Dependence of dielectric behavior on the physical property of fillers in the polymer-matrix composites*, Synth. Met. 146, 79, (2004).

[DAN 2004] Z. M. Dang, Y. H. Zhang, and S. C. Tjong, *Dependence of dielectric behavior on the physical property of fillers in the polymer-matrix composites*, Synth. Met. 146, 79 (2004).

[DAV 1982] G. T. Davis, T. Furukawa, A. J. Lovinger and M. G. Broadhurst, Macromolecules, 15, 329 (1982).

[DAV 1999] L.C. Davis, *Model of magnetorheological elastomers*, Journal of Applied Physics, 85(6), 3348-3351 (1999).

[DEV 2006] N. G. Devaraju and B. I. Lee, *Dielectric Behavior of Three Phase Polyimide Percolative Nanocomposites*, J. Appl. Polym. Sci. 99, 3018 (2006).

[DIA 2005] Diaconu, D. Dorohoi, *Properties of polyurethane thin films*, journal of

optoelectronics and advanced Materials. 7(2), 921-924 (2005).

[ELV 2001] N. G. Elvin, A. A. Elvin, and M. Spector, *A self-powered mechanical strain energy sensor*, Smart Materials & Structures. 10(2), 293-299 (2001).

[ENG 1994] Engdahl, Göran. *Handbook of Giant Magnetostrictive Materials*. (Academic Press, 1994).

[EST 1971] Estes, G.M., Seymour, R.W., Cooper, S.L., *Infrared studies of segmented polyurethane elastomers. II*, Macromol., 4, 452-457 (1971).

[FAR 1972] B.L. Farmer, A.J. Hopfinger and J.B.Lando, *Polymorphism of poly(vinylidene fluoride):potential energy calculations of the effects of head-to-head units on the chain conformation and packing of poly(vinylidene fluoride)*, J. Appl. Phys. 43, 4293-4303 (1972).

[FAY 1997] D.N. Fry, D.E. Holcomb, J.K. Munro, L.C. Oakes, and M.J. Maston, *Compact Portable Electric Power Sources*, Oak Ridge National Laboratory report, ORNL/TM-13360 (1997).

[FLE 2004] J. Fleming, W. Ng, and S. Ghamaty, *Thermoelectric-Based Power System for Unmanned-Air-Vehicle/Microair-Vehicle Applications*, Journal of Aircraft, 41,674–676 (2004).

[FRO 1950] H. Fr¨ ohlich, *Theory of dielectrics*, (Oxford University Press, London, 2nd edition, 1958).

[GAO 2005] R. X. Gao, and Y.Cui, *Vibration-based energy extraction for sensor powering:*
Design, analysis, and experimental evaluation, Proceedings of SPIE, 5765, 794-801 (2005).

[GLY 2004] P. Glynne-Jones, M. J. Tudor, S. P. Beeby, and N. M White, *An electromagnetic, vibration-powered generator for intelligent sensor systems*, Sensors and Actuators a-Physical.110(1-3), 344-349 (2004).

[GOU 2001] Y. Gourinat, *Introduction a la dynamique des structures*, (Cepadues edition, 2001).

[GUI 2003] F. M. Guillot and E. Balizer, *Electrostrictive Effect in Polyurethances*, J. Appl. Polym. Sci. 89, 399-404 (2003).

[GUI 2006] B. Guiffard, L. Seveyrat, G. Sebald, and D. Guyomar, *Enhanced electric field-induced strain in non-percolative carbon nanopowder/polyurethane*

composites, J. Phys. D: Appl. Phys. 39, 3053 (2006).

[GUI 2009] B. Guiffard, D. Guyomar, L. Seveyrat, Y. Chowanek, M. Bechelany D. Cornu and P. Miele, *Enhanced electroactive properties of polyurethane films loaded with carbon-coated SiC nanowires*, J. Phys. D: Appl. Phys. 40, 055503 (2009).

[GUY 1999] I.L.Guy, S.Muensit and E.M.Goldys, *Electrostriction in Gallium Nitride*, Appl. Phys.Lett. 75(23), 3641-3643 (1999).

[GUY 2005] D. Guyomar, A.Badel, E. Lefeuvre and C.Richard, *Toward energy harvesting using active materials and conversion improvement by nonlinear processing*, IEEE Transactions on Ultrasonics Ferroelectrics and Frequency Control. 52, 584-595 (2005).

[HEP 1982] Hepburn, C., *Polyurethane Elastomers*, (Applied Science, London 1982).

[HER 1982] J. M. Herbert, *Ferroelectric Transducers and Sensors* (Gordon and Breach, New York, 1982).

[HIR 1999] Hirai T, M. Watanabe, M. Yamaguchi, *PVC gel deforms like a tongue by applying an electric field*, WW-EAP Newsletter.1(2), 7-8 (1999).

[HUA 2003] J. Huang, R. C. O'Handley, and D.Bono, *New, high-sensitivity, hybrid magnetostrictive/electroactive magnetic field sensors*, Proceedings of SPIE, 5050 (2003).

[HUA 2004] C. Huang, R. Klein, H. Li, Q. M. Zhang, F. Bauer and Z.-Y. Cheng, *Poly(vinylidene floride-trifluoroethylene) Based High Performance Electroactive Polymers*, IEEE Trans. on Dielec. and Elec. Insul. 20, 299-311 (2004).

[HUN 2007] X. Y.Hung, P. K. Jiang and C. U. Kim, *Electrical properties of polyethylene/aluminum nanocomposites*, J. Appl. Phys. 102, 12410 (2007).

[IBR 2009] Ibrahim Sari, Tuna Balkan and Haluk Kulah, *An electromagnetic micro energy harvester based on an array of parylene cantilevers*, J. Micromech. Microeng. 19, 105023 (2009).

[IEEE 1988] IEEE Standard on Piezoelectricity, An American National Standard, ANSI/IEEE, (The Institute of Electrical and Electronics Engineers, Inc., New York, USA, 1988).

[INM 2001] Engineering Vibration: Second Edition. D.J. Inman, (Prentice-Hall, Inc.,

2001).

[JAN 1979] Jang, S.J., Ph.D.Dissertation, The Pennsylvania State University, University Park, PA, 1979.

[JEA 2007]. Jean-Mistral C, Basrour S., Chaillout J.J., and Bonvilain A, *DTIP of MEMS & MOEMS*, Stresa, Italy, 25-27 April 2007, ISBN :978-2-35500-000-3

[KAI 2007]. Kailiang Ren,Yiming Liu, H. Hofmann, Q. M. Zhang and John Blottman, *An active energy harvesting scheme with an electroactive polymer*, Applied Physics Letters 91, 132910 (2007).

[KIE 1991] J. J. Kiely, D. V. Morgan, and D. M. Rowe, *Low cost miniature thermoelectric generator*, Electronics Letters, 27, 2332-2334 (1991).

[KIM 2000] Kim J., J.-Y. Kim and S.-J. Choe, *Electro-Active Papers: Its Possibility as Actuators*, Y. Bar-Cohen Y., (Ed.), Proceedings of the SPIE's EAPAD Conf., part of the 7th Annual International Symposium on Smart Structures and Materials. 3987, 203-209 (2000). ISBN 0-8194-3605-4

[KRA 1999] I. Krakovsky, T. Romijn, and A. Posthuma de Boer, *A few remarks on the electrostriction of elastomers*, J. of applied physics, 85 (1), 628 (1999).

[KOF 2001] G. Kofod, *Dielectric elastomer actuators*, PhD Thesis, The Technical University of Denmark, 2001.

[KOR 2004] Kornbluh R., Harsha Prahlad, Ron Pelrine, Scott Stanford, Marcus A. Rosenthal, Philip A. von Guggenberg, *Rubber to rigid, clamped to undamped: towards composite materials with wide-range controllable stiffness and damping*, Proc. SPIE, 5388, 372-386 (2004).

[KOR 2006] Korley, L.T.J.; Pate, B.D.; Thomas, E.L.; Hammond, P.T.; *Effect of the Degree of Soft and Hard Segment Ordering on the Morphology and Mechanical Behavior of Semicrystalline Segmented Polyurethanes*; Polymer, *47*, 3073-3082 (2006).

[KYM 1998] J. Kymissis, C. Kendall, J. Paradiso and N. Gershenfeld, *Parasitic power harvesting in shoes*, the 2nd International Symposium on Wearable Computers, Pittsburgh, PA, USA, 132-9 (1998).

[LAM 2005] K. S. Lam, Y. Zhou, Y. W. Wong, and F. G. Shin, *Electrostriction of lead zirconate titanate/polyurethane composites*, J. Appl. Phys. 97, 104112, 2005.

[LAN 2006] S. B. Lang and S. Muensit, *Review of some lesser-known applications of piezoelectric and pyroelectric polymers*, Appl. Phys. A 85, 125–134 (2006).

[LAP 2007] Lapprand A., Mechin F., Pascault J.-P., *Synthesis and Properties of Self-Crosslinkable Thermoplastic Polyurethanes*, J. Appl. Polym. Sci. 105, 99 (2007).

[LEE 1995] J. B. Lee, Z. Z. Chen, M. G.Allen, A. Rohatgi, and R. Arya, *A miniaturized high-voltage solar-cell array as an electrostatic MEMS power-supply*. Journal of Microelectromechanical Systems. 4, 102-108 (1995).

[LEF 2005] E.Lefeuvre, A.Badel, C.Richard and D. Guyomar, *Piezoelectric energy harvesting device optimization by synchronous electric charge extraction*, Journal of Intelligent Material Systems and Structures.16(10), 865-876 (2005).

[LIU 2005] Yiming Liu, Kai Liang Ren, Heath F. Hofmann and Qiming Zhang, *Investigation Of Electrostrictive Polymers For Energy Harvesting*, IEEE transactions on ulrasonics, ferroelectric s and frequency control.52(12), 2411-2417 (2005).

[LUI 2000] Lui Z. and P. Calvert, *Multilayer hydrogels and muscle-like actuators*, Advanced Materials.12(4), 288-291 (2000).

[MAD 2004] J.D.W. Madden, A. N. Vandesteeg, P.A. Anquetil, P.G.A. Madden, A. Takshi, R.Z. Pytel, S.R. Lafontaine, P.A. Wieringa, and I.W. Hunter, *Artificial muscle technology: Physical principles and naval prospects*, IEEE Journal of Oceanic Engineering. 20(3), 706–728 (2004).

[MAT 2002] K. Matsubara, *Development of a High Efficient Thermoelectric Stack for a Waste Exhaust Heat Recovery of Vehicles*, Proc. of the 21st International Conference on Thermoelectronics, August 25-29th, Portland, OR, 418–423 (2002).

[MEN 2001] S. Meninger, J. O. Mur-Miranda, R. Amirtharajah, A. P. Chandrakasan, and J. H. Lang, *Vibration-to-electric energy conversion*, IEEE Transactions on Very LargeScale Integration (Vlsi) Systems. 9(1), 64-76 (2001).

[MIT 2004] B. S. Mitchell, *An Introduction to Materials Engineering and Science for Chemical and Materials Engineers* (Wiley-IEEE, 2004).

[MYK 2007] Mykola Pereyma, Perspectives of Smart RFID Tags Usage Fabricated by MEMS Technologies, MEMSTECH'2007, May 23-26, 2007 Lviv-Polyana, Ukraine.

[NAL 1995] Hari Singh Nalwa, *Ferroelectric polymers chemistry, physics and applications*, (Marcel Dekker, Inc. 1995).

[NEE 2009] Bret P. Neese, *The multifunctional properties of PVDF-based Polymers*, PhD Thesis, The Pennsylvania State University, 2009.

[NEW 1997] R. E. Newnham, V. Sundar, R. Yimnirun, J. Su, and Q. M. Zhang, *Electrostriction: Nonlinear Electromechanical Coupling in Solid Dielectrics*, J. Phys. Chem. B, 101 (48), 10141–10150 (1997).

[NUR 2006] Nurazreena, L. B. Hussain, H. Ismail, and M. Mariatti, *Metal Filled High Density Polyethylene Composites-Electrical and Tensile Properties*, J. Therm. Comp. Materials 19, 413 (2006).

[NYE 1985] J .F.Nye ,*Physical properties of crystals*, (Oxford university press,1985).

[OGU 1999] K. Oguro, N. Fujiwara, K. Asaka, K. Onishi, and S. Sewa, *Polymer electrolyte actuator with gold electrodes*, Proceedings of the SPIE's 6th Annual International Symposium on Smart Structures and Materials.3669, 64-71 (1999). ISBN 0-8194-3143-5

[OSA 1993] Osada Y., and R. Murphy, *Intelligent Gels*, Scientific American, 268, 82-87 (1993).

[OTT 2002] G. K. Ottman, H. F. Hofmann, A. C. Bhatt, and G. A. Lesieutre, *Adaptive piezoelectric energy harvesting circuit for wireless remote power supply*, IEEE Transactions on Power Electronics. 17(5), 669-676 (2002).

[PAR 2005] J.A. Paradiso and T. Starner, *Energy Scavenging for Mobile and Wireless Electronics*, IEEE Pervasive Computing. 4, 18–27 (2005).

[PAR 2008] C. Park, J. H. Kang, J. S. Harrison, R. C. Costen, and S. E. Lowther, *Actuating Single Wall Carbon Nanotube_Polymer Composites:Intrinsic Unimorphs*, Adv. Mater.20, 2074 (2008).

[PER 2007]. M. Pereyma, *Overview of the Modern State of the Vibration Energy Harvesting Devices*, IEEE international conference on Perspective Technologies and Methods in MEMS Design, MEMSTECH'2007, 107-

114 (2007).

[PET 1991] Petrovic, Z., Ferguson, J., *Polyurethane Elastomers*. Prog. Polym. Sci., 16, 695-836 (1991).

[PET 2008] Petit L, Guiffard B, Seveyrat L and Guyomar D, *Actuating abilities of electroactive carbon nanopowder/polyurethane composite films*, Sensors and Actuators. A 148(1), 105-110 (2008)**.**

[POU 2004] G. Poulin, E. Sarraute, and F. Costa, *Generation of Electrical Energy for Portable Devices Comparative Study of an Electromagnetic and a Piezoelectric System*, Sensors & Actuators.116, 461–471 (2004).

[QI 2006] L. Qi, B. I. Lee, W. D. Samuels, G. J. Exarhos and S. G. Plarler, *Three-Phase Percolative Silver-BaTiO3-Epoxy Nanocomposites with High Dielectric constants*. J. Appl. Polym. Sci. 102, 967 (2006).

[QUR 2008] A. Qureshi, A. Mergen, M. S. Eroglu, N. L. Singh and A. Gulluoglu, *Dielectric Properties of Polymer Composites Filled with Different Metals*. J. Macromol. Sci., Part A: Pure Appl. Chem. 45, 462 (2008).

[ROU 2003] S. Roundy, P. Wright, and J. Rabaey, *A Study of Low Level Vibrations as a Power Source for Wireless Sensor Nodes*, Computer Communications. 26, 1131–1144 (2003).

[ROU 2004] Roundy, S., Wright, P. K., and Rabaey, J. M., *Energy scavenging for wireless sensor networks: with special focus on vibrations*, (Kluwer Academic, Boston. 2004).

[ROU 2004b] S. Roundy and P. K. Wright, *A piezoelectric vibration based generator for wireless electronics*, Smart Materials & Structures. 13(5), 1131-1142 (2004).

[RUS 2001] Rusu,M.; sofian,N.; and rusu,D, *Mechanical and thermal properties of zine powder filled high density polyethylene composites*, polymer testing. 20, 407-417 (2001).

[SCH 2000b] H. B. Schreyer, G. Nouvelle, K. J. Kim, and M. Shahinpoor, *Electrical activation of artificial muscles containing polyacrylonitrile gel fibers*, Biomacromolecules. 1, 642–647 (2000).

[SHA 2000] M. Shahinpoor, *Elastically-Activated Artificial Muscles Made with Liquid Crystal Elastomers*, Y. Bar-Cohen, (Ed.), Proceedings of the SPIE's 7"

Annual International Symposium on Smart Strucmes and Materials, EAPAD Conf. 3987, 187-192 (2000). ISBN 0-18194-3605-4

[SHA 2005] Shashank Priya, *Modeling of electric energy harvesting using piezoelectric windmill*, Appl.Phys.Lett. 87,184101 (2005).

[SHA 2007] Shashank Priya, *Advances in energy harvesting using low profile piezoelectric transducers*, J electroceram. 19, 165-182 (2007).

[SOD 2003] H. A. Sodano, G. Park, D. J. Leo and D. J. Inman, *Use of piezoelectric energy harvesting devices for charging batteries*, Proceedings of SPIE. 5050, 101–108 (2003).

[SOD 2007] H. A. Sodano, G. E. Simmers, R. Dereux and D. J. Inman, *Recharging Batteries using Energy Harvested from Thermal Gradients*, Journal of Intelligent Material Systems and Structures.18, 3-10 (2007).

[STA 1996] T. Starner, *Human-powered wearable computing*, IBM Systems Journal, 35(3-4), 618-629 (1996).

[STA 2005] M. E. Staley and A. B. Flatau, *Characterization of energy harvesting potential of Terfenol-D and Galfenol*, Proceedings of SPIE, 5764, 630-40 (2005).

[STO 1997] M. Stordeur and I.Stark, *Low power Thermoelectric Generator – Self-sufficient Energy Supply for Micro Systems*, 16th International Conference on Thermoelectrics, 575-577, 1997.

[SU 1998] J. Su, Q. M. Zhang, P. Wang, A. G. Macdiarmid, and K. J. Wynne, *Preparation and Characterization of electrostrictive Polyurethane Films with conductive Polymer Electrodes*, Polym. Adv. Technol. 9, 317 (1998).

[SU 1999] Su J., J. S. Harrison, T. St. CIair, Y. Bar-Cohen, and S.Leary, *Electrostrictive Graft Elastomers and Applications*, MRS Symposium Proceedings. 600, Warrendale, PA,131-136 (1999). ISBN 1-55899-508-0

[SU 1999b] Su J., R. Yimnirun, V. Sundar, P. J. Moses, S. Jang, and R.E. Newnham, *Converse electrostriction in polymers and composites*, Mater. Chem and Phys. 61, 18-23 (1999).

[SU 2000] J. Su, J.S. Harrison, and T. St. Clair, *Novel polymeric elastomers for actuation*, Proceedings of IEEE International Symposium on Application of Ferroelectrics, 2:811–819 (2000).

[SUN 1996] V. Sundar and R.E. Newnham, *Converse method measurements of*

electrostriction coefficients in low-K dielectrics, Materials Research Bulletin 31(5), 545 (1996).

[SYL 1999] Sylvie Eury, R. Yimnirun, V. Sundar, P. J. Moses, Sei-Joo Jang, R. E. Newnham, *Converse electrostriction in polymers and composites*, Materials Chemistry and Physics. 61, 18-23 (1999).

[TOR 2005] Torah, R., *Cantilever generator*, University of Southampton. School of Electronics and Computer Science (2005). http:www.ecs.soton.ac.uk/~rnt/Cantilever_Gen_eire_v6.ppt

[UCH 1980] K. Uchino and L. E. Cross, *Electrostriction and Its Interrelation with Other Anharmonic Properties of Materials* ,Jpn. J. Appl. Phys., Part 2: 19, L171 (1980).

[UCH 2000] K. Uchino, *Ferroelectric devices*, (Marcel Dekker, Inc., New York, 2000).

[UME 2004] M. Umeda, K. Nakamura, and S Ueha, *Analysis of the transformation of mechanical impact energy to electric energy using piezoelectric vibrator*, Japanese Journal of Applied Physics Part 1-Regular Papers Short Notes & Review Papers, 35(5B), 3267-3273 (1996).

[WAN 1991] H. Wang, Q. M. Zhang, L. E. Cross, R. Ting, C. Coughlin, and K. Rittenmyer, *The Origins of Electromechanical Response in Polyurethane Elastomers*, Proceedings of the Ninth IEEE International Symposium.182, 1991. CH3416-5 0-7803-1/95

[WAN 2006] L. Wang and F. G. Yuan, *Structural vibration energy harvesting by magnetostrictive materials (MsM)*, The 4th China-Japan-US Symposium on Structural Control and Monitoring, Zhejiang University Press, Hangzhou, China,147-152 (2006).

[WAN 2007] Lei Wang and F.G. Yuan, Energy harvesting by magnetostrictive material (MsM) for powering wireless sensors in SHM,SPIE Smart Structures and Materials & NDE and Health Monitoring, 14th International Symposium (SSN07), 18-22 March, 2007.

[WAN 2008] Lei Wang and F G Yuan, *Vibration energy harvesting by magnetostrictive material*, Smart Mater. Struct.17, 045009 (14pp), 2008.

[WIL 1996] C. B. Williams, and R. B. Yates, *Analysis of a micro-electric generator for Microsystems*, Sensors and Actuators a-Physical, 52(1-3), 8-11 (1996).

[WOE 1998] van der Woerd, A. C., Bais, M. A., de Jong, L. P., and Van Roermund, A. H. M., *A highly efficient micro-power converter between a solar cell and a rechargeable lithium-ion battery*, Proceedings of SPIE 3328, San Diego, CA, USA, 315-25. 1998.

[XIA 2002] F. Xia, Z.-Y. Cheng, H. Xu, and Q. M. Zhang, G. Kavarnos, R. Ting, G. Abdul-Sedat and K. D. Belfield, *High Electromechanical Responses in Terpolymer of Poly(vinylidene fluoride trifluoroethylenechlorofluoroethylene)*, Adv. Mats. 14, 1574-1577 (2002).

[YAN 2006] J. Yang and T.Caillat, *Thermoelectric Materials for Space and Automotive Power Generation*, MRS Bulletin- Materials Research Society. 31(3), 199-205, 2006.

[YIM 1999] R. Yimnirun, S. Eury, V. Sundar, P. J. Moses, and R. E. Newnham, *Compressometer Based Method for Measuring Converse Electrostriction in Polymers*, IEEE Conference on Electrical Insulation and Dielectric Phenomena, 338 (1999).

[YUE 2004] S.C.L. Yuen, J.M.H. Lee, M.H.M, Lee, G.M.H. Chan, F.K. Lei, P.H.W. Leong,W.J. Li, and Y. Yeung, *A Size Micro Power Conversion Cell for Wireless Applications*, Proc. of the World Congress on Intelligent Control and Automation (WCICA). 6, 5629–5634 (2004).

[ZHA 1995] Q. M Zhang, J. Zhao, T. Shrout, N. Kim, L. E. Cross, A. Amin, and B. M. Kulwicki, *Characteristics of the Electromechanical Response and Polarization of Electric Field Biased Ferroelectrics*, J. Appl. Phys. 77, 2549-2555 (1995).

[ZHA 1998] Q. M. Zhang, V. Bharti, and X. Zhao, *Giant electrosb-iction and relaxor ferroelectric behavior in electron-irradiated poly(viny1idene fluoridetrifluorethylene) copolymer*, Science.280, 2101-2104 (1998).

[ZHA 2001] C. Zhang, C. Najafi, L. P. Bernal and P. Washabaugh, *An integrated combustor-thermoelectric micro power generator*, Twelfth IEEE Int. Conf. On Solid-State Sensors and Actuators (Trandsucers ’01), Munich, Germany, June 2001.

[ZHA 2004] Q. M. Zhang C. Huang, F. Xia, and J. Su, *Electroactive Polymer Actuators as Artificial Muscles*, Ed. Y. Bar-Cohen, SPIE Optical Engineering Press, WA, (2004).

[ZHE 1994] Ma Zhenyi, Jerry I. Scheinbeim *, Jar Wha Lee, Brian A. Newman, High field electrostrictive response of polymers, Journal of Polymer Science Part B: Polymer Physics, 32(16), 2721 – 2731 (1994).

[ZHI 2004] Y. Zhi, A. Chen, L.E. Cross, A. Petchsuk and T.C. Chung, *Dielectric and electroactive strain properties of poly(vinylidene fluoride-trifluoroethylene-chlorotrifluoroethylene) terpolymers,* Appl. Phys. Lett. 84(10) 1738 (2004).

[ZRI 1999] Zrinyi M., D. Szabo and J.Feher, *Comparative studies of electro- and magnetic field sensitive polymer gels*, Y. Bar-Cohen, (Ed.), Proceedings of the SPIE's 6th Annual International Symposium of Smart Structures and Materials, 3669, 406-413 (1999).

FOLIO ADMINISTRATIF

THESE SOUTENUE DEVANT L'INSTITUT NATIONAL DES SCIENCES APPLIQUEES DE LYON

NOM : **PUTSON** DATE de SOUTENANCE : **18 Novembre 2010**
(avec précision du nom de jeune fille, le cas échéant)

Prénoms : **Chatchai**

TITRE : ***RECUPEPATION D'ENERGIE A PARTIR DE MATERIAUX ELECTROACTIF. MODELISATION DU COMPORTEMENT DE CES DERNIERS***

NATURE : **Doctorat** Numéro d'ordre : **2010-ISAL-0097**

Ecole doctorale : **EEA**

Spécialité : **Electronique-Electrotechnique-Automatique**

Cote B.I.U. - Lyon : T 50/210/19 / et bis CLASSE :

RESUME :
Le besoin de systèmes auto-alimentés et sans fils est à l'origine d'une activité intense de recherches sur la récupération d'énergie électrique à partir de sources ambiantes d'origine thermique ou mécanique. Cette récupération ne peut se faire que si l'on dispose de matériaux de conversion adaptés, objet de cette thèse et de méthodes efficaces d'extraction d'énergie. Parmi les différents types de matériaux, les polymères électro-actifs occupent une place de choix car ils sont faciles de mise en œuvre et peuvent être déposés sur de très grandes surfaces quelles soient planes ou non.
Dans un premier temps, un modèle analytique a été réalisé pour obtenir l'expression du courant électrique et de la puissance disponible lorsqu'on récupère l'énergie électrique avec un film polymère collé sur une poutre métallique excitée mécaniquement sur son premier mode de flexion. Ce modèle a par exemple montré que la permittivité du film polymère est un des paramètres clefs pour augmenter la conversion. Ce modèle a été validé expérimentalement en utilisant des polymères du commerce et a permis aussi d'évaluer l'effet de l'épaisseur du film et de la fréquence de travail.
Dans un deuxième temps, des composites utilisant des charges conductrices de taille nanométriques ou micrométriques dispersées en volume dans le polymère ont été synthétisés. Il a été montré que l'emploi de charges conductrices permet d'augmenter la permittivité grâce à un mécanisme de polarisation interfaciale et, conformément à ce que le modèle prédit, d'accroitre les performances en récupération d'énergie.

MOTS-CLES : **Polymère électro-actifs, Polymère électrostrictif, Polyurethane, Composite, Récupération d'Energie Mécanique**

Laboratoire (s) de recherche : **Laboratoire de Génie Electrique et Ferroélectricité (LGEF) INSA Lyon**

Directeur de thèse: **Pr. Daniel GUYOMAR**
Co-directeur de thèse **Pr. Laurent LEBRUN**

Président de jury : **Pr. Amen AGBOSSOU**

Composition du jury : **Pr. Amen AGBOSSOU**
Dr. Eric DUHAYON
Pr. Daniel GUYOMAR
Dr. Olivier GIRAUDO
Pr. Laurent LEBRUN
Pr. Jean François ROUCHON